UNIVERSITÀ DEGLI STUDI DI MILANO

FACOLTÀ DI SCIENZE E TECNOLOGIE

Dipartimento di Matematica "Federigo Enriques"

Dottorato di Ricerca in Scienze Matematiche

Ciclo XXXVII

Tesi di Dottorato di Ricerca

MODELLING AND NUMERICAL STUDY OF MARBLE SULPHATION IN CULTURAL HERITAGE: A RANDOM PDE-ODE SYSTEM

Settore scientifico-disciplinare: MAT/06

Relatrici:
Prof. Daniela Morale
Prof. Stefania Ugolini

Coordinatore:
Prof. Giulio Ciraolo

Candidata:
Francesca Arceci

Anno Accademico 2023/2024

The doctoral scholarship was co-funded with resources in the frame of
the PON REACT-EU financing Program
Action IV.4 – Doctorates on innovation topics
This thesis reflects only the authors' views and opinions, neither the European Union nor
the European Commission can be considered responsible for them.

La borsa di dottorato è stata cofinanziata con risorse del
Programma di finanziamento PON REACT-EU
Azione IV.4 – Dottorati su tematiche dell'innovazione
Questa tesi riflette solo i punti di vista e le opinioni degli autori, né l'Unione Europea né la
Commissione Europea possono essere considerate responsabili per essi.

Abstract

The final scope of this thesis is to investigate from a numerical point of view a new approach to the mathematical modelling of the degradation process in the context of Cultural Heritage, focusing on the description of the marble sulphation chemical reaction.

Our contribution is a numerical analysis of a novel random model of the sulphation reaction on the half-line. Given a system of non-linear reaction-diffusion partial and ordinary differential equations (PDE-ODE) system, already present in the literature and describing the penetration of sulphur dioxide through the pores of a calcium carbonate-based surface which reacts with a consequent formation of gypsum, a source of randomness has been introduced as a Dirichlet dynamical boundary condition, with the aim to better model the sulphur dioxide evolution in the air.

A direct observation of some recent sulphur dioxide time series recorded in Milan suggests that an appropriate model needs to incorporate a significant stochastic fluctuation component, boundedness and a mean-reverting behaviour. The novelty relies on the choice of a class of stochastic processes with such properties, known as Pearson diffusions, and which can be introduced as solutions of an Itô's stochastic differential equations (SDE). For completeness, positiveness, boundedness, and stability for the Pearson SDE, as well as its numerical scheme, known as Lamperti Sloping Smooth Truncation, based on the well-known Euler-Maruyama method, are discussed and implemented, respectively.

The entirely original results are presented in the second part of the thesis. The numerical approximation of the overall system, combination of a non-linear reaction-diffusion PDE-ODE system with a stochastic boundary condition given by a specific Pearson process is investigated. Following recent theoretical results about the existence and uniqueness of a mild solution of this random system, a new numerical splitting scheme is proposed: an autonomous heat equation which inherits the stochastic boundary condition, and a non-linear and non local random system, coupled with the first, but with deterministic boundary conditions. We present an FTCS approximation and we provide the stability conditions for the discrete scheme. Furthermore, the order of spatial accuracy is numerically estimated to be one. Numerical quantitative and qualitative analyses of the impact of the randomness at the boundary are illustrated, both in the framework of single realizations of the process, i.e. in a pathwise sense, and also by considering distribution, first and second moments of large samples. We analyse both slow and accelerated regimes,

by considering increasing values of the reaction rates. In the fast reaction case, a formation of a moving stochastic front can be observed.

The final part of the thesis presents a theoretical convergence result. We consider a semi-discrete approximation of the system and prove the convergence of the discrete solution to the unique mild solution of the original random system, through a space-discrete approach. The same splitting strategy is adopted to derive some a priori estimates for the splitted discrete variables. Relevant results on compact embedding for time-space Besov spaces on the lattice as well some recent estimate results for the discrete heat kernel are exploited to prove a useful estimate for the solution to the discrete random heat equation. Furthermore, an L^2 a priori estimate for the second splitted variable together with its discrete derivative is provided. The final convergence result is obtained by a compactness argument, by first introducing piecewise constant interpolation and discretization operators on the lattice and by exploiting the uniform a priori estimate for the total system variable.

Keywords: Reaction-diffusion models; stochastic dynamical boundary condition; stochastic differential equation; PDE-ODE system; Pearson process; Lamperti transformation; numerical analysis; splitting scheme, convergence, semi-discrete scheme, Besov-spaces.

Research Project: PON 2021(DM 1061)-Università degli Studi di Milano *"Deterministic and stochastic mathematical modelling and data analysis within the study for the indoor and outdoor impact of the climate and environmental changes for the degradation of the Cultural Heritage"*

Acknowledgments

I would like to express my gratitude to my supervisors Prof.sse Stefania Ugolini and Daniela Morale for their help and support during my Ph.D. studies. Thank you for giving me the opportunity to restart my studies and for the encouragement during these three years.

I am deeply grateful to Prof. Francesco Carlo De Vecchi, whose expertise and knowledge are unquestionable.

I would like to thank the Referees for their feedback on this thesis and their comments and suggestions. I am so grateful you appreciated the interdisciplinary effort I have put into this work.

I thank all the students, researchers and professors I had the opportunity to meet at conferences and schools. I carry with me every little discussion and shared moment.

Finally, I would like to thank my family for the unconditional support I always had in all the choices I made. Thank you for the love and for always being there to look after me. To the friendships with deep roots that distance has only strengthened, you are my cornerstone. To the new friendship that Milan has brought into my life: I wasn't prepared for all the changes, but you showed me they were worth it.

Introduction: aim and results

This thesis is devoted to the complete numerical study of a new random mathematical model of the marble sulphation phenomenon in the context of Cultural Heritage preservation. The model describes the chemical aggression of calcium carbonate stones under the attack of sulphur dioxide [6, 7]. It is an initial, stochastic boundary value problem on the half-line: a non-linear PDE-ODE system, already known in the literature, of a not strongly parabolic reaction-diffusion type equations describing the penetration of sulphur dioxide through the pores of a calcium carbonate-based surface, forming gypsum, is made random since endowed with a stochastic Dirichlet dynamical boundary condition, to better model the sulphur dioxide evolution in the air. We face the problem of the numerical study of the whole highly non-linear random system by a suitable splitting strategy, which decomposes the original problem into two more manageable random subsystems. A first study regards a complete discrete forward in time and centred in space approximation of the random solution process is presented [8]. We state the theoretical stability and boundedness of the solutions and we perform a numerical accuracy study. By sampling the process, a qualitative parameter-dependent study is fulfilled and a numerical estimation of the distribution and the first two moments is carried out. A second theoretical achievement of the research project is a convergence result for a semi-discrete scheme to the solution of the random system in the continuum; by some a priori estimates and by taking advantage of immersion compactness arguments in (discrete) time-space Besov spaces, the convergence is proven [5].

The problem of the degradation of sandstones, limestones, and marble stones with different porosity used as building materials for thousands of years is a very important issue that has been observed in the last century. The first cause can be attributed to atmospheric pollutants, in particular the reaction of sulphur dioxide with calcareous surfaces, which then forms gypsum and black crusts, [17, 37, 35]. The dynamical evolution of the chemical reaction of sulphur dioxide with the surface of calcium carbonate stones in the cultural heritage degradation process is a complex system, due to the involvement of physical, chemical and biological processes, coupled with specific characteristics of the materials such as capillarity and porosity, [1, 9, 18]. To our knowledge, the study of degradation phenomena has been utilised primarily for pure statistical models or deterministic partial differential equations, [99]. Only in the last couple of years, stochastic evolution modelling has been introduced at both the microscale [86, 87] and the macroscale [6, 7, 82].

In the last decades, a great improvement to this research has been provided by a series of papers within the deterministic framework [1, 2, 9, 18, 19, 58, 60, 53, 90]. The basic elements of the models are introduced in [9], in which the authors propose a quantitative description of the diffusion of the sulphur dioxide SO_2 on the porosity of calcium carbonate stones $CaCO_3$. They assume that polluted air, and in particular the sulphur dioxide, diffuses through the pores of the carbonate stone and interacts with the surface of the pores, causing the following reaction:

$$CaCO_3 + SO_2 + 1/2\ O_2 + 2H_2O \longrightarrow CaSO_4 \cdot 2H_2O + CO_2.$$

The sequence of papers we refer to goes from a first basic model summarizing the above reaction [9, 60, 58] to more complex models taking into account other physical variables, such as the pressure [1, 2] and the stone surface rugosity [18] as well as damaging effects [19], with the aim to better study and reproduce the damages caused by the sulphation phenomenon. The reported analysis involves both well posedness results and numerical study above all for the models characterized by some technical difficulties that seem hard to overcome from a theoretical viewpoint [19].

The primary proposed deterministic model is a one-dimensional reaction-diffusion system of non-linear parabolic equations. Given the sulphur dioxide concentration ρ_s and the calcite density c, the model reads as following, [1, 9]

$$\begin{aligned} \frac{\partial}{\partial t}\rho_s &= \nabla \cdot (\varphi \nabla s) - \lambda \rho_s c, \qquad \text{in } (0,T) \times (0,\infty), \\ \partial_t c &= -\lambda \varphi s c, \end{aligned} \tag{1}$$

with constant initial and boundary conditions

$$\begin{aligned} \rho_s(0,x) = \rho_0, \quad c(0,x) = c_0; \\ \rho_s(t,0) = \bar{\rho}_0. \end{aligned} \tag{2}$$

Function s stands for the porous concentration of sulphur dioxide and it is such that $\rho_s = \varphi s$, whereas $\lambda \in \mathbb{R}_+$ is the reaction rate. The function $\varphi = \varphi(c)$ is the porosity of the material, which is usually a function of calcium carbonate

$$\varphi(c) = A + B\, c,$$

with $A \in \mathbb{R}_+$ and $B \in \mathbb{R}$. Calcium carbonate has a lower porosity than the transformed gypsum. Hence, we particularly focus on the specific case of $B \in \mathbb{R}_-$.

At the macroscale, a source of randomness has been proposed in [82]; with the aim to better model the sulphur dioxide evolution in the air, a Dirichlet stochastic dynamical boundary condition has been coupled with the system (1). More precisely, at the left boundary a Pearson process is considered, that is a solution to a Brownian motion-driven stochastic differential equation (SDE) with a mean reverting drift and a squared diffusion coefficient, which is a second-order polynomial of the state. As a consequence, instead of

the constant boundary condition in (2), the following Dirichlet dynamical condition is considered

$$\rho_s(t,0) = \Psi_t, \quad t \in (0,T],$$

where $\{\Psi_t\}_{t\in[0,T]}$ is the solution of the Itô type SDE

$$d\Psi_t = \alpha(\gamma - \Psi_t)dt + \sigma\sqrt{\Psi_t\,(\eta - \Psi_t)}dW_t, \tag{3}$$

with $\alpha, \sigma, \gamma, \eta \in \mathbb{R}_+$, and $\gamma \leq \eta$. Hence, the boundary condition has a lower regularity than the case faced in [9, 59]; indeed, it inherits the same regularity of the Wiener process W. Thus, despite the fact that the process Ψ has almost surely trajectories in C^β, for every $\beta \in (0, 1/2)$, i.e. the class of Hölder continuous functions of order less than one half, in [82] the authors, taking advantage of a splitting strategy, study the well posedness of the random system, by proving the existence of a pathwise unique mild solution of the random PDE-ODE system. First let us observe that if system (1) holds, c is explicitly given in terms of the porous sulphur dioxide $s = \rho_s/\varphi(c)$, i.e.

$$c(t,x) = Ac_0(x)\left[\varphi(c_0(x))e^{\lambda A\int_0^t s(r,x)dr} - Bc_0(x)\right]^{-1},$$

and the equation for s assumes the form

$$\begin{aligned} \partial_t s &= \partial_x^2 s + b_c(t,x)\partial_x s + \gamma_c(t,x)s(Bs-1) \\ \partial_t c &= -\lambda s(A+Bc)c, \end{aligned} \tag{4}$$

with $b_c(t,x) = B\partial_x c/(A+Bc), \quad \gamma_c(t,x) = \lambda c$.

The splitting strategy helps in overcoming the difficulty coming from the not strongly parabolic character of the system and the irregularity of the function at the boundary. It relies on the fact that, by splitting the porous sulphur dioxide s as $s = u + v$, one may decompose the random PDE equation into two sub-problems.

The first one is an autonomous heat equation: u is a solution of the following zero initial value problem which inherits the stochastic boundary condition

$$\begin{aligned} \partial_t u &= \partial_x^2 u, && (t,x) \in (0,T)\times(0,\infty); \\ u(0,x) &= 0, && x \in (0,\infty); \\ u(t,0) &= s(t,0) = \widetilde{\Psi}_t = \Psi_t/\varphi(c(t,0)), && t \in (0,T). \end{aligned}$$

The second problem is a non-linear and non local random system, coupled with the first, and with deterministic initial and boundary conditions, that is v is solution to the following system

$$\begin{aligned} \partial_t v &= \partial_x^2 v + \frac{B\partial_x c}{\varphi(c)}(\partial_x v + \partial_x u) - \left(\frac{B\partial_t c}{\varphi(c)} + \lambda c\right)(v+u), && (t,x) \in (0,T)\times(0,\infty); \\ v(0,x) &= s_0, && x \in (0,\infty); \\ v(t,0) &= 0, && t \in (0,T). \end{aligned}$$

The idea behind the splitting technique is to take advantage of the regularity properties of the solution of the heat equation, which involves just the diffusion part, and to exploit the smoothing effects of the Laplace operator to deal with the high irregularity at the boundary, given by the stochastic dynamical boundary condition. The specific choice of a Pearson diffusion as a dynamical boundary condition is an example of a stochastic process with such regularity; this choice is original in the context of the degradation of Cultural Heritage.

The original contribution of this thesis is the study of the numerical approximation of the random PDE system (1) endowed with the stochastic boundary condition Ψ_t. The starting point is the proposed model introduced in [82], where the existence and uniqueness of the mild solution are provided. Therefore, the investigation in this thesis is indeed focused on the one-dimensional space case to guarantee the well-posedness of the entire system. Moreover, the choice of the stochastic boundary condition proposed in this work is strictly related to the spatial dimension of the domain.

A first introductory paper [6], from one side, provides a preliminary numerical approximation of all the involved processes; on another side, it gives a justification of the choice of the Pearson type noise, starting by the direct observation of some recent sulphur dioxide time series recorded in Milan; the data suggest that an appropriate model needs to incorporate a significant stochastic fluctuation component, boundedness and a mean-reverting behaviour. More specifically, coherently with the observed data, the proposed process in (3) takes into account the tendency of the sulphur concentration ρ_s to return to a mean level (γ) in the dynamics described by the drift coefficient; the bounded behaviour is captured via the specific form of the diffusion coefficient, even though the SDE is driven by an unbounded Wiener process W. In applications, it is well-known that the issue of considering bounded noises is a crucial question ([40, 48]).

Regarding the literature on stochastic dynamical boundary conditions for evolution problems, some papers introduce white noise as a Neumann-type boundary condition (see, for instance [14, 16, 23, 42, 32, 45]). For our specific case, the experimental SO_2 concentration data are not compatible with a white noise behaviour. Moreover, since the boundary condition for the sulphur dioxide concentration on the positive real line is set in (2) to be of Dirichlet-type, it is reasonable to adopt a new modelling approach by considering the solutions of the stochastic process in (3) as a dynamical boundary condition.

For the convenience of the reader, in this thesis, we propose a self-contained presentation of the relevant mathematical properties associated with the Pearson stochastic boundary condition, in particular the uniqueness and the pathwise uniqueness, despite the non-Lipschitz diffusion coefficient; furthermore, we provide its boundedness throughout the classical Feller classification of the boundary of $\{0, \eta\}$ as *entrance boundary points*, whenever the following condition on the parameters of the SDE holds

$$\frac{2\alpha\gamma}{\eta\sigma^2} \wedge \frac{2\alpha(\eta-\gamma)}{\eta\sigma^2} > 1. \tag{5}$$

Furthermore, we face the two main problems arising in the application of the Eulero-Maruyama scheme for its numerical simulation: the not Lipschitz diffusion coefficient and the fact that the scheme is not domain preserving. In order to overcome both such problems, we consider a particular spatial change transformation of the process, known as the Lamperti transform,

$$Y_t = F(\Psi_t) = 2 \arcsin\left(\sqrt{\Psi_t/\eta}\right), \quad \Psi_t \in (0, \eta),$$

which allows to get rid of the not Lipschitz diffusion coefficient. The resulting additive noise Itô-type SDE shows a constant diffusion coefficient but a not Lipschitz drift, which is also periodic and monotone decreasing. Concerning this issue, we recall that in the standard Eulero-Maruyama scheme superlinearly growing coefficients produce divergent solutions, [31]. Furthermore, in the case of the one-sided Lipschitz continuous drift, with the derivative growing at most polynomially and global Lipschitz diffusion coefficient, one might consider a *tamed* Euler method, where the drift is modified to obtain a uniformly bounded coefficient [67]. Recently, a smooth truncation procedure has been proposed in [30], to overcome both the difficulty caused by the not Lipschitz drift coefficient, which has less regular properties, and to guarantee that monotonicity is maintained. In this thesis, we discuss the qualitative behaviour of the solution of the Pearson SDE and we provide a related error analysis, by considering samples of dimension 10000.

The entirely original results are presented in the second part of the thesis.

A first study regards a whole discrete forward in time and centred in space approximation of the random PDE-ODE process [8]. For a complete investigation of the random evolution problem, we propose a numerical *splitting scheme*, based on the same decomposition of the solution s of the porous sulphur concentration used in [82].

Let $\Xi_x \times \Xi_t = [0 = x_0, x_1, \ldots, x_M = \bar{x}] \times [0 = t_0, t_1, \ldots, t_N = T]$ be the equipartition of the space and time mesh, with $\Delta_t = T/N$ and $\Delta_x = \bar{x}/M$. Furthermore, let $\bar{\Delta}$ be such that

$$\bar{\Delta} = \frac{\Delta_t}{\Delta_x^2}.$$

We adopt the following notation for a general function g evaluated at the mesh nodes $g_m^n = g(t_n, x_m)$, for any $(n, m) \in \{0, \ldots, N\} \times \{0, \ldots, M\}$. Since at the simulation level we consider a bounded domain $[0, \overline{x}]$, we need to take into account a boundary conditions at $\overline{x}$ for function $s = u + v$: we take the following Neumann condition for u and v for the right boundary:

$$\partial_x u(t, \overline{x}) = \partial_x v(t, \overline{x}) = 0.$$

We denote by $(s_m^n, c_m^n) = (u_m^n + v_m^n, c_m^n)$ the discretized solutions in the nodes of the grid.

We solve the random PDE system pathwise, i.e. for any given realization $\{\tilde{\psi}^n\}_n(\omega), \omega \in \Omega_P$ of the discrete process

$$\widetilde{\psi}^n = \psi^n \left[\varphi\left(c_0 \exp(-\lambda \int_0^{t_n} \Psi_u du)\right)\right]^{-1},$$

where ψ^n is obtained via the LSST scheme introduced for the approximation of the solution of the SDE (3).

The splitting scheme is based on two main steps. First, a discrete forward time - centered space (FTCS) approximation $\{u_m^n\}_{n,m}$ of the heat equation is considered. It is coupled with a zero initial condition and with a discrete realization of the process ψ as a boundary condition. Given this discrete realization, for each trajectory, the *random heat equation* admits the following scheme , i.e. for any $n = 0, 1, \dots, N-1$

$$\begin{aligned} &u_m^{n+1} = \bar{\Delta}\, u_{m+1}^n + (1-2\bar{\Delta})u_m^n + \bar{\Delta}\, u_{m-1}^n, \quad m = 1, \dots, M-1; \\ &u_0^{n+1} = \widetilde{\psi}^{n+1}, \quad u_M^{n+1} = (1-2\bar{\Delta})u_M^n + 2\bar{\Delta}\, u_{M-1}^n; \\ &\quad u_0^0 = \widetilde{\psi}^0 \quad u_m^0 = 0, \quad m = 1, \dots, M. \end{aligned} \tag{6}$$

We state the following classical stability results.

Proposition 3.3 (Pathwise stability for u)**.** *Suppose that assumption* (5) *on the parameters of the stochastic boundary condition holds. Then for*

$$\bar{\Delta} \leq 1/2$$

the random process u_m^n is pathwise stable; precisely, there exists a constant C such that, for any $n \in \{1, \dots, N\}$, the vector solution U^n is such that

$$\|U^n(\omega)\|_{\Delta_x} \leq C_{T,\Delta_x}\widetilde{\eta},$$

where $\widetilde{\eta} = \eta/\varphi(c_0)$ and $\|\cdot\|_{\Delta_x}$ is the usual Euclidian norm. Moreover, also the mean square stability holds. Furthermore, the stability property holds also in the maximum norm case both pathwise and in mean

$$\mathbb{E}\left[\|U^n\|_{\max}\right] \leq C_T\widetilde{\eta}.$$

The second step of the splitting scheme is provided as follows. Given the discrete heat solution u_m^n, by using again an explicit first-order finite difference approximation, centred in space and forward in time, for any $n = 0, \dots, N-1$ and $m = 1, ..., M-1$ the variables v_m^n and c_m^n are the solutions to the scheme

$$\begin{aligned} v_m^{n+1} &= v_m^n + \bar{\Delta}\left(v_{m+1}^n - 2v_m^n + v_{m-1}^n\right) \\ &\quad + \bar{\Delta}\frac{B}{4\varphi(c_m^n)}\left(c_{m+1}^n - c_{m-1}^n\right)\left(v_{m+1}^n - v_{m-1}^n\right) \\ &\quad + \bar{\Delta}\frac{B}{4\varphi(c_m^n)}(c_{m+1}^n - c_{m-1}^n)(u_{m+1}^n - u_{m-1}^n) \\ &\quad + \Delta_t\lambda c_m^n\left(B(v_m^n + u_m^n) - 1\right)(v_m^n + u_m^n); \\ c_m^{n+1} &= c_m^n\, e^{-\lambda\Delta_t\,(v_m^n + u_m^n)\,\varphi(c_m^n)}, \end{aligned}$$

coupled with (6) and with initial conditions for $m \in \{1, \dots, M-1\}$ given by $v_m^0 = s_0 \leq \widetilde{\eta}, \quad c_m^0 = c_0$. Coherently with u, the Neumann boundary condition in $x = \overline{x}$ leads to the following condition at the boundary mesh points, for any $n = 1, \dots, N-1$

$$\begin{aligned} v_0^n &= 0; \\ v_M^{n+1} &= 2\bar{\Delta} v_{M-1}^n + (1 - 2\bar{\Delta}) v_M^n + \lambda \Delta_t c_m^n \left(B(v_m^n + u_m^n) - 1\right)(u_M^n + v_M^n). \end{aligned}$$

We derive explicit conditions to ensure both the positivity and the boundedness of the numerical solutions. An upper bound for the initial data for c and some restrictions on the time step of the discretization are provided in dependence on both the spatial step and the parameters governing the dynamics in order to guarantee the stability of the solutions, both in the pathwise and in the mean sense, according with the following statements.

Proposition 3.4 (Pathwise stability and boundedness)**.** *Let us suppose that the initial condition $s_0 \leq \widetilde{\eta}$, $c_m^0 = c_0$, $m \in \{1, \dots, M-1\}$ and the stability condition $\Delta_t / \Delta_x^2 \leq 1/2$ for the discretized solution u_m^n hold. If the following further conditions are satisfied*

$$\begin{aligned} c_0 &< -\frac{4}{5}\frac{A}{B} = \frac{4}{5}\frac{A}{|B|}; \\ \Delta_t &\leq \frac{\Delta_x^2}{2 + \lambda c_0 \Delta_x^2 (1 - B\widetilde{\eta})}. \end{aligned}$$

then the discretized solutions (s_m^n, c_m^n) is such that, for any $(n, m) \in \{1, \dots, N\} \times \{1, \dots, M\}$, and any $\omega \in \Omega$

$$(s_m^n(\omega), c_m^n(\omega)) \in [0, \widetilde{\eta}) \times [0, c_0].$$

Corollary 3.1 (Bounds for v_m^n)**.** *Let us suppose that the hypothesis of the previous proposition are satisfied. Then for any $(n, m) \in \{1, \dots, N\} \times \{1, \dots, M\}$, and any $\omega \in \Omega$,*

$$-\widetilde{\eta} \leq -u_m^n(\omega) \leq v_m^n(\omega) \leq \widetilde{\eta} - u_m^n.$$

Also the stability for the full scheme is proven; indeed, the following result is stated.

Proposition 3.5 (Pathwise stability for numerical v)**.** *Let us suppose that the hypothesis of previous propositions are satisfied. Then there exist positive constants $C_{\Delta_x, T, \bar{x}}, C_{\Delta_x, T}$ for any $n \in \{1, \dots, N\}$, the solution vector V^n at time step n is such that*

$$\|V^n(\omega)\|_{\Delta_x} \leq C_{\Delta_x, T, \bar{x}} \widetilde{\eta},$$

and

$$\|V^n(\omega)\|_{\max} \leq C_T \widetilde{\eta}.$$

The same stability results in mean follow.

Finally, the spatial accuracy order one is numerically estimated.

An extensive qualitative investigation of the numerical solutions for the entire system is provided for different levels of noise at the boundary, and different values of the porosity of the material, both in the slow and fast regime of the reaction. The fast regime is obtained by increasing the value of the reaction rate parameter λ. Indeed, as discussed in [59], an accelerated regime for the reaction obtained by assuming increasing values of the parameter λ is equivalent to analysing the asymptotic behaviour of the system by accelerating time by a factor of λ_i and taking a space expansion $\sqrt{\lambda_i}x$. By changing the parameter λ, the role of the activation energy in the penetration of the sulphur dioxide and the consequent degradation of the calcium carbonate is captured.

In the thesis we discuss the pathwise behaviour of the random system, by underlying the particular contribution of each single splitted variable to the evolution of the whole system, specifically the dynamics of the random heat equation problem and the role played by the second non-linear reaction system. Furthermore, we also face the problem of investigating the probability distribution, and the first and second moments of large trajectory samples, showing how the variability at the boundary spreads out into the domain. One can see that as σ increases, the impact of the noise on the entire domain also increases, gradually in the slower regime and instead with high fluctuations in a faster reaction regime. In the latter case, the transition zone gets smaller: the interior remains unaffected by sulphur dioxide without penetration of the gas in the marble, and more evident calcite deterioration at the boundary of the sample is highlighted with a subsequent formation of a stochastic moving front. Finally, in order to quantitative estimate the impact of the noise on the boundary, an L^2-mean distance among solutions (ρ_σ, c_σ) with different levels of noise σ at the boundary and the deterministic one $(\rho_{\sigma_0}, c_{\sigma_0})$ driven only by the mean-reverting dynamics is provided to account for the influence of the boundary in the dynamics. More precisely, we compute the *root mean square difference* (RMSD),[52]

$$RMSD(\rho_\sigma, \rho_{\sigma_0})(t,x) = \sqrt{\mathbb{E}\left[|\rho_{\sigma_3}(t,x) - \rho_{\sigma_0}(t,x)|^2\right]},$$
$$RMSD(c_\sigma, c_{\sigma_0})(t,x) = \sqrt{\mathbb{E}\left[|c_{\sigma_3}(t,x) - c_{\sigma_0}(t,x)|^2\right]}.$$

The impact of the noise is well-understood, displaying that the noise at the boundary propagates immediately throughout the entire domain: this happens more slowly for the slow reaction rate regime. Moreover, in the latter configuration, the impact of the noise at the boundary for the calcium carbonate density is almost zero everywhere. On the other hand, in the case of a fast reaction configuration, there is a more significant impact of the noise for the calcite around the formation of the front, whereas it is almost zero for the SO_2 concentration, coherently with the rest of our analysis.

The final chapter of the thesis is devoted to a theoretical convergence result. Indeed, it is considered a space-discrete approximation of the process (s, c) and the convergence to the

unique mild solution of the random reaction-diffusion system in the continuum, whose existence and uniqueness is stated in [82], is stated. In the framework of a discretization approach, which is discrete in space and continuous in time, to the same random system (s, c), we first give some a priori estimates on the discrete solutions (s, c) via the same splitting argument described above. We remark that the splitting argument is often utilized in facing stochastic partial differential equations (SPDEs). Here we adopt it for taking advantage of the linearity and the regularization effect of the discrete heat equation to compensate the strong irregularity of the boundary condition.

We present a complete, detailed analysis of the space-discrete random heat equation in the lattice $\Omega_h^+ = h\mathbb{Z}_+$ (and continuous in time). The derivation of the fundamental solution on the positive lattice is performed by starting from the fundamental solution to the whole one-dimensional lattice and by doing an odd reflection as in the classical framework. Furthermore an explicit representation of the solution for the initial boundary value problem (IBVP) is derived. By considering the boundary value problem (BVP) (with zero initial condition), we also provide an explicit representation of its solution in terms of the (*difference*) derivative of the discrete heat kernel on $\Omega_h = h\mathbb{Z}$. In order to prove some a priori estimates on the positive lattice for the solution of the random heat equation, we take advantage of some recent results in discrete time-space Besov spaces. In particular, by exploiting some properties of the discrete heat kernel derived in [13] to gain more regularity in space, we give a final estimate for the discrete random heat equation. As a final achievement, we prove that the $L_t^\infty W_x^{p,r}$ norm of u is controlled by the C^κ norm of the general boundary condition ψ with $\kappa \in (1/4, 1/2)$, according with the following proposition.

Proposition 4.7. *Let u be the solution of the semi-discrete random heat problem:*

$$\begin{aligned} \partial_t u = &\quad \Delta_x^D u, && \text{for } (t,x) \in [0,T] \times \Omega_h^+ \\ u(0,x) = &\quad 0 && \text{for } x \in \Omega_h^+ \\ u(t,0) = &\quad \psi(t) && \text{for } \psi(t) \in C^\kappa(\mathbb{R}_+). \end{aligned}$$

where Δ^D is the discrete Laplacian operator. Let us suppose that ψ is such that $\psi(0) = 0$ and $\kappa \in \left(\frac{1}{4}, \frac{1}{2}\right)$. Then, for every $\alpha \in (0,1)$ and $p \in (1, 1/\alpha)$, there exists a constant C' not depending on ψ such that P-almost surely

$$||u||_{L_t^\infty W_x^{p,r}} \leq C' ||\psi||_{C^\kappa}, \quad \frac{1}{p} + 2\kappa > r \tag{7}$$

Moreover, the estimation on the (difference) derivative of u in $L^2(\Omega_h)$ directly derives from (7) by taking $p = 2$ and $r = 1$.

We note that the result is not related to the particular stochastic model (3) assumed as a dynamical boundary condition, but it holds for every process that shares the regularity property of being β -Hölder continuous, with $1/4 < \beta < 1/2$. This class of processes is quite large, including, for example, the fractional Brownian motion with Hurst index

$\frac{1}{4} < H$, or solutions to rough path equations with driving noise having β Hölder regularity with $1/4 < \beta < 1/2$.

Concerning the estimates for the system (v, c), we first introduce a simplification strategy consisting of a sort of linearization of the whole system. Following [59] and [82], we introduce an auxiliary function f with good regularity properties in place of the variable s in the ODE of the system (4), which allows to obtain an independent ODE. While maintaining the coupling between the PDE and the ODE, this strategy returns a *linear* equation for the variable, although the system remains complexively non-linear. In this setting, for the second problem (v, c), a useful a priori bound for the L^2-norm in space of v and its discrete derivative is proved. The lines of the proof are similar to those applied in [82] but, coherently with the numerical pathwise estimatesusually carried out in L^2, we consider an interpolation between the spaces $L^2_t H^1_x$ and $L^\infty_t L^2_x$. to give our final estimate for v. Finally, a uniform bound for the solution s is provided by gathering the previous estimates on u and v together, leading to the following final estimate.

Proposition 4.11. *Let (s, g) be the couple of solutions of the following semi-discrete version of system (4) in $[0, T] \times \Omega_h^+$:*

$$\begin{aligned} \partial_t s &= \Delta_x^D s + b_g(t,x)[D_x^+ c D_x^+ s + D_x^- c D_x^- s] + \gamma_g s(Bf - 1) \\ \partial_t g &= -\lambda f \varphi(g) g \end{aligned}$$

where D_x^+, D_x^- are respectively the forward and backward finite difference operators and

$$b_g = \frac{1}{2}\frac{B}{\varphi(g)}, \qquad \gamma_g = \lambda g.$$

Then, for any $T > 0$, the following estimate on s holds with K a constant depending on T and the constants for the estimates for v:

$$\sup_{t\in[0,T]} \|s(t,\cdot)\|^2_{L^2(\Omega_h^+)} + \int_0^T \|D_x^+ s(t,\cdot)\|_{L^2(\Omega_h^+)} dt \le K$$

These a priori estimates allow to obtain our main convergence result, via compactness properties of time-space Besov spaces. More precisely, we first introduce simple extension operators (in terms of piecewise constant functions) associating to any function defined on the lattice Ω_h a function on the continuum Ω. This operator has good continuity and convergence properties with respect to the discrete and continuum Besov spaces. Furthermore, we also consider some not trivially defined discretization operators, which associate to each regular function on $\mathbb{R}_+$ a value at each lattice point given by the mean value of the function on a square centered on the lattice points. By introducing a weak formulation of our semi-discrete system solution, we first state that a weak solution is also a mild solution and, then, we prove the convergence of the piecewise constant extension of a solution of the semi-discrete random PDE-ODE system to the unique solution of the random system (1) for any $p \in [1, 2]$ and for any $k < 1/p$, in $L^p([0, T], B^k_{p,p}(\mathbb{R}_+))$, according with the following theorem.

Theorem 4.3. *Let (s_h, c_h) be the unique solution to the semi-discrete system defined in $[0,T] \times \Omega_h^+$:*

$$\begin{cases} \partial_t(\varphi(c_h)s_h) & = \frac{1}{2}\left(D_x^+(\varphi(c_h)D_x^- s_h) + D_x^-(\varphi(c_h)D_x^+ s_h)\right) - \lambda\varphi(c_h)s_h c_h \\ \partial_t c_h & = -\lambda\varphi(c_h)s_h c_h. \end{cases}$$

Then (s_h, c_h) converges to the solution (s, c) of the system (3.7) - (3.8), in the following sense: denoting by $\tilde{s}_h = \mathcal{E}_h(s_h)$ and $\tilde{c}_h = \mathcal{E}_h(c_h)$ the piecewise linear extension, for any $p \in [1,2]$ and for any $k < \frac{1}{p}$, we have that $(\tilde{s}_h, \tilde{c}_h)$ converges in $L^p([0,T], B^k_{p,p}(\mathbb{R}_+))$ to the unique solution (s, c) of the equations (4).

The outline of the thesis is the following.

In Chapter 1 we provide a detailed derivation of the deterministic mathematical model (1) describing the marble sulphation. Numerical simulations, carried out with different reaction rate, together with a complete stability analysis are provided to better understand the system and the dynamics of the reaction-diffusion system under consideration. Successively, the choice of a possible stochastic boundary condition for the SO_2 evolution is discussed as a consequence of a preliminary and qualitative analysis of the time series for the dioxide sulphur registered in Milan.

Chapter 2 is devoted to the formal remind of the mathematical framework for the Pearson process. For sake of completeness, a complete study is presented. Existence and uniqueness are provided by adapting Skorokhod and Yamada-Watanabe results for processes in one dimension to deal with the non-Lipschitz diffusion coefficient. A brief discussion on the role of *scale function* and *speed measure* is given for applying the Feller theory of the classification of boundary point with the aim to impose the boundedness of the process. The discussion on the problems arising with the numerical approximation via a Euler-Maruyama scheme is carried out into details. Numerical results are provided for different configurations of parameters, together with the convergence of the process to the invariant probability distribution.

Chapter 3 contains the main novelty of the work. The deterministic differential system (1) is combined with (3). Since it is necessary for the forthcoming analysis, we briefly recall the existence and uniqueness result of the solution to the PDE-ODE system with stochastic boundary conditions established in [82]. The new splitting scheme for the discretization of the whole random system is here proposed. Results are illustrated either for a single realization of the process as well as for the mean behaviour of the solutions. Particularly, we focus on both the quantitative and qualitative analysis of the impact of the noise at the boundary on the solutions. Pathwise stability of the scheme is rigorously established and its accuracy is numerically described.

Finally, Chapter 4 establishes a rigorous bridge between the numerical solutions and the mild solutions for the original system. Within a semi-discrete approach, discrete in space and continuous in time, and applying the same splitting strategy for the solution s, we derive some a priori estimates both for the splitted variables u and v. In particular, we derive the fundamental solution for the discrete random heat kernel and we exploit compact embeddings of time-space discrete Besov spaces to gain regularity in time. The convergence of the discrete solution to the one in the continuum is provided by a compactness argument, via interpolated functions and by some a priori uniform estimates.

Acknowledgement. The research presented in the thesis is carried out within the research project PON 2021(DM 1061) *"Deterministic and stochastic mathematical modelling and data analysis within the study for the indoor and outdoor impact of the climate and environmental changes for the degradation of the Cultural Heritage"* of the Università degli Studi di Milano.

Contents

Chapter 1

Modelling the sulphation phenomenon

The problem of the degradation of sandstones, limestones, and marble stones with different porosity, used as building materials for thousands of years, is a very important issue that has been observed in the last century. In this first chapter, we provide a general introduction to the mathematical modelling of the surface deterioration in Cultural Heritage, due to the chemical reaction of sulphur dioxide with the surface of calcium carbonate stones. We review the deterministic models widespread in literature, deriving into details the equations describing the sulphation evolution, starting point of the work in the thesis. We end the chapter giving a reasoning of the choice done for introducing a source of randomness in the model at the macroscale.

1.1 Introduction to the problem

Cultural heritage plays a crucial role in our society; not only it represents a connection with the past, preserving traditions and keeping individual identities, but it also helps bridge differences, fostering mutual respect and understanding between diverse communities. Of course, it represents a central part in the economic side: in 2015, cultural tourism in Europe was deemed to be responsible for 40% of European tourism contributing to the economy of any country and promoting the preservation of cultural heritage [36]. For these and other reasons, governmental institutions and organizations such as the United Nations Educational, Scientific and Cultural Organization (*UNESCO*) take care of cultural heritage all over the world. Especially in Italy, there are 60 recognized world heritage sites [1]; hence the interest to preserve them is very strong.

Historical buildings and monuments, often mainly composed of carbonate-based stone materials with calcite as their main component, are susceptible to deterioration caused by

[1] *https://www.unesco.org/en/countries/it*

acidic substances. The problem of the degradation of sandstones, limestones, and marble stones with different porosity used as building materials for thousands of years is a very important issue that has been observed in the last century.

Nowadays, atmospheric pollutants continue to be a major contributor to the degradation of heterogeneous structures made from a mixture of different materials, especially when complex structures with articulated geometries are involved. Among these, calcareous stones are particularly susceptible to damage. However, the mechanisms of stone degradation and the factors influencing them are difficult to identify due to the interplay of coupled processes. In particular, the phenomenon is very complex since physical, chemical and biological processes, coupled with specific characteristics of the materials such as capillarity and porosity, are involved.

For this reason, modelling the degradation phenomena and, more precisely, the surface recession of the stone, is an essential tool for the care and protection of our monuments. In [99], authors propose an interesting review of the latest mathematical models whose aim is to describe the deterioration of these structures over time; in particular, they highlight the lack of an inclusive model, capable of encompassing all the possible deterioration processes that, time by time, could be adapted to different case studies in the various parts of the world and with usually different conditions nearby, at least for structures build with similar materials. The geographic location and the microclimate surrounding pollution conditions are effectively very different from place to place and thus, finding a mathematical model able to explain different scenarios without neglecting any factors is very challenging.

In this work, we particularly focus on the *carbonation* phenomena, which plays an important role in the weathering process: the presence of carbon dioxide CO_2 in the air, indeed, dissolves in water forming carbonic acid

$$2H_2O + CO_2 \longrightarrow H_2CO_3,$$

that, combined with calcium carbonate, forms calcium bicarbonate. The latter is highly soluble in water and this causes the stone dissolution [34, 88, 99]:

$$CaCO_3 + H_2CO_3 \longrightarrow Ca(HCO_3)_2$$

Combined with the carbonation process, the *sulphation* phenomenon is considered. The sulphur dioxide (SO_2) present in the air reacts with the calcium carbonate due to the presence of water in the stone's surface and forms the calcium sulphite (1.1)

$$CaCO_3 + SO_2 + nH_2O \longrightarrow CaSO_3 \cdot nH_2O + CO_2 \tag{1.1}$$

$$CaCO_3 + SO_2 + 2H_{20} + \frac{1}{2} \longrightarrow CaSO_4 \cdot 2H_2O + CO_2. \tag{1.2}$$

Moreover, in the presence of sufficient water and oxygen in the air, when the sulphuric acid reacts with calcium carbonate leads to a decomposition of carbonate and, consequentially to the formation of anhydrous calcium sulphate (see (1.2)). The latter, when hydrated by


Figure 1.1: Examples of black crust in outdoor monuments. Pictures from *Wikimedia Commons*, Author: *Père-Lachaise*.

the relative humidity of the air, expands by up to 30 % in volume and readily adsorbs external colourful substances on its surface. This hydrated form is commonly referred to as gypsum. In particular, the phenomenon is observable in stone buildings and monuments exposed to atmospheric pollutants with the formation on their surfaces of dark colour *patinas*, known as *black crust*. Furthermore, gypsum has a higher porosity than carbonate calcium at the beginning of the reaction: thus,it is more susceptible to physical degradation caused by climatic agents, [17, 37, 35].

Nonetheless, we have to mention that nowadays the role of SO_2 in the degradation process of the monumental estate is becoming of secondary importance, due to the green campaigns adopted by many western countries in the last thirty years, which has produced a decreasing of SO_2 level in most of our cities. It could be very reasonable now to introduce variables such as HNO_3 or NO_2 that significantly increase the vulnerability of the stone: in particular, they increase the superficial porosity of the material, leading to an easier entry of water and pollutants. However, the inclusion of additional factors in the mathematical modelling is crucial; nonetheless, it lies beyond the scope of this thesis. In this work, we consider a model in which sulphur dioxide reacts with calcareous surfaces. We aim to investigate whether introducing some form of randomness into the phenomenon under study is feasible and, lately, introduce a proper mathematical modelling which could be generalized to different problems.

For the study of the evolution of degradation phenomena, either pure statistical models or deterministic partial differential equations have been proposed. In the 80's most of the models were based on statistical studies and were mainly related to the quantitative descriptions of damage correlated to the mass loss of stone materials with the deposition rate and pH of rainfall. Among such models the Lipfert formula is the most used, based on statistical models of atmospheric corrosion; it quantifies the annual surface recession of carbonate stone, due to the effects of clean rain, acid rain and dry deposition of pollutants [78]. However, during the present century, the rainfall contribution to surface recession is likely to have a small effect, while nowadays the increase in atmospheric CO_2

concentration is shown to be the main factor in increasing weathering via the karst effect [17]. The interested reader may refer to [99] for a review of such models.

With the work [9], a new approach in the framework of hydrodynamic models has been proposed. The starting points for the derivation of a differential model are the basic physical relations, the balance laws of the chemical reactions, and Fick's law. As a particular feature, the model takes into account the effects of sulphation on carbonate rocks, by assuming a direct linear dependence of porosity and diffusivity on the density of calcium carbonate. The permeability of the medium is neglected. A proper determination of the thickness of the formed gypsum crust ($CaSO_4 \cdot 2H_2O$) as a product of the reaction of SO_2 with calcium carbonate stones is determined. As explained in [9], the path of reaction of SO_2 suggests that, since the $CaSO_3$ (*calcium sulphite*) reaches equilibrium soon after the initial reaction, and then the amount of gypsum continues to increase with the progress of the reaction, one can consider the one-step reaction in (1.2) [50, 51, 73, 107]. In this model, all heat effects are neglected and it is assumed that the air contains enough water to give rise to the reaction and that the change in concentrations of oxygen (O_2), water (H_2O), and carbon dioxide (CO_2) does not affect the reaction [1, 9].

Our investigation starts precisely from the mathematical model introduced in [9], where a degenerate nonlinear parabolic system gives a quantitative description of the diffusion and the chemical action of sulphur dioxide on the porosity of calcium carbonate stones; it is assumed that polluted air (and so the sulphur dioxide) is diffused through the pores of the stones and interacts with the surface of the pores. The reaction-diffusion model gives a macroscopic description of the formation of calcium sulfate (gypsum) from the calcium carbonate (calcite) on the surface of a stone. The model reads as following, for $(t,x) \in [0,T] \times \mathbb{R}_+$, $T > 0$:

$$\begin{cases} \partial_t(\varphi(c(t,x))s(t,x)) &= d\,\partial_x(\varphi(c(t,x))\partial_x s(t,x)) - \lambda_1\varphi(c(t,x))s(t,x)c(t,x) \\ \partial_t c(t,x) &= -\lambda_2\varphi(c(t,x))s(t,x)c(t,x) \end{cases} \tag{1.3}$$

where s stands for the porous concentration of SO_2 (mol/cm^3) (see below for definition) and c for the local density of $CaCO_3$ (g/cm^3). The function $\varphi(c)$ is the porosity (volume of pores/total volume); it is supposed to depend only on the density of calcite. Denoting by m_s, m_c the masses of single molecules of sulphur dioxide and calcite respectively, the reaction speed λ_1, λ_2 are given by

$$\lambda_1 = \bar{A}/m_c; \quad \lambda_2 = \bar{A}/m_s, \tag{1.4}$$

where $\bar{A}$ is considered here as constant (in general, it might depend on the temperature, the presence of catalysers and the activation energy). Finally, d is the scalar effective molecular diffusive coefficient. Note that s is the *porous* concentration, namely the fraction of porous volume occupied by SO_2; it is related to the concentration ρ_s of SO_2 (fraction of total volume occupied by SO_2) by the relation

$$\rho_s = \varphi(c)s.$$

For the convenience of the reader, the detailed derivation of system (1.3) is presented in Section 1.2.

The initial conditions for s and c given by

$$s(0,x) = s_0(x), \quad c(0,x) = c_0(x), \quad x \in [0,\infty)$$

are coupled with the boundary condition for s, expressed as

$$s(t,0) = \psi(t), \quad t \in [0,T].$$

In [9] the boundary condition for s is assumed to be constant, i.e. $s(t,0) = \bar{s}_0$, even though, at least as far as numerical analysis is concerned, the authors state that the same analysis may be performed in the case where $s(t,0)$ is a given pre-selected bounded measurable positive function $\psi(t)$.

The above differential model (1.3) can be related to reactive flows in porous media [20, 27, 28]. A great advantage is that one can numerically simulate the dynamics of the damage process in monumental stones and compare the results with experimental data ([90]). The case $x \in \mathbb{R}$ has been studied in [58], while in the case on the half-line, $x \in \mathbb{R}_+$, as here, when the boundary condition ψ for $\in W^{1,1}$ regularity (in time), the work [59] states the well-posedness of the model; it also studies the fast reaction limit and the large time behaviour. See also [60] for the mathematical study of a generalization of the previous model (1.3), with Dirichlet boundary conditions for the unknown s expressed in terms of an assigned space-time function. In [53] a validation of the model both by numerical simulations and some experimental tests in the laboratory is provided, by giving especially a quantitative law for the penetration of the sulphation front inside the stone. Free boundary problems are faced in [33] for other simpler models by considering also the influence of humidity and discussing the agreement with experimental data. The introduction, in this first model (1.3), of the pressure p and the permeability $\kappa = \kappa(x,c)$ of the limestone specimen, as physical important quantities conditioning the phenomenon, was proposed in [1]; the model takes into account both the pressure gradient effects due to the Darcy law and the diffusivity given by the Fick law. The same model was studied from a numerical point of view in [2]. In such model as in [33] other phenomena, such as the effect of high permeability, swelling and the effects of humidity, were considered. All these models were analysed in depth in [3, 58, 59, 60, 61] where some analytical results were established, also with respect to the qualitative behaviour of the materials. In [18] a new nonlinear differential system for marble sulphation including the surface rugosity, a function obeying a damage-like equation which describes the microscopic variation of a surface with respect to a flat configuration, is introduced. An important novelty is the introduction of Robin boundary conditions for the flux of SO_2 through the external surface of the marble, depending on porosity, external concentration of sulphur dioxide and surface rugosity. During the numerical simulations, a random surface rugosity on the boundary based on Weibull's statistics is considered. As discussed in recent works [37, 38, 35], in urban and industrial areas the formation of gypsum on the stone surface is often accelerated by the deposition of particulate matter rich in metals and metal oxides, which

act as catalysts in the sulphation reaction. Hence, to improve the physical accuracy of the mathematical model, one could consider the dependence of the reaction rate (1.4) on the internal temperature, on the degree of wetness and on the catalysts. Recently, the authors in [19] perform another step in building an effective damage theory of stones, by coupling the chemical effect considered by the model in [18] with elastic damage due to mechanical stress introduced in [49], partially inspired by the results in [90]. This model is characterized by some technical difficulties that seem hard to overcome from a theoretical viewpoint. Therefore, by now they introduce some physically reasonable modifications to establish the existence of a suitable notion of solution on a given time interval. Numerical simulations are presented and discussed, also in view of further research.

To the best of our knowledge, all the dynamical systems considered so far describing the degradation of calcium carbonate due to the attack of sulphur dioxide are deterministic ones, except for [18] introducing random surface rugosity in simulations. Only in the last couple of years, stochastic evolution modelling has been introduced more systematically. In particular, at the microscale an interacting particle model has been proposed,[86] and a probabilistic interpretation of the deterministic model proposed in [9] has been derived,[87].

The work of this thesis follows the line of the modelling at macroscale started in [82] with the introduction of a random PDE-ODE system and then followed by the papers [6, 7] and [5, 8].

1.2 The deterministic model: a starting point

As previously introduced, a first attempt to mathematically model the sulphation phenomena in marble stones has been derived in [9].

For the mathematical modelization of the chemical reaction (1.2), let us introduce the notation that we will use in this thesis: let Ω be the domain occupied by the specimen of calcite and let ρ_s, c, g be the concentration of SO_2, $CaCO_3$ and $CaSO_4 \cdot 2H_2O$, respectively, defined with respect to the whole volume and depending on the position $x \in \Omega$ and the time $t \in [0, T]$.

The previous reaction can be expressed in terms of variation of the concentrations and products of balance's law, given by:

$$\begin{aligned} \partial_t \rho_s + \nabla \cdot (\rho_s V_s) &= \dot{r}_s &&= -m_s\, \omega, \\ \partial_t c &= \dot{r}_c &&= -m_c\, \omega, \end{aligned}$$

where

V_s : is the SO_2 fluid velocity;

$\dot{r}_s, \dot{r}_c$: rates of production or consummation of SO_2 and $CaCO_3$;

m_c, m_s, m_g : masses of single molecules of sulphur dioxide, calcite and gypsum;

$\omega > 0$: is the rate of reaction.

More precisely, ω is given by:

$$\omega = \bar{A}\left(\frac{\rho_s}{m_s}\right)\left(\frac{c}{m_c}\right),$$

where $\bar{A}$ is a constant depending on the temperature, the activation energy and the catalysts of the reaction. In [9], as the very first work in the field, the parameter $\bar{A}$ has been set to be constant, but it could play a fundamental role in the reaction.

As previously introduced, the porosity is here considered as a linear function of the gypsum (equivalently, of the amount of calcite), since the transformation of calcite in gypsum alters the volume of void (occupied by air and sulphur dioxide). Let φ_0 be the initial value of porosity ($c = c_0, g = 0$ the gypsum is not already formed) and $\varphi_{\tilde{g}}$ the final product of the sulphation ($c = 0$, $\tilde{g} = \frac{m_g}{m_c}c_0$)

$$\varphi(c) = \varphi_{\tilde{g}} + (\varphi_0 - \varphi_{\tilde{g}})\frac{c}{c_0}.$$

Let now s be the porous concentration of the sulphur dioxide, more precisely, the SO_2 concentration with respect to the volume of the pores, which is related to the concentration by the porosity ($\rho_s = \varphi(c)s$) and the seepage velocity, related to the fluid velocity by the Dupuit-Forchheimer relation ($v_s = \varphi(c)V_s$).

Finally, the balance law becomes:

$$\begin{aligned} \partial_t(\varphi(c)s) + \nabla\cdot(sv_s) &= -\left(\frac{\bar{A}}{m_c}\right)\varphi(c)sc, \\ \partial_t c = -m_c\bar{A}\left(\frac{\varphi(c)s}{m_s}\right)\left(\frac{c}{m_c}\right) &= -\left(\frac{\bar{A}}{m_s}\right)\varphi(c)sc. \end{aligned}$$

Following [9], the seepage velocity could be expressed by the Fick's law

$$sv_s = -D(c)\nabla s$$

where $D(c) = d\varphi(c)$ where d is (scalar) effective molecular diffusive coefficient; from now on, we will always assume $d = 1$.

We can finally give the equations system for the sulphation phenomena:

$$\partial_t(\varphi(c)s) = \nabla\cdot(\varphi(c)\nabla s) - \left(\frac{\bar{A}}{m_c}\right)\varphi(c)sc, \tag{1.5}$$

$$\partial_t c = -\left(\frac{\bar{A}}{m_s}\right)\varphi(c)sc, \tag{1.6}$$

which is a closed set of parabolic degenerate nonlinear partial differential equations, coupled with initial conditions at time $t = 0$, and Dirichlet or Neumann type condition at the boundary. Note that the system is equivalent to (1.3) with $\lambda_1 = \frac{\bar{A}}{m_c}$ and $\lambda_2 = \frac{\bar{A}}{m_s}$.

Existence and uniqueness for the global solution to problem (1.5)-(1.6) are stated in [58], [60]. Numerical approximations of its solutions via finite elements and finite differences are provided in [9]. Numerical stability is also established for the adopted approximation schemes.

In recent years, more complex models capable of incorporating additional aspects within the previous framework have been proposed in the literature. The authors in [33] propose a model for the evolution of carbonate stones under the aggression of sulphur dioxide, taking into account both the swelling of the external gypsum layer and the influence of humidity. In [1], a high permeability regime is considered: the effects of neglecting the convective contributions due to the pressure term are analysed and included in the model. Numerical experiments are conducted. More recently, a novel model that accounts for the rugosity of the surface has been proposed in [18]. More precisely, both piecewise constant and random rugosity are investigated.

Nonetheless, the final aim of this thesis is to incorporate a stochastic component into the model and to study both the well-posedness and numerical behaviour of the solutions in the new configuration. To achieve this, we consider the simplest model to better understand the role of the stochastic component within the new framework.

1.2.1 From the scaled to the adimensionalized model

For the convenience of the reader, following [9], we derive the adimensionalized system starting from (1.5)-(1.6) for a better understanding of the physics dynamics that will be useful in view of the reproduction of numerical simulations. We consider the change of variables:

$$y = \sqrt{\frac{\bar{A}}{m_c}}x, \quad \tau = \frac{\bar{A}}{m_c}t, \quad \tilde{s} = \frac{m_c}{m_s}s. \tag{1.7}$$

Starting from the spatial change of variable:

$$\begin{aligned}
\nabla_x(\varphi(c)\nabla_x s) &= \frac{\partial}{\partial_{x_1}}\varphi(c)\partial_{x_1}s + \cdots + \frac{\partial}{\partial_{x_n}}\varphi(c)\partial_{x_n}s \\
&= \sqrt{\frac{\bar{A}}{m_c}}\left(\frac{\partial}{\partial_{y_1}}\varphi(c)\partial_{x_1}s + \cdots + \frac{\partial}{\partial_{y_n}}\varphi(c)\partial_{x_n}s\right) \\
&= \sqrt{\frac{\bar{A}}{m_c}}\sqrt{\frac{\bar{A}}{m_c}}\left(\frac{\partial}{\partial_{y_1}}\varphi(c)\partial_{y_1}s + \cdots + \frac{\partial}{\partial_{y_n}}\varphi(c)\partial_{y_n}s\right) \\
&= \frac{\bar{A}}{m_c}\nabla_y(\varphi(c)\nabla_y s)\,,
\end{aligned}$$

and by substituting the previous expression in (1.5)-(1.6):

$$\partial_t(\varphi(c)s) = \frac{\bar{A}}{m_c}\nabla_y \cdot (\varphi(c)\nabla_y s) - \left(\frac{\bar{A}}{m_c}\right)\varphi(c)sc$$
$$\partial_t c = -\left(\frac{\bar{A}}{m_s}\right)\varphi(c)sc\,.$$

The change of variables in time leads to the following system:

$$\left(\frac{\bar{A}}{m_c}\right)\partial_\tau(\varphi(c)s) = \frac{\bar{A}}{m_c}\nabla_y \cdot (\varphi(c)\nabla_y s) - \left(\frac{\bar{A}}{m_c}\right)\varphi(c)sc\,,$$
$$\left(\frac{\bar{A}}{m_c}\right)\partial_\tau c = -\left(\frac{\bar{A}}{m_s}\right)\varphi(c)sc\,,$$

that reduces in

$$\partial_\tau(\varphi(c)s) = \nabla_y \cdot (\varphi(c)\nabla_y s) - \varphi(c)sc$$
$$\partial_\tau c = -\left(\frac{m_c}{m_s}\right)\varphi(c)sc\,.$$

Finally, the last change of variable for s gives :

$$\partial_\tau\left(\varphi(c)\frac{m_s}{m_c}\tilde{s}\right) = \nabla_y \cdot \left(\varphi(c)\nabla_y\frac{m_s}{m_c}\tilde{s}\right) - \varphi(c)\frac{m_s}{m_c}\tilde{s}c$$
$$\partial_\tau c = -\left(\frac{m_c}{m_s}\right)\varphi(c)\frac{m_s}{m_c}\tilde{s}c\,,$$

that is equivalent to

$$\partial_\tau(\varphi(c)\tilde{s}) = \nabla_y \cdot (\varphi(c)\nabla_y\tilde{s}) - \varphi(c)\tilde{s}c$$
$$\partial_\tau c = -\varphi(c)\tilde{s}c\,.$$

To avoid abuse of notation, the final system is rewritten in terms of s, x, t respectively to reset the initial notation.

$$\begin{aligned}\partial_t(\varphi(c)s) &= \nabla_x \cdot (\varphi(c)\nabla_x s) - \varphi(c)sc\\ \partial_t c &= -\varphi(c)sc\,.\end{aligned} \tag{1.8}$$

Global well-posedness and regularity for the problem (1.8) have been studied in [58] on the full line ($x \in \mathbb{R}$) and in [59] on the half line ($x \in (0,\infty)$). More precisely, in [9], finite element and finite difference schemes are provided and numerical stability is investigated under suitable conditions.

To understand the effect of a random boundary condition, we consider a simulation study of the system, following [1, 2, 9].

To this end, we rewrite system (1.5)-(1.6) for the rescaled total air concentration of SO_2

$$\rho_s = \varphi(c)s\,, \tag{1.9}$$

and an equivalent formulation of the problem is gained:

$$\begin{aligned} \partial_t(\rho_s) &= \nabla_x \cdot (\varphi(c)\nabla_x s) - \rho_s c \\ \partial_t c &= -\rho_s c\,. \end{aligned} \tag{1.10}$$

In [9] authors studied the previous system for $x \in [0,1]$ and $t \geq 0$. The porosity function $\varphi(c)$ is directly dependent on the density of calcite, since the transformation of calcite in gypsum alters the volume of void (occupied by air and sulphur dioxide) [1, 9], and the dependence is assumed to be linear, i.e.

$$\varphi(c) = A + Bc. \tag{1.11}$$

with $B = \frac{1}{c_0}(\varphi_0 - \varphi_{\tilde{g}}))$, $A = \varphi_{\tilde{g}}$, where the initial calcite density c_0 is assumed to be a positive constant, φ_0 is the porosity of the pure calcite specimen and $\varphi_{\tilde{g}}$ is the porosity of the final sulphation product, i.e. when all the calcium carbonate has been converted in gypsum.

System (1.10) is coupled with the initial conditions, for $x \in [0,1]$,

$$\begin{aligned} \rho(0,x) &= 0 \\ c(0,x) &= c_0 \end{aligned}$$

and boundary condition, for $t \in [0,T]$,

$$\begin{aligned} \rho(t,0) &= \rho_{s_0} \\ \partial_x \rho_s(t,1) &= 0 \\ c(t,0) &= c_0 e^{-\rho_{s_0} t} \end{aligned} \tag{1.12}$$

with ρ_{s_0}, c_0 are positive constant.

We perform numerical simulations of system (1.10)-(1.12) by a finite element scheme in space and by θ-method in time, in the class where s is a continuous piecewise linear function and c is a piecewise constant function. In [9] numerical stability for this scheme is established for the case $B > 0$. For completeness, in the following, we provide stability results when the parameter $B < 0$, since this is the case more interesting for the marble sulphation: the porosity increases as the reaction occurs and the calcium carbonate decreases and transform in gypsum. Hence, $B < 0$, the porosity level of the calcite at the beginning of the reaction is lower than the final level of porosity of the gypsum. The following proposition provides conditions on parameters when the parameter $\theta = 1$ in the time-discretization of the method (see Appendix A.1 for a more detailed derivation of the finite element method).

Proposition 1.1. *Let φ be the porosity defined in* (1.11)*, with $A \in \mathbb{R}_+$ and $B < 0$. Given the time and mesh step Δt and Δx, suppose that $\Delta x^2 < 6/c_0$, while the time step satisfies the following not empty condition*

$$\Delta t > \frac{\Delta x^2}{6 - c_0 \Delta x^2}\,. \tag{1.13}$$

Then, for all $x \in [0,1]$, the approximation of c is a non increasing function of time bounded by c_0 and the approximated ρ_s is non negative. Moreover, the numerical solution has the following upper bound:

$$0 \leq \rho_{s,h}(t,x) \leq \frac{A\rho_{s_0}}{\varphi_0}\,.$$

Differently from the case where $B > 0$ in [9], no additional hypotheses on Δt and ρ_{s_0} are requested.
Remark 1.1. Let us precise that condition (1.13) is explicitly derived in Proposition A.1.

Proof. Coherently with the derivation of the finite element scheme presented in Appendix A, let (s_h, c_h) be the couple of solutions approximated as follows:

$$s_h(t,x) = \sum_{i=1}^{N+1} \xi_i(t)p_i(x), \quad c_h(t,x) = \sum_{k=1}^{N} \eta_k(t)q_k(x)$$

where p_i, q_k are the canonical basis defined by (A.4). From proposition (A.1), we already know that the positivity is preserved and that for all $n \geq 0$ and $i \in \{0,\dots,N\}$ we have:

$$0 < \eta_i^{n+1/2} \leq \eta_i^n \leq c_0 \tag{1.14}$$

Let us denote $X_n = \max\limits_{0\leq j\leq N} \xi_j^n$. For all $(t,x) \in [t_n, t_{n+1}[\times[x_n, x_{n+1}[$ the numerical solution can be written as

$$\rho_{s,h}(t,x) = \varphi(\eta_k^n)[\xi_k^n p_k(x) + \xi_{k+1}^n p_{k+1}]$$

Since $B < 0$, as η_k^n decreases, $\varphi(\eta_k^n)$ increases. Recalling the definition (1.11) for $\varphi(c)$, then

$$0 < \varphi_0 \leq \varphi(\eta_k^n) \leq \varphi(\eta_k^{n+1/2}) \leq A = \varphi_{\tilde{g}}.$$

Therefore,

$$0 < \rho_{s,h}(t,x) \leq \varphi_{\tilde{g}} X_n = AX_n$$

We now want to prove that $X_n = \max\limits_{0\leq j\leq N} \xi_j^n \leq \frac{\rho_{s_0}}{\varphi_0}$ If $n{=}0$:

$$X_0 = \max_{0\leq j\leq N} \xi_j^o = \xi_1^0 = \frac{\rho_{s_0}}{\varphi_0}$$

Suppose now it is true for n and let us verify it for $n+1$:
If $j = 1$, let $X_{n+1} = \xi_1^{n+1}$. Then from (A.20) we get:

$$X_{n+1} = \xi_1^{n+1} = \frac{\rho_{s_0}}{\varphi\left(\eta_1^{n+1}\right)} \leq \frac{\rho_{s_0}}{\varphi_0}$$

Let $j \geq 2$, then $X_{n+1} = \xi_j^{n+1}$. It is sufficient to prove that $X_{n+1} \leq X_n$ to get the claim. From Proposition A.1 we have the following condition to ensure the positivity of U and G:

$$m_{ij}^{n+1/2} + \theta\Delta t k_{ij}^{n+1/2} < 0$$
$$m_{ij}^n + (1-\theta)\Delta t k_{ij}^n \geq 0$$

These conditions imply

$$\begin{aligned}\sum_{j=i-1}^{i+1}\left(m_{ij}^{n+1/2}+\Delta t\theta k_{ij}^{n+1/2}\right)X_{n+1} &\le \sum_{j=i-1}^{i+1}(m_{ij}^{n}-(1-\theta)\Delta t k_{ij}^{n})\xi_j^n\\ &\le \sum_{j=i-1}^{i+1}(m_{ij}^{n}-(1-\theta)\Delta t k_{ij}^{n})\max_{0\le j\le N}\xi_j^n\\ &= \sum_{j=i-1}^{i+1}(m_{ij}^{n}-(1-\theta)\Delta t k_{ij}^{n})X_n\end{aligned}$$

The inequality reads as

$$\begin{aligned}X_{n+1}&\left[\left(\varphi_{j-1}^{n+1/2}+\varphi_j^{n+1/2}\right)+\Delta t\theta\left(\varphi_{j-1}^{n+1/2}\eta_{j-1}^{n+1/2}+\varphi_j^{n+1/2}\eta_j^{n+1/2}\right)\right]\\ &\le X_n\left[(\varphi_{j-1}^n-\varphi_j^n)-\Delta t(1-\theta)(\varphi_{j-1}^n\eta_{j-1}^n+\varphi_j^n\eta_j^n)\right]\end{aligned}$$

By denoting

$$\Lambda=\frac{2}{\Delta x}\sum_{j=i-1}^{i+1}\left(m_{ij}^{n+1/2}+\Delta t\theta k_{ij}^{n+1/2}\right),\quad e_j=\eta_j^n-\eta_j^{n+1/2}$$

and using (1.14) we get

$$\begin{aligned}\Lambda X_{n+1}&\le X_n\Big[\Lambda+(\varphi_{j-1}^n+\varphi_j^n)-(1-\theta)\Delta t(\varphi_{j-1}^n\eta_{j-1}^n+\varphi_j^n\eta_j^n)\\ &\quad-(\varphi_{j-1}^{n+1/2}+\varphi_j^{n+1/2})-\theta\Delta t(\varphi_{j-1}^{n+1/2}\eta_{j-1}^{n+1/2}+\varphi_j^{n+1/2}\eta_j^{n+1/2})\Big]\\ &\le X_n\Big[\Lambda+(\varphi_{j-1}^n-\varphi_{j-1}^{n+1/2})+(\varphi_j^n-\varphi_j^{n+1/2})\\ &\quad-\Delta t(\varphi_{j-1}^n\eta_{j-1}^n+\varphi_j^n\eta_j^n)\\ &\quad+\theta\Delta t(\varphi_{j-1}^n\eta_{j-1}^n+\varphi_j^n\eta_j^n)\\ &\quad-\theta\Delta t(\varphi_{j-1}^{n+1/2}\eta_{j-1}^{n+1/2}+\varphi_i^{n+1/2}\eta_j^{n+1/2})\Big]\\ &\le X_n\Big[\Lambda+Be_{j-1}+Be_j-\Delta t(\varphi_{j-1}^n\eta_{j-1}^n+\varphi_j^n\eta_j^n)\\ &\quad+\theta\Delta t\varphi_{j-1}^{n+1/2}(\eta_{j-1}^n+\eta_{j-1}^{n+1/2})\\ &\quad+\theta\Delta t\varphi_i^{n+1/2}(\eta_j^n-\eta_j^{n+1/2})\Big]\end{aligned}$$

From the last inequality, since $B<0$, we get that $X_{n+1}\le X_n$ if

$$-\Delta t(\varphi_{j-1}^n\eta_{j-1}^n+\varphi_j^n\eta_j^n)+\theta\Delta t\varphi_{j-1}^{n+1/2}(\eta_{j-1}^n-\eta_{j-1}^{n+1/2})+\theta\Delta t\varphi_j^{n+1/2}(\eta_j^n-\eta_j^{n+1/2})\le 0$$

Since $\eta_j^n > 0, \varphi_j^n > 0$ for all $j \geq 0$ and for all $n \geq 0$, the first term is always negative; moreover, from (1.14) we know that $\eta_j^{n+1/2} \leq \eta_j^n$ and so the second and the third terms are always negative. Thus the inequality holds for all j, n and we got the claim

$$X_{n+1} \leq X_n \leq \frac{\rho_{s_0}}{\varphi_0}.$$

The numerical solution $\rho_{s,h}(t,x)$ has indeed an upper bound:

$$\rho_{s,h}(t,x) \leq \frac{A\rho_{s_0}}{\varphi_0}$$

□

Moreover, coherently with [9], we provide in Appendix (B) the derivation of the finite differences for the numerical discretization of (1.10).

All the parameters considered in [9] are listed in Table 1.1.

1.2.2 Simulation results for the deterministic system

At first, we consider the simulation results for the non-rescaled system (1.5)-(1.6), in the domain $[0, \bar{x}] \times [0, T] = [0, 1] \times [0, 1]$. In [9] the authors observe that the implemented implicit finite element method can be used with a hyperbolic like time step $\Delta t \propto \Delta x$, which allows fast computations; hence, the following mesh steps and initial parameters may be considered: $\Delta x = \Delta t = 0.0031$. Furthermore, the initial calcite and concentration of SO_2 are set as $c_0 = 10, \rho_{s_0} = 1$.

Parameter	Value	Dimension	Parameter	Value	Dimension
B	-0.01	cm^2/g	A	0.2	adimensional
m_c	100.09	g/mol	m_s	64.06	g/mol
d	1	cm^2/sec			

Table 1.1: Physical parameters consider in the model.

Simulation results for slow reaction rate $\bar{A} = 1$ and fast reaction rate $\bar{A} = 10000$ are performed, as in [9]. Figure 1.2 shows the spatial evolution profile of the solution at fixed times, from time $t = 0$ to $t = 0.5$ and time step 0.1, in the case $\bar{A} = 1$, which corresponds to reaction rates $\lambda_1 = 0.01, \lambda_2 = 0.016$. It is clear how reaction is quite slow: the sulphur dioxide leaks into domain, since the degradation is slow and there is enough calcite also inside the domain. Figure 1.3 shows, still in the case $\bar{A} = 1$, the time evolution of the SO_2 concentration and calcite density at points $x = 0.25$ and $x = 0.5$. Profiles are coherent with what discussed: the SO_2 concentration increases slowly at the beginning but at the

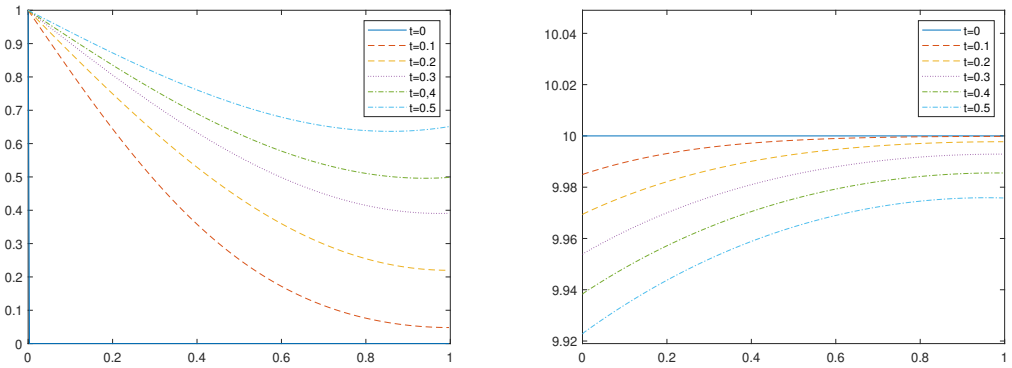

(a) (b)

Figure 1.2: Deterministic solution from $t = 0$ to $t = 0.5$ with $A = 1$. x-axis : $x \in [0, 1]$. (a) SO2 concentration ρ; (b) calcite density c.

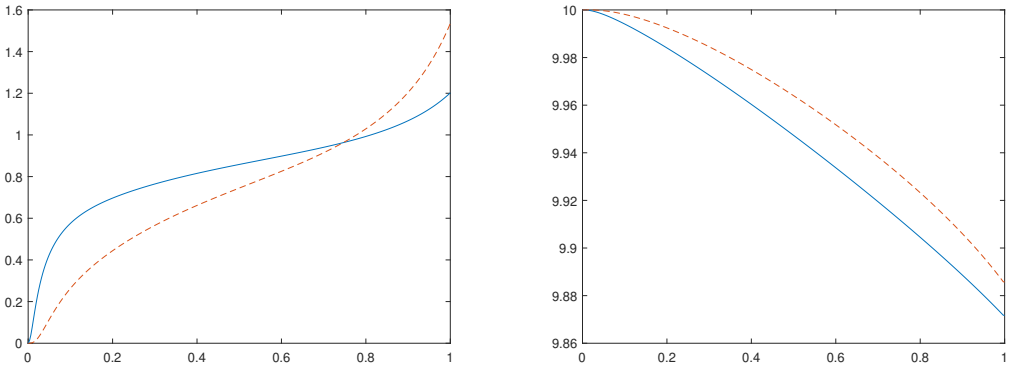

(a) (b)

Figure 1.3: Deterministic time evolution with $\bar{A} = 1$ at the points $x = 0.25$ (solid line) and $x = 0.5$ (dashed line). x-axis : $t \in [0, 1]$. (a) SO_2 concentration ρ; (b) calcite density c.

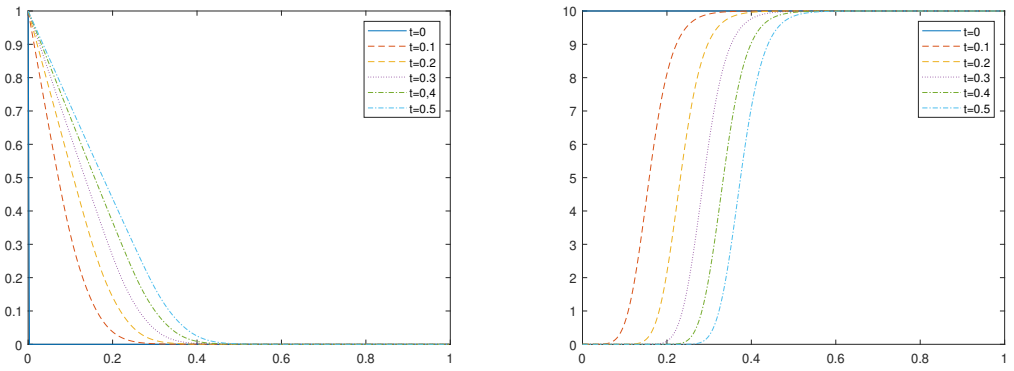

(a) (b)

Figure 1.4: Deterministic solution from $t = 0$ to $t = 0.5$ with $\bar{A} = 10000$. x-axis : $x \in [0, 1]$. (a) SO_2 concentration ρ; (b) calcite density c.

end is large in $x = 0.5$, since in Figure 1.2 we see that as the time increases the profile is going to change convexity.

These results are compared with the solution of a faster reaction obtained by considering $\bar{A} = 10000$. From the change of variable in (1.7) it is clear that in the case of the rescaled system this would impose an acceleration of time. From Figure 1.4, which gives the spatial profile of the solutions at fixed times, we see that the transition zone (roughly speaking, where c is neither close to 0 nor close to c_0) is smaller, so that the calcite deterioration is higher near the boundary of the sample, while the interior of the spatial domain is not touched by SO_2. We observe an effective calcite degradation near the boundary already at $t = 0.1$, while for $\bar{A} = 1$ the calcite density is close to its initial level, pointing out the degradation phenomenon.

The faster reaction and the faster degradation of calcite are clear also comparing the time evolution of the SO_2 concentration and calcite density at point $x = 0.25$ and $x = 0.5$ of Figure 1.3 with the one in Figure 1.5. Calcite fast decreases to zero while the SO_2 leakes slower into domain.

Finally, an intermediate case with $\bar{A} = 100$ in a larger domain $[0, \bar{x}] \times [0, T] = [0, 10] \times [0, 10]$ is considered. The space and time mesh steps are $\Delta x = 0.01$ and $\Delta x = 0.02$, respectively. Figure 1.6 represents profiles at different times for SO_2 and calcite. One can appreciate the formation of the front. We have at the boundary $c(0, t) = c_0 e^{-\lambda_2 t}$ and this gives $c(0, 5) = 0.004$ and $10^{-7} < c(0, 10) < 10^{-6}$. Indeed, after the time $t = 5$, we already observe the profile from 10 to 0 on the calcite density, obtained in the case of fast reaction.

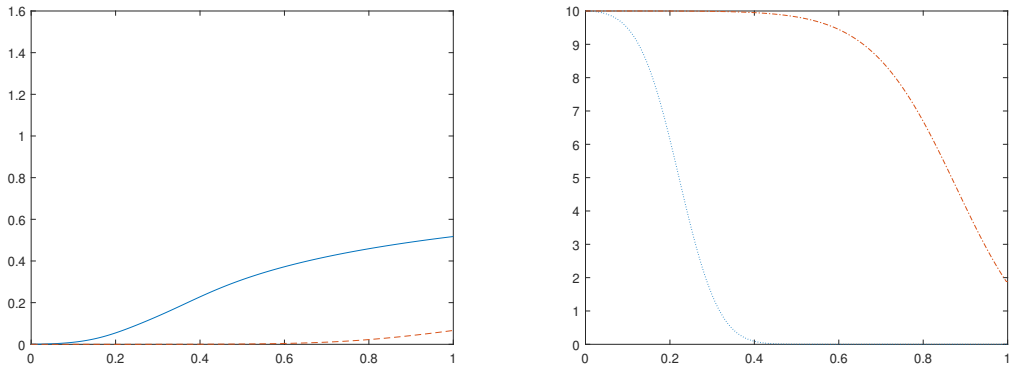

(a) (b)

Figure 1.5: Deterministic time evolution with $\bar{A} = 10000$ at the points $x = 0.25$ (solid line) and $x = 0.5$ (dashed line). x-axis : $t \in [0, 1]$. (a) SO_2 concentration ρ; (b) calcite density c.

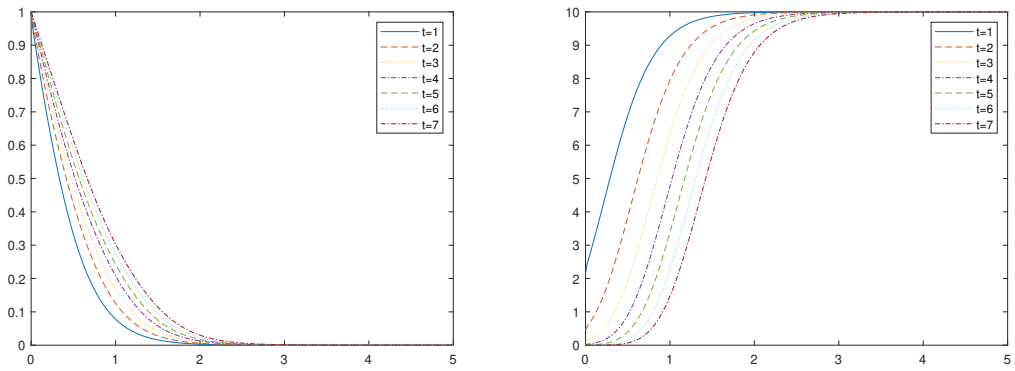

(a) (b)

Figure 1.6: Deterministic front formation with $\bar{A} = 100$. x-axis : $x \in [0, 5]$. (a) SO_2 concentration ρ; (b) calcite density c.

1.3 Introduction of a source of randomness

As previously discussed, most of the models describing the sulphation phenomenon presented in the literature are deterministic ones. The scope of this thesis is to investigate, from a numerical point of view, the dynamics of the calcite and the sulphur dioxide when a source of randomness is introduced in the settings described in Section 1.2.

Numerous factors influence the reaction, including temperature, the presence of catalysts, and, most notably, the amount of pollutants present in the air. It is precisely this latter factor that motivated a deeper investigation into its behaviour, strongly driven by the

availability of historical environmental data series. From a statistical perspective, having access to such a substantial datasets constitutes a significant advantage.

For this reason, we focus our attention on the first of the boundary conditions in (1.12), namely the boundary condition at the interface $x = 0$ for the concentration of the sulphur dioxide in the air ρ_s. As already mentioned, in [9] the authors consider it constant, even though, as far as numerics is concerned, they state that the same analysis may be carried out in the case where the constant is replaced by a bounded measurable function.

Precisely, the boundary condition describes the dynamics of the sulphur dioxide penetration from the air into the pores of calcite.

Figure 1.7 shows a historical SO_2 concentration time series; data are recorded hourly during the year 2021 at the meteorological station located in Via Pascal in Milano, Italy.

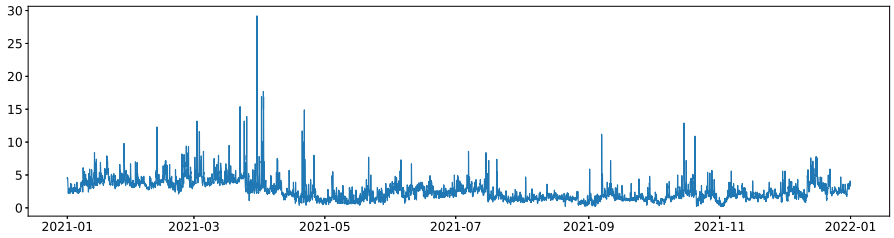

Figure 1.7: Time series of SO_2: data registered in the station of Milano-Pascal, 2021 ($\mu g/m^3$). Preprocessed data.

The shown data series has been preprocessed, in order to clean out the wrong records and to impute the missing data, since atmospheric sensors are always prone to malfunctioning, causing missing data in time series. The interested reader may refer to [6] and above all [96] for more details of the preprocessing analysis. Here we do not go into details since it goes beyond the aim of the present thesis.

What is interesting for us is that by observing the behaviour of the time series of the SO_2, it is evident that such behaviour is far from being constant. Furthermore, a clear randomness is shown. This observation inspired the idea of introducing the intrinsic randomness of the pollutant's behaviour on the surface as the boundary condition of the previously described system in (1.8).

Real data in Figure 1.7 are subject to seasonality and the presence of peaks. This means that a possible model to describe the SO_2 time series should include a deterministic trend, a noise composed by a general Levy process, an overlapping of a point process and, finally, a continuous noise. So an important step is the separation of the different signals from the data time series. This is not an easy task, as discussed in our preliminary work [6], where a preliminary study of the SO_2 time series has been performed using an estimation procedure similar to the one introduced in [54]. More studies in this direction have been done in [96, 101, 116], where the problems of the identification of the jumps

and the estimation of possible processes modelling the time series have been addressed. In particular, in [96] a pure statistical decomposition procedure has been carried out, with the final aim of isolating the possible continuous noise.

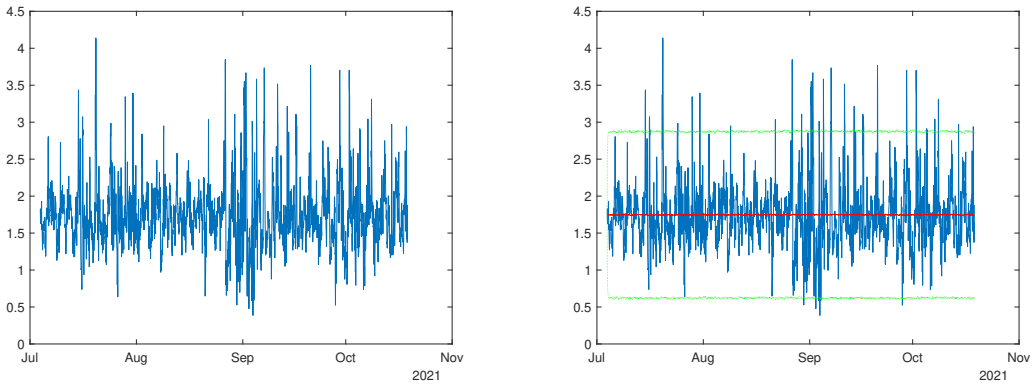

(a) (b)

Figure 1.8: (a) SO_2 filtered data in the period July-October 2021. (b) Real filtered data, the mean of the simulated realization and the interval of the usual (values mean ± 2.5 standard deviation).

Figure 1.8-(a) shows the signal obtained after the filtering process, where seasonality effects and jumps have been removed. A mean reverting behaviour with oscillations around a mean value of the concentration can be observed. Hence, a possible model one can consider as the boundary condition could be

$$d\psi_{1,t} = \eta_1(\gamma_1 - \psi_{1,t})dt + \eta_2 dW_t,$$

where $\{W_t\}_t$ is a Wiener process. However, since the process $\psi_{1,t}$ is driven by a Wiener process and thus inherits its unboundedness, from the modeling point of view, this is not reasonable. In other words a bounded noise would be more appropriate. Indeed, preprocessed real data in Figure 1.7-(b) suggest that the data series shows the presence of a bounded continuous noise: all fluctuations are confined within a limited range. The issue of considering a bounded noise, is a very important point above all in applications, [40, 48].

This is the main reason why we choose the solution of the following SDE

$$d\psi_{2,t} = \eta_1(\gamma_1 - \psi_{2,t})dt + \eta_2\sqrt{\psi_{2,t}(\gamma_2 - \psi_{2,t})}dW_t,$$

with a mean reverting drift coefficient and bounded squared diffusion coefficient which is a second-order polynomial of the state. The process $\psi_{2,t}$ is a mean reverting process with a noise characterized by a bounded diffusion coefficient. The drift is such that on average the solution is pulled to a mean level γ_1 at a rate η_1. It is also bounded between 0 and

γ_2; this is evident since, as soon as the solution encounters either $\psi_{2,t} = 0$ or $\psi_{2,t} = \gamma_2$ the randomness disappears and only the drift acts.

The process $\{\psi_{2,t}\}_t$ belongs to the class of Pearson diffusions. Such processes are often considered in financial applications; for instance, the very special case of Cox–Ingersoll–Ross process is well known; furthermore, they are often involved in the evolution of interest rates, [46] or as a model for correlation, [108]; recently, an example also in the context of the first passage time is provided, [41]. We also mention that Pearson processes have been popular in applications such as population genetics, under the name of Wright-Fisher diffusion, [57, 56, 94].

In this thesis we consider the Pearson process $\psi_{2,t}$ as a candidate for the stochastic dynamical boundary condition to be coupled with the PDE-ODE system (1.10).

In conclusion, the novelty we propose here is the description of the evolution of air pollutants, such as sulphur dioxide via a version of a Pearson process as the dynamical boundary condition of a partial differential system which is nonlinear and not strongly parabolic, describing the evolution inside the material.

Evolution problems with stochastic dynamical boundary conditions have been studied with particular attention to the case in which at the boundary the solution acts as a white noise, [14, 16, 23, 32, 42, 45]. To the best of our knowledge, there are a couple of studies closer related to our setting in [16, 32], where the solution of the PDE satisfies a SDE at the boundary. We stress that the analysed experimental data for SO_2 are not compatible with a white noise behaviour. Furthermore, since we do not use Neumann type boundary conditions which could admit a white noise type condition, a process driven by a Brownian motion seems more appropriate in the case of a Dirichlet boundary condition. From the mathematical point of view, the regularity of the noise considered here is better than the regularity of the white noise, even though it is much more irregular than the boundary conditions assumed in the existing literature,[18, 58, 59, 19]. Finally, even though the noise is not Lipschitz, it is naturally bounded, which is important from a modelling point of view.

A deeper and complete study of the proposed model is presented in Chapter 2.

Chapter 2

A stochastic boundary condition: the Pearson process

In this chapter, for sake of completeness, we carry out a complete study of the proposed model of the sulphur dioxide concentration in the air via a Pearson diffusion, based on the qualitative preliminary study of the time series discussed in Section 1.3. The observed characteristics of the data namely, the presence of random fluctuations, the bounded behaviour, and the mean-reverting properties, are captured by a Pearson-type diffusion. The boundedness arises intrinsically from the definition of the diffusion coefficient in the stochastic dynamics. Nonetheless, the Lipschitz continuity property is not satisfied.

In the following, we discuss the existence, uniqueness and we impose conditions on parameters to guarantee the boundedness of the solutions of the process. Numerical approximation via a novel approach to encompass the non-Lipschitz property of the diffusion coefficient and to preserve the boundedness is discussed [30]. Numerical simulations and an error analysis via Monte Carlo approach are provided, together with a numerical convergence of the solution's distribution to an invariant measure.

2.1 The class of Pearson processes: properties

As mention above we introduce as a stochastic dynamical boundary condition $s(t,0) = \Psi_t$, where the process $\{\Psi_t\}_{t\in[0,T]}$ is solution of the following stochastic differential equation of the Itô type

$$d\Psi_t = \alpha(\gamma - \Psi_t)dt + \sigma\sqrt{\Psi_t\,(\eta - \Psi_t)}dW_t,$$

with $\alpha, \sigma, \gamma, \eta \in \mathbb{R}_+$, and $\gamma \leq \eta$.

This is a novelty in the field of Cultural Heritage [6, 7].

Definition 2.1 ([70])**.** A Pearson diffusion is a stationary solution to a stochastic differential equation of the form

$$dX_t = -\theta(X_t - \mu)dt + \sqrt{2\theta(\tilde{a}X_t^2 + \tilde{b}X_t + \tilde{c})}dW_t \tag{2.1}$$

where $\theta > 0$, $\tilde{a}, \tilde{b}, \tilde{c}$ are such that the square root is well defined when X_t varies in the state space, and W_t is a Wiener process.

Parameters in (2.1) are referred to as a *canonical representation:* $\theta > 0$ is a scaling of time that determines how fast the diffusion moves; $\mu, \tilde{a}, \tilde{b}, \tilde{c}$ determine the state space of the diffusion as well as the shape of the invariant distribution. More precisely, μ is the mean of the invariant measure.

Remark 2.1. In the case where $\tilde{a} < 0$ and the diffusion coefficient is given by $b^2(x) = 2\theta\tilde{a}x(x-1)$, then the diffusion process is mainly known as *Jacobi* process since its related eigenfunctions are Jacobi polynomials. Particularly, we will generalize this specific case in further sections.

Returning to our case, the evidence of random fluctuation, boundedness and mean reverting effect are the three main characteristics of the studied time series. As authors declare in [104], one shall use Pearson diffusion for any stationary distribution solution of a stochastic differential equation specified by a mean reverting linear drift and a squared diffusion coefficient which is a second-order polynomial of the state. Moreover, this class of stochastic process is often used because they fit the data particularly well (see [104] and references therein for further details).

In further paragraphs, following [70, 97], we prove the existence and uniqueness results for our solution of a class of a specific Pearson process.

2.1.1 Existence, uniqueness and boundedness

Let $\bar{\Omega}_P := (\Omega_P, \mathcal{F}, \{\mathcal{F}_t\}_t, P)$ be a filtered probability space. We define $\Psi = (\Psi_t)_{t\in[0,T]}, T \in \mathbb{R}_+$, in $\bar{\Omega}_P$ to be the solution of the following autonomous stochastic differential equation, for $t \in [0, T]$

$$\begin{aligned} d\Psi_t \quad &= \alpha(\gamma - \Psi_t)dt + \sigma\sqrt{\Psi_t(\eta - \Psi_t)}\, dW_t, \\ &\qquad\qquad \Psi_0 \in (0, \eta), \end{aligned} \tag{2.2}$$

with $\alpha, \gamma, \sigma, \eta \in \mathbb{R}_+$, $\gamma < \eta$ and $W = (W_t)_{t\in[0,T]}$ is a standard Wiener process, so that the process $\Psi = \{\Psi_t\}_{t\in\mathbb{R}}$ is a diffusion.

It is easy to check that the process (2.2) is in the class of Pearson processes accordingly with definition (2.1): by a rearrangement of parameters, (2.2) is in the class of processes introduced in (2.1). Furthermore, it has a mean reverting drift, for $x \in \mathbb{R}$

$$a(x) = \alpha\,(\gamma - x)\,,$$

and a noise characterized by a bounded squared diffusion coefficient which is a second order polynomial of the state

$$b(x) = \sigma\sqrt{x(\eta - x)}. \tag{2.3}$$

In the mathematical biology, the case $\eta = 1$ is better known as *Wright-Fisher* diffusions ([94]) or *Jacobi* processes [55]. Since in our case this is not at all a natural assumption, we let $\eta \in \mathbb{R}_+$. The mean reverting drift is such that on average the solution is pulled to a mean level γ at a rate α, while fluctuations are bounded due to physical constraints and all the parameters model are strictly positive quantities.

It is well-known that the classical notion of the uniqueness of the solution of a stochastic differential equation requires the Lipschitz continuity property. It is easy to verify that the proposed model (2.2) does not verify such property in the diffusion coefficient (2.3). To provide a result on the existence and uniqueness of our SDE, we need to recover some preliminary classical results from Skorokhod and Yamada-Watanabe which will be useful within the proof of the main results on the existence and uniqueness of the solution for our process (2.2).

A classical result by Skorokhod [103] shows the existence of solutions under the condition that coefficients are only continuous in the general case for a process with jumps. In this work, we do not consider jumps in the mathematical modelling of the sulphur dioxide concentration, thus we provide the results to our case.

Theorem 2.1 ([103])**.** *Let ξ be the following process on $[t_0, T] \times \mathbb{R}^m$:*

$$\xi(t) = \xi(t_0) + \int_{t_0}^{t} a(s, \xi(s))ds + \sum_{k=1}^{l} \int_{t_0} b_k(s, \xi(s))dW_k(s) \tag{2.4}$$

Suppose the following conditions are fulfilled:

1. *$a(t,x), b_1(t,x), \ldots, b_l(t,x)$ are continuous with respect to the set of variables with $x \in \mathbb{R}^m, t \in [t_0, T]$.*
2. *There exists K such that*

$$|a(t,x)|^2 + \sum_{k=1}^{l} |b(t,x)|^2 \leq K(1 + |x|^2) \tag{2.5}$$

then the process in (2.4) has a bounded solution with probability 1.

Concerning the proof of the uniqueness of the solution of the process, we provide the following result by Yamada-Watanabe [114]: since the diffusion coefficient of the process does not satisfy the Lipschitz continuity property, the classical results from Itô's theory to prove the uniqueness of the solution cannot apply directly. In [114], authors declare that under appropriate conditions on the diffusion and drift coefficient, the pathwise uniqueness of the solution is guaranteed in one dimension.

Theorem 2.2 ([114]). *Let $(\Omega, \mathcal{F}, \{\mathcal{F}_t\}_t, P)$ a probability space. Let be $W = \{W_t\}_t$ a Wiener process adapted to the given filtration. Let us consider the following SDE*

$$dX_t = a(X_t)dt + b^2(X_t)dW_t. \tag{2.6}$$

Let us suppose that

1. *there exists a positive increasing function $\rho(u)$, $u \in (0, \infty)$ such that*

$$|b_i^2(x) - b_i^2(y)| \leq \rho(|x - y|), \quad \forall x, y \in \mathbb{R}, \quad i = 1, 2, \ldots, n$$

and

$$\int_{0^+}^{\infty} \rho^{-2}(u)du = +\infty$$

2. *there exists a positive increasing concave function $k(u)$, $u \in (0, \infty)$, such that*

$$|a_i(x) - a_i(y)| \leq k(|x - y|), \quad \forall x, y \in \mathbb{R}, \quad i = 1, 2, \ldots, n$$

and

$$\int_{0^+}^{\infty} k^{-1}(u)du = +\infty$$

then the pathwise uniqueness of the solution of (2.6) *holds, i.e. solutions are almost surely indistinguishable, given the same Brownian motion.*

An alternative result can be found in [97] by Revuz and Yor: here the pathwise uniqueness is ensured by taking a Borel function ρ from $]0, \infty[$ into itself such that $\int_{0^+}^{\infty} \frac{1}{\rho(a)}da = +\infty$.

Theorem 2.3 ([97]). *Pathwise uniqueness holds for the following SDE*

$$dX_t = a(X_t)dt + b^2(X_t)dW_t. \tag{2.7}$$

in each of the following cases:

1. $$|b^2(x) - b^2(y)|^2 \leq \rho(|x - y|), \quad |b^2| \geq \epsilon > 0 \text{ and } b \text{ is bounded};$$

2. $$|b^2(s, x) - b^2(s, y)|^2 \leq \rho(|x - y|)$$

   and b is Lipschitz continuous, i.e. for each t there exists a constant K_t such that for every $x, y \in \mathbb{R}$ and $s \leq t$

   $$|a(s, x) - a(s, y)| \leq K_t|x - y|$$

3. $$|b^2(x) - b^2(y)|^2 \leq |f(x) - f(y)|$$

   where f is increasing and bounded, $|b^2| \geq \epsilon > 0$ and a is bounded.

Remark 2.2. Pathwise uniqueness implies the uniqueness in the sense of probability law for strong solutions (see [97]).

Combining the previous results, we can establish the existence and uniqueness of a strong solution for (2.2):

Proposition 2.1. *Let $(\Omega_P, \mathcal{F}, \{\mathcal{F}_t\}_t, P)$ be a filtered probability space and let $W = \{W_t\}_t$ be an $\mathcal{F}_t$ - Wiener process. Let $\alpha, \gamma, \sigma, \eta \in \mathbb{R}_+$ and $\gamma < \eta$. Then, there exists a pathwise unique solution, and then a unique strong solution, of equation (2.2), for $x \in [0, \eta]$.*

Proof. The existence of the solution is a direct application of Skorokhod result in Theorem 2.1. In the following, let us define the drift and diffusion coefficients as:

$$\begin{aligned} a(t,x) &= a(x) &= \alpha(\gamma - x), \\ b(t,x) &= b(x) &= \sigma\sqrt{x(\eta - x)}. \end{aligned}$$

The drift coefficient $a(x)$ is continuous for all $x \in \mathbb{R}$, while the diffusion coefficient $b(x)$ is continuous for $x \in [0, \eta]$.

We need to find a constant K such that condition (2.5) of the theorem 2.1 holds:

$$\begin{aligned} |a(x)|^2 &= |\alpha\gamma - \alpha x|^2 \\ &\leq \alpha^2(|\gamma|^2 + |2\gamma x| + |x|^2) \\ &\leq k(\alpha, \gamma)\left(1 + |x|^2\right) \end{aligned}$$

For $|x| < 1$ we have:

$$\alpha^2(|\gamma|^2 + |2\gamma x| + |x|^2) \leq \alpha^2(|\gamma|^2 + |2\gamma| + 1). \tag{2.8}$$

On the other hand, for $|x| \geq 1$:

$$\alpha^2(|\gamma|^2 + |2\gamma x| + |x|^2 \leq \alpha^2(|\gamma|^2 + |2\gamma + 1||x|^2). \tag{2.9}$$

Thus, there exists a constant K such that both inequalities (2.8)-(2.9) hold.

For the diffusion coefficient $b(x)$, we proceed with the following estimate:

$$\begin{aligned} |b(x)|^2 &= |\sigma\sqrt{x(\eta - x)}|^2 \\ &= |\sigma|^2|\sqrt{x(\eta - x)}|^2 \\ &= |\sigma|^2|x(\eta - x)| \\ &\leq |\sigma|^2(|\eta x| + |x|^2) \\ &\leq K(\sigma, \eta)(1 + |x|^2) \end{aligned}$$

Thus, both coefficients $a(x)$ and $b(x)$ exhibit sub-quadratic growth, i.e., there exists a constant $k = k(\alpha, \gamma, \sigma, \eta)$ such that

$$|a(x)|^2 + |b(x)|^2 \leq k(1 + |x|^2)$$

Indeed, the existence of a bounded solution to the stochastic differential equation (2.2) on $[0, \eta]$ with probability one is provided.

To address the uniqueness of the solution, we apply Theorem (2.2) and its corollary from [114]. According to these results, the existence of a unique strong solution requires proving the Lipschitz continuity of the drift coefficient and the Hölder continuity of the diffusion coefficient. More specifically,

$$|b(x) - b(y)| \leq \sigma\sqrt{|\eta x - x^2 - \eta y + y^2|} \leq \sigma\sqrt{|x - y|}\sqrt{|\eta - x - y|} \leq \beta \cdot |x - y|^{1/2},$$

with $\beta = \sigma\eta$. Hence, the diffusion coefficient $b(x)$ is Hölder continuous with index $1/2$. This ensures the well-posedness of the stochastic differential equation and the proof is completed. □

Remark 2.3. The hypothesis $x \in [0, \eta]$ is not restrictive, since by employing specific constraints on the parameters of equation (2.2), one can prove that $x = 0$ and $x = \eta$ are *entrance boundaries* and the solution $\Psi_t \in (0, \eta)$ for $t \in (0, T]$, whenever $\Psi_0 \in [0, \eta]$. More details on the classical boundary classification are provided in Section 2.1.3.

2.1.2 Scaled function and speed measure

It is well-known that diffusion processes and second-order parabolic equations are strongly connected. More specifically, when the fundamental solution to the parabolic equation is given, it provides the transition density of the diffusion process, enabling the computation of nearly any quantity of interest. However, in most cases, finding an explicit form for the transition density is not feasible. Despite this, a notable advantage of one-dimensional diffusions is that many quantities can be determined explicitly. This is possible because mostly all one-dimensional diffusions can be transformed into Brownian motion (except at certain singular points, which under our conditions will only occur at the endpoints of the interval where the diffusion takes place). This transformation is achieved by first altering the space variable using the scale function, followed by a time change via the speed measure.

Following [97], let us recall the definition of the infinitesimal generator for the diffusion $\Psi = \{\Psi_t\}_{t\in[0,T]}$ for $f \in C_b((0, \eta])$:

$$\mathcal{A}f(x) = a(x)f'(x) + \frac{1}{2}b^2(x)f''(x).$$

and two basic characteristics: the *scale function* and the *speed measure*.

Definition 2.2 (Scale function)**.** Given a diffusion X_t on $(0, \eta)$ with drift a and variance $b^2 > 0$ and given arbitrary $x_0, x_1 \in (0, \eta)$, the *scale function* is defined by

$$S(x) = \int_{x_0}^{x} \exp\left(- \int_{x_1}^{y} \frac{2a(z)}{b^2(z)} \right) dz \tag{2.10}$$

Moreover, if $S(x)$ can be taken to be linear, then the diffusion is in *natural scale*.

Definition 2.3 (Speed measure)**.** The *speed measure* for a process X_t is given by

$$M(x) = \int_{x_0}^{x} m(\xi) d\xi$$

with $x_0 \in (0, \eta)$. The function

$$m(\xi) = \frac{1}{b^2(\xi) S'(\xi)} \tag{2.11}$$

is called the speed density of the process X_t.

Remark 2.4 (Martingale property). Authors in [97] show in Proposition 3.5 that, up to an affine transformation, there exists at most a Borel function f such that $f(X_t)$ is a martingale. Indeed, the scale function is such that $\mathcal{A}s(x) = 0$, so that $Y_t = S(X_t)$ is a local martingale:

$$dY_t = dS(X_t) = s(X_t) b(X_t) dW_t = \tilde{b}(Y_t) dW_t,$$

where $\tilde{b}(\cdot) = s(S^{-1}(\cdot)) b(S^{-1}(\cdot))$.

Furthermore, the Markov transition kernel associated to the process X is absolutely continuous with respect to the speed measure, i.e.

$$P(t, x, dy) = P(X_t \in dy | X_0 = x) = \int p(t, x, y) M(dx) = \int p(t, x, y) m(x) dx.$$

The relation between the scale function, the speed measure and the infinitesimal generator is given by Theorem 3.12 in [97] and for a bounded function f can be summarized by:

$$\mathcal{A} f = \frac{1}{2} \frac{d}{dM} \frac{d}{dS} f, \tag{2.12}$$

which is also known as the *canonical representation of the differential infinitesimal operator* associated to the diffusion process (see [70]).

Furthermore, let us denote by $T_x = \inf\{t \geq 0 : X_t = x\}$ the first passage time that X reaches $x \in (0, \eta)$ (see [97, 98]). Then, the probability that the process X reaches u_2 before u_1, for $0 < u_1 < x < u_2 < \eta$, is defined as:

$$u(x) = \mathbb{P}\{T_{u_2} < T_{u_1} | X(0) = x\}.$$

Together with boundary conditions $u(u_1) = 0$, $u(u_2) = 1$, the differential equation (2.12) becomes:

$$\frac{1}{2}\frac{d}{dM}\left[\frac{du(x)}{dS}\right] = 0, \qquad \text{for } u_1 < x < u_2.$$

Finally, the solution comes naturally from two successive integrations and it is expressed in terms only of the scale function:

$$u(x) = \frac{S(x) - S(u_1)}{S(u_2) - S(u_1)}, \quad \text{for } u_1 < x < u_2$$

In conclusion, the scale function allows for a rescaling of the state space in terms of the probabilities of reaching different levels. Conversely, the speed density represents the rate at which the process's internal clock advances when the system is positioned at a given point.

More precisely, this means that there is a not trivial bridge between scale function, speed measure and the infinitesimal transition of the process, in particular via the passage times. Therefore, the study of the boundary points becomes crucial.

2.1.3 Feller boundary classification

Authors in [70] provide a modern classification of the boundary points based on the values of functionals involving the scale function and speed measures assumed at the boundary. In this work, we focus our attention on the *entrance boundary*, the class of points that either are never reached by the process if the initial point X_0 lies in their interior, or immediately push the process into the domain if X_0 is a boundary point. Such a definition can be given in terms of the scale and speed measures: a boundary point is of type *entrance* if the transition towards it (infinitesimal close) is possible, but it never reaches it ([97, 98]). Formally:

Definition 2.4 (Entrance boundary)**.** Let $x \in [l, r] \subseteq (0, \eta)$. The right boundary r is an *entrance boundary* if

$$S(l, x] = \lim_{a \to l} \int_a^x s(v)dv = \infty, \qquad M(l, x] = \lim_{a \to l} \int_a^x m(v)dv < \infty \tag{2.13}$$

The left boundary l is an *entrance boundary* if

$$S[x, r) = \lim_{a \to r} \int_x^a s(v)dv = \infty, \qquad M[x, r) = \lim_{a \to r} \int_x^a m(v)dv < \infty \tag{2.14}$$

In the following, we apply the previously introduced definitions of the scale function and speed measure. Precisely, we impose conditions (2.14)-(2.13) on the parameters of the process (2.2) to determine whether $l = 0$ and $r = \eta$ are entrance boundaries.

More precisely, conditions (2.14)-(2.13) for $x = 0$ and $x = \eta$ being, respectively, entrance boundary are expressed in terms of integrability conditions for $s(x)$ and $m(x)$ close to the boundary.

Proposition 2.2. *Given the process* (2.2)*, then the scale function is defined as*

$$s(x) = \frac{x_0^p(\eta - x_0)^q}{x^p(\eta - x)^q},$$

while the speed density admits the following expression

$$m(x) = \frac{x^{p-1}(\eta - x)^{q-1}}{\sigma^2 x_0^p(\eta - x_0)^q},$$

with

$$p = \frac{2\alpha\gamma}{\eta\sigma^2}, \quad q = \frac{2\alpha(\eta - \gamma)}{\eta\sigma^2} \tag{2.15}$$

Proof. The proof involves just a little algebra. We start by finding the primitive function $s(x)$ of the scale function defined in (2.10): for $x_0 \in [0, \eta]$

$$s(x) = S'(x) = \exp\left(-\int_{x_0}^x \frac{2a(\xi)}{b^2(\xi)}d\xi\right).$$

Then, by taking the logarithmic we get:

$$-\log s(x) = -\log\left(\exp\left\{-\int_{x_0}^x \frac{2a(\xi)}{b^2(\xi)}d\xi\right\}\right) = \int_{x_0}^x \frac{2a(\xi)}{b^2(\xi)}d\xi = \int_{x_0}^x \frac{2\alpha(\gamma - \xi)}{\sigma^2(\eta - \xi)}d\xi.$$

We look for the primitive of the integrand function

$$\frac{2\alpha(\gamma - \xi)}{\sigma^2\xi(\eta - \xi)} = \frac{A}{\sigma^2\xi} + \frac{B}{\eta - \xi} = \frac{A(\eta - \xi) + \sigma^2 B\xi}{\sigma^2\xi(\eta - \xi)}$$

and we found the coefficient A, B:

$$\begin{cases} 2\alpha\gamma &= A\eta \\ -2\alpha &= -A + \sigma^2 B\,. \end{cases} \quad \rightsquigarrow \quad \begin{cases} A &= \frac{2\alpha\gamma}{\eta} \\ B &= \frac{2\alpha(\gamma-\eta)}{\sigma^2\eta} \end{cases}$$

Going back to the integral we obtain:

$$\begin{aligned} \int_{x_0}^x \frac{2\alpha\gamma - 2\alpha\xi}{\sigma^2\xi(\eta - \xi)}d\xi &= \int_{x_0}^x \frac{2\alpha\gamma}{\sigma^2\eta\xi}d\xi + \int_{x_0}^x -\frac{2\alpha(\eta - \gamma)}{\sigma^2\eta(\eta - \xi)}d\xi \\ &= \frac{2\alpha\gamma}{\sigma^2\eta}\log\xi\Big|_{x_0}^x + \frac{2\alpha(\eta - \gamma)}{\sigma^2\eta}\log(\eta - \xi)\Big|_{x_0}^x \\ &= \log x^p + \log(\eta - x)^q - \log(x_0)^p - \log(\eta - x_0)^q \\ &= \log\frac{x^p(\eta - x)^q}{x_0^p(\eta - x_0)^q} \end{aligned}$$

where p, q are defined in (2.15). In conclusion, an explicit formula for the scale function is derived:

$$-\log s(x) = \log \frac{x^p(\eta - x)^q}{x_0^p(\eta - x_0)^q}$$
$$s(x) = \frac{x_0^p(\eta - x_0)^q}{x^p(\eta - x)^q}.$$

On the other hand, the speed density is defined by (2.11):

$$m(x) = \frac{1}{b^2(x)s(x)} = \frac{x^p(\eta - x)^q}{\sigma^2 x(x - \eta)(x_0^p(\eta - x_0)^q)} = \frac{x^{p-1}(\eta - x)^{q-1}}{\sigma^2(x_0^p(\eta - x_0)^q)}.$$

□

The following proposition gives the conditions to ensure that $\{0, \eta\}$ are entrance boundary points for our process (2.2):

Proposition 2.3. *Let $\Psi = \{\Psi_t\}_{t\in[0,T]}$ be the solution of the Pearson diffusion (2.2) and p, q defined in (2.15). Then, if the following condition on the parameter holds*

$$\nu = p \wedge q > 1 \tag{2.16}$$

then $\{0, \eta\}$ are respectively left and right entrance boundary. Hence, if $x_0 \in [0, \eta]$, then the trajectories of Ψ stay in $(0, \eta)$ with probability one.

Furthermore, the following bound holds, for any $T \in \mathbb{R}_+$ and any $r < \nu$:

$$\left(\sup_{t\in[0,T]} \mathbb{E}\left[\Psi_t^{-r}\right] \vee \sup_{t\in[0,T]} \mathbb{E}\left[(\eta - \Psi_t)^{-r}\right] \right) \leq C_{T,r}.$$

Proof. We need to ensure that the definition 2.13 of entrance boundary is verified for both left and right boundaries. Let us start with 0 as left boundary:

$$S(0, x] = \int_0^x s(\xi)d\xi = +\infty \iff \int_0^x \frac{1}{\xi^p(\eta - \xi)^q} = +\infty \iff p \geq 1$$
$$M(0, x] = \int_0^x m(\xi)d\xi < +\infty \iff \int_0^x \xi^{p-1}(\eta - \xi)^{q-1} < +\infty \iff p - 1 \geq 0$$

Similarly, for the right boundary η

$$S[x, \eta) = \int_x^\eta s(\xi)d\xi = +\infty \iff \int_x^\eta \frac{1}{\xi^p(\eta - \xi)^q} = +\infty \iff q \geq 1$$
$$M[x, \eta) = \int_x^\eta m(\xi)d\xi < +\infty \iff \int_x^\eta \xi^{p-1}(\eta - \xi)^{q-1}d\xi < +\infty \iff q - 1 \geq 0$$

It is easy to check that conditions in (2.16) are obtained by imposing $p \geq 1$ and $q \geq 1$. To conclude, we note that while we have set $x_0 = 0$, the definition remains valid for any general $x_0 \in [0, \eta]$. For the bound on inverse moments, see [104]. □

Remark 2.5. From (2.16), in particular $q > 1$, then $\eta - \gamma \geq 0$; hence, naturally the mean-reverting level lies in the interval $(0, \eta)$.

2.1.4 The invariant measure

For completeness, we would like to briefly discuss the role of speed and scale functions in the definition of the invariant measure for equation (2.2). Indeed, if it exists, its density has the form

$$\Phi(x) = c_1 \frac{S(x)}{s(x)b^2(x)} + c_2 \frac{1}{s(x)b^2(x)} = c_1 S(x) + c_2 m(x),$$

with c_1 and c_2 such that p is positive and it is the density of a probability measure (see [66] for a detailed derivation).

In our specific case, we get that the invariant density is given by

$$\Phi(x) = \frac{1}{\eta^{p+q-2}} \frac{\Gamma(p+q)}{\Gamma(p)\Gamma(q)} x^{p-1}(\eta - x)^{q-1}, \tag{2.17}$$

which is a $Beta(p, q)$ probability density with support in $[0, \eta]$, where parameters p and q are defined in (2.15).

2.2 Numerical approximation of a Pearson process

The numerical approximation of the process (2.2) is a crucial point in our work: since the diffusion coefficient does not satisfy the Lipschitz property, finding an analytical solution to the SDE is not feasible. Thus, providing a good numerical approximation for the process becomes crucial. Specifically, we have already proved that there exists a bounded solution with probability one. Therefore the numerical scheme must preserve this property.

The most natural choice when dealing with numerical approximation of a stochastic differential equation is the well-known Eulero-Maruyama scheme (see [72]): the scheme has the advantage of being very simple and easy to implement but it is unable to preserve the boundary for (2.2). The algorithm should be modified to control step by step what happens when the realization of the process reaches the boundary: either one could *kill* the realization whenever it reaches the boundaries or impose some a priori conditions to force the boundary to be whether absorption or reflecting types. This could introduce bias within the numerical solution. Moreover, the problem of the non-Lipschitz property would still be unresolved.

In literature, especially in finance and biology contexts, various numerical schemes are studied to avoid these issues. Different versions of the Eulero-Maruyama scheme, involving implicit scheme [47, 43], semi-implicit [89] as well as tamed Eulero-Maruyama [118] are proposed for specific problems with non-Lipschitz property on the diffusion coefficient. Here it is proven that the positivity of the solution is preserved.

More recently, regarding the class of Wright-Fisher processes, in [63] authors generalize a numerical semi-discrete scheme and they prove a strong convergence result. Authors in

[71] build a numerical scheme based on the backward Euler combined with the Lamperti transform. The same idea was adopted in [64] and [30] but, whereas the first authors show convergence up to $\frac{1}{2}$, in the latter strong convergence is proven to be up to 1. In this work, we adopt the latter work by generalizing their result for the class of Wright-Fisher processes living in $[0, \eta]$.

To better explain the numerical algorithm involved, we introduce the Lamperti transform.

2.2.1 The Lamperti transform

The Lamperti transform is motivated by a straightforward idea: by applying a simple transformation f to the process and exploiting Itô's lemma, one could get new stochastic dynamics with constant diffusion. This is particularly useful to bypass some issues typically connected to state-dependent diffusion coefficients. On the other hand, one should verify some conditions on the diffusion component of the stochastic process in order to apply such transformation (see [85], [112]). A typical way to transform the process to get a constant diffusion σ is to perform a time-change for the Brownian motion [26].

We start by recalling Itô's lemma:

Lemma 2.1 (Itô formula, [93])**.** *Let X_t be an Itô process with dynamics*

$$dX_t = a(t, X_t)dt + b(t, X_t)dW_t$$

and let $F = F(t, X_t) \in C^2(\mathbb{R} \times [0, +\infty[)$, then it holds that

$$Z(t) = F(t, X_t)$$

is again an Itô process with dynamics:

$$dZ_t = \frac{\partial F(t, X_t)}{\partial t}dt + \frac{\partial F(t, X_t)}{\partial X}dX_t + \frac{1}{2}\frac{\partial^2 F(t, X_t)}{\partial X^2}(dX_t)^2 \tag{2.18}$$

where $(dX_t)^2$ is computed by stating that

$$(dt)^2 = dW_t dt = 0, \quad (DW_t)^2 = dt$$

Proof. See [93]. □

Following [85], we introduce the main result for the Lamperti transform.

Theorem 2.4 (Lamperti transform)**.** *Let X_t be an Itô process with dynamics as in Lemma* (2.1) *containing a diffusion term that is continuously differentiable and strictly positive or strictly negative on the domain of the process. Define*

$$F(t, X_t) := \int \frac{1}{b(t, x)}dx\bigg|_{x=X_t}, \quad F(0, X_0) = 0$$

If F is a one-to-one mapping from the state space of X_t to $\mathbb{R}$ for $t \in [0, +\infty[$, let $Z_t = F(t, X_t)$. In the other case, define

$$Z_t := F(t, X_t) := \int_{\xi}^{x} \frac{1}{b(t,u)} du \Big|_{x=X_t}$$

where ξ is an arbitrary point inside the state-space of X_t such that b does not change sign in the resulting integration interval.
Then Z_t is a one-to-one mapping from the state-space of X_t to $\mathbb{R}$ for $t \in [0, +\infty[$ and it has the following dynamics with unit diffusion:

$$dZ_t = \left(\frac{\partial F(F^{-1}(t, Z_t), t)}{\partial t} + \frac{a(F^{-1}(t, Z_t), t)}{b(F^{-1}(t, Z_t), t)} - \frac{1}{2} \frac{\partial b(F^{-1}(t, Z_t), t)}{\partial X} \right) dt + dW_t$$

Proof. Let us start by rewriting 2.18:

$$\begin{aligned} dZ_t &= \frac{\partial F(t, X_t)}{\partial t} dt + \frac{\partial F(t, X_t)}{\partial X} dX_t + \frac{1}{2} \frac{\partial^2 F(t, X_t)}{\partial X^2} (dX_t)^2 \\ &= \frac{\partial F(t, X_t)}{\partial t} dt + \frac{\partial F(t, X_t)}{\partial X} (a(t, X_t)dt + b(t, X_t)dW_t) + \frac{1}{2} \frac{\partial^2 F(t, X_t)}{\partial X^2} b^2(t, X_t)dt \\ &= \left(\frac{\partial F(t, X_t)}{\partial t} + \frac{\partial F(t, X_t)}{\partial X} a(t, X_t) + \frac{1}{2} \frac{\partial^2 F(t, X_t)}{\partial X^2} b^2(t, X_t) \right) dt \\ &\quad + \frac{\partial F(t, X_t)}{\partial X} b(t, X_t) dW_t \end{aligned}$$

Then, the unit diffusion could be obtained by choosing:

$$Z_t := F(t, X_t) := \int_{\xi}^{x} \frac{1}{b(u,t)} du \Big|_{x=X_t}.$$

Following Leibniz's integration theorem we obtain:

$$\frac{\partial F(t, X_t)}{\partial X} = \frac{1}{b(t, X_t)}.$$

Furthermore,

$$\frac{\partial F(t, X_t)}{\partial t} = \frac{\partial}{\partial t} \int_{\xi}^{x} \frac{1}{b(t,u)} du \Big|_{x=X_t}, \quad \frac{\partial^2 F(t, X_t)}{\partial X^2} = -\frac{\frac{\partial b(t, X_t)}{\partial X}}{b^2(t, X_t)}.$$

Now, combining this with the anti-transform $X_t = F^{-1}(t, Z_t)$ we get:

$$\begin{aligned} dZ_t &= \left(\frac{\partial}{\partial t} \int_{\xi}^{x} \frac{1}{b(t,u)} du \Big|_{x=X_t} + \frac{a(t, X_t)}{b(t, X_t)} - \frac{1}{2} \frac{\partial b(t, X_t)}{\partial X} \right) dt + dW_t \\ &= \left(\frac{\partial F(F^{-1}(t, Z_t), t)}{\partial t} + \frac{a(F^{-1}(t, Z_t), t)}{b(F^{-1}(t, Z_t), t)} - \frac{1}{2} \frac{\partial b(F^{-1}(t, Z_t), t)}{\partial X} \right) dt + dW_t \end{aligned} \tag{2.19}$$

Thus the claim is provided. □

In other words, the Lamperti transform is a transformation of the process to get a constant diffusion by performing a time-change for the Brownian motion.

Let us apply this result to our stochastic dynamics (2.2). To get a constant diffusion coefficient σ, the most natural choice is the following:

$$y = F(z) = \sigma \int^z \frac{du}{b(u)} = \int^z \frac{du}{\sqrt{u(\eta - u)}} = 2 \arcsin\left(\sqrt{\frac{z}{\eta}}\right).$$

Thus, by applying the Lamperti transform to (2.2), we obtain a new process Y with constant diffusion σ by considering the following transformation:

$$Y = F(\Psi) = 2 \arcsin\left(\sqrt{\frac{\Psi}{\eta}}\right), \tag{2.20}$$

which is well-defined. In fact, from Proposition 2.3 we know that $\Psi \in (0, \eta)$ with probability one, so that the anti-transform is well defined and we can recover our original process:

$$\Psi = F^{-1}(Y) = \eta \sin^2\left(\frac{Y}{2}\right). \tag{2.21}$$

Proposition 2.4. *Let $\Psi \in (0, \eta)$ be the unique pathwise solution of the SDE (2.2), such that condition (2.16) is fulfilled. For $t \in [0, T], T \in \mathbb{R}_+$, the process $Y_t = F(\Psi_t) \in [0, \pi]$, with F given by (2.20) is solution of the following SDE*

$$dY_t = \left[a_1 \cot\left(\frac{Y_t}{2}\right) - a_2 \tan\left(\frac{Y_t}{2}\right)\right] dt + \sigma dW_t. \tag{2.22}$$

with a_1, a_2 are positive constants given by

$$a_1 = \frac{4\alpha\gamma - \sigma^2\eta}{4\eta}, \qquad a_2 = \frac{4\alpha(\eta - \gamma) - \sigma^2\eta}{4\eta}. \tag{2.23}$$

Furthermore, there is a unique point

$$y^* = 2 \arctan\left(\sqrt{\frac{4\alpha\gamma - \sigma^2\eta}{4\alpha(\eta - \gamma) - \sigma^2\eta}}\right) \tag{2.24}$$

such that the non Lipschitz drift

$$f(y) = a_1 \cot\left(\frac{y}{2}\right) - a_2 \tan\left(\frac{y}{2}\right), \tag{2.25}$$

is such that $f(y^*) = 0$.

Proof. Let us start by remark that the process Ψ and, thus, the transform (2.20) depend only on the state. Hence, we can rewrite the dynamics in (2.19) as follows:

$$\begin{aligned} dY_t &= \left(F'(F^{-1}(Y_t))a(F^{-1}(Y_t)) + \frac{1}{2}F''(F^{-1}(Y_t))b^2(F^{-1}(Y_t)) \right) dt + F'(F^{-1}(Y_t))dW_t \\ &= \left(\sigma \frac{a(F^{-1}(Y_t))}{b(F^{-1}(Y_t))} - \frac{\sigma^2}{4} \frac{\eta - 2F^{-1}(Y_t))}{\sqrt{\Psi(\eta - \Psi)}} \right) dt + \sigma dW_t, \end{aligned}$$

where the drift and the diffusion coefficient are obtained by applying Itô's formula. Thus, the new drift $\tilde{a}$ becomes, for any t and $Y_t \in (0, \pi)$

$$\begin{aligned} \tilde{a}\left(Y_t\right) &= \sigma \frac{a(F^{-1}(Y_t))}{b(F^{-1}(Y_t))} - \frac{\sigma^2}{2} \frac{\partial b(F^{-1}(Y_t))}{\partial Y} \\ &= \frac{\alpha(\gamma - (F^{-1}(Y)))}{\sqrt{F^{-1}(Y)(\eta - (F^{-1}(Y)))}} - \frac{\sigma^2}{4} \frac{\eta - 2(F^{-1}(Y))}{\sqrt{F^{-1}(Y)(\eta - (F^{-1}(Y)))}} \\ &= \frac{\alpha(\gamma - \eta \sin^2\left(\frac{Y}{2}\right))}{\sqrt{\eta \sin^2\left(\frac{Y}{2}\right)\left(\eta - \eta \sin^2\left(\frac{Y}{2}\right)\right)}} - \frac{\sigma^2}{4} \frac{\eta - 2\eta \sin^2\left(\frac{Y}{2}\right)}{\sqrt{\eta \sin^2\left(\frac{Y}{2}\right)\left(\eta - \eta \sin^2\left(\frac{Y}{2}\right)\right)}} \\ &= \frac{\alpha\left(\gamma - \eta \sin^2\left(\frac{Y}{2}\right)\right)}{\sqrt{\eta^2 \sin^2\left(\frac{Y}{2}\right)\left(1 - \sin^2\left(\frac{Y}{2}\right)\right)}} - \frac{\sigma^2}{4} \frac{\eta\left(1 - 2\sin^2\left(\frac{Y}{2}\right)\right)}{\sqrt{\eta^2 \sin^2\left(\frac{Y}{2}\right)\left(1 - \sin^2\left(\frac{Y}{2}\right)\right)}} \\ &= \frac{\alpha\gamma}{\eta \sin\left(\frac{Y}{2}\right)\cos\left(\frac{Y}{2}\right)} - \frac{\alpha\eta \sin^2\left(\frac{Y}{2}\right)}{\eta \sin\left(\frac{Y}{2}\right)\cos\left(\frac{Y}{2}\right)} - \frac{\sigma^2 \cos Y}{4 \sin\left(\frac{Y}{2}\right)\cos\left(\frac{Y}{2}\right)} \\ &= \frac{\alpha\gamma\left(\sin^2\left(\frac{Y}{2}\right) + \cos^2\left(\frac{Y}{2}\right)\right)}{\eta \sin\left(\frac{Y}{2}\right)\cos\left(\frac{Y}{2}\right)} - \frac{\alpha \sin\left(\frac{Y}{2}\right)}{\cos\left(\frac{Y}{2}\right)} - \frac{\sigma^2 \cos Y}{2 \sin Y} \\ &= \frac{\alpha\gamma \cos^2\left(\frac{Y}{2}\right)}{\eta \sin\left(\frac{Y}{2}\right)\cos\left(\frac{Y}{2}\right)} + \frac{\alpha\gamma \sin^2\left(\frac{Y}{2}\right)}{\eta \sin\left(\frac{Y}{2}\right)\cos\left(\frac{Y}{2}\right)} - \alpha \tan\left(\frac{Y}{2}\right) - \frac{\sigma^2}{2}\cot Y \\ &= \frac{\alpha\gamma}{\eta}\cot\left(\frac{Y}{2}\right) + \frac{\alpha\gamma}{\eta}\tan\left(\frac{Y}{2}\right) - \alpha\tan\left(\frac{Y}{2}\right) - \frac{\sigma^2}{4}\left(\cot\left(\frac{Y}{2}\right) - \frac{1}{\cot\left(\frac{Y}{2}\right)}\right) \\ &= \cot\left(\frac{Y}{2}\right)\left[\frac{\alpha\gamma}{\eta} - \frac{\sigma^2}{4}\right] - \tan\left(\frac{Y}{2}\right)\left[\alpha - \frac{\alpha\gamma}{\eta} - \frac{\sigma^2}{4}\right] \\ &= \cot\left(\frac{Y}{2}\right)\left[\frac{4\alpha\gamma - \sigma^2\eta}{4\eta}\right] - \tan\left(\frac{Y}{2}\right)\left[\frac{4\alpha\eta - 4\alpha\gamma - \sigma^2\eta}{4\eta}\right] \\ &= a_1 \cot\left(\frac{Y}{2}\right) - a_2 \tan\left(\frac{Y}{2}\right) \end{aligned}$$

Where $a_1 = \frac{4\alpha\gamma - \sigma^2\eta}{4\eta}$, $a_2 = \frac{4\alpha\eta - 4\alpha\gamma - \sigma^2\eta}{4\eta}$ are exactly the coefficient in (2.23).

Following [30], we show the existence of a fixed point y^* such that $f(y^*) = 0$:

$$\begin{aligned}
0 &= \cot\left(\frac{y}{2}\right)\left(\frac{4\alpha\gamma - \sigma^2\eta}{4\eta}\right) - \tan\left(\frac{y}{2}\right)\left(\frac{4\alpha\eta - 4\alpha\gamma - \sigma^2\eta}{4\eta}\right) \\
&= \frac{1}{\tan\left(\frac{y}{2}\right)}\left(\frac{4\alpha\gamma - \sigma^2\eta}{4\eta}\right) - \tan\left(\frac{y}{2}\right)\left(\frac{4\alpha\eta - 4\alpha\gamma - \sigma^2\eta}{4\eta}\right) \\
&= \left(\frac{4\alpha\gamma - \sigma^2\eta}{4\eta}\right) - \tan^2\left(\frac{y}{2}\right)\left(\frac{4\alpha\eta - 4\alpha\gamma - \sigma^2\eta}{4\eta}\right)
\end{aligned}$$

Then

$$\tan^2\left(\frac{y}{2}\right) = \frac{4\alpha\gamma - \sigma^2\eta}{4\alpha\eta - 4\alpha\gamma - \sigma^2\eta},$$

and the fixed point in (2.24) is reached. □

Proposition 2.5. *The drift* (2.25) *shows a superlinear growth in* $[0, \pi]$ *and for any* $y \in [0, \pi]$

$$f'(y) \leq -C_0, \tag{2.26}$$

where $C_0 = (2\alpha - \sigma^2)/4 > 0$.

Proof. The inequality (2.26) is simply obtained by the derivation of (2.25):

$$\begin{aligned}
f'(y) &= \left[\left(\frac{4\alpha\gamma - \sigma^2\eta}{4\eta}\right)\cot\left(\frac{y}{2}\right) - \left(\frac{4\alpha\eta - 4\alpha\gamma - \sigma^2\eta}{4\eta}\right)\tan\left(\frac{y}{2}\right)\right]' \\
&= -\frac{1}{2}\left(\frac{4\alpha\gamma - \sigma^2\eta}{4\eta}\right)\frac{1}{\sin^2\left(\frac{y}{2}\right)} - \frac{1}{2}\left(\frac{4\alpha\eta - 4\alpha\gamma - \sigma^2\eta}{4\eta}\right)\tan\left(\frac{y}{2}\right)\frac{1}{\cos^2\left(\frac{y}{2}\right)} \\
&\leq -\frac{1}{2}\left(\frac{4\alpha\gamma - \sigma^2\eta + 4\alpha\eta - 4\alpha\gamma - \sigma^2\eta}{4\eta}\right) \\
&= -\frac{1}{4}\left(2\alpha - \sigma^2\right)
\end{aligned}$$

Denoting $C_0 = \frac{2\alpha - \sigma^2}{4}$, the condition $C_0 > 0$ derives from the fact that by (2.16) one has that $\alpha > \sigma^2$. □

In conclusion, the Lamperti transform is useful to overcome the issue to a deal with a SDE (2.2) with a non-Lipschitz diffusion coefficient. In particular, this would lead to problems in the numerical approximation of the equation, since the typical numerical schemes are not able to preserve the boundaries. Thus the monotonicity in (2.26) could not be preserved and stability problems would arise.

2.2.2 Smooth slope truncation

We are interested in the numerical approximation of the stochastic diffusion (2.2) whose solution stays in the domain $(0, \eta)$. Our goal is to construct an explicit numerical scheme that preserves that structure. It is well-known that the Eulero-Maruyama scheme does not preserve the boundary of the domain, since, in the approximation close to the boundary, the Wiener increment at the next time step could be large enough to force the solution out of the interval $(0, \eta)$ [72, 44].

Boundedness of the numerical solution can be maintained by absorption or reflection at boundary [80], but this introduces bias into the numerical solution. Hence, to overcome such a problem, we apply the Lamperti transform (2.22), to overcome the problem of the boundary. We discretize the new dynamics and by the anti-transform (2.21), we recover the original stochastic process ([30]).

Concerning the numerical scheme for the additive model (2.22), let us start by noticing that the drift function (2.25) is only one-side Lipschitz, periodic decreasing in $[0, \pi]$ as shown by Proposition 2.5; hence, it is necessary a regularization approach in order both to preserve the monotonicity and avoid the production of divergence solutions by the Eulero-Maruyama scheme [67, 31]. The drift's properties suggest a way to truncate the drift and overcome the problem of monotonicity.

Smooth truncation is involved to overcome the difficulty caused by the non-Lipschitz and super-growing drift coefficient (see, for instance, [67]), while the sloping truncation allows the method to maintain the monotonicity of the drift [31, 30]. Monotonicity is also important for the stability of the distribution.

Therefore, the proposed algorithm combines the *Lamperti transform* so that a new process with constant diffusion is derived and the *smooth truncation* for the approximation of the new drift coefficient; the idea is to smooth the drift close to the boundary via a first-order Taylor expansion and regularized outside $(0, \pi)$, by ensuring that the monotonicity the approximated drift [30]. Finally, the initial process is recovered by the anti-transform.

More precisely, let $y^* \in (0, \pi)$ be the fixed point defined in (2.24) and let $k > 0$ a fixed constant and define

$$\Delta^* = (y^* \wedge (\pi - y^*) \wedge 1)^{\frac{1}{k}}. \tag{2.27}$$

For every $\Delta < \Delta^*$, let us define the following partition of $\mathbb{R}$

$$P = \{P_1, P_2, P_3, P_4, P_5\} = \{(-\infty, 0), [0, \Delta^k), [\Delta^k, \pi - \Delta^k], (\pi - \Delta^k, \pi], (\pi, \infty)\},$$

and let f_Δ be the new truncated drift function for the SDE (2.22):

$$f_\Delta(y) := \begin{cases} f(\pi-\Delta^k) + \frac{1}{2}\Delta^k f'(\pi-\Delta^k) - C_0(y-\pi+\frac{1}{2}\Delta^k), & y \in P_5; \\ f(\pi-\Delta^k) + f'(\pi-\Delta^k)(y-\pi+\Delta^k) & \\ \qquad -\frac{1}{2\Delta^k}(f'(\pi-\Delta^k)+C_0)(y-\pi+\Delta^k)^2, & y \in P_4; \\ f(x), & x \in P_3; \\ f(\Delta^k) + f'(\Delta^k)(x-\Delta^k) + \frac{1}{2\Delta^k}(f'(\Delta^k)+C_0)(y-\Delta^k)^2, & y \in P_2; \\ f(\Delta^k) - \frac{1}{2}\Delta^k f'(\Delta^k) - C_0(y-\frac{1}{2}\Delta^k), & y \in P_1. \end{cases}$$

Figure 2.1 shows the effect of the smoothing truncation on the drift f given by (2.25) for a specific set of parameters and different diffusion coefficients.

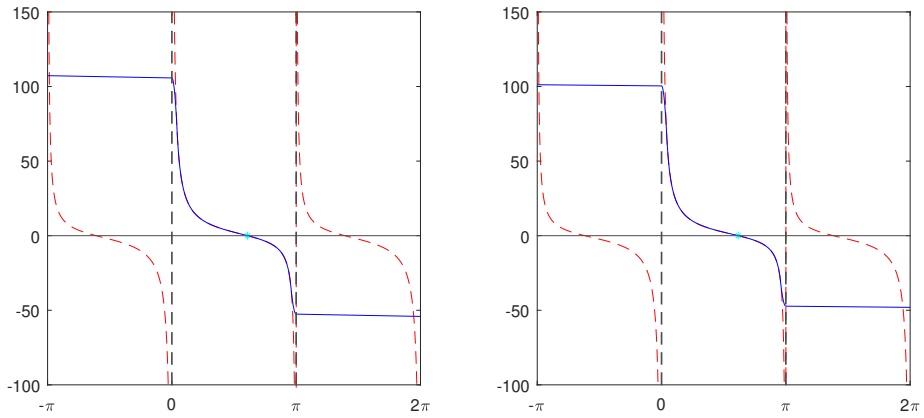

(a) (b)

Figure 2.1: Drift $f(x)$ of equation (2.22) (dashed line) and the LSST drift $f_\Delta(x)$, (solid line) for $\alpha = 7, \gamma = 1, \eta = 1.5, \Delta = 10^{-4}, k = 0.22$. (a) $\sigma_1 = 0.25$, $x^* = 1.912$, $C_0 = 0.48$; (b) $\sigma_3 = 1$, $x^* = 1.938$, $C_0 = 0.25$.

The drift f is monotone decreasing, periodic of period π and super-growing to infinity and minus infinity close to 0 and π, while f_Δ is smoothly truncated close to the boundary and regularized outside to preserve the monotonicity. Note that for smaller diffusion coefficient f_Δ grows a bit faster outside the boundaries. The new drift f_Δ is Lipschitz continuous and one-side Lipschitz continuous. Furthermore, the drift f_Δ is a good approximation of the drift f. Indeed, the following result ensures the desired Lipschitz property for the drift approximation f_Δ and the convergence to the continuous drift of the process is provided in [30].

Proposition 2.6. *Suppose assumption* (2.16) *holds. Let* $0 < k < 1$ *and* $\Delta < \Delta^*$ *be given. Then, for any* $x \in [0, \eta]$

$$f'_\Delta(x) \leq -C_0;$$

and for any $x, y \in [0, \eta]$

$$\begin{aligned} |f_\Delta(x) - f_\Delta(y)| &\leq \pi^2 C_0 \Delta^{-2k} |x - y|, \\ (x - y)\,(f_\Delta(x) - f_\Delta(y)) &\leq -C_0 |x - y|^2. \end{aligned}$$

Furthermore, if $\nu > 3$*, where* ν *is defined in* (2.16)*, for any* $1 < p < \nu$*, and* $\kappa_1 = 2k(p-1)$

$$\sup_{t \in [0,T]} \mathbb{E}\left[|f(Y_t) - f_\Delta(Y_t)|^2 \right] \leq C_{T,p} \Delta^{\kappa_1}.$$

The overall numerical procedure is called the *Lamperti Sloping Smooth Truncation* (LSST).

Let us consider

$$\Xi_t = [0 = t_0, t_1, \ldots, t_N = T], \tag{2.28}$$

an equi-partition of $[0, T]$, where $\Delta_t = \frac{T}{N}$, $N \in \mathbb{N}$. From now on, the following notation for a general function u evaluated at the mesh nodes $u^n = u(t_n)$, for any $n \in \{0, \ldots, N\}$ is adopted.

The scheme of the stochastic boundary condition Ψ solution of equation (2.2) is obtained by numerically sampling (Y, Ψ) solution of (2.22) and (2.21), respectively employing the LSST procedure that reads as follows: given $\Psi_0 = \psi^0$, set $y^0 = 2\arcsin\left(\sqrt{\psi^0/\eta}\right)$ then, for $n = 0, \dots, N-1$

$$\begin{aligned} &\textit{LSST Scheme:} \qquad && y^{n+1} = y^n + f_\Delta(y^n)\Delta_t + \sigma\Delta W^n, \\ & && \psi^{n+1} = \sin^2\left(y^{n+1}/2\right), \end{aligned} \tag{2.29}$$

where $\Delta W^j,\ j = 1, \dots, N$ are independent Brownian increments.

Given the LSST scheme (2.29), let y_t, ψ_t be the time continuous LSST approximation (TC-LSST) defined for any $t \in [0, T]$ as follows. Let $\bar{f}_\Delta$ be the function defined as

$$\bar{f}_\Delta(y_t) = f_\Delta(y^n), \quad t \in [t_n, t_{n+1}).$$

Therefore, the time continuous LSST approximation of the scheme (2.29), given a Wiener process $W = (W_t)_{t\in[0,T]}$, is given by

$$\begin{aligned} &\textit{TC-LSST Scheme:} \qquad && y_t = y^0 + \int_0^t \bar{f}_\Delta(y_t)dt + \sigma W_t, \\ & && \psi_t = \sin^2\left(y_t/2\right). \end{aligned} \tag{2.30}$$

In [30] authors show that the numerical approximation with the LSST scheme has strong convergence and, furthermore, the rate of convergence may be up to one under specific assumptions on the coefficients.

Proposition 2.7. *Suppose $\nu > 3$ and take $\tilde{p}, k, \bar{r}$ in the ranges according to the following cases*

Case	ν	$\tilde{p}$	k	$\bar{r}$
Case 1	$(3, 13/4]$	$(3, \nu)$	$1/4$	*1*
Case 2	$(13/4, \infty)$	$(\sqrt{13\nu}/2, \nu)$	$2\tilde{p}/9\nu$	$2k(\tilde{p}-1) \wedge 2$

Then, for any $\Delta_t < \Delta^*$, the TC-LSST scheme $(y_t, \psi_t)_{t\in[0,1]}$ defined by (2.30) have the following strong convergence

$$\sup_{t\in[0,T]} \mathbb{E}\left[|Y_t - y_t|^2\right], \sup_{t\in[0,T]} \mathbb{E}\left[|\Psi_t - \psi_t|^2\right] \le C_{T,\tilde{p}}\Delta^{\bar{r}}.$$

Remark 2.6. Note that whenever $\nu > 11/2$, the $\bar{r} = 2$; as a consequence, the order of convergence is always one.

2.2.3 Numerical error investigation and simulations

Let us consider the Pearson process $\Psi = \{\Psi_t\}_{t\in[0,1]}$ in the range $[0, \eta] = [0, 1.5]$. In the further investigation, the mean reverting level is set $\gamma = 1$ and the rate $\alpha = 7$, whereas two different diffusion coefficients $\sigma_1 = 0.25$ and $\sigma_3 = 1$ are investigated.

In the LSST scheme (2.29) we consider $\Delta_t = 2^{-15}$ and $k = 0.22$.

For diffusion coefficients $\sigma_1 = 0.25$ and $\sigma_3 = 1$, we obtain that the condition (2.16) is given by $\nu = p = 74.67$ and $\nu = q = 4.67$, respectively. Hence, only for the first parameter set we get the condition $\nu = p > 11/2 = 5.5$ of Remark 2.6 is satisfied and, accordingly with theoretical results, we expect strong order convergence one in the sense of (2.31). In the second case, we expect $\bar{r} \in (1.27, 1.6)$, so we the order of convergence should be in $(0.637, 0.80)$.

We have performed numerical experiments and the approximation error are tested both in terms of the $L^2(\Omega)$ at the final time $T = 1$, i.e.

$$e_{2,T,\Delta} = (\mathbb{E}[|Y_T - y_T|^2])^{\frac{1}{2}}. \tag{2.31}$$

and in terms of the uniform in time $L^2(\Omega)$ norm along the discretization partition

$$\epsilon_{2,\Delta} = \sup_{t_n\in\Xi_t} (\mathbb{E}[|Y_{t_n} - y_{t_n}|^2])^{\frac{1}{2}}, \tag{2.32}$$

where Ξ_t is the time mesh in (2.28).

Since we don't have an explicit formula for the solution, we approximate the true solution with a *reference* solution Y_T, which is identified as the LSST approximation with the finer step-size $\delta = 2^{-15}$.

For any larger $\Delta_t \in \delta \cdot [2^4, 2^5, 2^6, 2^7, 2^8]$, we define by $(y_j^n)_{n=0,\dots,T/\Delta}$ the discrete j-the trajectory out of $N \in \mathbb{N}$ given by (2.29). Precisely, we use trajectory samples of dimension $N = 10000$ and estimate for any Δ_t the error (2.31) through the sample mean

$$\hat{e}^2_{2,T,\Delta} = \frac{1}{N}\sum_{k=1}^{N} \left|Y_T - y_j^{T/\Delta}\right|^2, \tag{2.33}$$

while the time uniform error (2.32) is estimates by

$$\hat{\epsilon}^2_{2,\Delta} = \sup_{t_n\in\Xi_t} \frac{1}{N}\sum_{j=1}^{N} \left|Y_{t_n} - y_j^n\right|^2. \tag{2.34}$$

Experimental estimates are shown in Table 2.1.

By assuming a power law relation for the error e, i.e, $e = C\Delta^{\bar{q}}$, where $\bar{q} = \bar{r}/2$, where $\bar{r}$ in (2.7) since $\log e = \log C + \bar{q}\log\Delta_t$ we estimate the order of strong convergence $\bar{q} = \bar{r}/2$ by means of a least squares fit, given the error sample $(\Delta, \hat{e})_\Delta$. For $\hat{e} = \hat{e}_{2,T,\Delta}$ the estimates of $\bar{q}$ are 1.016 and 1.022 in the case $\sigma_1 = 0.25$ and $\sigma_2 = 1$, respectively.

	$\sigma_1 = 0.25$	$\sigma_3 = 1$
Δ/δ	$\hat{e}_{2,T,\Delta}$	$\hat{e}_{2,T,\Delta}$
2^8	1.19E-03	4.65E-03
2^7	5.94E-04	2.29E-03
2^6	2.93E-04	1.13E-03
2^5	1.45E-04	5.57E-04
2^4	7,12E-05	2.72E-04

(a)

	$\sigma_1 = 0.25$	$\sigma_3 = 1$
Δ/δ	$\hat{\epsilon}_{2,\Delta}$	$\hat{\epsilon}_{2,\Delta}$
2^8	1.16E-02	1.90E-02
2^7	5.10E-03	9.79E-03
2^6	2.33E-03	5.36E-03
2^5	1.06E-03	5.57E-03
2^4	8.82E-04	4.35E-03

(b)

Table 2.1: Convergence error estimates for $\alpha = 7, \gamma = 1, \eta = 1.5$ and different diffusion coefficients: $\sigma_1 = 0.25$ and $\sigma_3 = 1$. (a) $L^2(\bar{\Omega}_P)$ approximation error at time T: estimation (2.33). (b) Time uniform $L^2(\bar{\Omega}_P)$ approximation error: estimation (2.34).

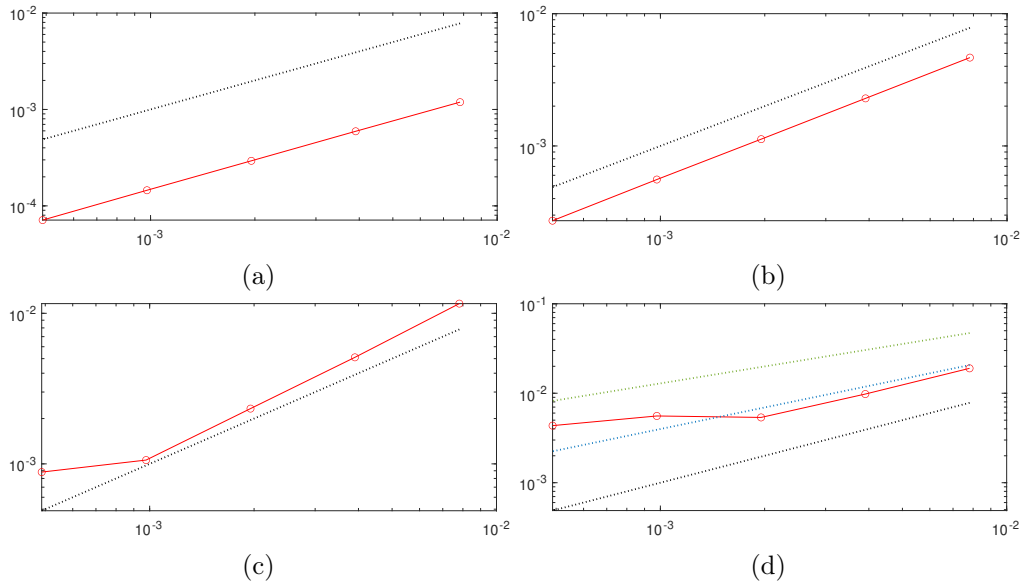

Figure 2.2: Log-log of the estimations of the L^2-errors at time T $(\Delta, \hat{e}_{2,T,\Delta})_\Delta$ (solid line-first raw), and the uniform one $(\Delta, \hat{\epsilon}_{2,\Delta})_\Delta$ (solid line-second row). Parameters are: $\alpha = 7, \gamma = 1, \eta = 1.5$ and different diffusion coefficients: (a)-(c) $\sigma_1 = 0.25$; (b)-(d) $\sigma_3 = 1$. Dashed black line: Slope reference 1; dashed blue line: slope reference 0.8; dashed green line: slop reference 0.6.

Figure 2.2 (first row) shows the points $(\Delta, \hat{e}_{2,T,\Delta})_\Delta$ in the log-log scale for (a) $\sigma_1 = 0.25$ and (b) $\sigma_2 = 1$; for $\hat{e} = \hat{e}_{2,\Delta}$ the estimates of q are 0.97 and 0.51, respectively. Figure 2.2 (second row) shows the points $(\Delta, \hat{e}_{2,\Delta})_\Delta$ in the log-log scale for (c) $\sigma_1 = 0.25$ and (d) $\sigma_2 = 1$. Hence, evidence of first-order strong convergence of LSST scheme is experimentally proven. Let us stress that, even though we are in the Case 1 of the Proposition 2.7, the convergence rate could equal one since conditions are only sufficient (see [30], Theorem 8 for more details).

Indeed, we investigate a new configuration accordingly with the following data: $\alpha = 3.9, \gamma = 0.9, \eta = 1.5$ and $\sigma_3 = 1$. In this set of parameters, the condition $3 < \nu < 13/4$ holds, therefore we would expect a convergence rate equal to $1/2$ but actually from Figure 2.3-(a) we observe that the L^2 convergence rate at the final time T may be equal to 1, while the uniform error rate as shown in Figure 2.3-(b) is closed to 0.5.

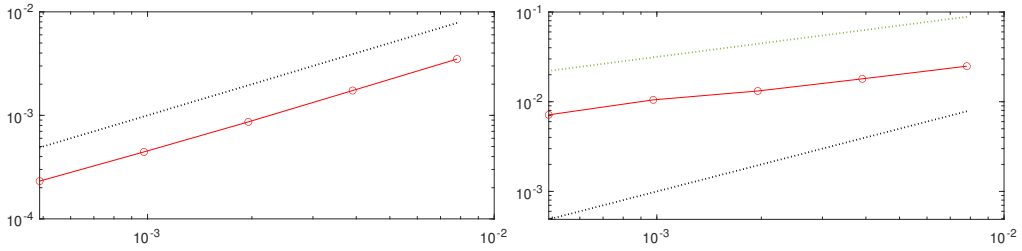

(a) (b)

Figure 2.3: Log-log representation of the estimations of the L^2-errors at time T $(\Delta, \hat{e}_{2,T,\Delta})_\Delta$ (a), and the uniform one $(\Delta, \hat{\epsilon}_{2,\Delta})_\Delta$ (b). Parameters are: $\alpha = 3.9, \gamma = 0.9, \eta = 1.5$ and $\sigma_3 = 1$. Dashed black line: Slope reference 1; dashed green line: slop reference 0.5.

Figure (2.4) represents a single realization of the reference solution Y_T of the approximated solutions $(y_j^n)_{n=0,\dots,T\delta/\Delta}$ in the configuration $\sigma_3 = 1$ with different time steps: $\Delta/\delta = 2^8\,(a)$, $2^6\,(b)$, $2^4\,(c)$. It is important to remark that, for every larger time step adopted, the Brownian increments of the reference solution in the common nodes have been considered and not the reference solution itself. One can appreciate that, since large time steps, the numerical approximated solution converges pathwise to the reference one (see Figure (2.4)).

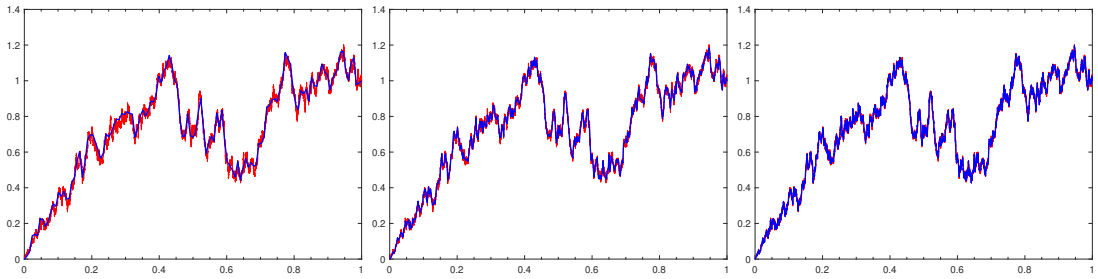

(a) (b) (c)

Figure 2.4: Comparison for a single realization between the reference solution (red line) and approximated solution for different time steps: $\Delta/\delta = 2^8\,(a)$, $2^6\,(b)$, $2^4\,(c)$.

Figure 2.5 shows some random trajectories of the SDE solution process small and large diffusion.

Different values of the diffusion coefficient σ are considered for the SDE to capture how the variability of the noise intensity may influence the sulphation process evolution. Note

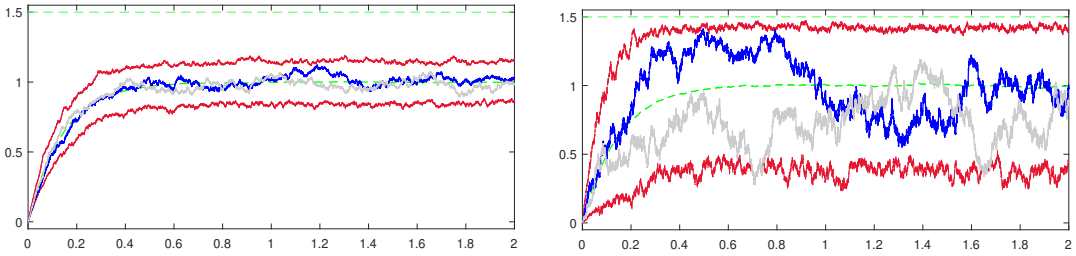

(a) (b)

Figure 2.5: Two random trajectories (filled line) kept within the max and the min of all the trajectories (dotted lines); the sampled mean process (dashed centered line) and boundary of the domain (lower and higher dashed lines) $[0, \eta]$ for $\alpha = 7, \gamma = 1, \eta = 1.5$, $\Psi_0 = 0$ and different diffusion coefficients: (a) $\sigma_1 = 0.25$; (b) $\sigma_3 = 1$.

that all the involved configurations of parameters satisfy the well-posedness condition (2.16).

We see in Figure 2.5-(a) how in the case of a small noise $\sigma_1 = 0.25$ the process moves around the mean $\gamma = 1$ with low excursions in the domain $[0, \eta]$. Indeed, the minimum and the maximum of the sample at each time are both very far from the boundary of the domain. A higher value of the mean reverting rate $\alpha = 7$ together with a low value of the diffusion coefficient induces a lower variability. For a higher value of the diffusion coefficient such as $\sigma_3 = 1$ in Figure 2.5-(b), the process may instead arrive close to the boundary even though it oscillates around $\gamma = 1$ with a longer deviation in the excursion. Indeed, a higher mean reversion helps the return to the average.

2.2.4 Convergence to the invariant measure

For the completeness of the numerical discussion of the stochastic process, we provide the numerical convergence of the distribution to the invariant measure *Beta(p,q)* provided in (2.17).

Figure (2.6) shows the theoretical *Beta(p,q)* (red solid line) with p, q given by (2.15) and the distribution of solution for different time steps at final time T (black dashes line) and at time $T/2$ for two different levels of noise $\sigma_1 = 0.25$ and $\sigma_3 = 1$, respectively. One can notice that the convergence at final time T is achieved even when the time discretization is big (see Figures (2.6) cases (a) and (c)). Moreover, in both configurations, the theoretical distribution is almost reached at time $T/2$.

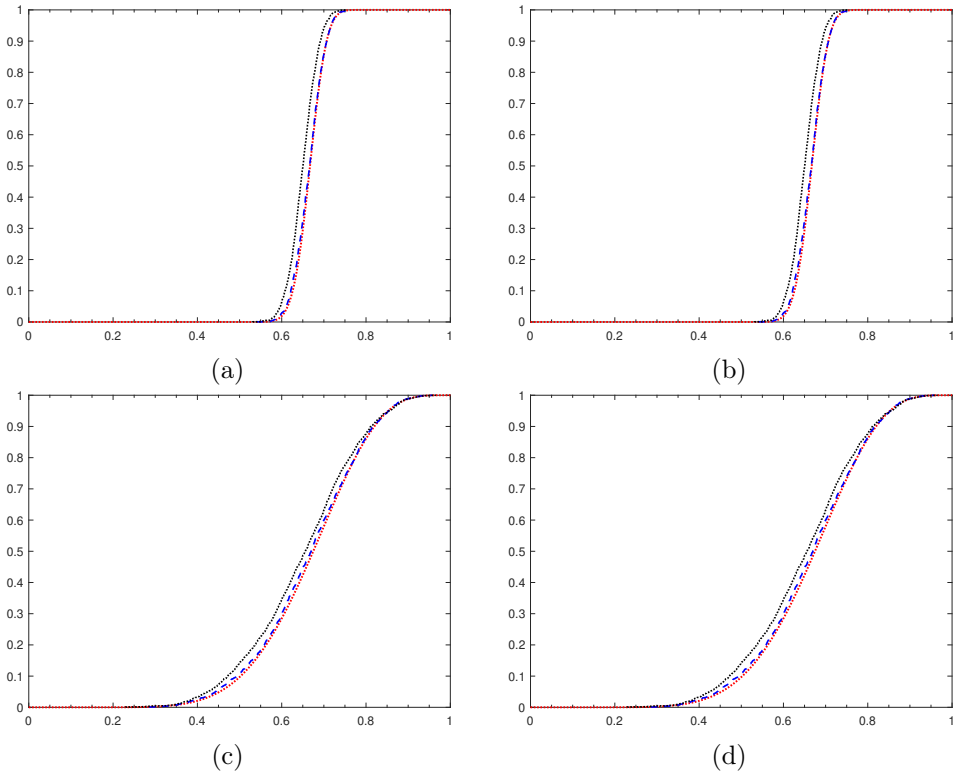

Figure 2.6: Invariant distribution for $\sigma_1 = 0.25$ (first row) and $\sigma_3 = 1$ (second row) for different time steps. $\Delta/\delta = 2^8$ (a)-(c), $\Delta/\delta = 2^4$ (b)-(d). Theoretical distribution *Beta(p,q)* red dashed line, distribution at final time T blue dashed line, distribution at time $T/2$ black line.

Chapter 3

A random PDE system for the sulphation phenomenon

This chapter represents the first original contribution of the thesis [7, 8]. A new numerical splitting scheme for the approximation of the PDE-ODE system with stochastic boundary dynamics based on a splitting strategy is provided.

In Section 3.1 we recall the results of the well-posedness of the PDE-ODE system coupled with boundary conditions provided in [82]. In Section 3.2, we present the original part of the thesis. We perform a complete qualitative and numerical analysis of system (1.8) coupled with stochastic boundary condition, given by the stochastic diffusion $\widetilde{\Psi}_t$ in (2.2), deeply discussed in Chapter 2. We aim, essentially from a modelling point of view, to illustrate the role of randomness in the dynamical evolution of the chemical reaction, either pathwise or in the mean sense.

Numerical pathwise stability and accuracy are provided. Furthermore, we illustrate different configurations to capture the role of randomness at the boundary and in the evolution of solutions. Slow and fast regimes are investigated. A quantitative study of the impact of the noise at the boundary on the solutions is finally described.

3.1 Well-posedness of the PDE-ODE system with stochastic dynamical conditions

For the convenience of the reader, in this first section, we recall a result on the well-posedness of the PDE-ODE system with a stochastic dynamical condition given by the solution of the diffusion process (2.2). The global existence and pathwise uniqueness for the solution to the random system, in a mild sense, is given in [82]. A brief discussion on the result can be found in [7], In the following we describe the main steps.

As in [58, 60], rather than working directly with the local concentration ρ_s, authors work

with the porous concentration $s = \rho_s/\varphi$ (as in (1.9)), while c stands for the local density of calcite. Thus system (1.8) is considered:

$$\begin{aligned} \partial_t(\varphi(c)s) &= \partial_x(\varphi(c)\partial_x s) - \lambda\varphi(c)sc, \\ \partial_t c &= -\lambda\varphi(c)sc. \end{aligned} \tag{3.1}$$

with the parameter $\lambda \in \mathbb{R}_+$ to control the velocity of the reaction.

From now on, the previous system will be the central study of this thesis, coupled with initial conditions for s and c:

$$s(0,x) = s_0(x) = \frac{\rho_s(0,x)}{\varphi(c(0,x))}, \quad c(0,x) = c_0(x), \tag{3.2}$$

and boundary conditions for s

$$s(t,0) = \widetilde{\Psi}_t := \frac{\Psi_t}{\varphi(c(t,0))}, \tag{3.3}$$

with Ψ_t given by the solution of the diffusion process (2.2). Again, the porosity is described as a linear function of the calcite density:

$$\varphi(c) = A + Bc. \tag{3.4}$$

From (3.3) and the second equation in (3.1), we easily derive that the boundary condition at $x = 0$ for the calcium carbonate is the solution of the following linear ODE

$$\partial_t c(t,0) = -\lambda\Psi_t\, c(t,0), \qquad c(0,0) = c_0.$$

Hence, the stochastic boundary conditions in $x = 0$, for the couple solution (s,c), are given by

$$\begin{aligned} c(t,0) &= c_0 \exp\left(-\lambda \int_0^t \Psi_u du\right), \\ s(t,0) = \widetilde{\Psi}_t &= \frac{\Psi_t}{\varphi\left(c_0 \exp(-\lambda \int_0^t \Psi_u du)\right)}. \end{aligned} \tag{3.5}$$

The following proposition ensures the boundedness of solutions.

Proposition 3.1. *Let condition* (2.16) *be satisfied. Then the boundary function* (3.5) *are bounded for any* $t \in [0,T]$. *More precisely,*

$$\begin{aligned} c(t,0) &< c_0, \\ 0 < s(t,0) = \widetilde{\Psi}_t &< \frac{\eta}{\varphi_1 + c_0\varphi_2} =: \widetilde{\eta} \end{aligned} \tag{3.6}$$

Proof. The thesis easily derives from Proposition 2.3. □

The high oscillation property of $s(t,0)$ corresponds to poor regularity of the path of $\widetilde{\Psi}$: from the analytical point of view, this poor regularity is the main feature of the model. Precisely, Ψ and, thus, $\widetilde{\Psi}$ have β-Hölder continuous paths, for every $\beta \in (0, 1/2)$, but have no better regularity ([82]). In the deterministic case, the well-posedness is achieved for a boundary condition $\psi \in W^{1,1}([0,T])$ (see [60]), while existence and uniqueness in the present case is proven in [82], as follows.

Let us derive an equivalent formulation for the system (3.1):

Proposition 3.2. *Let* (3.4) *be the model for the porosity. The system* (3.1)*, coupled with initial and boundary conditions* (3.2)-(3.5) *could be rewritten as:*

$$\partial_t s = \partial_x^2 s + b_c(t,x)\partial_x s + \gamma_c(t,x)s(Bs-1) \tag{3.7}$$
$$\partial_t c = -\lambda s(A+Bc)c \tag{3.8}$$

with

$$b_c(t,x) = B\frac{\partial_x c}{(A+Bc)} \tag{3.9}$$
$$\gamma_c(t,x) = \lambda c \tag{3.10}$$

Proof. We start with the first equation in system (3.1) and we derive the products:

$$\begin{aligned}
\partial_t(\varphi(c)s) &= \partial_x(\varphi(c)\partial_x s) - \lambda\varphi(c)sc \\
(\partial_t\varphi(c))\, s + \varphi(c)\partial_t s &= \partial_x\varphi(c)\partial_x s + \varphi(c)\partial_x^2 s - \lambda\varphi(c)sc \\
(B\partial_t c)\, s + \varphi(c)\partial_t s &= B\partial_x c\partial_x s + \varphi(c)\partial_x^2 s - \lambda\varphi(c)sc \\
\left(\frac{B}{\varphi(c)}\partial_t c\right) + \partial_t s &= \frac{B}{\varphi(c)}\partial_x c\partial_x s + \partial_x^2 s - \lambda sc \\
\partial_t s &= \partial_x^2 s + \frac{B}{\varphi(c)}\partial_x c\partial_x s + B(\lambda sc)s - \lambda sc
\end{aligned}$$

where we have used the fact that $\partial_t\varphi(c) = \partial_t(A+Bc) = B\partial_t c$ and, symmetrically, for the spatial derivative. Moreover, in the last equality, we have pulled the second equation for the dynamics of c into the equation for s. By rearranging the terms and denoting

$$b_c(t,x) = B\frac{\partial_x c}{A+Bc}, \quad \gamma_c(t,x) = \lambda c,$$

the formulation in (3.7)-(3.8) is gained. □

Then, a precise definition of *mild solution* is provided.

Definition 3.1 (Bounded positive mild solution)**.** A couple (s,c), with $s \in L^\infty([0,T], W^{1,2}(\mathbb{R}_+)) \cap L^\infty([0,T]\times\mathbb{R}_+)$ and $c \in B_b([0,T]\times\mathbb{R}_+)$, the space of bounded Borel functions, is *a*

bounded positive mild solution of the nonlinear PDE (3.7),(3.8)-(3.10) if, for every $x \in \mathbb{R}_+$, the function $c(\cdot, x)$ solves (3.8)-(3.10), that is c is explicitly given by

$$c(t,x) = \frac{Ac_0(x)}{\varphi(c_0(x))e^{\lambda A \int_0^t s(\tau,x)d\tau} - Bc_0(x)}, \tag{3.11}$$

and the function s satisfies

$$0 \leq s(t,x) \leq \widetilde{\eta} \quad \text{for every } (t,x) \in [0,T] \times \mathbb{R}_+,$$

and it is a $L^\infty([0,T], W^{1,2}(\mathbb{R}_+))$-mild solution of (3.7), that is

$$\begin{aligned} s(t,\cdot) = &-2\int_0^t \partial_x G(t-\tau,\cdot)\psi(\tau)d\tau + G(t,\cdot) * s_0 \\ &+ \int_0^t G(t-\tau,\cdot) * \left(b_c(\tau,\cdot)\partial_x s(\tau,\cdot) + \gamma_c(\tau,\cdot)s(\tau,\cdot)\right)(Bs(\tau,\cdot)-1))ds, \end{aligned} \tag{3.12}$$

where b_c and γ_c are defined as (3.9) and (3.10), respectively and $G(t,\cdot) * f$ denotes the convolution-type operator with the heat kernel G, which is defined as

$$G(t,x) = \frac{1}{\sqrt{4\pi t}} e^{-x^2/4t}.$$

Following [82], the time horizon T is supposed to vary in a compact interval $[0, T_{fin}]$.

The following theorem provides the global existence of a pathwise unique solution of the random system.

Theorem 3.1 (Well-posedness, [82])**.** *Let conditions* (2.16) *on the parameters of* Ψ *be satisfied. Then, the trajectories of* Ψ *are almost surely in* C^β*, with* $\beta \in (1/4, \infty)$ *and let* $\widetilde{\Psi}(0) = 0$*. Then, for any* $T \in [0, T_{fin}]$ *there exists a pathwise unique mild solution* (s,c) *to system* (3.1) *coupled with initial and boundary conditions* (3.2)-(3.3)*, in the sense of definition* (3.1)*.*

Theorem 3.1 is proven via a splitting argument. Here we do not state the main feature of the proof since we will take advantage of the same splitting strategy to numerical sampling the random couple of solutions (s,c) in $[0,T] \times \mathbb{R}_+$ in Chapter 4.

3.2 Numerical approximation: a splitting scheme

In the following, we introduce a novel *splitting scheme* for the numerical approximation of problem (3.1) coupled with random dynamical conditions in (3.3).

Well-posedness of the previous system is provided in Section 3.1 via a splitting argument. Coherently, towards the numerical discussion of the problem, we decompose s as the sum

$$s = u + v, \tag{3.13}$$

where u is the solution to the diffusion equation (*heat equation*) with zero initial condition and boundary condition $\widetilde{\Psi}$:

$$\begin{aligned} \partial_t u &= \partial_x^2 u, \\ u(0,x) &= 0, \\ u(t,0) &= \widetilde{\Psi}(t). \end{aligned} \tag{3.14}$$

Therefore, function u neglects the reaction term, and so the non linearity, and handles the randomness and the consequent low regularity of the system. The heat equation is very well studied in literature and its highly oscillating boundary behaviour becomes smoother in the indoor environment, due to diffusion. We can then use this smoothing effect to study the full system which has also a reaction component. Indeed, $u \in C^\infty$ in the interior $(t,x) \in (0,T] \times (0,\infty)$ and for $\beta \in (1/4,\infty)$, $u \in L^\infty([0,T]; W^{1,2}(0,\infty))$, in particular it is weakly differentiable in x. This additional regularity plays an important role in the study of the system for v.

The term v satisfies an equation of the same form of the equation for s with terms depending on u, but with zero boundary condition, namely for any $(t,x) \in [0,T] \times [0,\infty)$

$$\begin{aligned} &\partial_t v = \partial_x^2 v + \frac{B\partial_x c}{\varphi(c)}(\partial_x v + \partial_x u) - \left(\frac{B\partial_t c}{\varphi(c)} + \lambda c\right)(v+u), \\ &v(0,x) = s_0(x), \\ &v(t,0) = 0, \end{aligned} \tag{3.15}$$

where c is explicitly given in terms of $s = u + v$ by:

$$c(t,x) = \frac{A c_0(x)}{\varphi(c_0(x)) e^{\lambda A \int_0^t s(r,x)dr} - B c_0(x)}, \tag{3.16}$$

Thanks to the regularity of u and $\partial_x u$, existence and uniqueness for v and hence for s is proven in [82], as discussed in [7].

We introduce a discrete version of the system (3.1)-(2.2) in $[0,T] \times [0,\overline{x}]$ with $\overline{x} \in \mathbb{R}_+$ and let us consider an equi-partition of the space and time intervals with space-time meshes

$$\Xi_x \times \Xi_t = [0 = x_0, x_1, \ldots, x_M = \overline{x}] \times [0 = t_0, t_1, \ldots, t_N = T]. \tag{3.17}$$

From now on, we consider the following notations

$$\Delta_x = \frac{\overline{x}}{M}, \quad \Delta_t = \frac{T}{N}, \quad \bar{\Delta} = \frac{\Delta_t}{\Delta_x^2},$$

with $N \in \mathbb{N}$ such that $\Delta_t < \Delta^*$, where Δ^* is as in (2.27) and Proposition 2.7. For a general function u evaluated at the mesh nodes we denote $u_m^n = u(t_n, x_m)$, for any $(n,m) \in \{0,\ldots,N\} \times \{0,\ldots,M\}$.

Since, at the simulation level, we consider a bounded domain $[0, \overline{x}]$, we need to specify the boundary condition in $x = \overline{x}$ for the solutions $s = u + v$ and c. Therefore, the following Neumann conditions for u, v and c are set for the right boundary $x = \bar{x}$:

$$\begin{aligned} \partial_x u(t, \overline{x}) = \partial_x v(t, \overline{x}) &= 0. \\ \partial_x c(t, \overline{x}) &= 0. \end{aligned} \tag{3.18}$$

We consider the discrete version of the splitted solution (3.13) of system (3.1), that is for any $(m, n) \in \{1, ..., M\} \times \{1, ..., N\}$

$$s_m^n = u_m^n + v_m^u.$$

According to the theoretical results obtained in [82], s solves the discrete SDE-PDE system in a pathwise way.

3.2.1 The discrete random heat equation: definition and stability

We solve the random PDE system pathwise, i.e. for any given realization $\{\tilde{\psi}^n\}_n(\omega), \omega \in \Omega_P$ of the discrete process

$$\widetilde{\psi}^n = \frac{\psi^n}{\varphi\left(c_0 \exp(-\lambda \int_0^{t_n} \Psi_u du)\right)}. \tag{3.19}$$

First, we consider a forward time, centered space (FTCS) approximation $\{u_m^n\}_{n,m}$ of the heat equation in (3.14), for $(n, m) \in \{0, \ldots, N-1\} \times \{1, \ldots, M\}$

$$\frac{u_m^{n+1} - u_m^n}{\Delta_t} = \frac{u_{m+1}^n - 2u_m^n + u_{m-1}^n}{\Delta_x^2}.$$

A slight improvement in computational efficiency can be obtained with a small rearrangement of the discrete system, by considering that the right boundary conditions lead to the condition $u_{M+1}^n = u_{M-1}^n$, for any n. This comes from the approximation of the Neumann condition at the boundary in (3.18) by centered finite differences in space, coherently with the numerical scheme for the internal points.

Therefore, for any $n = 0, 1, \ldots, N-1$ we consider the following complete numerical scheme

$$\begin{aligned} &u_m^{n+1} = \bar{\Delta}\, u_{m+1}^n + (1 - 2\bar{\Delta}) u_m^n + \bar{\Delta}\, u_{m-1}^n, \quad m = 1, \ldots, M-1; \\ &u_0^{n+1} = \widetilde{\psi}^{n+1}, \quad u_M^{n+1} = (1 - 2\bar{\Delta}) u_M^n + 2\bar{\Delta}\, u_{M-1}^n; \\ &\quad u_0^0 = \widetilde{\psi}^0 \quad u_m^0 = 0, \quad m = 1, \ldots, M. \end{aligned} \tag{3.20}$$

The discrete bounded process $\left(\widetilde{\psi}^n\right)_n$ in (3.19) is given by the transformation (3.5) of the process solution of the LSST scheme (2.29).

System (3.20) is equivalent to solve for any $n = 0, \dots, N-1$ the following linear system for the internal nodes

$$U^{n+1} = AU^n + \bar{\Delta}\, \widetilde{U}_0^n, \tag{3.21}$$

where $U^n = (u_1^n, ..., u_M^n)^T \in \mathbb{R}^M$ for any $n = 0, \dots, N-1$, the matrix $A \in \mathbb{R}^M \times \mathbb{R}^M$ is given by

$$A = \begin{bmatrix} 1-2\bar{\Delta} & \bar{\Delta} & 0 & 0 & 0 & \dots & 0 \\ \bar{\Delta} & 1-2\bar{\Delta} & \bar{\Delta} & 0 & 0 & \dots & 0 \\ 0 & \bar{\Delta} & 1-2\bar{\Delta} & \bar{\Delta} & 0 & \dots & 0 \\ \vdots & \vdots & \vdots & \vdots & \vdots & \vdots & \vdots \\ 0 & \dots & 0 & 0 & \bar{\Delta} & 1-2\bar{\Delta} & \bar{\Delta} \\ 0 & \dots & 0 & 0 & 0 & 2\bar{\Delta} & 1-2\bar{\Delta}. \end{bmatrix} \tag{3.22}$$

Note that the matrix A is the classical matrix associated to the first-order finite difference approximation and it is tridiagonal and positive whenever $\bar{\Delta} \leq \frac{1}{2}$. Here, we lose the symmetry property of the matrix by imposing centred finite differences at the right boundary. In fact, equation (3.21) is associated to the following boundary condition $\widetilde{U}_0^n$ at $x = 0$, coupled with the second rescaling in (3.5), and the $t = 0$ condition U^0:

$$\begin{aligned} \widetilde{U}_0^n &= \left(\widetilde{\psi}^n, 0, \dots, 0, 0\right)^T; \\ U^0 &= (0, \dots, 0)^T. \end{aligned} \tag{3.23}$$

Furthermore, the initial condition U^0 is given by the null matrix. By an iteration of (3.21), we get that a solution of (3.21)- (3.23) is, for any $n \in \{1, ..., N\}$

$$U^n = A^n U^0 + \bar{\Delta} \sum_{j=0}^{n} A^{n-j}\, \widetilde{U}_0^j. \tag{3.24}$$

Mean-square stability of the solution to a random partial differential equation refers to the property that the expected value of the square of the solution remains is limited in the amount of growth that can occur in a finite time. We first have a result of pathwise stability. Let us consider the Euclidean norm in space and time for U^n and $\widetilde{U}_0$, respectively

$$\|U^n\|_{\Delta_x} = \left(\Delta_x \sum_{m=0}^{M} |u_m^n|^2\right)^{1/2}, \quad \|\widetilde{U}_0\|_{N,\Delta_t} = \left(\Delta_t \sum_{j=0}^{N} \left|\widetilde{U}_0^j\right|^2\right)^{1/2}, \tag{3.25}$$

A notion of stability ([106]) for the initial-condition boundary-value problem (3.21) is the following.

Definition 3.2. The discrete scheme (3.21) is L^2-pathwise stable if, for any n such that $0 \leq n\Delta_t \leq T$, and for any $\omega \in \Omega$, there exists a positive constant C_T such that

$$\|U^n(\omega)\|_{\Delta_x} \leq C_T \left(\|U^0\|_{\Delta_x} + \|\widetilde{U}_0(\omega)\|_{n,\Delta_t}\right).$$

If the scheme is L^2-pathwise stable, it is also L^2 stable in mean. Indeed, following the classical stability results in the deterministic case, the following results may be stated.

Proposition 3.3 (Pathwise stability for u)**.** *Suppose that assumption* (2.16) *on the parameters of the stochastic boundary condition holds. Then for*

$$\bar{\Delta} \leq 1/2 \tag{3.26}$$

the random process, solution of (3.21)- (3.23) *is pathwise stable; precisely, there exists a constant C such that, for any $n \in \{1, \ldots, N\}$*

$$\|U^n(\omega)\|_{\Delta_x} \leq C_{T,\Delta_x} \widetilde{\eta},$$

where $\widetilde{\eta}$ is defined in (3.6)*. Moreover, also the mean square stability holds. Furthermore, the stability property holds also in the maximum norm case both pathwise and in mean*

$$\mathbb{E}\left[\|U^n\|_{\max}\right] \leq C_T \widetilde{\eta}. \tag{3.27}$$

Proof. Let us observe that the matrix A is similar to the matrix symmetric

$$\widetilde{A} = \begin{bmatrix} 1-2\bar{\Delta} & \Delta & 0 & 0 & 0 & \ldots & 0 \\ \bar{\Delta} & 1-2\bar{\bar{\Delta}} & \bar{\Delta} & 0 & 0 & \ldots & 0 \\ 0 & \bar{\Delta} & 1-2\bar{\Delta} & \bar{\Delta} & 0 & \ldots & 0 \\ \vdots & \vdots & \vdots & \vdots & \vdots & \vdots & \vdots \\ 0 & \ldots & 0 & 0 & \bar{\Delta} & 1-2\bar{\Delta} & \sqrt{2}\bar{\Delta} \\ 0 & \ldots & 0 & 0 & 0 & \sqrt{2}\bar{\Delta} & 1-2\bar{\Delta} \end{bmatrix},$$

i.e. $\widetilde{A} = S^{-1}AS$, with $S = diag(1, 1, .., 1, \sqrt{2}) \in \mathbb{R}^M$. Then

$$\|A^n\|_2 = \left\| \left(S^{-1}\widetilde{A}S \right)^n \right\|_2 = \left\| S^{-1}\widetilde{A}^n S \right\|_2 \leq \|S^{-1}\| \|\widetilde{A}^n\| \|S\|_2 \leq \frac{1}{\sqrt{2}} \rho\left(\widetilde{A}\right)^n,$$

where $\rho\left(\widetilde{A}\right)$ is the largest eigenvalue of the symmetric matrix $\widetilde{A}$ which is of the form $|1 - 4\bar{\Delta}\sin^2(\xi)|$, with $\xi \in (0, 1)$, a function of Δ_x, [109]. Since $|1 - 4\bar{\Delta}\sin^2(\xi)| \leq 1$ if and only if $\bar{\Delta} \leq 1/2$. Hence, by (3.26) we get that, for any $n \in \{1, ..., N\}$

$$\|A^n\|_2 \leq 1.$$

Finally, by (3.24), (3.25) and (3.23) we get

$$\begin{aligned} \|U^{n+1}(\omega)\|_{\Delta_x} &\leq \|U^0(\omega)\|_{\Delta x} + \frac{\Delta_t}{\Delta_x^2} \left\| \sum_{j=0}^{n} \widetilde{U}_0^j \right\|_{\Delta_x} \leq \frac{\Delta_t}{\Delta_x^2} \left(\Delta_x \sum_{j=0}^{n} |\psi^n|^2 \right)^{1/2} \\ &\leq \frac{\Delta_t^{1/2}}{\Delta_x^{1+1/2}} \left(\Delta_t \sum_{j=0}^{n} |\psi^n|^2 \right)^{1/2} = \frac{\bar{\Delta}^{1/2}}{\Delta_x^{1/2}} \|\widetilde{\Psi}\|_{n,\Delta_t} \leq C_{T,\Delta_x} \widetilde{\eta}, \end{aligned}$$

that is the thesis is proven. The mean case and (3.27) may be easily proven. □

Remark 3.1. Pathwise and mean stability are provided whether condition (3.26) holds: stability condition for classical heat equation by first-order finite differences is reached (see, for instance, [75]). Moreover, condition (3.26) is equivalent to asking the matrix A in (3.22) to be positive defined.

3.2.2 The random non-linear dynamics with deterministic boundary condition

Given the solution $\{u_m^n\}_{m,n}$ of the discrete heat equation (3.20) or equivalently, (3.21) -(3.23) with $x = 0$-boundary condition $\{\widetilde{\psi}^n\}_n$ in the class C^β, with $(\beta < 1/2)$, we take the discrete version of the equation (3.15) for v coupled with the explicit solution for the calcite c given by (3.16), where s is defined by (3.13).

For any $m \in \{1, \ldots, M\}, n \in \{1, \ldots, N\}$, let $s_m^n = u_m^n + v_m^n$ and c_m^n be the discrete version of s and c, respectively. Again, by using an explicit first-order finite difference approximation, centred in space and forward in time for (3.15), we obtain the following forward system of equations for any $n = 0, \ldots, N-1$ and $m = 1, ..., M-1$

$$\begin{aligned} v_m^{n+1} &= v_m^n + \bar{\Delta}\left(v_{m+1}^n - 2v_m^n + v_{m-1}^n\right) \\ &\quad + \bar{\Delta}\frac{B}{4\varphi(c_m^n)}\left(c_{m+1}^n - c_{m-1}^n\right)\left(v_{m+1}^n - v_{m-1}^n\right) \\ &\quad + \bar{\Delta}\frac{B}{4\varphi(c_m^n)}(c_{m+1}^n - c_{m-1}^n)(u_{m+1}^n - u_{m-1}^n) \\ &\quad + \Delta_t \lambda c_m^n \left(B(v_m^n + u_m^n) - 1\right)(v_m^n + u_m^n); \\ c_m^{n+1} &= c_m^n \, e^{-\lambda\Delta_t \left(v_m^n + u_m^n\right)\varphi(c_m^n)} \end{aligned}$$

coupled with the discrete solution u_m^n given by (3.20). By denoting the functions

$$\begin{aligned} b_m^n = b_m^n(c) &:= \frac{B}{4\varphi(c_m^n)}(c_{m+1}^n - c_{m-1}^n) = \frac{\varphi(c_{m+1}^n) - \varphi(c_{m-1}^n)}{4\varphi(c_m^n)}; \\ h_m^n = h_m^n(c,u,v) &:= \lambda\Delta_t c_m^n \left(B(v_m^n + u_m^n) - 1\right), \end{aligned}$$

a small rearrangement leads to the following scheme for (v_m^n, c_m^n)

$$\begin{aligned} v_m^{n+1} &= \bar{\Delta}\left(1 + b_m^n(c)\right) v_{m+1}^n + \bar{\Delta}\left(1 - b_m^n(c)\right) v_{m-1}^n \\ &\quad + \left[1 - 2\bar{\Delta} + h_m^n(c,u,v)\right] v_m^n \\ &\quad + \bar{\Delta} b_m^n(c) u_{m+1}^n + h_m^n(c,u,v) u_m^n - \bar{\Delta}\, b_m^n(c) u_{m-1}^n; \qquad (3.28) \\ c_m^{n+1} &= c_m^n \, e^{-\lambda\Delta_t \left(v_m^n + u_m^n\right)\varphi(c_m^n)}, \qquad (3.29) \end{aligned}$$

coupled with u_m^n, given by (3.20) and initial conditions given by

$$v_m^0 = s_0 \leq \widetilde{\eta}, \quad c_m^0 = c_0, \quad m \in \{1, \ldots, M-1\}. \qquad (3.30)$$

Coherently with u, the Neumann boundary condition in $x = \overline{x}$ reads as

$$v_{M+1}^n = v_{M-1}^n, \qquad c_{M+1}^n = c_{M-1}^n,$$

so that, for any $n = 1, \dots, N$,

$$b_M^n := \frac{B}{4\varphi(c_M^n)}(c_{M+1}^n - c_{M-1}^n) = 0.$$

Therefore, this leads to the boundary equation for v, that is, for any $n = 1, \dots, N-1$

$$\begin{aligned} v_0^n &= 0; \\ v_M^{n+1} &= 2\bar{\Delta} v_{M-1}^n + (1 - 2\bar{\Delta} + h_M^n) v_M^n + h_M^n u_M^n. \end{aligned} \tag{3.31}$$

We may express the system (3.28), (3.30) and (3.31) in a matrix form.

For any $n = 0, \dots, N-1$, let V^n be the vector $V^n = (v_1^n, ..., v_M^n)^T \in \mathbb{R}^M$, and let the matrices $G(n), P(n) \in \mathbb{R}^M \times \mathbb{R}^M$ be the following

$$G(n) = \begin{bmatrix} 1 - 2\bar{\Delta} + h_1^n & \bar{\Delta}(1 + b_1^n) & 0 & \dots & 0 \\ \bar{\Delta}(1 - b_2^n) & 1 - 2\bar{\Delta} + h_2^n & \bar{\Delta}(1 + b_2^n) & \dots & 0 \\ \vdots & \vdots & \vdots & \vdots & \vdots \\ 0 & \dots & \bar{\Delta}(1 - b_{M-1}^n) & 1 - 2\bar{\Delta} + h_{M-1}^n & \bar{\Delta}(1 + b_{M-1}^n) \\ 0 & \dots & 0 & 2\bar{\Delta} & 1 - 2\bar{\Delta} + h_M^n \end{bmatrix};$$

$$P(n) = \begin{bmatrix} h_1^n & \bar{\Delta} b_1^n & 0 & \dots & \dots & 0 \\ -\bar{\Delta} b_2^n & h_2^n & \bar{\Delta} b_2^n & \dots & \dots & 0 \\ \vdots & \vdots & \vdots & \vdots & \vdots & \vdots \\ 0 & \dots & 0 & -\bar{\Delta} b_{M-1}^n & h_{M-1}^n & \bar{\Delta} b_{M-1}^n \\ 0 & \dots & \dots & 0 & 0 & h_M^n \end{bmatrix}.$$

Then, for $n = 0, 1, \dots N$, the system (3.28), (3.30) and (3.31) reads as

$$V^{n+1} = G^n V^n + P^n U^n + \bar{\Delta} \widetilde{V}^n, \tag{3.32}$$

where $\widetilde{V}^n = \left(-b_1^n \tilde{\psi}^n, 0, \dots, 0\right)$.

3.2.3 Pathwise boundedness and stability

The first step of the analysis regards boundedness result for $(s_m^n, c_m^n) = (u_m^n + v_m^n, c_m^n)$, solution of the following system, easily obtained from systems (3.20) and (3.28)-(3.29).

For any $(n, m) \in \{0, \dots, N-1\} \times \{1, \dots, M\}$,

$$\begin{aligned} s_m^{n+1} &= \bar{\Delta}\left(1 + \frac{\varphi(c_{m+1}^n) - \varphi(c_{m-1}^n)}{4\varphi(c_m^n)}\right) s_{m+1}^n + \bar{\Delta}\left(1 - \frac{\varphi(c_{m+1}^n) - \varphi(c_{m-1}^n)}{4\varphi(c_m^n)}\right) s_{m-1}^n \\ &\quad + \left[1 - 2\bar{\Delta} - \lambda \Delta_t c_m^n (1 - B s_m^n)\right] s_m^n \qquad (3.33) \\ c_m^{n+1} &= c_m^n \, e^{-\lambda \Delta_t s_m^n \varphi(c_m^n)} \qquad (3.34) \end{aligned}$$

Proposition 3.4 (Pathwise stability for discretized s)**.** *Let us consider the linear porosity defined in* (3.4) *and the initial condition* (3.30) *with A, B and c_0 independent on the size of the grids in space and time such that*

$$5Bc_0 + 4A > 0. \tag{3.35}$$

Given the first stability condition (3.26)*, let us suppose that the following further condition is satisfied*

$$\Delta_t \leq \frac{\Delta_x^2}{2 + \lambda c_0 \Delta_x^2 (1 - B\widetilde{\eta})}, \tag{3.36}$$

with $\widetilde{\eta}$ defined in (3.6)*. Then, the solution of the system* (3.33)-(3.34) *is such that, for any $(n, m) \in \{1, \dots, N\} \times \{1, \dots, M\}$, and any $\omega \in \Omega$*

$$(s_m^n(\omega), c_m^n(\omega)) \in [0, \widetilde{\eta}) \times [0, c_0].$$

Proof. Let us observe that from the expression of c_m^{n+1}, it is clear that if $s_m^n \in [0, \tilde{\eta})$, then $c_m^{n+1} \in [0, c_m^n]$. This is true for $n = 0$. Let us suppose it is true for all $k \leq n$. Then for any $k \in \{1, \dots, n+1\}$, $c_m^n \in [0, c_0]$ and then, for any $m \in \{1, \dots, M\}$,

$$0 < \varphi(c_0) = A + Bc_0 \leq \varphi(c_m^k) \leq A < 1. \tag{3.37}$$

By the induction hypothesis, for all $k \leq n$, $s_{m+1}^k, s_m^k, s_{m-1}^k$ are positive: we should check the positivity for $k = n + 1$ in (3.33); indeed,

$$\begin{aligned} 1 - \frac{\varphi(c_{m+1}^n) - \varphi(c_{m-1}^n)}{4\varphi(c_m^n)} &= \frac{4\varphi(c_m^n) - \varphi(c_{m+1}^n) + \varphi(c_{m-1}^n)}{4\varphi(c_m^n)} \\ &\geq \frac{5\varphi(c_0) - \varphi(c_{m+1}^n)}{4\varphi(c_m^n)} \geq \frac{5\varphi(c_0) - A}{4\varphi(c_m^n)} \\ &\geq \frac{5\varphi(c_0) - A}{4\varphi(c_m^n)} \geq 0. \end{aligned}$$

We need to guarantee that the previous quantitive is positive:

$$\begin{aligned} \frac{5\varphi(c_0) - A}{4\varphi(c_m^n)} \geq \frac{5\varphi(c_0) - A}{4A} = \frac{5(A + Bc_0)}{A} - 1 \geq 0 \\ Bc_0 \geq -4A \end{aligned}$$

Thus, condition (**??**) ensures the positivity of the solutions. Note that whenever $B > 0$, the condition is always fulfilled, since the parameter A is strictly positive from (3.37). On the other hand, the case $B < 0$ specifies a lower bound for the initial level of the calcite density.

In a similar way, we obtain the same estimation for the coefficient of s_{m+1}^n:

$$1 + \frac{\varphi(c_{m+1}^n) - \varphi(c_{m-1}^n)}{4\varphi(c_m^n)} \geq \frac{5\varphi(c_0) - \varphi(c_{m-1}^n)}{4\varphi(c_m^n)} \geq \frac{5\varphi(c_0) - A}{4\varphi(c_m^n)} \geq 0.$$

Then, for the induction hypothesis we may prove the upper bound for s_m^{n+1}; since $(1 - Bs_m^n) > 0$, we get

$$\begin{aligned} s_m^{n+1} &\leq \bar{\Delta} s_{m+1}^n + \bar{\Delta} s_{m-1}^n + \left[1 - 2\bar{\Delta} - \lambda \Delta_t c_m^n \left(1 - B s_m^n\right)\right] s_m^n \\ &\leq 2\bar{\Delta}\widetilde{\eta} + \left[1 - 2\bar{\Delta}\right] s_m^n \\ &\leq 2\bar{\Delta}\widetilde{\eta} + \left[1 - 2\bar{\Delta}\right] \widetilde{\eta} = \widetilde{\eta} \end{aligned}$$

For the proof of the lower bound, we need to prove that also the last coefficient of the equation is positive; we have the following

$$\begin{aligned} 1 - 2\bar{\Delta} - \lambda \Delta_t c_m^n \left(1 - B s_m\right) &= 1 - 2\frac{\Delta_t}{\Delta_x^2} - \lambda \Delta_t c_m^n + \lambda \Delta_t c_m^n B s_m \\ &\geq 1 - 2\frac{\Delta_t}{\Delta_x^2} - \lambda \Delta_t c_0 + \lambda \Delta_t B c_0 \widetilde{\eta} \\ &= \frac{1}{\Delta_x^2}\left[\Delta_x^2 - \Delta_t\left(2 + \Delta_x^2 \lambda c_0 (1 - B\widetilde{\eta})\right)\right] \end{aligned}$$

The last is greater then zero if and only if condition (3.36) is satisfied. Then, the thesis is achieved. □

It naturally follows from the decomposition of $s = u + v$ that the discretised solution v_m^n admits admits upper and lower bounds:

Corollary 3.1 (Bounds for v_m^n)**.** *Let us suppose that the hypothesis of Proposition 3.4 are satisfied. Then the solution of* (3.20) *and* (3.28)-(3.29) *are such that for any* $(n, m) \in \{1, \ldots, N\} \times \{1, \ldots, M\}$*, and any* $\omega \in \Omega$*,*

$$-\widetilde{\eta} \leq -u_m^n(\omega) \leq v_m^n(\omega) \leq \widetilde{\eta} - u_m^n. \tag{3.38}$$

Proof. The result easily follows from Proposition 3.4 and the fact that $u_M^n \in [0, \eta)$. □

Therefore, the pathwise stability is provided for the numerical solution v:

Proposition 3.5 (Pathwise stability for numerical v)**.** *Let us suppose that the hypothesis of Proposition* (3.4) *are satisfied. Then there exist positive constants* $C_{\Delta_x,T,\bar{x}}, C_{\Delta_x,T}$ *for any* $n \in \{1, \ldots, N\}$*, the solution* V^n *of* (3.32) *is such that*

$$\|V^n(\omega)\|_{\Delta_x} \leq C_{\Delta_x,T,\bar{x}} \widetilde{\eta}, \tag{3.39}$$

and

$$\|V^n(\omega)\|_{\max} \leq C_T \widetilde{\eta}.$$

The same stability results in mean follow.

Proof. From the bound (3.38), we get that for any $(n, m) \in \{1, \dots, N\} \times \{1, \dots, M\}$,

$$\sum_{m=1}^{M} |v_m^n|^2 \leq \sum_{m=1}^{M} |u_m^n|^2 + M|\widetilde{\eta}|^2.$$

Then, for $V^n = (v_1^n, \dots, v_M^n)^T, H = id(\widetilde{\eta}) \in \mathbb{R}^M$ the following bound, for any $n = 0, \dots, N-1$,

$$\|V^{n+1}(\omega)\|_{\Delta_x} \leq \|U^{n+1}(\omega)\|_{\Delta_x} + \|H\|_{\Delta_x} \leq C_{\Delta_x,T} + \bar{x}\widetilde{\eta} \leq C_{\Delta_x,.T,\bar{x}}\widetilde{\eta}$$

Then, bound (3.39) follows from Proposition 3.3. The rest of the thesis easily follows with the same arguments and by considering the mean. □

Remark 3.2. Condition (**??**) is equivalent to a condition on the initial porosity, that is $\varphi(c_0) > A/5$: thus, the initial porosity needs to be not too small. On the other hand, condition (3.36) says that $\bar{\Delta} \leq 1/2$ is not sufficient for both the positivity and stability of v: a more restrictive condition is then introduced. Moreover, the stability restriction on the time step Δ_t in (3.36) involves also the parameter λ, which controls the velocity of the reaction: hence, it is relevant to guarantee the stability for numerical solutions in accelerated configurations.

3.3 Sampling the system

This section is devoted to the numerical sampling of the PDE-ODE system (3.1) with stochastic boundary dynamics (3.3) via the splitted numerical system introduced in Section 3.2. All further simulations are performed in MATLAB R2023a. Codes are available upon request.

We sample the solution of the system by considering a time horizon $[0, T] = [0, 1.5]$ and a spatial domain $[0, \bar{x}] = [0, 1.5]$. In the following, we show the numerical results of the random PDE in the smaller space window $[0, 1]$, to avoid the influence at the boundary condition at $\bar{x} = 1.5$. The time step is $\Delta_t = 1.99e^{-5}$, while the spatial one is $\Delta_x = 10^{-2}$. Let us stress that Δ_t is chosen so that stability restriction in (2.27) for the SDE at the boundary are verified simultaneously with conditions (3.26) and (3.36) for the PDE-ODE model.

We aim to test the behaviour of the diffusion-advection-reaction system under the influence of the stochastic dynamical boundary condition. Concerning the sampling of the complete system, we perform simulations for different values of diffusion parameters for the SDE; furthermore, to catch the role of the activation energy in the penetration of the sulphur dioxide and the consequent degradation of the calcium carbonate, we also consider different reaction rates λ, by considering a slow ($\lambda_1 = 1$) and fast ($\lambda_3 = 100$) regimes. An intermediate case $\lambda_2 = 10$ is also considered. The case of a diffusion coefficient $\sigma_0 = 0$ in equation (2.2) corresponds to the deterministic case; in particular, we consider a

configuration in which the deterministic boundary condition for ρ in $x = 0$ is not constant as in [9, 60], but it is a function $\Psi_0 \in C_b([0,T])$, i.e. for $t \in [0,T]$

$$\rho_{\sigma_0}(t,0) = \Psi_0(t) = \gamma\left(1 - e^{-\alpha t}\right). \tag{3.40}$$

Note that the constant boundary condition $\rho_{\sigma_0}(t,0) = 1$ studied in Ref. [9] corresponds to the time asymptotic limit of equation (3.40).

Table 3.1 shows the parameters considered in the numerical sampling.

SDE	α	γ	η	σ_0	σ_1	σ_2	σ_3	
	7	1	1.5	0	0.25	0.7	1	
PDE	s_0	c_0	A	$\widetilde{A}$	B	λ_1	λ_2	λ_3
	0	10	0.2	0.7	-0.01	1	10	100

Table 3.1: Parameter sets for the simulation of the PDE system (3.20) and (3.28)-(3.31).

3.3.1 Pathwise results

This first paragraph focuses on a single realization of the diffusion process at the boundary to highlight the evolution of the solutions (u, v) of the splitted algorithm proposed in this work and the couple (s, c) solutions to the original problem. This paragraph aims to underline how the randomness at the boundary affects the behaviour of the solutions.

Results for different sets of parameters for the SDE at the boundary accordingly with Table 3.1 are presented: different configurations for the discretization of the PDE-ODE are considered. It is important to remark that the following results are associated with a single realization among the $\overline{N} = 500$ we have realized for each configuration of parameters.

Before going into the different realizations, let us recall that the solution of the sulphur dioxide s is given by the sum of two contributions u and v. More precisely, u is the solution of the stochastic heat equation with Neumann boundary condition in $\overline{x}$, with initial condition $s_0 = 0$ and boundary condition given by:

$$s(t,0) = \widetilde{\Psi}_t = \frac{\Psi_t}{\varphi\left(c_0 \exp(-\lambda \int_0^t \Psi_u du)\right)} \tag{3.41}$$

Let us firstly focus on the role of the linear porosity $\varphi(c) = A + Bc$: in Section 3.2 we proved that, whenever $B < 0$, the function $\varphi(c)$ is an increasing function of the time t:

$$0 < \varphi(c_0) = A + Bc_0 \leq \varphi(c_m^n) \leq \varphi(c_m^{n+1}) \leq A < 1$$

From the definition of the boundary for the solution s in (3.41), it is easy to see that the range of values assumed by $\varphi(c)$ modify the boundary condition for s, and thus for u.

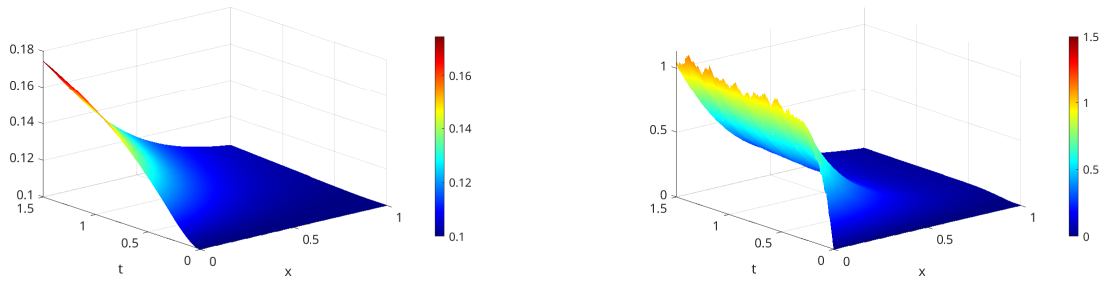

(a) $\varphi(c)$ (b) ρ_s

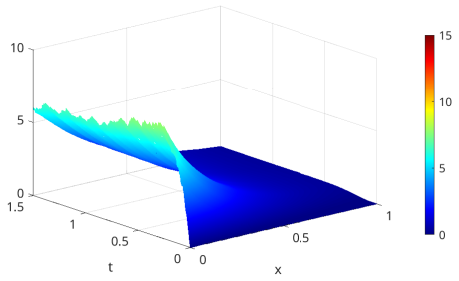

(c) s

Figure 3.1: Single realization of $\varphi(c)$ (top left), ρ_s (top right) and s (bottom) for the slow regime $\lambda_1 = 1$ and $\sigma = 0.25$.

Smaller values for the porosity lead to higher values of SO_2 porous concentration at the boundary. Moreover, as $\varphi(c)$ is an increasing function of the time (see Fig. 3.1a), the process at the boundary will slowly decrease during the time (see Fig 3.1c). Figure (3.1) shows the effect of the porosity in the dynamics of s: the level of noise $\sigma = 0.25$ is low, but one could appreciate the fact that the profile of the sulphur concentration in Figure (3.1c) slowly decreasing when time increases.

Physically, this behaviour makes absolute sense: s describes the porous concentration of the sulphur dioxide and its value at the boundary decreases over time as the gas progressively enters the porous medium. The decrease in sulphur dioxide concentration is directly influenced by the level of porosity, as a higher porosity allows for more efficient diffusion of the gas into the medium, leading to a faster reduction of its concentration at the boundary.

To better understand the role of v, a different angulation for the solution is presented here. This first configuration of parameters (see Fig. 3.3b) does not properly underline the non-linear behaviour of the solution, but it will be clearer in the other cases (see, for instance, Figure 3.7b,3.9b). As stated in Corollary (3.38), the function v takes values in $[-\widetilde{\eta}, \widetilde{\eta} - u]$. Since the initial condition here is $s_0 = 0$, the results is that v is always

negative. The role of the non-linear stochastic solution is to lower the stochastic heat solution to incorporate the reaction term within the final solution s. The result of the splitting method is illustrated in the sulfur evolution shown in Fig. 3.3c. Notable, the contribution of the solution u to the final solution s is due to the smoothing effect of the Laplacian operator, while the reaction effect is driven by the solution v. Here, little variability at the boundary is considered and the solution becomes very regular at early times. A similar behaviour is observed in the solution c (Fig. 3.3d), where the boundary randomness is negligible and does not significantly impact the calcite degradation.

Slow dynamics

First of all, we consider the case of slower dynamics, where the activation energy, or reaction rate, $\lambda = \lambda_1 = 1$. The case of a porosity function (3.4) with $A = 0.2$ is examined (see Table (3.1)). In this section we illustrate the dynamics pathwise, focusing on a single realization of the involved random processes. Following the splitting strategy, we firstly discuss the paths of $\left(u^n, \widetilde{\psi}^n\right)_n$ as the solution of the discrete stochastic system (3.20), together with $(v^n, c^n)_n$, or, equivalently, $(s^n = u^n + v^n, c^n)_n$ via system (3.28)-(3.31). The following results are presented in a smaller space window $[0, 1]$ to avoid the influence at the boundary condition at $\bar{x} = 1.5$.

Figure 3.2 shows a sample path of the random heat equation (3.20) coupled with conditions (3.23) for different diffusion coefficients σ for the dynamical stochastic boundary condition in $x = 0$. Randomness is concentrated at the boundary: thanks to the smoothing properties of the Laplace operator, the solution becomes more regular whenever it moves inside the domain. As the noise intensity σ grows, the corresponding solution oscillates more and more and oscillations spread all over the domain. We may also appreciate the contribution of the porosity acting at the boundary condition, as expressed by (3.19): when the SDE reaches a stationary distribution, the action of increasing porosity let the boundary profile decrease. This is much more evident in the deterministic case (Fig. 3.2a) and for the smaller σ (Fig. 3.2b).

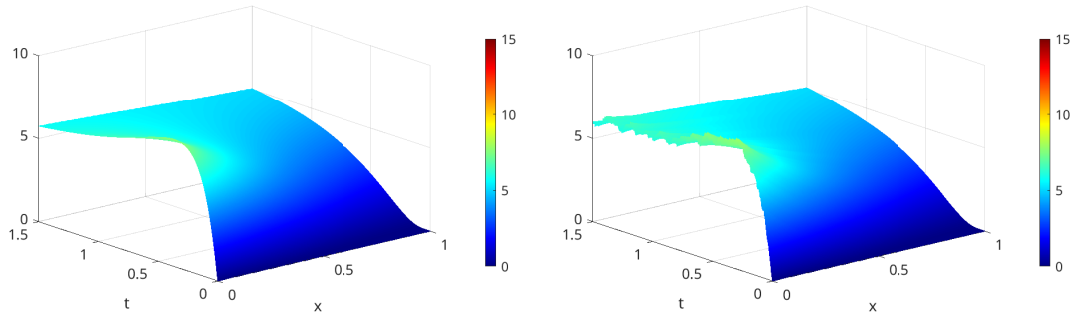

(a) $\sigma = 0$

(b) $\sigma = 0.25$

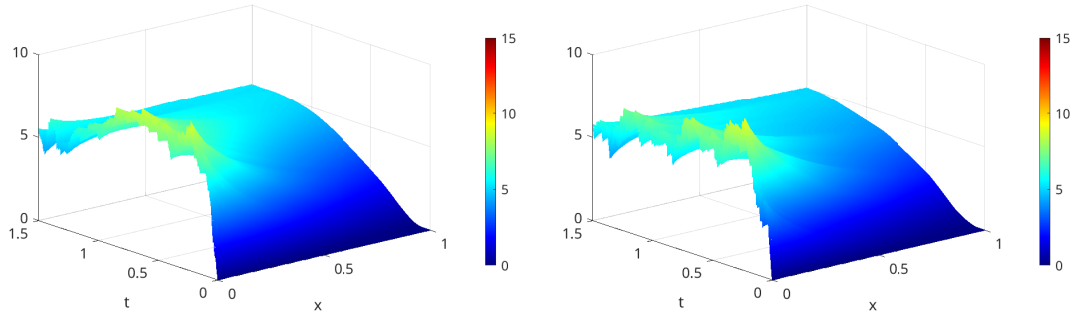

(c) $\sigma = 0.7$

(d) $\sigma = 1$

Figure 3.2: Random heat solution in the case $A = 0.2$, for different values of σ. (a) $\sigma_0 = 0$; (b) $\sigma_1 = 0.25$; (c) : $\sigma_2 = 0.7$; (d) $\sigma_3 = 1$.

Figure 3.3 depicts the single contribution of a path of the process $(s = u + v, c)$ that may be derived by the splitting strategy. The case of diffusion coefficient at the boundary $\sigma_1 = 0.25$ is considered. The solution v of the nonlinear equation (3.28) includes the reaction of the sulphur dioxide; since the initial and boundary conditions are zero, from (3.5) and (3.38) it gives a complete negative contribution bounded from below by $-\widetilde{\eta} = -15$. This is the reason why the sulphur dioxide porous concentration $s = u + v$ oscillates as u, but as soon as it moves away from the boundary, oscillations slow down to zero. As the profile of the calcite c in (3.29) concerns, we see how the degradation occurs as time increases, with a slower degradation of the calcite profile far from the boundary.

Figure (3.4) shows the four single realizations for (u, v, s, c) in the slow regime as in Figure (3.3) but with a higher level of $\sigma_3 = 1$ at the boundary. The effect of the stochasticity is more visible in the dynamics for v, while the profile of the calcite remains very smooth.

Figure 3.5 illustrates the evolution of a pathwise solution of $\rho = \varphi(c)s$ sampled, for any

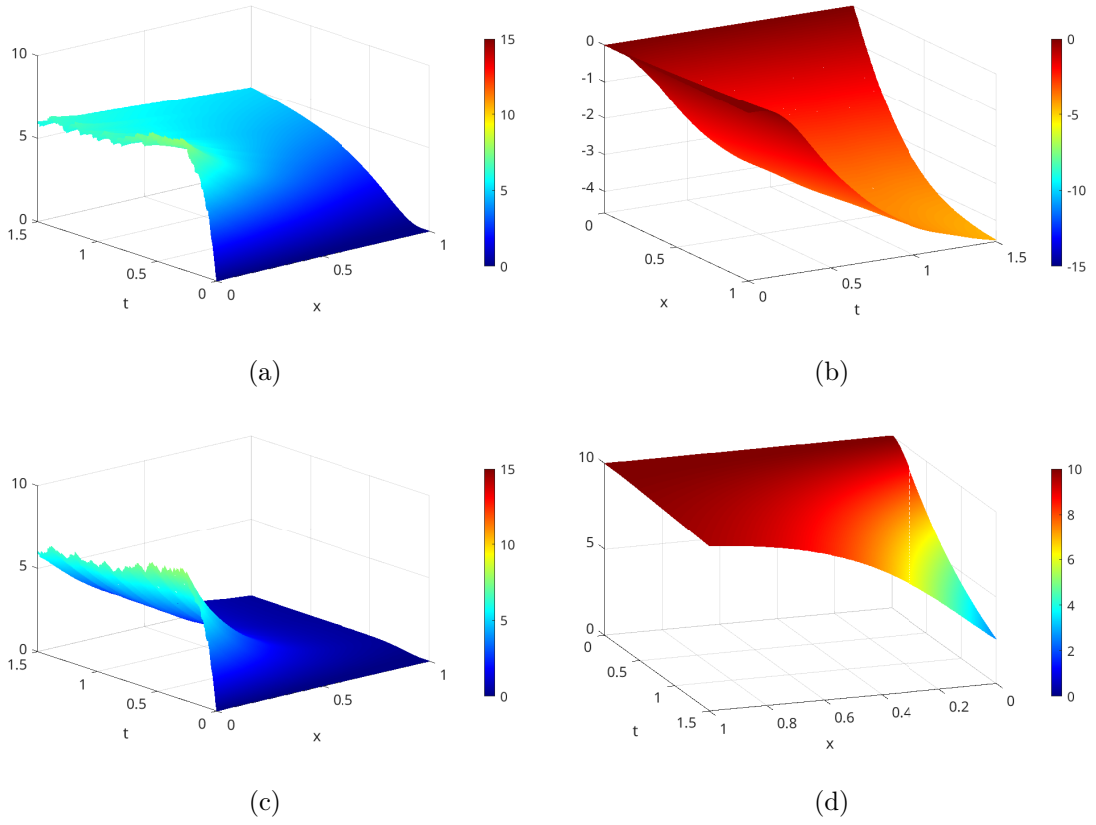

Figure 3.3: Different contributions to a single realization of the complete PDE with $\sigma_1 = 0.25$. First row: a pathwise random heat equation solution u (left) and the solution v of the non-linear equation (3.28) (right). Second row: the sulphur dioxide evolution $s = u + v$ (left) and the evolution of the calcite c, solution of (3.29).

$(n, m) \in \{0, 1, \ldots, N\} \times \{0, 1, \ldots, M\}$, by

$$\rho_m^n = (v_m^n + u_m^n)\, \varphi(c_m^n),$$

with c_m^n defined in (3.29). As the noise at the boundary increases, the perturbation is much more detected far from the boundary, even though the effect is mitigated by the low reaction rate and the quite low porosity of the transformed material.

Gypsum porosity may reach a level of 70%. The higher the porosity, the faster the penetration of the sulphur dioxide and, thus, the degradation. The effect may be detected in Figure 3.6: the evolutions of a realization of the SO_2 and the corresponding calcium carbonate density for a lower porosity $A = 0.02$ are compared with the ones with higher porosity $\widetilde{A} = 0.7$. All other parameters involved remain unchanged.

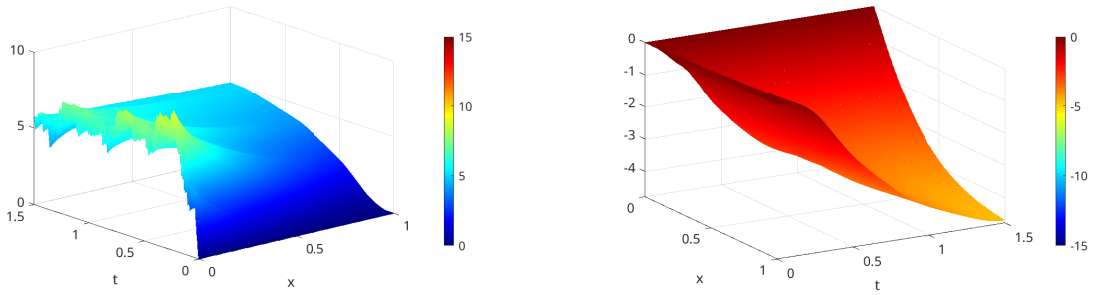

(a) (b)

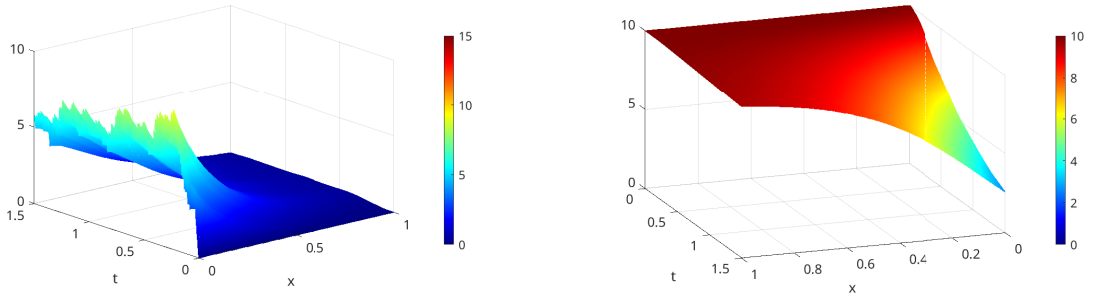

(c) (d)

Figure 3.4: Different contributions to a single realization of the complete PDE with $\sigma_3 = 1$. First row: a pathwise random heat equation solution u (a) and the solution v of the non-linear equation (3.28) (b). Second row: the sulphur dioxide evolution $s = u + v$ (c) and the evolution of the calcite c (d), solution of (3.29).

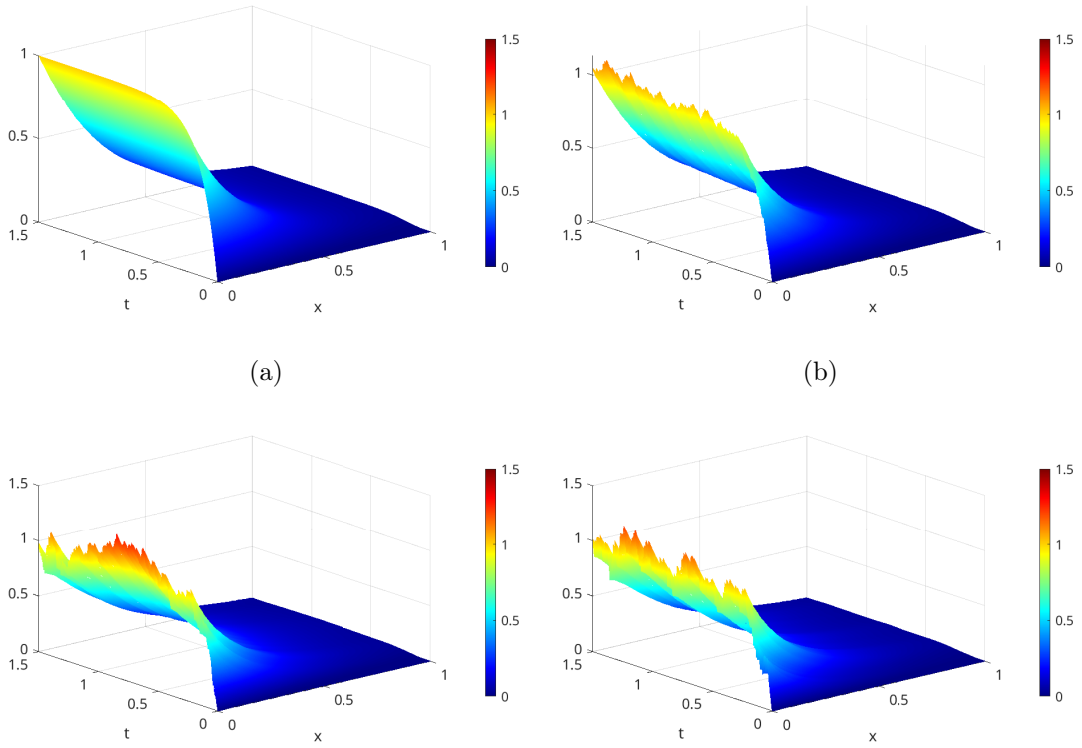

Figure 3.5: The role of the diffusion σ. A single path of the SO_2 concentration $\rho = \varphi s$ for different levels of boundary noise. (a): $\sigma_0 = 0$; (b): $\sigma_1 = 0.25$; (c): $\sigma_2 = 0.7$; (d): $\sigma_3 = 1$.

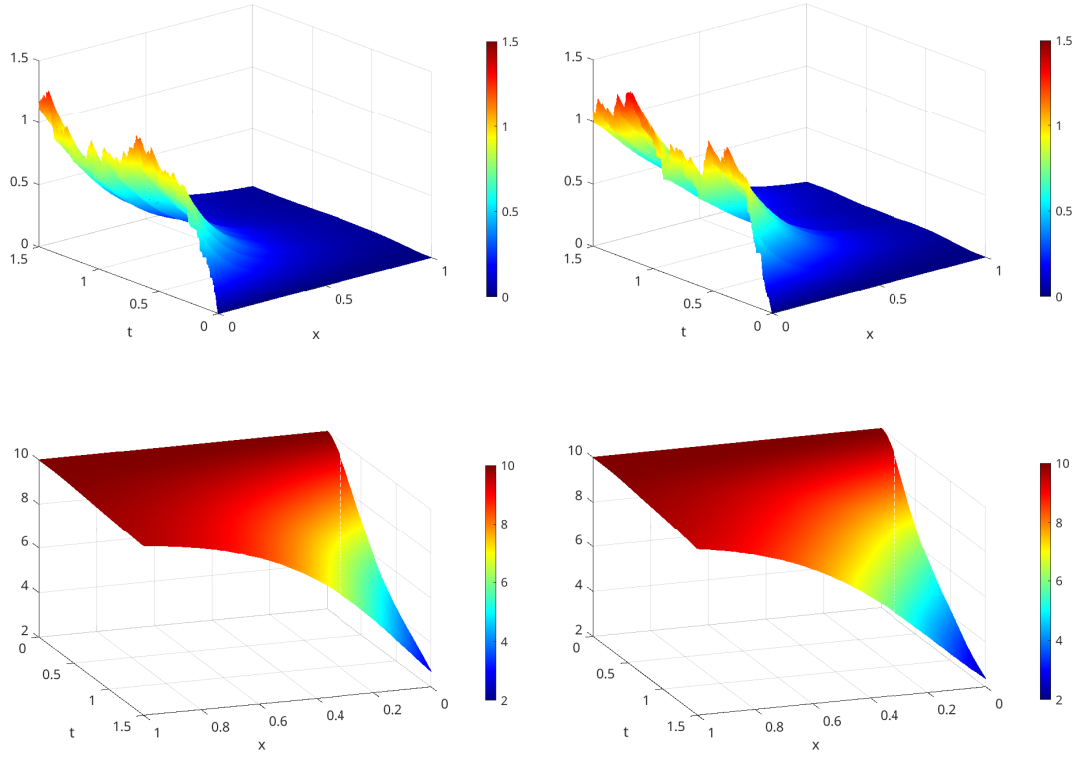

Figure 3.6: The role of the gypsum porosity via the parameter A. Evolution of a realization of SO_2 (first row) and the corresponding marble concentration (second row) for $A = 0.02$ (left) and a higher porosity $\widetilde{A} = 0.7$ (right). Other parameters: $B = -0.01$, $\lambda = 1$, $\sigma_2 = 0.7$.

Faster dynamics: the accelerated case

In this paragraph, we consider different values of the parameter $\lambda \in \mathbb{R}_+$ in System (3.1), (3.2) and (3.3). As discussed in [59], an accelerated regime for the reaction by assuming different values λ_i, $i = 2, 3$ accordingly to Table 3.1 is considered. This is equivalent to analysing the asymptotic behaviour of the system by accelerating time by a factor of λ_i and taking a space expansion $\sqrt{\lambda_i}x$. By changing the parameter λ, the role of the activation energy in the penetration of the sulphur dioxide and the consequent degradation of the calcium carbonate is captured. Figure 3.7 illustrates the evolution of the solutions for an intermediate acceleration rate, $\lambda_2 = 10$. The impact of acceleration is particularly pronounced, especially in the dynamics of v and c. At early times, the reaction variable v exhibits a highly irregular behaviour due to the random penetration of sulphur dioxide concentration into the medium. This irregular penetration of the pollutant strongly influences the calcite dynamics, as the $CaCO_3$ levels near the boundary rapidly go to zero. This behaviour highlights the tendency for the reaction to degrade more rapidly in regions closer to the boundary. This is more evident when the reaction rate parameter is set to $\lambda = \lambda_3 = 100$. The solution has a very different qualitative aspect: as the interaction coefficient λ increases, the transition zone gets smaller, leading to more evident calcite deterioration at the boundary of the sample, while the interior remains unaffected by sulphur dioxide. In particular, in Fig 3.8 we may see the formation of a moving front.

Figures 3.8 and 3.9 describe the same accelerated case where $\lambda_3 = 100$ but the level of noise increases from $\sigma_1 = 0.25$ to $\sigma_3 = 1$. One can notice that for higher levels of noise at the boundary, the reaction part v (see Figs 3.8b and 3.9b) becomes more irregular; on the other hand, the profile of the calcite (Figs 3.8d, 3.9d) remains very smooth. In the given system, the stochasticity is confined to the boundary of the domain, influencing the behaviour of the solution s (Figs 3.8c, 3.9c). This behaviour indicates that the reaction is predominantly localized at the boundary, as evidenced by the dynamics of calcite. Near the boundary, the level of calcite material is zero, emphasizing that the reaction leading to degradation occurs intensely in these regions. Thus, the system exhibits increased sensitivity to degradation in accelerated regimes.

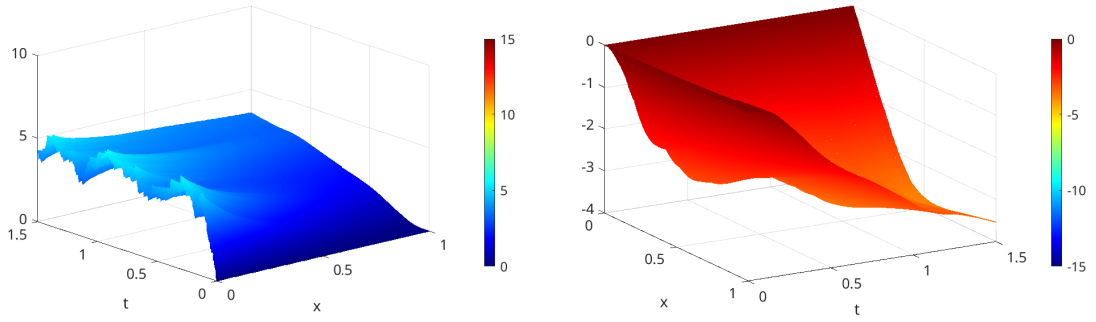

(a) (b)

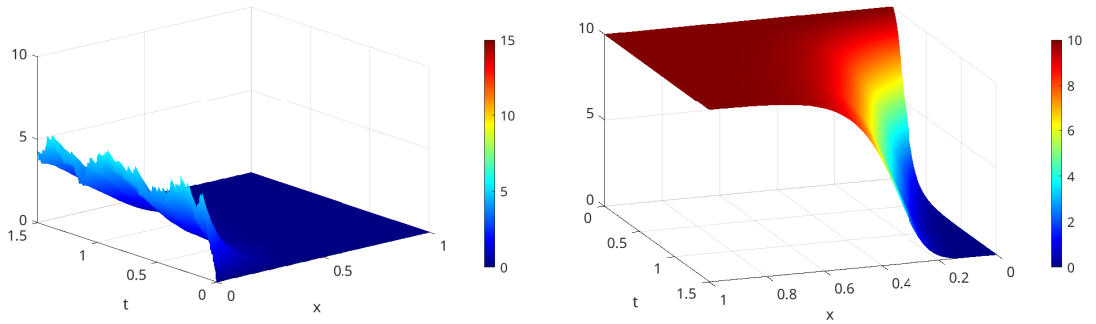

(c) (d)

Figure 3.7: Different contributions to a single realization of the complete PDE with $\sigma_2 = 0.7$ in the accelerated configuration with $\lambda = \lambda_2 = 10$. First row: a pathwise random heat equation solution u (left) and the solution v of the non-linear equation (3.28) (right). Second row: the sulphur dioxide evolution $s = u + v$ (left) and the evolution of the calcite c.

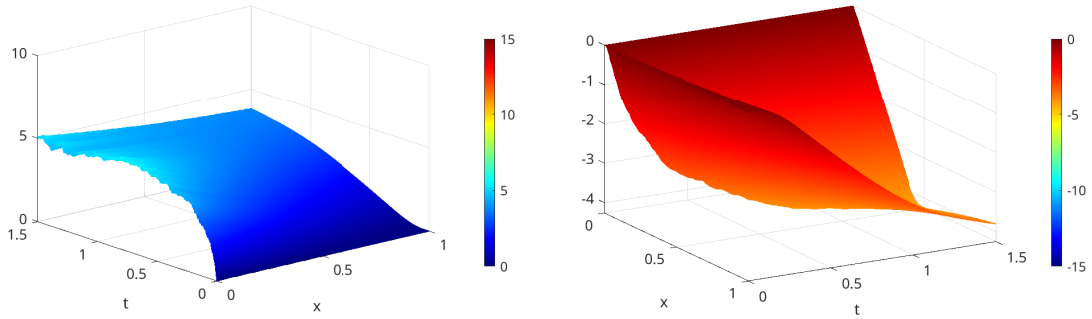

(a) (b)

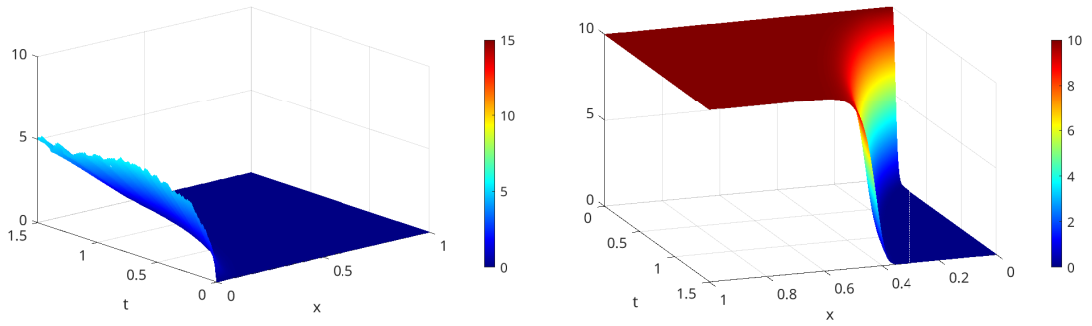

(c) (d)

Figure 3.8: Different contributions to a single realization of the complete PDE with $\sigma_1 = 0.25$ in the accelerated configuration with $\lambda = \lambda_3 = 100$. First row: a pathwise random heat equation solution u (left) and the solution v of the non-linear equation (3.28) (right). Second row: the sulphur dioxide evolution $s = u + v$ (left) and the evolution of the calcite c.

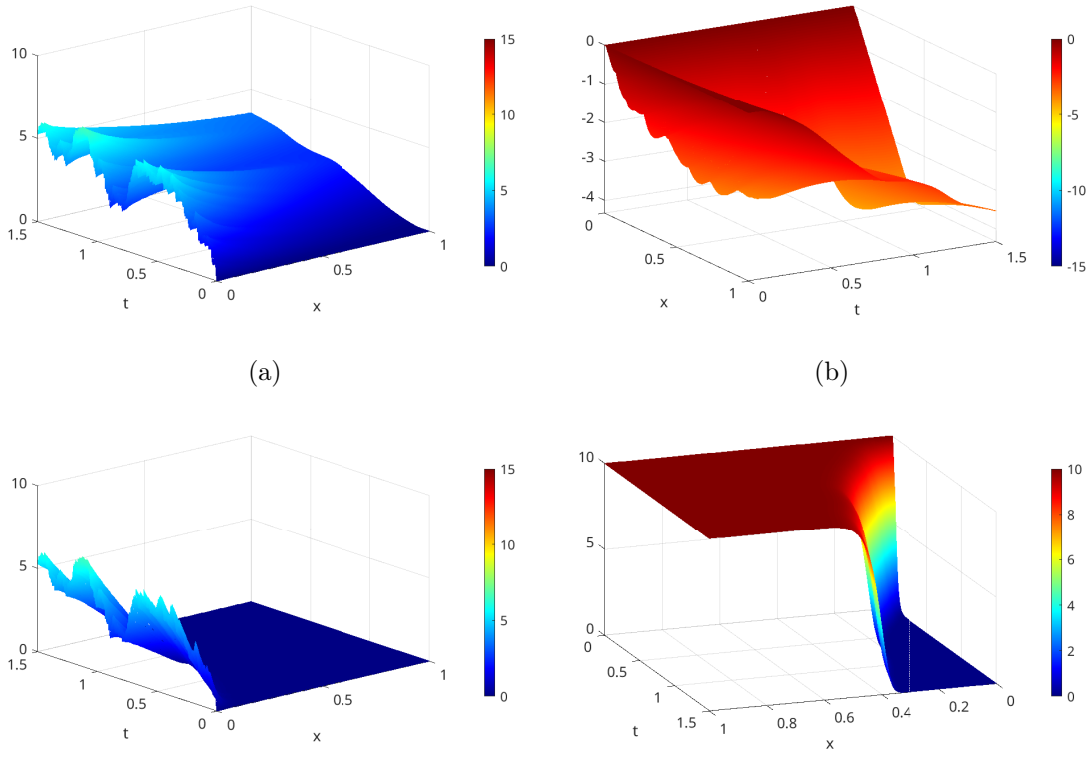

Figure 3.9: Different contributions to a single realization of the complete PDE with $\sigma_3 = 1$ in the accelerated configuration with $\lambda = \lambda_3 = 100$. First row: a pathwise random heat equation solution u (left) and the solution v of the non-linear equation (3.28) (right). Second row: the sulphur dioxide evolution $s = u + v$ (left) and the evolution of the calcite c.

3.3.2 Estimation results

In paragraph 3.3.1, we analysed a typical but single realization of the process at the boundary, to describe the evolution of the PDE-ODE system and the role of splitted solution (u, v).

Now we perform a statistical estimation of the dynamics for appreciating the variability of the process. We consider the estimation in $(t, x) \in [0, 1.5] \times [0, 1]$ by means of a sample $\overline{N} = 500$ trajectories of both processes ρ and c. Concerning the variability of the distribution, we provide the mean and the standard deviation of the empirical distribution at each point of the mesh: for any $(n, m) \in \{0, 1, \dots, N\} \times \{0, 1, \dots, M\}$ and the occurrences $\omega_j \in \Omega$, $j = 1, 2, \dots, \overline{N}$,

$$\overline{\rho}_m^n = \frac{1}{\overline{N}} \sum_{j=1}^{\overline{N}} \rho_m^n(\omega_j), \quad \overline{c}_m^n = \frac{1}{\overline{N}} \sum_{j=1}^{\overline{N}} c_m^n(\omega_j),$$

and

$$[S_\rho]_m^n = \sqrt{\frac{1}{\overline{N} - 1} \sum_{j=1}^{\overline{N}} (\rho_m^n(\omega_j) - \overline{\rho}_m^n)^2}, \quad [S_c]_m^n = \sqrt{\frac{1}{\overline{N} - 1} \sum_{j=1}^{\overline{N}} (c_m^n(\omega_j) - \overline{c}_m^n)^2},$$

In particular, we discuss the case $\sigma_3 = 1$, i.e. the highest level of noise, for both slow and fast regimes.

Figures 3.10, 3.11 present the mean distribution for the slow case $\lambda = \lambda_1 = 1$ and the accelerated $\lambda_3 = 100$ for ρ_s and c respectively. We present results with a different angulation, to better capture the dynamics of the solutions. One can appreciate the fact that the mean distribution has the same shape as the single trajectories previously described. Notably, the mean distribution of the process at the boundary tends to the mean level $\gamma = 1$.

The standard deviation distribution for (ρ_s, c) is captured in figures 3.12,3.13, again for slow and fast regimes and the highest level of noise $\sigma_3 = 1$. For the slow regime (Figures 3.12a,3.13a), the variability is low for both distributions. On the other hand, for the accelerated configuration (Figures 3.12b,3.13b), it is notable that the order of magnitude of the standard deviation for ρ_s is the same as the slower case; concerning the calcium carbonate, the orders are quite different: precisely, in the fast regime is one order bigger. Focusing on (3.13), one can appreciate the different behaviour of the variance for the calcite: in the slow regime the variability is concentrated at the boundary and slowly decades within the domain, whereas, for the faster configuration $\lambda_3 = 100$, the variance is always zero except for an interval around the forming front. It seems that the spatial distribution of the variance is always the same but with a time-dependent translation. This is interesting and it is worth performing further experiments to identify a possible invariant distribution around the moving front.

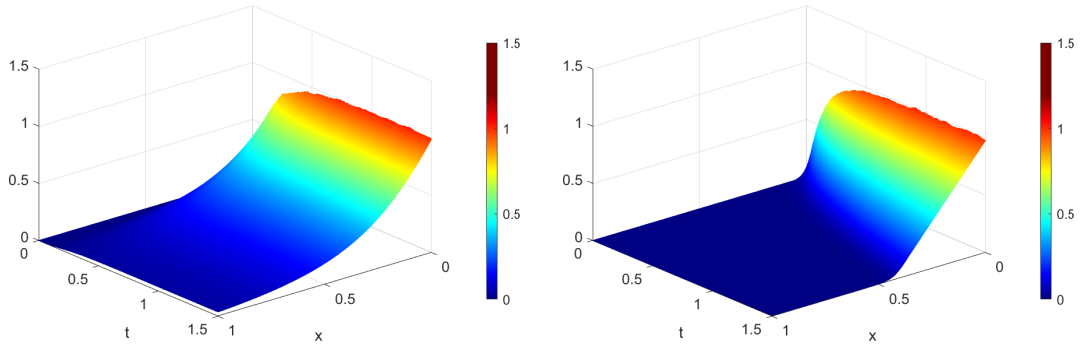

(a) (b)

Figure 3.10: Mean distribution for ρ_s with $\sigma_3 = 1$. Slow reaction (left), Fast reaction (right)

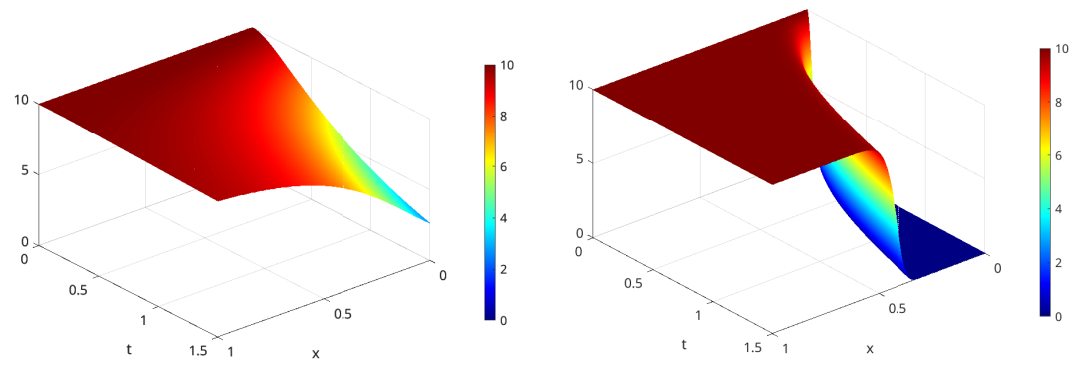

(a) (b)

Figure 3.11: Mean distribution for c with $\sigma_3 = 1$. Slow reaction (left), Fast reaction (right)

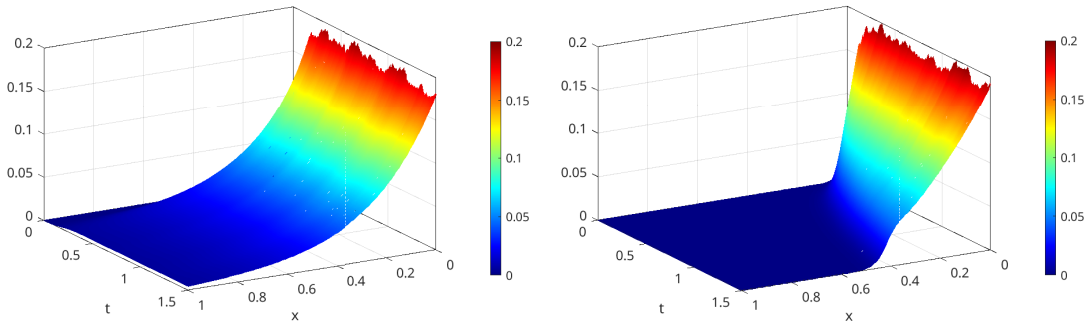

(a) (b)

Figure 3.12: Standard deviation distribution for ρ_s, with $\sigma = 1$. Slow reaction (left), Fast reaction (right)

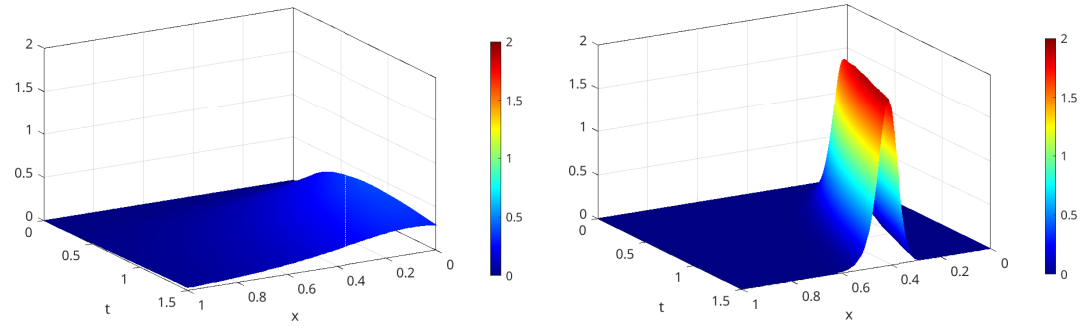

(a) (b)

Figure 3.13: Standard deviation distribution for c, with $\sigma = 1$. Slow reaction (left), Fast reaction (right)

Figure 3.14,3.15 presents a graph of the 25%, 50% and 75% percentile of the sample for each grid point. Hence, the figure shows the intervals of the usual points of the distribution, which means the intervals within which the central 50% of the distribution is located. We compare the case of $\sigma_3 = 1$, for both the slow reaction with $\lambda_1 = 1$ and the fast reaction case with $\lambda_3 = 100$. We observe that, after a small time interval, all the percentiles at the boundary oscillate around some fixed points; in particular, the median oscillates around $\gamma = 1$. This suggests the existence of an invariant measure, coherently with the invariant measure of the Pearson process at the boundary with unitary mean as in (2.17). For the slow regime $\lambda_1 = 1$, from Figures 3.14a,3.15a, the variability in $t = 0$ is not detected but increases over time. Furthermore, fluctuations around the median are stronger close to the boundary, even though they are present almost everywhere. This is coherent with the evidence from the standard deviation analysis in Figures 3.12a,3.13a.

A different scenario comes up in the case of the fast reaction (Figs 3.14b,3.15b): the transition zone gets smaller and it is located at the boundary; the interior is not touched by the sulphur dioxide penetration. As previously mentioned, the formation of a front is visible and the variability is detectable, even if is very small. This underlines that, even with a random process at the boundary, the mean behaviour is very close to the deterministic one presented in [9]. In the next paragraph, we quantify the difference between the deterministic solution and the mean behaviour of the random one.

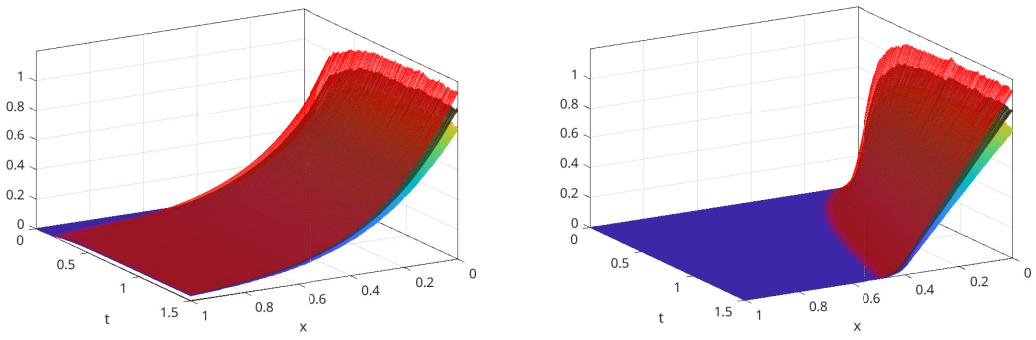

(a) (b)

Figure 3.14: Estimation of the distribution : 25% (green-blue), 50% (black) and 75% (red) percentile of an $\overline{N} = 500$ sample of the processes ρ_s at each mesh point. Parameters: $A = 0.2$, $\sigma_3 = 1$. (a) slow reaction $\lambda_1 = 1$; (b) fast reaction $\lambda_3 = 100$.

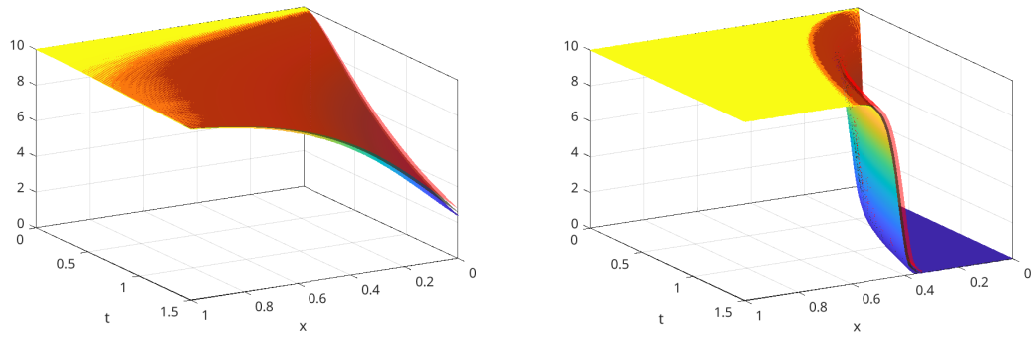

(a) (b)

Figure 3.15: Estimation of the distribution : 25% (green-blue), 50% (black) and 75% (red) percentile of an $\overline{N} = 500$ sample of the processes c at each mesh point. Parameters: $A = 0.2$, $\sigma_3 = 1$. (a) slow reaction $\lambda_1 = 1$; (b) fast reaction $\lambda_3 = 100$.

Comparison with deterministic solution: impact of the boundary

From paragraph 3.3.2, it can be observed that the average behaviour of numerical solutions tends to the deterministic one described in Section 1.2.2. In the following, we would like to quantify the impact of the noise on the solutions in terms of the computation of an $L^1(\Omega)$ distance between the deterministic solution $(\rho_{\sigma_0}, c_{\sigma_0})$ and the noise solutions (ρ_σ, c_σ), both for slow and fast reactions.

More specifically, the couple solution $(\rho_{\sigma_0}, c_{\sigma_0})$ refers to the solution where the level of noise σ is set to be zero. Therefore, just the drift part in the process survives and the boundary condition is given in Fig 3.16: here, the time asymptotic limit behaviour towards the mean level $\gamma = 1$ is illustrated.

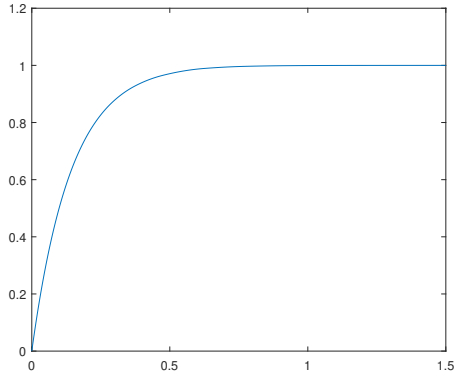

Figure 3.16: Boundary condition for $\sigma = 0$, $\lambda_1 = 1$ for the solutions ρ_s. Other parameters are listed in table 3.1.

Figures 3.17 and 3.18 illustrate the L^1-distance between the random solutions (ρ_s, c) under varying levels of σ and the corresponding deterministic solution in the slow regime. It is observed that the difference increases with the noise level σ, but the impact of the noise on the solution remains confined to the boundary and remains small.

A similar behaviour is evident in the fast regime. Specifically, Figure 3.19 demonstrates that the magnitude of the error for ρ_s remains comparable to the one observed in the slow regime. Meanwhile, Figure 3.20 depicts the formation of a front across all three noise configurations. Consistent with the estimates provided in Section 3.3.2, it is evident that higher noise levels lead to greater variability in the distributions.

Following the approach in [52][113], we present a different quantitative analysis of the impact of boundary randomness on the numerical solutions $(\rho_{\sigma_i}, c_{\sigma_i})$, $i = 1, 2, 3$, accordingly with Table 3.1. Specifically, we would like to measure the difference between the solution with a random boundary condition and the solution with a deterministic boundary, where no noise is introduced. Again, we vary the level of noise σ in the discretization of the stochastic boundary condition and, for each level of σ, we compute the root mean square

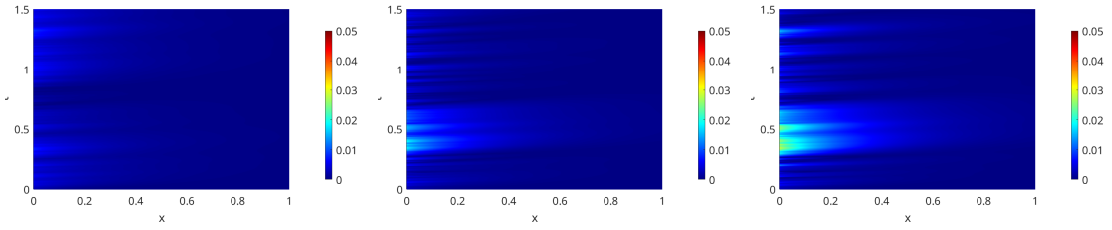

(a) $\sigma = 0.25$ (b) $\sigma = 0.7$ (c) $\sigma = 1$

Figure 3.17: Comparison in terms of L^1-distance of the mean trajectories of ρ_s with deterministic processes $\lambda = 1$. $\sigma_2 = 0.25$; $\sigma_2 = 0.7$; $\sigma_3 = 1$.

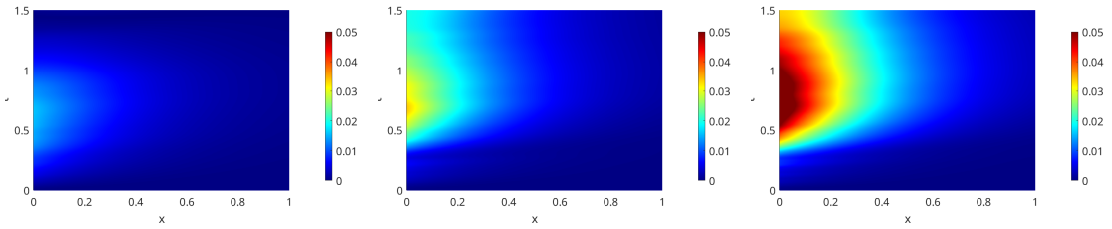

(a) $\sigma = 0.25$ (b) $\sigma = 0.7$ (c) $\sigma = 1$

Figure 3.18: Comparison in terms of L^1-distance of the mean trajectories of c with deterministic processes $\lambda = 1$. $\sigma_2 = 0.25$; $\sigma_2 = 0.7$; $\sigma_3 = 1$.

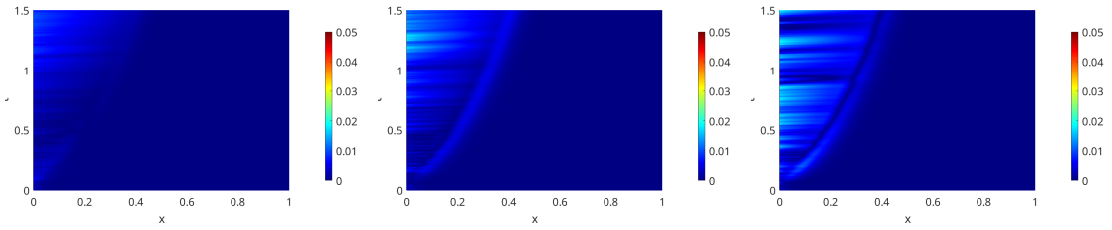

(a) $\sigma = 0.25$ (b) $\sigma = 0.7$ (c) $\sigma = 1$

Figure 3.19: Comparison in terms of L^1-distance of the mean trajectories of ρ_s with deterministic processes $\lambda = 100$. $\sigma_2 = 0.25$; $\sigma_2 = 0.7$; $\sigma_3 = 1$.

difference ($RMSD$) between the numerical solution with noise at the boundary and the deterministic one.

Accordingly to the set of parameters for the SDE at the boundary listed in Table 3.1, we compute the root mean squared difference between the numerical solutions $(\rho_{\sigma_i}, c_{\sigma_i})$, $i = 1, 2, 3$ of the original system and the deterministic solution $(\rho_{\sigma_0}, c_{\sigma_0})$ in the

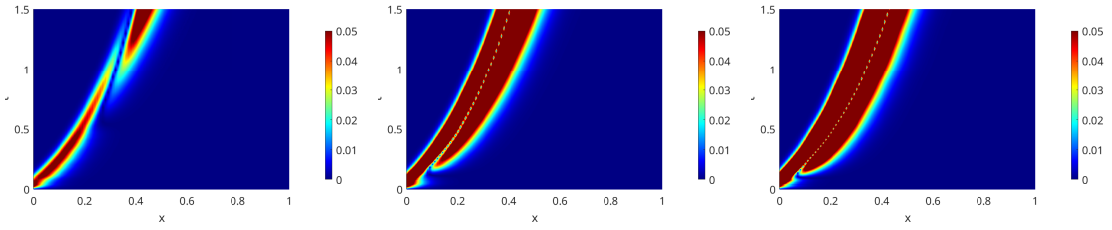

(a) $\sigma = 0.25$ (b) $\sigma = 0.7$ (c) $\sigma = 1$

Figure 3.20: Comparison in terms of L^1-distance of the mean trajectories of c with deterministic processes $\lambda = 100$. $\sigma_2 = 0.25$; $\sigma_2 = 0.7$; $\sigma_3 = 1$.

following metric, for $i = 1, 2, 3$:

$$RMSD(\rho_{\sigma_i}, \rho_{\sigma_0})(t, x) = \sqrt{\mathbb{E}\left[|\rho_{\sigma_i}(t, x) - \rho_{\sigma_0}(t, x)|^2\right]},$$
$$RMSD(c_{\sigma_i}, c_{\sigma_0})(t, x) = \sqrt{E\left[|c_{\sigma_i}(t, x) - c_{\sigma_0}(t, x)|^2\right]}.$$

We present in the following the color-maps for different configurations of σ for the solution $(\rho_{\sigma_i}, \rho_{\sigma_0})$ where $\sigma_1 = 0.25, \sigma_2 = 0.7, \sigma_3 = 1.2$ and we observe how the randomness behave within the space x in time t.

The effect of the boundary randomness increases whenever the level of the parameter σ is higher: however, the mean of the difference between the realization of the solution with stochastic boundary condition and the one with deterministic one rapidly goes to zero. From the color-bar one can notice that for the solution ρ_s in Fig 3.21, the difference is almost zero everywhere for the configuration with $\sigma = 0.25, 0.7$. The impact of the boundary is significant only in the last configuration where $\sigma = 1$. On the other hand, when looking at the color-maps for the calcite in the slow regime (Figure 3.22, there is no significative impact of the randomness at the boundary. This is because the effect of the stochasticity for c is mitigated by the exponential function.

In the accelerated configuration with $\lambda = 100$ (see Figures 3.23,3.24), the behaviour of the solutions exhibits significant changes compared to previous configurations. Notably, the influence of the boundary on the sulphur dioxide concentration, ρ_s is markedly different. This happens because, under the accelerated reaction regime, nearly all the sulphur dioxide concentration becomes localized at the boundary. The boundary's influence is substantial, even for small values of the parameter σ, but it rapidly vanishes as one moves further into the interior of the spatial domain.

In contrast, when examining the impact on the calcite concentration, the effect shifts toward the interior of the spatial domain. This indicates that, asymptotically, the evolution of the calcite forms a distinct front. This front represents a sharp boundary where one can clearly distinguish between the region where the calcite is entirely degraded, with

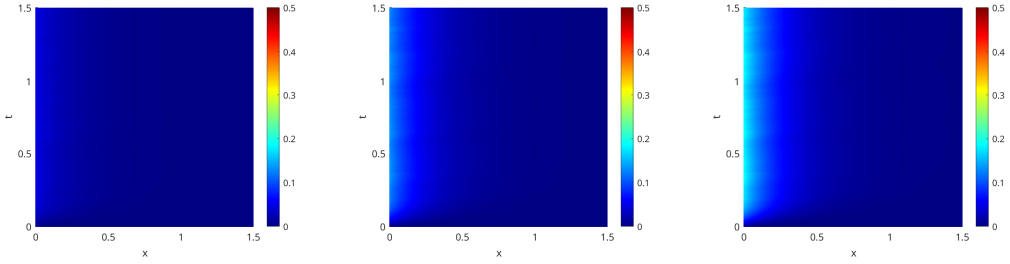

(a) (b) (c)

Figure 3.21: Estimation of the impact of the noise at the boundary: $RMSD(\rho_\sigma, \rho_{\sigma_0})$ at each mesh point for $\sigma = 0.25$ (a), $\sigma = 0.7$ (b) and $\sigma = 1$ (c). Parameters: $A = 0.2$, slow reaction $\lambda_1 = 1$

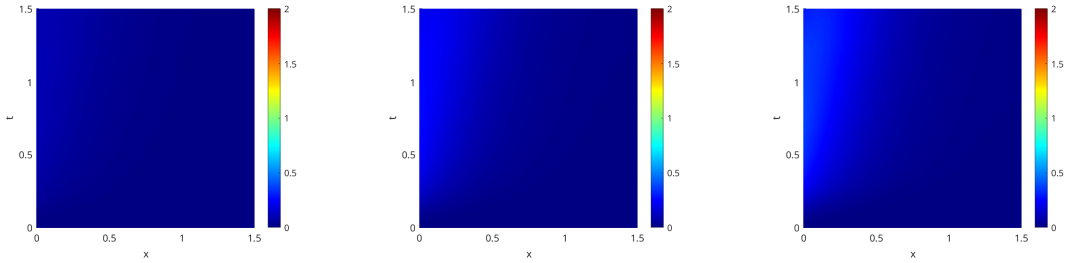

(a) (b) (c)

Figure 3.22: Estimation of the impact of the noise at the boundary: $RMSD(c_\sigma, c_{\sigma_0})$ at each mesh point for $\sigma = 0.25$ (a), $\sigma = 0.7$ (b) and $\sigma = 1$ (c). Parameters: $A = 0.2$, slow reaction $\lambda_1 = 1$

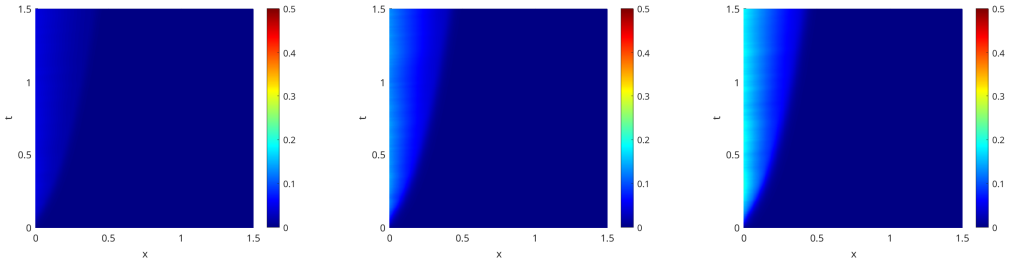

(a) (b) (c)

Figure 3.23: Estimation of the impact of the noise at the boundary: $RMSD(\rho_\sigma, \rho_{\sigma_0})$ at each mesh point for $\sigma = 0.25$ (a), $\sigma = 0.7$ (b) and $\sigma = 1$ (c). Parameters: $A = 0.2$, fast reaction $\lambda_1 = 100$.

concentration $c = 0$, and the region where the calcite retains its initial concentration value, $c = 10$.

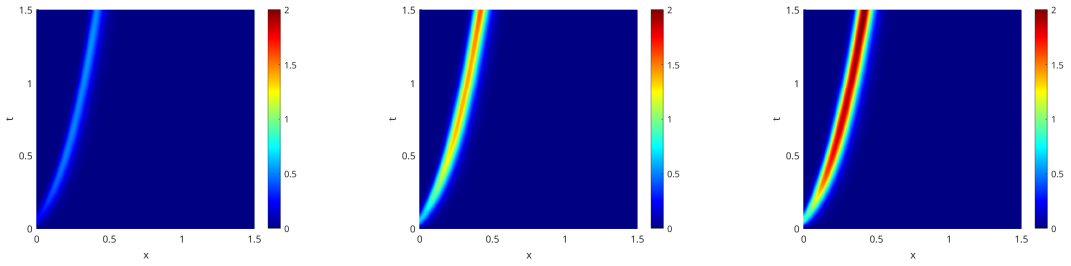

(a) (b) (c)

Figure 3.24: Estimation of the impact of the noise at the boundary: $RMSD(c_\sigma, c_{\sigma_0})$ at each mesh point for $\sigma = 0.25$ (a), $\sigma = 0.7$ (b) and $\sigma = 1$ (c). Parameters: $A = 0.2$, fast reaction $\lambda_1 = 100$.

Finally, it should be emphasized that the impact of the front is higher whenever the level of σ increases: from Fig 3.22 to Fig. 3.24 one can notice the change in the squared mean difference.

3.3.3 Pathwise Accuracy

In the context of numerical analysis, the concept of *rate of convergence* is defined as how fast the discretized solution converges to the exact solution of the original problem. Formally, the rate of convergence is defined as the order of accuracy of the numerical method.

When dealing with partial differential equations, the definition of accuracy order should involve both spatial and time steps [109]. Let $\Omega = [0, \bar{x}]$ be the spatial domain, and Δ_x, Δ_t be respectively the space and time steps of the discretization on the grid. Then, for $t \in [0, T]$ the *pointwise convergence rate* for a difference scheme approximating a partial differential equation is defined in the following way:

Definition 3.3 (Pointwise convergence rate, [109])**.** A difference scheme $L_m^n z_m^n = G_m^n$ approximating the partial differential equation $\mathcal{L}w = F$ is a pointwise convergent scheme of order (p, q) if for any t, as $(n+1)\Delta t$ converges to t,

$$\|z^{n+1} - w^{n+1}\|_{L^2(\Omega)} = \mathcal{O}(\Delta_x^p) + \mathcal{O}(\Delta_t^q) \tag{3.42}$$

as Δx and Δt converge to 0.

In other words, when addressing time-dependent problems, both the contributions in time and space must be considered.

Remark 3.3. It should be noted that the notation $\mathcal{O}(\Delta_x^p + \Delta_t^q)$ always involved a constant C . More specifically, Definition 3.3 implies that there exists a constant C such that

$$\|z^{n+1} - w^{n+1}\| \leq C(\Delta_x^p + \Delta_t^q)$$

Moreover, C will depend on time in this case.

In the context of parabolic problems, there is a strong relationship between Δ_t and Δ_x due to the stability conditions of the method. It is essential that these constraints are respected to achieve a convergence rate (p, q) consistent with the stability estimates. Consequently, this may require working with very small discretization values.

When the exact solution w is unknown there are two possible approaches in the investigation of the discrepancy between the numerical solution and the classical (3.42): the first one is to compute a numerical reference solution with a very small discretization step and treat it as the *real* solution. This could be expansive in terms of numerical computational costs. The second approach consists of comparing the ratio of consecutive solutions obtained by reducing the discretization step by half.

Thus, following [75], to derive the *rate of accuracy* for our proposed numerical scheme and to avoid high computational costs, we compare the ratios of two successive different solutions by decreasing the discretization step $\delta = \Delta_x$ at each simulation. Moreover, we fix the time step Δ_t and we calculate the order p for the time discretization at final time T. From now on we omit the dependence $n + 1$:

$$\|z_T^{\delta} - z_T^{\delta/2}\|_{\Delta_x} \leq C(\delta^p)$$

Here, $\|\cdot\|_{\Delta_x}$ is the Euclidean norm in space defined in (3.25).

We ensure that the difference decays to zero with the same speed as the actual error $\|z_T^\delta - w_T\|_{\Delta_x}$:

$$\begin{aligned}
\left\|z_T^\delta - z_T^{\delta/2}\right\|_{\Delta_x}^2 &= \frac{1}{M}\sum_{i=1}^{M}\left(z_T^\delta - z_T^{\delta/2}\right)^2 \\
&= \frac{1}{M}\sum_{i=1}^{M}\left(z_T^\delta - w_T + w_T - z_T^{\delta/2}\right)^2 \\
&\leq \frac{1}{M}\sum_{i=1^M}\left(\left(z_T^\delta - w_T\right)^2 + \left(w_T - z_T^{\delta/2}\right)^2\right) \\
&= \frac{1}{M}\sum_{i=1}^{M}\left(z_T^\delta - w_T\right)^2 + \frac{1}{M}\sum_{i=1}^{M}\left(w_T - z_T^{\delta/2}\right)^2 \\
&\leq C\delta^{2p} + C\left(\frac{\delta}{2}\right)^{2p}
\end{aligned} \tag{3.43}$$

By introducing the following definition, we would like to generalize the definition of *accuracy order* for every realization of the process at the boundary. Specifically, we aim to estimate the magnitude of the error as the grid size decreases.

Definition 3.4. Let $z_T^\delta(\omega) = (s_T^\delta(\omega), c_T^\delta(\omega))$ be the numerical bivariate solution to system (3.33)-(3.34) associated to the spatial discretization δ and to the realization ω of the process at the boundary. The *spatial pathwise accuracy rate* p for a fixed time step Δ_t at final time T is defined as, for every $\omega \in \Omega$:

$$\gamma_z^\delta = \log_2\left(\frac{\left\|z_T^\delta(\omega) - z_T^{\delta/2}(\omega)\right\|_{\Delta_x}}{\left\|z_T^{\delta/2}(\omega) - z_T^{\delta/4}(\omega)\right\|_{\Delta_x}}\right) = p$$

Remark 3.4. The previous definition for the spatial accuracy rate p follows directly from (3.43):

$$\frac{\left\|z_T^\delta(\omega) - z_T^{\delta/2}(\omega)\right\|_{\Delta_x}}{\left\|z_T^{\delta/2} - z_T^{\delta/4}(\omega)\right\|_{\Delta_x}} = \frac{C\delta^p\left(1 + 2^{-p}\right)}{C\left(\frac{\delta}{2}\right)^p\left(1 + 2^{-p}\right)} = 2^p.$$

Thus, by taking the 2-logarithm, (3.43) is achieved.

The previous definition is in a *pathwise* sense: once we fix the trajectory at the boundary, we reduce to a deterministic problem.

Tables (3.2),(3.3) show the *pathwise spatial accuracy orders* accordingly to the definition (3.4) and the norms of two different solutions for fixed $\Delta_t = 1.907e-06$ for different values

of $\delta = \Delta_x$. Note that the time-step Δ_t here adopted satisfies the stability conditions (3.3)-(3.39) for every value δ involved in this analysis.

$\sigma = 0.25$				
δ	$\gamma^{\delta}_{\rho_s}$	$\|\rho^{\delta}_s - \rho^{\delta/2}_s\|_{\Delta_x}$	γ^{δ}_c	$\|c^{\delta} - c^{\delta/2}\|_{\Delta_x}$
0.1250	1.3035	0.01591	1.3300	0.1007
0.0625	1.1569	0.00649	1.1806	0.0400
0.0313	-	0.00292	-	0.0177
0.0156	-	-	-	-

Table 3.2: Pathwise spatial order of accuracy and norms of two consecutive solutions for ρ_s and c respectively. $\sigma_1 = 0.25$, $\lambda = 1$.

$\sigma = 1$				
δ	$\gamma^{\delta}_{\rho_s}$	$\|\rho^{\delta}_s - \rho^{\delta/2}_s\|_{\Delta_x}$	γ^{δ}_c	$\|c^{\delta} - c^{\delta/2}\|_{\Delta_x}$
0.1250	1.2889	0.01590	1.3317	0.0996
0.0625	1.1505	0.00651	1.1818	0.0396
0.0313	-	0.00293	-	0.0174
0.0156	-	-	-	-

Table 3.3: Pathwise spatial order of accuracy and norms of two different solutions for ρ_s, c respectively. $\sigma_3 = 1$, $\lambda = 1$.

Thus, as expected, the pathwise spatial accuracy order does not change with the level of the noise at the boundary. To ensure that the spatial accuracy order is independent of the choice of the trajectory at the boundary, we provide in Table 3.4. the values for $\gamma^{\delta}_{\rho_s}, \gamma^{\delta}_c$ for three different realizations ω_1, ω_2 and ω_3. In all the presented configurations, the pathwise accuracy order is shown to be greater than 1.

δ	$\|\rho_s^\delta - \rho_s^{\delta/2}\|_{\Delta_x}$			γ_ρ^δ		
	ω_1	ω_2	ω_3	ω_1	ω_2	ω_3
0.125	0.016	0.014	0.017	1.304	1.316	1.283
0.0625	0.006	0.006	0.007	1.157	1.167	1.146
0.03125	0.003	0.002	0.003			
0.015625						
Δ_x	$\|c^\delta - c^{\delta/2}\|_{\Delta_x}$			γ_c^δ		
	ω_1	ω_2	ω_3	ω_1	ω_2	ω_3
0.125	0.101	0.095	0.104	1.330	1.337	1.329
0.0625	0.040	0.037	0.041	1.181	1.185	1.180
0.03125	0.018	0.016	0.018			
0.015625						

Table 3.4: Numerical estimation of the Euclidean L^2 norms and the spatial accuracy order for three different random paths at the boundary for ρ and c at final time $T = 1$. Parameters: $\sigma_3 = 1, A = 0.2$ and $\lambda = 1$; other parameters in Table 3.1.

3.3.4 Local Truncation Error

The local truncation error (LTE) of a given numerical scheme verifies the consistency with the original PDE involved. It is defined by replacing in the finite difference formulation (FTCS) the true solution: since the latter does not satisfy the equation exactly, the discrepancy is called *Local Truncation Error*. Whenever the explicit solution is not given, a Taylor expansion of the continuous solution in the nodes of the discretization is considered.

Proposition 3.6. *Given the equi-partition of the space and time* (3.17) *and given the proposed FTCS scheme for the discretization of the solution* ($s = u + v,$) *in* (3.33)-(3.34)*, let us suppose that the stability conditions* (3.26)-(3.36) *hold. Then, the proposed scheme has order one in time and four in space.*

Proof. Given the PDE in (3.7)

$$\partial_t s = \partial_x^2 s + \frac{B}{2\varphi}\partial_x c \partial_x s - \frac{B\partial_t c}{\varphi} s + \lambda c s,$$

the local truncation error is defined by:

$$\begin{aligned}\tau(t,x) = &\frac{s(t+\Delta_t,x)-s(t,x)}{\Delta_t} - \frac{s(t,x+\Delta_x)-2s(t,x)+s(t,x-\Delta_x)}{\Delta_x^2} \\ &- \frac{B}{2\varphi(c(t,x))}\frac{c(t,x+\Delta_x)-c(t,x-\Delta_x)}{2\Delta_x}\frac{s(t,x+\Delta_x)-s(t,x-\Delta_x)}{2\Delta_x} \\ &+ \frac{B}{2\varphi(c(t,x))}\frac{c(t+\Delta_t,x)-c(t-\Delta_t,x)}{\Delta_t} s(t,x) - \lambda c(t,x)s(x,t).\end{aligned} \tag{3.44}$$

To determine the consistency, the exact continuous solutions $s(t,x), c(t,x)$ are replaced by their discrete values using Taylor expansions around (t_n, x_m):

$$\begin{aligned}
s(t_n+\Delta_t,x_m) &= s(t_n,x_m) + \Delta_t\partial_t s(t_n,x_m) + \frac{\Delta_t^2}{2}\partial_t^2 s(t_n,x_m) + \mathcal{O}(\Delta_t^3) \\
s(t_n,x_m+\Delta_x) &= s(t_n,x_m) + \Delta_x\partial_x s(t_n,x_m) + \frac{\Delta_x^2}{2}\partial_x^2 s + \frac{\Delta_x^3}{6}\partial_x^3 s + \mathcal{O}(\Delta_x^4) \\
s(t_n,x_m-\Delta_x) &= s(t_n,x_m) - \Delta_x\partial_x s(t_n,x_m) + \frac{\Delta_x^2}{2}\partial_x^2 s + \frac{\Delta_x^3}{6}\partial_x^3 s - \mathcal{O}(\Delta_x^4) \\
c(t_n,x_m+\Delta_x) &= c(t_n,x_m) + \Delta_x\partial_x c(t_n,x_m) + \frac{\Delta_x^2}{2}\partial_x^2 c + \frac{\Delta_x^3}{6}\partial_x^3 c + \mathcal{O}(\Delta_x^4) \\
c(t_n,x_m-\Delta_x) &= c(t_n,x_m) - \Delta_x\partial_x c(t_n,x_m) + \frac{\Delta_x^2}{2}\partial_x^2 c + \frac{\Delta_x^3}{6}\partial_x^3 c - \mathcal{O}(\Delta_x^4)
\end{aligned}$$

Thus

$$\frac{s(t_n,x_m+\Delta_x)-2s(t_n,x_m)+s(t_n,m_x-\Delta_x)}{\Delta_x^2} = \partial_x^2 s + \mathcal{O}(\Delta_x^2)$$

For the sake of simplicity in notation, in the following, we write $s_m^n = s(t_n, x_m)$, $c(t_n, x_m) = c_m^n$ and $\varphi_m^n = \varphi(c(t_n, x_m))$. Going back to the definition of local truncation error (3.44) and pushing the Taylor expansions within the formula we get:

$$\begin{aligned}
&\tau(t_n, x_m) = \frac{s_m^n}{\Delta_t} + \partial_t s_m^n + \mathcal{O}(\Delta_t) - \frac{s_m^n}{\Delta_t} - \partial_x^2 s_n^n + \mathcal{O}(\Delta_x^2) \\
&- \frac{B}{2\varphi_m^n}\left(\frac{c_m^n}{2\Delta_x} + \frac{\partial_x c_m^n}{2} - \frac{c_m^n}{2\Delta_x} + \frac{\partial_x c_m^n}{2} + \mathcal{O}\left(\frac{\Delta_x^2}{2}\right)\right) \cdot \left(\frac{s_m^n}{2\Delta_x} + \frac{\partial_x s_m^n}{2} - \frac{s_m^n}{2\Delta_x} + \right. \\
&\left. + \frac{\partial_x s_m^n}{2} + \mathcal{O}\left(\frac{\Delta_x^2}{2}\right)\right) + \frac{B}{\varphi_m^n}\left(\frac{c_m^n}{2\Delta_t} + \frac{\partial_t c_m^n}{2} - \frac{c_m^n}{2\Delta_t} + \frac{\partial_t c_m^n}{2} + \mathcal{O}\left(\frac{\Delta_t^2}{2}\right)\right) s_m^n - \lambda c_m^n s_m^n \\
&= \partial_t s_m^n + \mathcal{O}(\Delta_t) - \partial_x^2 s_m^n + \mathcal{O}(\Delta_x^2) - \left(\partial_x c_m^n + \mathcal{O}(\Delta_x^2)\right)\left(\partial_x s_m^n + \mathcal{O}(\Delta_x^2)\right) \\
&\quad + \frac{B}{\varphi_m^n}\left(\partial_t c_m^n + \mathcal{O}\left(\frac{\Delta_t}{2}\right)\right) s_m^n - \lambda c_m^n s_m^n \\
&= \partial_t s_m^n - \partial_x^2 s_m^n - \frac{B}{\varphi_m^n}\left(\partial_x c_m^n \partial_x s_m^n\right) + B(-\lambda c_m^n s_m^n) s_m^n - \lambda c_m^n s_m^n + \\
&\quad + \mathcal{O}(\Delta_t) + s_m^n \mathcal{O}(\Delta_t) + \mathcal{O}(\Delta_x^2)(1 + \partial_x c_m^n + \partial_x s_m^n) + \mathcal{O}(\Delta_x^4)
\end{aligned}$$

Where the last equality is obtained by rearranging terms.

What we gained is exactly the continuous equation evaluated in the nodes of the time-space discretization. We need to deal with the infinitesimal terms to determine the order of consistency in time and space respectively. Since $\partial_x c_m^n$ and $\partial_x s_m^n$ depends on the space step Δ_x, then

$$\mathcal{O}(\Delta_x^2)(1 + \partial_x c_m^n + \partial_x s_m^n) \simeq \mathcal{O}(\Delta_x^2)\left(1 + \frac{C}{\Delta_x}\right) \simeq \mathcal{O}(\Delta_x^2) + \mathcal{O}(\Delta_x).$$

Thus the spatial step is governed by the term $\mathcal{O}(\Delta_x^4)$, whereas the time step is governed by the $\mathcal{O}(\Delta_t)$ term.

Therefore, following the classical definition of local truncation error, we have shown that the numerical scheme has consistency order 1 in time and order 4 in space discretization. □

3.3.5 Other simulation results

In this section, we propose the first analysis of the numerical simulation for the system (3.1) with initial condition (3.2) and boundary condition given by the solution of the stochastic process as in (3.3) that we have conducted. These first results are presented in [6] and constitute our first numerical approach for the discretization of the random system.

Indeed, we propose a numerical scheme which combines the finite element scheme previously introduced and presented in Appendix A for the numerical approximation of the original system (3.1). Give the discrete realization of the process at the boundary $\{\widetilde{\psi}^n\}_n(\omega)$, $\omega \in \Omega_P$ via the LSST scheme discussed in Section (2.2), the couple of solutions (ρ_s, c) is discretized via finite elements in space and a θ-Eulero method in time.

Numerical simulations are performed in the domain $[0, \bar{x}] \times [0, T] = [0, 1] \times [0, 1]$, letting $\rho_s(0, x) = 1$, $c_0 = 10$ and assuming the parameters values as in Table 1.1. More precisely, we firstly discretize the $\bar{N} = 500$ solutions of the process for the boundary condition by the LSST scheme proposed in (2.29) and, for each realization, we solve the deterministic system (3.1) via finite elements.

It is important to underline that the stability conditions found in Proposition (1.1) still apply *pathwise* for the finite elements with stochastic boundary conditions; hence if we fix the trajectory at the boundary, we exploit the positivity and the boundedness of the solutions of the diffusion process to ensure the stability of the numerical scheme.

The parameters for the process at the boundary (2.2) are set to be: $\alpha = 0.22, \gamma = 1, \sigma = 0.1, \eta = 2$. Note that, in this first study, we consider a mean reversion model for the concentration density value ρ_s. We provide, as in [9] and in Section 1.2, simulation results both for a slow reaction rate $\lambda = 0.01$ and a fast reaction rate $\lambda = 100$. Note that, in the actual settings in (3.1), the parameter λ has the same order of magnitude of the coefficient $\frac{\bar{A}}{m_c}$ in the settings (1.5)-(1.6). Thus, coherently with the physical parameters in Table (1.1) this is equivalent to considering the cases where $\lambda = 0.01$ and $\lambda = 100$ respectively.

In Figures (3.25)-(3.26) we show two stochastic solutions (sample paths), the mean behaviour out of $\bar{N} = 500$ trajectories and the interval between 5% and 95% percentiles of the (space or time) marginal at point x or time t.

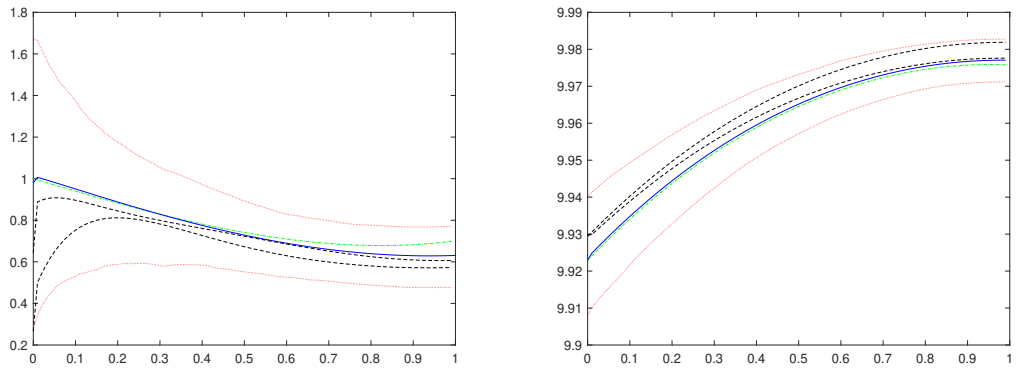

Figure 3.25: Stochastic solution at $t = 0.5$ with $\lambda = 0.01$. x-axis : $x \in [0, 1]$. Average Solution (solid line), 95% quantile bounds (dotted lines), some sample paths (dashed lines), and the deterministic solution (dashed-dotted line). Left: SO_2 concentration ρ; right: calcite density c.

Figure 3.25 shows the spatial evolution profile of the solution at time $t = 0.5$, in the case of slow reaction rate, that is with $\lambda = 0.01$. We can observe that while the average solution is comparable with the deterministic one, the variability upon the interface at $x = 0$ produces stochastic trajectories with higher variance close to the boundary and starts to reduce and stabilize just after $x = 0.5$. Single realizations of course may behave

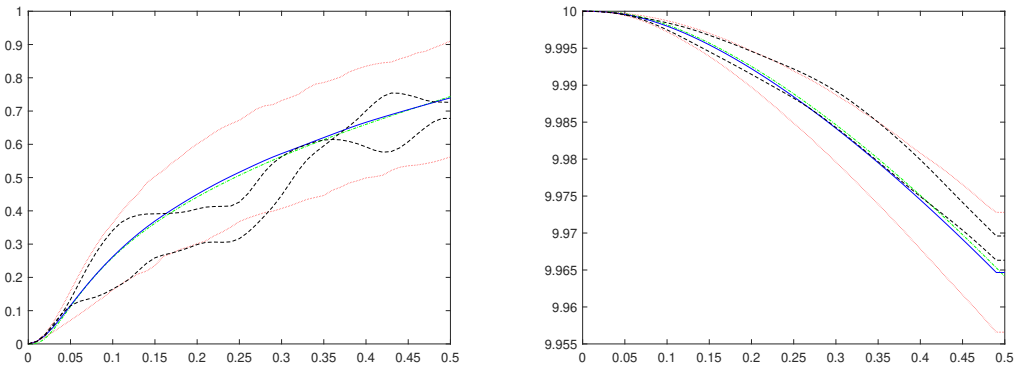

Figure 3.26: Stochastic solution time evolution with $\lambda = 0.01$ at the point $x = 0.5$. Average Solution (solid line), 95% quantile bounds (dotted lines), some sample paths (dashed lines), and the deterministic solution (dashed-dotted line). x-axis : $t \in [0, 0.5]$. Left: SO_2 concentration ρ; right: calcite density c.

differently in dependence on the initial condition at the boundary. Calcite is reduced at the boundary as well. Compared with the deterministic framework, what really changes is the speed of degradation in the sample path, although the average is similar. Variability emerges clearly from Figure 3.26, which shows the time evolution of the SO_2 concentration and calcite density at points $x = 0.5$. The deterministic solution is always in the 95% percentile interval, but the single trajectories exhibit highly smooth oscillations in time, due to the parabolicity of the PDE for s. The calcite profile exhibits variability in its velocity but not much in its shape.

As one could expect, from Figures 3.27-3.29 one can see that in the fast reaction case $\lambda = 100$ the qualitative behaviour, compared to the deterministic case, does not change in a significative way: the transition zone is smaller, so that the calcite deterioration is more important near the boundary of the sample; both in the deterministic case and in the stochastic case, at $t = 0.5$ the degradation in $[0, 0.2]$ is evident, while the interior of the (spatial) domain, i.e. $[0.5, 1]$, is not occupied by SO_2.

Still, in the fast reaction regime, the front formation is visible with a clearly reduced variability. From these first simulation results, we remark that, as one might expect, the introduction of stochasticity is more relevant at the beginning of the reaction and very close to the boundary.

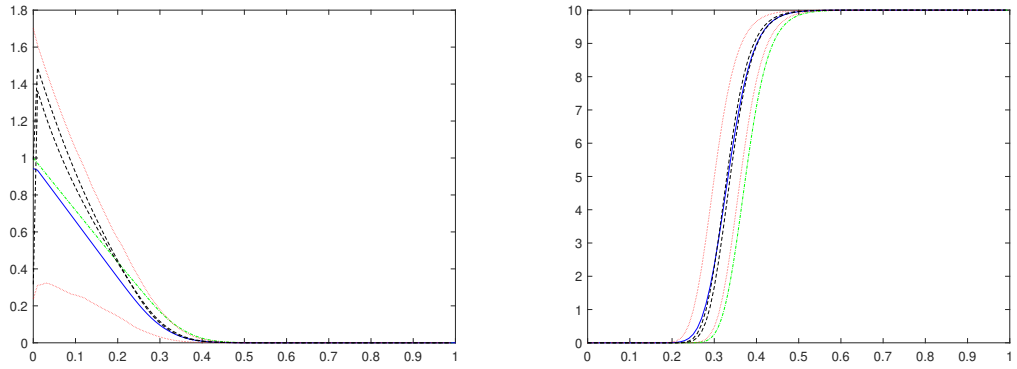

Figure 3.27: Stochastic solution at $t = 0.5$ with $\lambda = 100$. Average Solution (solid line), 95% quantile bounds (dotted lines), some sample paths (dashed lines), and the deterministic solution (dashed-dotted line). x-axis : $x \in [0, 1]$. Left: SO_2 concentration ρ; right: calcite density c.

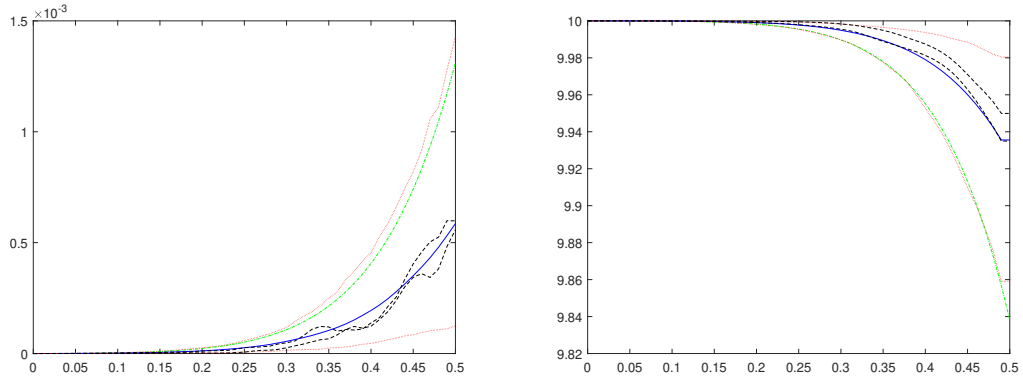

Figure 3.28: Stochastic time evolution with $\lambda = 100$ at the point $x = 0.5$. Average Solution (solid line), 95% quantile bounds (dotted lines), some sample paths (dashed lines), and the deterministic solution (dashed-dotted line). x-axis : $t \in [0, 0.5]$. Left: SO_2 concentration ρ; right: calcite density c.

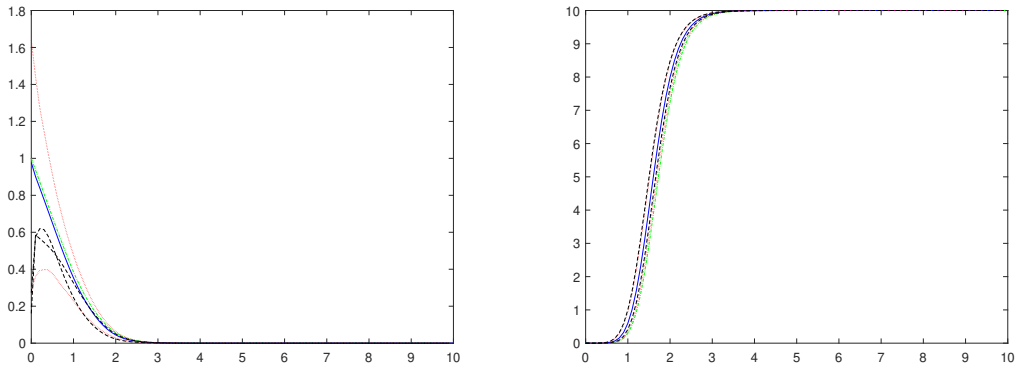

Figure 3.29: Front at $t = 10$ for the stochastic model. Average Solution (solid line), 95% quantile bounds (dotted lines), some sample paths (dashed lines), and the deterministic solution (dashed-dotted line). x-axis : $x \in [0, 10]$.Left: SO_2 concentration ρ; right: calcite density c.

Chapter 4

A convergence result for a semi-discrete approximation

In the final chapter of the thesis, we prove the convergence of a semi- discrete solution to the unique mild solution of the random PDE-ODE [5]. To this aim, we consider a semi-discrete version of the continuous system, where a space finite-difference approximation is assumed while the time remains continuous, coupled with (2.2) as a dynamical boundary condition.

Coherently with the numerical approximation of the problem presented in Section 3.2, we split the solution of the semi-discrete scheme (s, c) as $(u + v, c)$; here u is a solution to the semi-discrete heat equation in the positive lattice $\Omega_h^+ = h\mathbb{Z}_+$ coupled with the stochastic boundary condition. We derive the fundamental solution for this random heat equation in the lattice Ω_h^+ by an odd reflection technique starting from the fundamental solution in the whole space $\Omega_h = h\mathbb{Z}$. We explicitly express the solution of the boundary value problem in terms of the (difference) derivatives of the discrete heat kernel. Moreover we obtain some a priori estimates on the solution to the random discrete heat equation by exploiting, differently from [82], recent results on the discrete heat kernel in time-space Besov spaces [13]. Regarding the couple (v, c), we introduce a simplification strategy which consists in a sort of linearization of the whole system (following [90, 82]) which allows to prove an a priori bound for the L^2-norm of v and its discrete derivatives in the lattice.

The main convergence result is based on the previous a priori estimates, together with piecewise constant interpolation and compactness properties of time-space Besov spaces. More precisely we first prove that, given a weak solution of the semi-discrete problem, then it is also a mild solution. By considering piecewise constant interpolation and extension operators which are able to properly connect the solution on the lattice to the one on the continuum space, we finally prove the convergence of the semi-discrete solution to the unique mild solution of the random system (3.1)-(3.3).

4.1 Random PDE-ODE system: semi-discretization and splitting

In the following, we introduce the semi-discrete version of system (3.1) - (3.3) by a finite-difference approximation in space and continuous in time. We start by providing the general settings for our specific case.

Definition 4.1 (Discrete spaces and norms)**.** Let $h > 0$ and define the lattice of points as the set whose coordinates are integer multiples of h:

$$\Omega_h = h\mathbb{Z}, \quad \Omega_h^+ = h\mathbb{Z}_+, \quad \Omega_h^- = h\mathbb{Z}_-.$$

More specifically, $z \in \Omega_h$ if $z = (hn)$, $n \in \mathbb{Z}$. With the discrete topology and with the Lebesgue measure, for any integrable function $f : \Omega_h \to \mathbb{R}$, the following equivalence holds:

$$\int_{\Omega_h} f(z)dz = h \sum_{z \in \Omega_h} f(z)$$

One can also define the Lebesgue space $L^p(\Omega_h)$, with $p \in [1, +\infty]$, equipped with the norm

$$\|f\|_{L^p(\Omega_h)} := \left(h \sum_{i=0}^{\infty} |f(x)|^p \right)^{\frac{1}{p}}$$

Thus, for $f : \Omega_h \to \mathbb{R}$ or, equivalently, $f : \Omega_h^+ \to \mathbb{R}$, we can define the $L^2(\Omega_h)-$norm in the lattice as:

$$\|f\|_{2,\Omega_h} := \left(h \sum_{i=0}^{\infty} |f(x)|^2 \right)^{\frac{1}{2}},$$

while the supremum norm is usual denoted by $\|f\|_{L^\infty(\Omega_h)}$.

With $\mathcal{S}(\Omega_h)$ we refer to the Schwartz test function space defined on Ω_h, meaning the sequence descreasing at infinity less than any polynomial, and by $\mathcal{S}'(\Omega_h)$ its topological dual space, i.e. the set of functions defined on Ω_h with at most polynomial growth. Thus it is possible to define the Fourier transform. Given the $\mathcal{F}_h : \mathcal{S}(\Omega_h) \to C^\infty(\mathbb{T}_h)$, where $\mathbb{T}_h$ is the torus of length $\frac{2\pi}{h}$, i.e. $\mathbb{T}_h = \left[-\frac{\pi}{h}, \frac{\pi}{h}\right]$, which has the following form

$$\mathcal{F}_h(f)(x) := \hat{f}(x) = \int_{\Omega_h} e^{iz \cdot h} f(z)dz, \tag{4.1}$$

where $x \in \mathbb{T}_h$. In the usual way it is possible to define the inverse Fourier transform $\mathcal{F}_h^{-1} : C^\infty(\mathbb{T}_h) \to \mathcal{S}(\Omega_h)$

$$\mathcal{F}_h^{-1}(\hat{f})(z) := \frac{1}{(2\pi)} \int_{\mathbb{T}_h} e^{-iz \cdot x} \hat{f}(x)dh,$$

We can extend the Fourier transform $\mathcal{F}_h$, and the inverse Fourier transform $\mathcal{F}_h^{-1}$ from the space $\mathcal{S}'(\Omega_h)$ into $\mathcal{D}'(\mathbb{T}_h)$ (where $\mathcal{D}'(\mathbb{T}_h)$ is the space of distributions, i.e. the topological

dual of $C^\infty(\mathbb{T}_h)$), and from $\mathcal{D}'(\mathbb{T}_h)$ into $\mathcal{S}'(\Omega_h)$ respectively.
For simplicity reasons, in this chapter, we will denote the integral symbol also for spatial variables, except when it is strictly necessary. For the same reason, we continue to indicate lattice functions in the standard manner.

We recover the definitions of first-order finite forward and backward shift and differences operators to approximate the space-derivatives terms in the first equation of (3.1) in the one-dimensional case.

Definition 4.2 (Shift and finite-difference operators)**.** Given a smooth function $f : \Omega_h^+ \to \mathbb{R}$, the forward and backward *shift operators* for f are defined as:

$$\tau_h f(x) := f(x+h), \quad \tau_{-h} f(x) := f(x-h).$$

Furthermore, the backward and forward *finite difference operators* read as:

$$D_x^+ f(x) = \frac{f(x+h) - f(x)}{h}, \qquad D_x^- f(x) = \frac{f(x) - f(x-h)}{h}$$

while the *symmetric* discrete Laplacian is given by:

$$\Delta_x^D = \frac{1}{2}\left(D_x^+ D_x^- + D_x^- D_x^+\right). \tag{4.2}$$

Remark 4.1. There is a well-known relation between shift and finite-difference operators. Precisely, let $f : \Omega_h^+ \to \mathbb{R}$ be a smooth function, then

$$\begin{aligned} D_x^+ f &:= f(x+h) - f(x) = \tau_h f(x) - f(x) = (\tau_h - \mathcal{I}) f(x), \\ D_x^- f &:= f(x) - f(x-h) = f(x) - \tau_{-h} f(x) = (\mathcal{I} - \tau_{-h}) f(x) \end{aligned}$$

where $\mathcal{I}$ denotes the identity function.

Moreover,

$$D_x^+(\tau_{-h} f) = D_x^+(f(x-h)) = f(x) - f(x-h) = D_x^- f$$

Since the operators D_x^+ and D_x^- do not commute, the following Leibniz's rule for the discrete case is recalled for the convenience of the reader.

Lemma 4.1 (Leibniz's rule)**.** *For any $n \geq 0$ the following discrete Leibniz's rule holds:*

$$D_x^{+,n}(fg) := \sum_{j=0}^{n} \binom{n}{j} (D_x^{+,j} f)(D_x^{+,n-j} \tau_h^j g).$$

In particular, for $n = 1$ we get:

$$\begin{aligned} D_x^+(fg) &= f(D_x^+ g) + D_x^+ f \cdot (\tau_h g) \\ &= f(x)(g(x+h) - g(x)) + (f(x+h) - f(x))g(x+h) \end{aligned} \tag{4.3}$$

Symmetrically,

$$D_x^+(fg) = (D_x^+ f)g + (\tau_h f) D_x^+ g$$

Proof. See [68]. □

We now provide the semi-discrete version of the original system (3.1) by exploiting the finite-difference operators for the discretization in the lattice.

Proposition 4.1. *The system* (3.1) *can be rewritten by introducing the discrete Laplacian and finite differences as:*

$$\begin{cases} \frac{\partial}{\partial t}(\varphi s) = \varphi \Delta_x^D s + \frac{1}{2}[D_x^+ \varphi D_x^+ s + D_x^- \varphi D_x^- s] - \lambda \varphi s c, & \text{in } [0,T] \times \Omega_h^+ \\ \frac{\partial}{\partial t} c = -\lambda \varphi s c, & \text{in } [0,T] \times \Omega_h^+. \end{cases} \tag{4.4}$$

Proof. We should find a proper discretization for the term $\nabla \cdot (\varphi \nabla s)$. Applying the Leibniz's rule (4.3) for $D_x^+(\tau_{-h} f)$ we obtain:

$$\begin{aligned} D_x^-(fg) &= D_x^+(\tau_{-h}(fg)) = D_x^+(f(x-h)g(x-h)) \\ &= f(x-h) D_x^+ g(x-h) + D_x^+ f(x-h)(\tau_h g(x-h)) \\ &= f(x-h)(g(x) - g(x-h)) + (f(x) - f(x-h))g(x) \\ &= \tau_{-h} f \cdot D_x^- g(x) + D_x^- f \cdot g(x) \\ &= \tau_h g \cdot D_x^- f + D_x^- g \cdot f(x), \end{aligned}$$

where in the first line we have used the commutation property of the shift: $\tau_h(fg) = \tau_h(f)\tau_h(g)$.

Under these assumptions, let us calculate

$$\begin{aligned} D_x^+(\varphi D_x^- s)) &= \tau_h \varphi D_x^+(D_x^- s) + D_x^+ \varphi D_x^- s \\ &= \varphi(x+h)(D_x^+(s(x) - s(x-h))) + D_x^+ \varphi D_x^- s \\ &= \varphi(x+h)(D_x^+ s(x) - D_x^+(s(x-h))) + D_x^+ \varphi D_x^- s \\ &= \varphi(x+h)(D_x^+ s - D_x^- s) + D_x^+ \varphi D_x^- s \\ &= \varphi(x+h)\Delta_x^D s + D_x^+ \varphi D_x^- s. \end{aligned}$$

Symmetrically,

$$\begin{aligned} D_x^+(\varphi(D_x^- s)) &= (D_x^+ \varphi)\tau_h(D_x^- s) + \varphi D_x^+(D_x^- s) \\ &= D_x^+ \varphi(\tau_h(s(x) - s(x-h))) + \varphi D_x^+(s(x) - s(x-h)) \\ &= D_x^+ \varphi(\tau_h(s(x)) - \tau_h(s(x-h))) + \varphi(D_x^+ s(x) - D_x^+ s(x-h)) \\ &= D_x^+ \varphi(s(x+h) - s(x)) + \varphi(D_x^+ s(x) - D_x^- s(x)) \\ &= D_x^+ \varphi D_x^+ s + \varphi \Delta_x^D s. \end{aligned}$$

On the other hand

$$\begin{aligned} D_x^-(\varphi(D_x^+ s)) &= (\tau_{-h}\varphi)D_x^-(D_x^+ s) + D_x^-\varphi D_x^+ s \\ &= (\tau_{-h}\varphi)D_x^-(s(x+h) - s(x)) + D_x^-\varphi D_x^+ s \\ &= (\tau_{-h}\varphi)(D_x^- s(x+h) - D_x^- s(x)) + D_x^-\varphi D_x^+ s \\ &= (\tau_{-h}\varphi)\left(s(x+h) - s(x) - (s(x) - s(x-h))\right) + D_x^-\varphi D_x^+ s \\ &= (\tau_{-h}\varphi)(D_x^+ s - D_x^- s) + D_x^-\varphi D_x^+ s \\ &= \varphi(x-h)\Delta_x^D s + D_x^-\varphi D_x^+ s, \end{aligned}$$

and again,

$$\begin{aligned} D_x^-(\varphi D_x^+ s) &= (\tau_{-h}D_x^+ s)D_x^-\varphi + \varphi D_x^- D_x^+ s \\ &= \tau_{-h}(s(x+h) - s(x))D_x^-\varphi + \varphi D_x^-(s(x+h) - s(x)) \\ &= (\tau_{-h}s(x+h) - \tau_{-h}s(x))D_x^-\varphi + \varphi(D_x^- s(x+h) - D_x^- s(x)) \\ &= (s(x) - s(x-h))D_x^-\varphi + \varphi(D_x^+ s(x) - D_x^- s(x)) \\ &= D_x^- s D_x^-\varphi + \varphi\Delta_x^D s. \end{aligned}$$

Thus, two equivalent expressions for the $\nabla\cdot(\varphi\nabla s)$ term are gained:

$$\begin{aligned} \frac{1}{2}\left[D_x^+(\varphi D_x^- s) + D_x^-(\varphi D_x^+ s)\right] &= \frac{1}{2}[D_x^+\varphi D_x^+ s + D_x^-\varphi D_x^- s] + \varphi\Delta_x^D s \qquad (4.5) \\ \frac{1}{2}\left[D_x^+(\varphi D_x^- s) + D_x^-(\varphi D_x^+ s)\right] &= \frac{1}{2}[D_x^+\varphi D_x^- s + D_x^-\varphi D_x^+ s] + \frac{\varphi(x+h)+\varphi(x-h)}{2}\Delta_x^D s, \end{aligned}$$

where

$$\frac{\varphi(x+h)+\varphi(x-h)}{2} = \frac{\tau_h\varphi + \tau_{-h}\varphi}{2}.$$

By taking the first expression in (4.5), the semi-discrete system in (4.4) is achieved. □

From now on, we will adopt the first expression in (4.5) for the discretization of $\nabla\cdot(\varphi\nabla s)$ in system (3.1).

Remark 4.2 (The discrete Laplacian and a uniform homogeneous Markov chian). Let us recall that a stochastic process can be identified from its infinitesimal generator. Here, we focus on processes whose infinitesimal generator is the discrete Laplacian. We first note the following simple fact for our difference operator with $h = 1$:

$$\Delta^D f = \frac{f(x+1) - 2f(x) + f(x-1)}{2} = \frac{f(x+1) + f(x-1)}{2} - f(x),$$

where the first addendum on the right-hand side can be interpreted as the transition probabilities of a symmetric random walk.

Let us now introduce the symmetric random walk $\tilde{X}$ as a discrete time Markov chain with transition matrix $\tilde{P} = (p_{xy})_{xy}$ with $p_{xy} = 1/2$ when $y = x + h$ and $y = x - h$. It

is well-known that we can see the transition matrix $\tilde{P}$ as a linear operator on bounded measurable real functions f as:

$$\tilde{P}f(x) = \sum_y p_{xy}^{(n)} f(x) = \mathbb{E}_x[f(X_n)],$$

and the corresponding infinitesimal generator takes the form

$$A = \tilde{P} - I.$$

Let N be a homogeneous Poisson process on $\mathbb{R}_+$ with intensity $\lambda > 0$ and assume that N and $\tilde{X}$ are independent. We consider the process $X_t := \tilde{X}_{N(t)}$, usually called the uniform Markov chain. Its semigroup operator is given by

$$P(t) = \sum_{n=0}^{\infty} \exp(-\lambda t) \frac{(\lambda t)^n}{n!} \tilde{P}$$

and the corresponding generator assumes the form

$$L = \lambda(\tilde{P} - I).$$

Therefore, by choosing $\lambda = \frac{2}{h^2}$, the generator of X_t coincides with the discrete Laplacian operator:

$$\Delta^D f = Lf = \frac{2}{h^2}(\tilde{P} - I) = \frac{2}{h^2}\left[\frac{f(x+h) + f(x-h)}{2} - f(x)\right].$$

Finally, we can provide the semi-discretization version of the initial model (3.1). Accordingly to Chapter 3, let us stress that the porosity function φ defined in (3.4) is a linear function of the total amount of calcite c.

Proposition 4.2. *A discrete version in space and continuous in time of system* (3.1) *is given by:*

$$\partial_t s = \Delta^D s + b_c(t,x)\Big[D_x^+ c D_x^+ s + D_x^- c D_x^- s\Big] + \gamma_c B s^2 - \gamma_c s, \qquad \text{in } [0,T] \times \Omega_h^+ \quad (4.6)$$

$$\partial_t c = -\lambda \varphi s c, \qquad \text{in } [0,T] \times \Omega_h^+ \quad (4.7)$$

where $b_c(t,x) = \frac{1}{2}\frac{B}{A+Bc}$ *and* $\gamma_c = \lambda c$.

Proof. By deriving with respect to t and x we get:

$$\begin{aligned}\partial_t((A+Bc)s) &= (A+Bc)\Delta^D s + \frac{1}{2}[D_x^+(A+Bc)D_x^+ s + D_x^-(A+Bc)D_x^- s] \\ &\quad - \lambda(A+Bc)sc \\ &= (A+Bc)\Delta^D s + \frac{1}{2}\left[\frac{1}{h}(A+Bc(x+h)-(A+c(x)))D_x^+ s + \right. \\ &\quad \left. + \frac{1}{h}(A+Bc(x)-(A+c(x-h)))D_x^- s\right] - \lambda(A+Bc)sc \\ &= (A+Bc)\Delta^D s + \frac{1}{2}B\left[D_x^+ cD_x^+ s + D_x^- cD_x^- s\right] - \lambda(A+Bc)sc\end{aligned}$$

and by denoting $b_c(t,x) = \frac{1}{2}\frac{B}{A+Bc}$ and $\gamma_c = \lambda c$ we obtain the final expression for the dynamic of s (4.6). □

Coherently with the Chapter 3, we split the solution s of the first equation by the sum of two functions $v+u$, where u is the solution of the *discrete heat equation* and inherits the stochastic boundary condition, while v solves a non-linear equation coupled with u but with zero boundary condition.

Theorem 4.1. *Let us consider the system* (4.4) *and let* $s = u + v$ *where* u *is the solution of the following stochastic discrete heat equation:*

$$\begin{cases}\partial_t u = \Delta_x^D u & (t,x) \in [0,T] \times \Omega_h^+ \\ u(0,x) = 0, & x \in \Omega_h^+ \\ u(t,0) = \psi(t), & t \in [0,T]\end{cases} \tag{4.8}$$

with a discrete stochastic dynamical boundary condition $\psi(t)$ *at* $x = 0$ *and where* v *is the solution of the following non linear system:*

$$\begin{cases}\partial_t v = \Delta_x^D v + b_c(t,x)[D_x^+ cD_x^+ v + D_x^- cD_x^- v] - \gamma v & +b_c(t,x)[D_x^+ cD_x^+ u + D_x^- cD_x^- u] \\ \qquad -\gamma_c(t,x)u + \gamma_c(t,x)B(u+v)^2, & (t,x) \in [0,T] \times \Omega_h^+ \\ v(0,x) = s_0, & x \in \Omega_h^+ \\ v(t,0) = 0, & t \in [0,T]\end{cases} \tag{4.9}$$

Remark 4.3. Note that a possible reflecting boundary condition in (4.8) can be imposed in $x = X$ if we restrict to the space interval $[0,X] \subset \Omega_h^+, X < +\infty$:

$$\frac{1}{2}(D_x^+ + D_x^-)u(t,X) = 0, \quad t \in [0,T]$$

Proof. We split the solution $s = u + v$ and exploiting the linearity of the operator Δ_x^D and D_x^+, D_x^- we get:

$$\begin{aligned}\partial_t u + \partial_t v = \Delta_x^D u + \Delta_x^D v + b_c(t,x)\Big[D_x^+ c(D_x^+ u + D_x^+ v) + D_x^- c(D_x^- u + D_x^- v)\Big] \\ + \gamma_c(t,x)B(u^2 + 2uv + v^2) - \gamma_c(t,x)u - \gamma_c(t,x)v.\end{aligned}$$

We divide the problem into two different systems: the first one involves the discrete heat equation in u:

$$\partial_t u = \Delta_x^D u$$

and the second one involves all the terms in v and all the terms that are not in the previous equation:

$$\begin{aligned}\partial_t v = \Delta_x^D v + b_c(t,x)\Big[D_x^+ c D_x^+ v + D_x^- c D_x^- v\Big] - \gamma_c(t,x)v \\ + b_c(t,x)\Big[D_x^+ c D_x^+ u + D_x^- c D_x^- u\Big] + \gamma_c(t,x)B(u^2 + 2uv + v^2) - \gamma_c(t,x)u\end{aligned}$$

$$\begin{aligned}\partial_t v = \Delta_x^D v + \frac{b_c(t,x)}{2\varphi}[D_x^+ v D_x^+ \varphi + D_x^- v D_x^- \varphi] + \gamma B v^2 - \gamma v + 2\gamma B u v \\ + \frac{b_c(t,x)}{2\varphi}[D_x^+ u D_x^+ \varphi + D_x^- u D_x^- \varphi] + \gamma B u^2 - \gamma u\end{aligned}$$

Now we recover system (4.8) by equipping the heat equation with the stochastic dynamical boundary condition given by $\psi(t)$ and zero initial condition, while for system (4.9), we consider zero boundary condition and the non zero initial condition of the original system. □

4.2 Semi-discrete heat equation with stochastic boundary condition

In this section we study the semi-discrete heat equation, by explicitly calculating the fundamental solution and by deriving an explicit representation of the solution to the Initial Value Problem (IVP) and to the Boundary Value Problem (BVP).

4.2.1 Semi-discrete heat kernel

In analogy with the continuous case, we find a definition for the discrete heat kernel on the positive lattice Ω_h^+. Let us denote with $H^D(t,x)$ the fundamental solution for the discrete heat equation, then $H^D(t,x)$ solves the following problem on Ω_h:

$$\begin{cases}\partial_t H^D(t,x) = D_x^- D_x^+ H^D(t,x) & \text{in } [0,T]\times\Omega_h \\ H^D(0,x) = \delta_0(x) & \text{in } \Omega_h\end{cases} \tag{4.10}$$

where H^D is the transition probability associated with the process admitting the semigroup (4.2).

Lemma 4.2. *The discrete heat kernel on Ω_h^+ is obtained by an odd reflection of the fundamental solution $H^D(t,x)$ for the heat equation in Ω_h:*

$$G^D(t,x,y) = H^D(t,x-y) - H^D(t,x+y) \tag{4.11}$$

Proof. The proof follows the same procedure as in the continuous case: we start from the problem defined on the whole lattice and we construct an odd extension for the initial condition.

Let $u(t,x)$ be the solution of the heat equation on the lattice Ω_h:

$$\begin{cases} \dfrac{\partial u}{\partial t}(t,x) = \dfrac{1}{h^2}(u(t,x+h) - 2u(t,x) + u(t,x-h)) & \text{in } \Omega_h \\ u(0,x) = f(x) & \text{in } \Omega_h \end{cases}$$

Then $u(t,x)$ admits the following representation:

$$u(t,x) = h \sum_{y \in \Omega_h} H^D(t,x-y) f(y).$$

Now, let us consider the problem for a w defined on the positive reticle Ω_h^+:

$$\begin{cases} \frac{\partial w}{\partial t}(t,x) = \frac{1}{h^2}(w(t,x+h) - 2v(t,x) + w(t,x-h)) & \text{in } \Omega_h^+ \\ w(0,x) = f(x) & \text{in } \Omega_h^+ \end{cases} \tag{4.12}$$

We extend by an odd reflection the initial data:

$$g(x) = \begin{cases} f(x) & \text{if } x \in \Omega_h^+ \\ -f(-x) & \text{if } x \in \Omega_h^- \\ 0 & \text{if } x = 0 \end{cases}$$

Then $u(t,x)$ with initial condition $g(x)$ solves the heat equation in Ω_h:

$$\begin{cases} \frac{\partial u}{\partial t}(t,x) = \frac{1}{h^2}(u(t,x+h) - 2v(t,x) + u(t,x-h)) & \text{in } \Omega_h \\ u(0,x) = g(x) & \text{in } \Omega_h \end{cases}$$

and admits the following representation:

$$u(t,x) = h \sum_{z \in \Omega_h} H^D(t,x-z) g(z).$$

We show that $w(t,x) = u(t,x)|_{x\in\Omega_h^+}$ with initial data $w(0,x) = u(0,x)|_{x\in\Omega_h^+} = f(x)$ is the solution of (4.12):

$$\begin{aligned}
u(t,x) &= h\sum_{z\in\Omega_h} H^D(t,x-z)g(z) \\
&= h\sum_{z\in\Omega_h^-} H^D(t,x-z)g(z) + h\sum_{z\in\Omega_h^+} H^D(t,x-z)g(z) \\
&= h\sum_{z\in\Omega_h^-} -H^D(t,x-z)f(-z) + h\sum_{z\in\Omega_h^+} H^D(t,x-z)f(z) \\
&= h\sum_{z\in\Omega_h^+} -H^D(t,x+z)f(z) + h\sum_{z\in\Omega_h^+} H^D(t,x-z)f(z) \\
&= h\sum_{z\in\Omega_h^+} (H^D(t,x-z) - H^D(t,x+z))f(z)
\end{aligned}$$

where we performed a change of variable $z \mapsto -z$.

Thus by denoting

$$G^D(t,x,y) = H^D(t,x-y) - H^D(t,x+y),$$

we have the claim (4.11). □

Corollary 4.1. *Given the discrete heat kernel in Ω_h^+ in (4.11), then the solution of the stochastic heat equation $u(t,x)$ solves the following problem on the positive reticle with initial condition f:*

$$\begin{cases} \dfrac{\partial u}{\partial t}(t,x) = \dfrac{1}{h^2}(u(t,x+h) - 2u(t,x) + u(t,x-h)) & \text{in } \Omega_h^+ \\ u(0,x) = f(x) & \text{in } \Omega_h^+. \end{cases}$$

Moreover, $u(t,x)$ admits the following representation:

$$u(t,x) = h\sum_{y\in\Omega_h^+} G^D(t,x,y)f(y)$$

Proof. The claim descends directly from Lemma 4.2. □

Before giving an explicit representation of the solution to the above IBVP, we introduce a preliminary lemma which is the discrete counterpart of the integration by parts formula.

Lemma 4.3. *Let $A, B : \Omega_h^+ \to \mathbb{R}$, with h the uniform spatial step of the discretization. Then*

$$\int_h^{+\infty} A(t,y)(D_y^- B(t,y))dy = -A(t,0)B(t,0) - \int_0^{+\infty} (D_y^+ A(t,y))B(t,y)dy$$

and

$$\int_h^{+\infty} A(t,y) D_y^- D_y^+ C(t,y) dy = - A(t,0) D^+ C(t,0) + (D_y^+ A(t,0)) C(t,0) + \int_h^{+\infty} (D_y^+ D_y^- A(t,y)) C(t,y) dy$$

Remark 4.4. The dependence on the time variable t will be omitted to overcome the abuse of notation, but the result still holds for A, B function of (t,x) where the time variable is continuous.

Proof. (Lemma 4.3)
Let us start by calculating

$$\begin{aligned}
\int_h^{+\infty} A(y)(D_y^- B(y)) dy &= h \sum_{x=h}^{+\infty} A(x)(D_y^- B(x)) = h \sum_{x=h}^{+\infty} A(x) \frac{B(x) - B(x-h)}{h} \\
&= \sum_{x=h}^{+\infty} A(x)B(x) - \sum_{x=h}^{+\infty} A(x)B(x-h) \\
&= \sum_{x=h}^{+\infty} A(x)B(x) - \sum_{x=0}^{+\infty} A(x+h)B(x) \\
&= -A(0)B(0) + \sum_{x=0}^{+\infty} A(x)B(x) - \sum_{x=0}^{+\infty} A(x+h)B(x) \\
&= -A(0)B(0) + h \sum_{x=0}^{+\infty} \frac{A(x) - A(x+h)}{h} B(x) \\
&= -A(0)B(0) - h \sum_{x=0}^{+\infty} (D_y^+ A(x))B(x) \\
&= -A(0)B(0) - \int_0^{+\infty} (D_y^+ A(y))B(y) dy
\end{aligned}$$

To prove the second statement, we apply the first integration by parts formula with $B(y) = D_y^+ C(y)$, $B(0) = D_y^+ C(0)$ we get:

$$\int_h^{+\infty} A(y) D_y^- D_y^+ C(y) dy = -A(0)B(0) - \int_0^{+\infty} (D_y^+ A(y))(D_y^+ C(y)) dy \tag{4.13}$$

Focusing on the integral term on the right-hand side we have:

$$\begin{aligned}
\int_0^{+\infty} (D_y^+ A(y)) D_y^+ C(y) dy &= h \sum_{y=0}^{+\infty} (D_y^+ A(y)) D_y^+ C(y) \\
&= h \sum_{y=0}^{+\infty} (D_y^+ A(y)) \frac{C(y+h) - C(y)}{h} \\
&= \sum_{y=0}^{+\infty} (D_y^+ A(y)) C(y+h) - \sum_{y=0}^{+\infty} (D^+ A(y)) C(y) \\
&= \sum_{y=h}^{+\infty} (D_y^+ A(y-h)) C(y) - (D_y^+ A(0)) C(0) - \sum_{y=h}^{+\infty} (D_y^+ A(y)) C(y) \\
&= -(D^+ A(0)) C(0) + \sum_{y=h}^{+\infty} [D_y^+ A(y-h) - D_y^+ A(y)] C(y) \\
&= -(D_y^+ A(0)) C(0) - h \sum_{y=h}^{+\infty} D_y^+ \left(\frac{A(y) - A(y-h)}{h} \right) C(y) \\
&= -(D_y^+ A(0)) C(0) - \int_h^{+\infty} (D_y^+ D_y^- A(y)) C(y) dy
\end{aligned}$$

We get the claim by inserting the latter expression in (4.13). □

Remark 4.5 (Chain rule for D^+D^-). We need to cover the case where the order of the operator is inverted: when applying firstly the D_x^- operator, the behaviour close to the boundary must be considered.

$$\begin{aligned}
\int_h^{+\infty} A(y) D_x^+ B(y) dy &= h \sum_{x=h}^{+\infty} \frac{B(x+h) - B(x)}{h} \\
&= \sum_{x=h}^{+\infty} B(x+h) - \sum_{x=h}^{+\infty} A(x) B(x) \\
&= \sum_{x=0}^{+\infty} A(x) B(x+h) - A(0) B(h) - \sum_{x=0}^{+\infty} A(x) B(x) + A(0) B(0) \\
&= A(0) B(0) - A(0) B(h) - h \sum_{x=0}^{+\infty} \frac{(A(x+h) - A(x)) B(x)}{h} \\
&= -A(0) D_x^+ B(0) - \int_0^{+\infty} (D_y^+ A(y)) B(y) dy
\end{aligned}$$

Let now $B(y) = D_y^- C(y+h)$, then

$$\begin{aligned}\int_0^{+\infty} D_y^+ A(y) D_y^- C(y+h)dy &= D_y^+ A(0) D_y^- C(h) + h\sum_{x=h}^{+\infty} D_x^+ A(x) D_x^- C(x) \\ &= D_x^+ A(0) D_x^- C(h) + \sum_{x=h}^{+\infty} D_x^+ A(x) C(x) - \sum_{x=0}^{+\infty} D_x^+ A(x) C(x-h) \\ &= D_x^+ A(0) D_x^- C(h) - D_x^+ A(0) C(0) + \sum_{x=0}^{+\infty} D_x^+ A(x) C(x) - \sum_{X=0}^{+\infty} D_x^+ A(x+h) C(x) \\ &= D_x^+ A(0) D_x^- C(h) - D_x^+ A(0) C(0) - \sum_{x=0}^{+\infty} D_x^- D_x^+ A(x) C(x)\end{aligned}$$

Finally, the following result gives an explicit representation of the solution to the BVP in terms of the discrete heat kernel:

Proposition 4.3. *For a bounded, measurable and positive function ψ such that $\psi(0) = 0$, the function*

$$u(t,x) = -\int_0^t (D_x^- + D_x^+) H^D(t-s,x)\psi(s)ds$$

solves the problem

$$\begin{cases} \partial_t u = \Delta_x^D u & \text{in } [0,T] \times \Omega_h^+ \\ u(x,0) = 0 & \text{in } \Omega_h^+ \\ u(0,t) = \psi(t) & \text{in } [0,T] \end{cases} \tag{4.14}$$

Proof. Let $G^D(t,x)$ be the fundamental solution defined in Lemma 4.2 on the positive lattice Ω_h^+. We start by assuming that $u(t,x)$ is the solution of the (4.14). This means that

$$\begin{aligned} 0 &= \int_0^t \int_h^{+\infty} u(s,y)\Big[\partial_s G^D(t-s,x,y) + D_y^+ D_y^- G^D(t-s,x,y)\Big]dyds \\ &= \int_0^t \int_h^{+\infty} u(s,y)\partial_s G^D(t-s,x,y)dyds + \int_0^t \int_h^{+\infty} u(s,y) D_y^+ D_y^- G^D(t-s,x,y)dyds \\ &= I_1 + I_2 \end{aligned}$$

Let us analyse the two contributions separately. Integrating by parts the variables s, y,

respectively, for the first addendum we get:

$$
\begin{aligned}
I_1 &= \int_0^t \int_h^{+\infty} u(s,y)\partial_s G^D(t-s,x,y)dyds \\
&= \int_h^{+\infty} \Big[u(s,y)G^D(t-s,x,y) \Big]_{s=0}^{s=t} dy - \int_0^t \int_h^{+\infty} \partial_s u(s,y) G^D(t-s,x,y)dyds \\
&= \int_h^{+\infty} u(t,y)G^D(0,x,y)dy - \int_h^{+\infty} u(0,y)G^D(t,x,y)dy \\
&\quad - \int_0^t \int_h^{+\infty} \partial_s u(s,y) G^D(t-s,x,y)dyds \\
&= \int_h^{+\infty} u(t,y)\delta_x(y)dy - \int_0^t \int_h^{+\infty} \partial_s u(s,y) G^D(t-s,x,y)dyds \\
&= u(t,x) - \int_0^t \int_h^{+\infty} \partial_s u(s,y) G^D(t-s,x,y)dyds
\end{aligned}
$$

where we have used the fact the initial condition $u(0,y) = 0$ for all $y \in \Omega_h^+$ and that $G^D(0,x,y) = \delta_x(y)$ by definition.

We now look to the second contribution I_2. We integrate by parts twice, more precisely, we apply the second rule in Lemma 4.3 with $A(y) = u(t,y)$, $C(y) = G^D(t,x,y)$:

$$
\begin{aligned}
&\int_h^{+\infty} u(t,y) D_y^- D_y^+ G^D(t,x,y)dy = \\
&= -u(t,0)D_y^+ G^D(t,x,0) + D_y^+ u(t,0) G^D(t,x,0) + \int_h^{+\infty} D_y^- D_y^+ u(t,y) G^D(t,x,y)dy \\
&= -\psi(t) D_y^+ G^D(t,x,0) + \int_h^{+\infty} D_y^- D_y^+ u(y,t) G^D(t,x,y)dy
\end{aligned}
$$

where we have exploited the definition of G^D in (4.11) in $y = 0$:

$$
G^D(t,x,0) = H^D(t,x) - H^D(t,x) = 0
$$

Thus I_2 has the following expression:

$$
\begin{aligned}
I_2 &= \int_0^t \int_h^{+\infty} u(s,y) D_y^- D_y^+ G^D(t-s,x,y)dyds \\
&= -\int_0^t u(s,0) D_y^+ G^D(t-s,x,0)ds + \int_0^t D_y^+ u(s,0) G^D(t-s,x,0)ds \\
&\quad + \int_0^t \int_h^{+\infty} D_y^- D_y^+ u(s,y) G^D(t-s,x,y)dyds \\
&= -\int_0^t \psi(s) D_y^+ G^D(t-s,x,0)ds + \int_0^t \int_h^{+\infty} D_y^- D_y^+ u(s,y) G^D(t-s,x,y)dyds
\end{aligned}
$$

Now we sum the two contributes and we exploit the definition of $u(t,x)$ to be the solution of (4.14):

$$\begin{aligned}
0 &= I_1 + I_2 \\
&= u(t,x) - \int_0^t \int_h^{+\infty} \partial_s u(s,y) G^D(t-s,x,y) dy ds \\
&\quad - \int_0^t \psi(s) D_y^+ G^D(t-s,x,0) ds + \int_0^t \int_h^{+\infty} D_y^- D_y^+ u(s,y) G^D(t-s,x,y) dy ds \\
&= u(t,x) - \int_0^t \psi(s) D_y^+ G^D(t-s,x,0) ds.
\end{aligned}$$

Therefore

$$- \int_0^t \int_h^{+\infty} \partial_s u(s,y) G^D(t-s,x,y) dy ds + \int_0^t \int_h^{+\infty} D_y^- D_y^+ u(s,y) G^D(t-s,x,y) dy ds = 0$$

Hence $u(t,x)$ solves (4.14) and admits the following representation:

$$u(t,x) = \int_0^t \psi(s) D_y^+ G^D(t-s,x,0) ds \tag{4.15}$$

We calculate $D_y^+ G^D$:

$$\begin{aligned}
D_y^+ G^D(t,x,y) &= D_y^+ H^D(t,x-y) - D_y^+ H^D(t,x+y) \\
&= \frac{1}{h}\left(H^D(t,x-(y+h)) - H^D(t,x-y)\right) - \frac{1}{h}\left(H^D(t,x+(y+h)) - H^D(t,x+y)\right) \\
&= \frac{1}{h}\left(H^D(t,(x-h)-y) - H^D(t,x-y)\right) - \frac{1}{h}\left(H^D(t,(x+h)+y) - H^D(t,x+y)\right) \\
&= -D_x^- H^D(t,x-y) - D_x^+ H^D(t,x+y)
\end{aligned}$$

When calculating for $y = 0$:

$$D_y^+ G^D(t,x,0) = -D_x^- H^D(t,x) - D_x^+ H^D(t,x)$$

and (4.15) becomes:

$$u(t,x) = -\int_0^t (D_x^- + D_x^+) H^D(t-s,x) \psi(s) ds$$

□

Remark 4.6. Note that working within the positive lattice Ω_h^+ implies the use of the operator D_x^+ to account for the boundary at 0.

Remark 4.7. Since it will be useful for the theoretical estimation, let us calculate the first derivative $D_x^- u(t,x)$ for $x \geq h$ and under the hypothesis that $\psi(0) = 0$:

$$\begin{aligned}
D_x^- u(t,x) &= D_x^- \left(- \int_0^t \left(D_x^- + D_x^+ \right) H^D(t-s,x)\psi(s)ds \right) \\
&= - \int_0^t D_x^- D_x^- H^D(t-s,x)\psi(s)ds - \int_0^t D_x^- D_x^+ H^D(t-s,x)\psi(s)ds \\
&\overset{(4.10)}{=} - \int_0^t \partial_s H^D(t-s,x-h)\psi(s)ds - \int_0^t \partial_s H^D(t-s,x)\psi(s)ds \\
&\overset{by\ parts}{=} - \left[H^D(t-s,x-h)\psi(s) \right]_{s=0}^{s=t} + \int_0^t H^D(t-s,x-h)\dot{\psi}(s)ds \\
&\quad - \left[H^D(t-s,x)\psi(s) \right]_{s=0}^{s=t} + \int_0^t H^D(t-s,x)\dot{\psi}(s)ds \\
&= \int_0^t H^D(t-s,x-h)\dot{\psi}(s)ds + \int_0^t H^D(t-s,x)\dot{\psi}(s)ds
\end{aligned}$$

where we have used that for $x > 0$ we have $H^D(0,x) = 0$.

Remark 4.8. For the convenience of the reader, we note that in [25] a different approach for the explicit formula of the discrete heat kernel is provided for $h = 1$. Let $H^D(t,x)$ be the fundamental solution of the discrete heat equation defined in the whole space $x \in \Omega_h$:

$$\begin{cases} \frac{\partial}{\partial t} H^D(t,x) = D_x^- D_x^+ H^D(t,x) & x \in \Omega_h,\ t > 0 \\ H^D(0,x) = \delta_0(x) & x \in \Omega_h \end{cases}$$

We rewrite the equation in the following notation:

$$\frac{\partial}{\partial t} H^D(t,x) = \frac{1}{2} \Big(H^D(t,x+1) - 2H^D(t,x) + H^D(t,x-1) \Big) \tag{4.16}$$

Lemma 4.4. *A solution of* (4.16) *is given by*

$$H^D(t,x) = \exp(-t) I_{x-y}(t)$$

where I is the modified Bessel function of the first kind.

Proof. Starting from (4.16) we multiply both sides for $\exp(ix\xi)$ and then we take the

sum over x:

$$\frac{\partial}{\partial t}H^D(t,x) = \frac{1}{2}\Big(H^D(t,x+1) - 2H^D(t,x) + H^D(t,x-1)\Big)$$

$$e^{ix\xi}\frac{\partial}{\partial t}H^D(t,x) = \frac{1}{2}\Big(e^{ix\xi}H^D(t,x+1) - 2e^{ix\xi}H^D(t,x) + e^{ix\xi}H^D(t,x)\Big)$$

$$\frac{\partial}{\partial t}\sum_{x\in\Omega_h} e^{ix\xi}H^D(t,x) = \sum_{x\in\Omega_h}\frac{1}{2}\Big(e^{i(x+1)\xi}H^D(t,x) - 2e^{ix\xi}H^D(t,x) + e^{i(x-1)\xi}H^D(t,x)\Big)$$

$$\frac{\partial}{\partial t}\hat{H}^D(t,\xi) = \sum_{x\in\Omega_h} e^{ix\xi}H^D(t,x)\left(\frac{e^{i\xi}+e^{-i\xi}-2}{2}\right)$$

$$\frac{\partial}{\partial t}\hat{H}^D(t,\xi) = \hat{H}^D(t,\xi)\left(\frac{2cos(\xi)-2}{2}\right)$$

$$\frac{\partial}{\partial t}\hat{H}^D(t,\xi) = -2\sin^2\left(\frac{\xi}{2}\right)\hat{H}^D(t,\xi)$$

where

$$\hat{H}^D(t,\xi) = \sum_{x=-\infty}^{+\infty} e^{ix\xi}H^D(t,x)$$

is the characteristic function for the fundamental solution (4.16). Now, to go back to the solution we use the anti-transform:

$$H^D(t,x) = \frac{1}{2\pi}\int_{-\pi}^{\pi} e^{-ix\xi}\hat{H}^D(t,\xi)d\xi.$$

Indeed, we obtained a ODE with the following dynamics

$$\frac{\partial}{\partial t}\hat{H}^D(t,\xi) = -2\sin^2\left(\frac{\xi}{2}\right)\hat{H}^D(t,\xi)$$

and the solution can be computed explicitly:

$$\hat{H}^D(t,\xi) = \hat{H}^D(0,\xi)e^{-2\sin^2(\xi/2)t}.$$

Combining these latest results, we get a solution

$$H^D(t,x) = \frac{1}{2\pi}\sum_{y\in\Omega_h} H^D(0,y)\int_{-\pi}^{\pi} e^{-i\xi(y-x)}e^{-2\sin^2(\xi/2)t}d\xi.$$

□

4.3 Some a priori bounds

We plan to establish some a priori bounds on the solution of the (initial) boundary value problem for the one-dimensional discrete heat equation (4.8) taking advantage of some relevant results on space-time Besov spaces on the lattice. After having introduced a sort of linearization for the system (v,c), we provide an useful L^2 bound for it.

4.3.1 Bounds on the solution of the discrete-space random heat equation

To study the regularity properties of the equation (4.8), we introduce the definition and the main properties of the time-space Besov space (see, e.g, Appendix C), starting with the standard Besov spaces.

Definition 4.3 (Besov space)**.** Consider $s \in \mathbb{R}$, and $p, q \in [1, +\infty]$. We say that a function $f \in \mathcal{S}'(\mathbb{R}^d)$ belongs to the Besov space $B^s_{p,q}(\mathbb{R}^d)$ if the following norm

$$\|f\|_{B^s_{p,q}(\mathbb{R}^d)} := \left(\sum_{j \geq -1} 2^{qsj} \|\Delta_j f\|^q_{L^p} \right)^{1/q}$$

is finite, where Δ_j are the Little-Paley operators (see Appendix C).

Remark 4.9. In the definition of a Besov space, the parameter s describes the regularity of the object, the parameter p the integrability and q an additional refinement of the regularity scale (see, e.g. [111]).

Remark 4.10. When $p = q = 2$ then one has $B^s_{2,2} = H^s$ and, whenever $0 < s < 1$, $B^s_{\infty,\infty} = C^s$

Furthermore, the following embedding property holds:

Proposition 4.4 (Besov embedding property)**.** *Let* $1 \leq p_1 \leq p_2 \leq +\infty$ *and* $1 \leq q_1 \leq q_2 \leq +\infty$*, then*

$$B^s_{p_1,q_1} \hookrightarrow B^{s-n\left(\frac{1}{p_1}-\frac{1}{p_2}\right)}_{p_2,q_2},$$

where the embedding is continuous.

Since in this paper we consider a random PDE-ODE system, it is convenient to introduce the time-space Besov spaces in $\mathbb{R}^d$.

Definition 4.4. Let I=[0,t] be an interval. For $p, q \in [1, +\infty]$ and $s \in \mathbb{R}$ we consider the space

$$L^r(I, B^s_{p,q}(\mathbb{R}^d))$$

with norm given, for any $f : I \to B^s_{p,q}(\mathbb{R}^d)$, by

$$||f||_{L^r(I,B^s_{p,q}(\mathbb{R}^d)} = \left(\int_0^t ||f(t)||^r_{B^s_{p,q}(\mathbb{R}^d)} dt \right)^{1/r}$$

To obtain a compact embedding it is useful to introduce the following space for $\bar{s} \in \mathbb{R}$;

$$B^{\bar{s}}_{r,r}(I, B^s_{p,q}(\mathbb{R}^d))$$

with the norm given by

$$||f||_{B^{\bar{s}}_{r,r}(I,B^s_{p,q}(\mathbb{R}^d))} = \sum_{j \geq -1} \int_0^t \|\Delta^\tau_j f\|_{B^s_{p,q}(\mathbb{R}^d)} d\tau$$

These spaces have a difference characterization of their norms according to the following proposition.

Proposition 4.5 (Difference characterization)**.** *Let $r, p, q \in [1, +\infty]$ and $s \in \mathbb{R}$. If $f \in B^{\bar{s}}_{r,r}(I, B^s_{p,q}(\mathbb{R}^d))$ then*

$$||f||_{B^{\bar{s}}_{r,r}(I,B^s_{p,q}(\mathbb{R}^d))} \equiv ||f||_{L^r(I,B^s_{p,q}(\mathbb{R}^d))} + \int_0^t \int_{|h|<1} \frac{||f(\tau+h) - f(\tau)||^r_{B^s_{p,q}(\mathbb{R}^d)}}{h^{1+rs}} dh d\tau.$$

Proof. See, e.g. [111] □

Finally, the following embedding result continues to hold.

Proposition 4.6 (Compact embedding)**.** *When $\bar{s} > \bar{s}'$ and $\bar{s} - \frac{1}{r} > \bar{s}' - \frac{1}{r'}$, if the immersion*

$$B^{s_1}_{p_1,q_1}(\mathbb{R}^d)) \subset B^{s_2}_{p_2,q_2}(\mathbb{R}^d))$$

is compact, then also the immersion

$$B^{\bar{s}}_{r,r}(I, B^{s_1}_{p_1,q_1}(\mathbb{R}^d)) \subset B^{\bar{s}'}_{r',r'}(I, B^{s_2}_{p_2,q_2}(\mathbb{R}^d))$$

is compact.

Proof. See, e.g. [111] □

We restrict to the case $d = 1$, which is the case of interest in the present paper.
Following [81][13], one can introduce the definition of a discrete Besov space on the lattice (see Appendix C) and show that all the previous properties still hold.

For sake of semplicity, when needed, for the Banach, Sobolev and Besov spaces we introduce the following notations: $L^p_x = L^p(\Omega^+_h)$, $W^{p,r}_x = W^{p,r}_x(\Omega^+_h)$, $B^s_{p,q} = B^s_{p,q}(\Omega^+_h)$ in space and $L^+_t L^q_x = L^p([0,T], L^q(\Omega^+_h))$ in time and space.

Since our final goal is to provide some estimates on the derivative of u, $D^+_x u$ (or equivalently $D^-_x u$), we need to consider some regularization properties of the discrete heat kernel. The following result allows us to gain some regularity in space, more precisely a $2m$ space-regularity (see [13] or [111]).

Lemma 4.5 (Heat-kernel regularization)**.** *Let $m > 0$, $s > 0$, $p, q \in [0, +\infty]$ and consider $g \in B^s_{p,q}(\Omega_h)$. For every $t > 0$*

$$\|e^{\Delta t} g\|_{B^{s+2m}_{p,q}(\Omega_h)} \leq C t^{-m} \|g\|_{B^s_{p,q}(\Omega_h)}$$

Specializing the previous lemma to our case in which $g = \delta_0$, we can state the following result.

Lemma 4.6 (Dirac-delta case)**.** *Let $k > 0, \alpha > 0$, $p \in [0, +\infty]$ and consider $\delta_0 \in B^{\alpha}_{p,p}(\Omega_h)$. For every $t > 0$*

$$\left\| \int_t^{t+\sigma} e^{\Delta s}\delta_0 \right\|_{B^{\alpha+k+1}_{p,p}(\Omega_h^+)} \leq \frac{C}{t^{\theta\frac{k+1}{2}+(1-\theta)\frac{k-1}{2}}}\sigma^{\theta}||\delta_0||_{B^{\alpha}_{p,p}(\Omega_h^+)}$$

Proof. Let us introduce $F(t) = \int_0^t De^{\Delta s}\delta_0 ds$. By Lemma 4.5 we can estimate the difference norm as

$$\begin{aligned} ||F(t+\sigma) - F(t)||_{B^{\alpha+k+1}_{p,p}} \leq & \int_t^{t+\sigma} ||e^{\Delta s}\delta_0||_{B^{\alpha+k+1}_{p,p}} ds \\ \leq & ||\delta_0||_{B^{\alpha}_{p,p}} \int_t^{t+\sigma} \frac{C}{s^{\frac{k+1}{2}}} ds. \end{aligned}$$

Now

$$\begin{aligned} \int_t^{t+\sigma} \frac{1}{s^{\frac{k+1}{2}}} ds = & \frac{2}{k-1}\left(\frac{1}{(t+\sigma)^{\frac{k+1}{2}-1}} - \frac{1}{(t)^{\frac{k+1}{2}-1}} \right) \\ \leq & C\frac{1}{t^{\theta\frac{k+1}{2}+(1-\theta)\frac{k-1}{2}}}\sigma^{\theta} \end{aligned}$$

and by inserting the latter estimate in the previous expression we get the claim. □

By giving more regularity to the spatial variable, we can obtain some bound to the solution u in Sobolev space, uniformly in time and for $\alpha \in (-1, 0)$. For the following result, we need more regularity on the stochastic boundary function.

Proposition 4.7. *Let u be the solution of the semi-discrete random heat problem:*

$$\begin{aligned} \partial_t u = & \quad \Delta_x^D u, \qquad & \text{for } (t,x) \in [0,T] \times \Omega_h^+ \\ u(0,x) = & \quad 0 \qquad & \text{for } x \in \Omega_h^+ \\ u(t,0) = & \quad \psi(t) \qquad & \text{for } \psi(t) \in C^{\kappa}([0,T]). \end{aligned}$$

Let us suppose that ψ is such that $\psi(0) = 0$ and $\kappa \in \left(\frac{1}{4}, \frac{1}{2}\right)$. Then, for every $\alpha \in (-1, 0)$ and $p \in (1, 1/(1+\alpha))$, there exist constants C, C' not depending on ψ such that P-almost surely

$$||u||_{L_t^{\infty}W_x^{p,r}} \leq C'||\psi||_{C^{\kappa}}, \quad \frac{1}{p} + 2\kappa > r$$

In particular, we get

$$||u||_{L_t^{\infty}H_x^1} \leq C||\psi||_{C^{\kappa}}, \quad \kappa \in \left(\frac{1}{4}, \frac{1}{2}\right). \tag{4.17}$$

Proof. We start from the representation of the solution u in terms of the heat kernel provided in Proposition 4.3, transferring some regularity from the boundary term ψ to

the spatial one:

$$u(t,x) = -\int_0^t \left(D_x^- + D_x^+\right) H^D(t-s,x)\psi(s)ds$$
$$= -\int_0^t D_x^- e^{-\Delta(t-s)}\delta_0\psi(s)ds - \int_0^t D_x^+ e^{-\Delta(t-s)}\delta_0\psi(s)ds.$$

We prove that $D_x^+ e^{-\Delta(t-s)}\delta_0 \in B_{1,1}^{-\kappa}([0,t], B_{p,p}^{\alpha+k}(\mathbb{R}_+))$ (for suitable $p \in (1,+\infty)$, $\alpha < 0$ and $k > 0$ to be determined below). The estimation for the other addendum is the same. Assuming that the boundary function $\psi(s) \in B_{\infty,\infty}^{\kappa}([0,t]) = C^{\kappa}([0,t])$ with $t \in [0,T]$, then the product $D_x^+ e^{-\Delta(t-s)}\delta_0\psi(s)$, as a distribution depending on the time s, is a well defined distribution. This implies the following estimate for the Besov norm of the integral

$$\left\| \int_0^t D_x^+ e^{-\Delta(t-s)}\delta_0\psi(s)ds \right\|_{B_{p,p}^{\alpha+k}(\mathbb{R}_+)} \leq \|D_x^+ e^{-\Delta(t-\cdot)}\delta_0\|_{B_{1,1}^{-\kappa}([0,t],B_{p,p}^{\alpha+k}(\mathbb{R}_+))} \|\psi(\cdot)\|_{C^{\kappa}([0,t])},$$

and from the inequality we get that the $L_t^{\infty}W_x^{p,r}$ norm of u is bounded whenever $r < \alpha + k$.

Now we prove the statement $D_x^+ e^{-\Delta(t-s)}\delta_0 \in B_{1,1}^{-\kappa}([0,t], B_{p,p}^{\alpha+k}(\mathbb{R}_+))$.

Let us define $F(s) = \int_0^s D_x^+ e^{-\Delta(t-\tau)}\delta_0 d\tau$. In order to prove that $D_x^+ e^{-\Delta(t-s)}\delta_0 \in B_{1,1}^{-\kappa}([0,t], B_{p,p}^{\alpha+k}(\mathbb{R}_+))$ we can equivalently establish the following $\int_0^s D_x^+ e^{-\Delta(t-\tau)}\delta_0 d\tau \in B_{1,1}^{-\kappa}([0,t], B_{p,p}^{\alpha+k}(\mathbb{R}_+))$, so overcoming the fact that the regularity of $D_x^+ e^{-\Delta(t-s)}\delta_0$, in the variable s, is negative. By the difference characterization of time-space Besov spaces recalling in Proposition 4.5 we have:

$$||F||_{B_{1,1}^{1-\kappa}([0,t],B_{p,p}^{\alpha+k})} = \int_0^t ||F(s)||_{B_{p,p}^{\alpha+k}} ds + \int_0^t \int_{|h|<1} \frac{||F(s+\sigma) - F(s)||_{B_{p,p}^{\alpha+k}(\Omega_h^+)}}{\sigma^{2-\kappa}} dh ds.$$

We start by giving an upper bound for $\|F\|_{L^1([0,t],B_{p,p}^{\alpha+k})}$. We have that

$$\|F\|_{L^1([0,t],B_{p,p}^{\alpha+k}(\Omega_h^+))} = \int_0^t \left\| \int_0^s D_x^+ e^{-\Delta(t-\tau)}\delta_0 d\tau \right\|_{B_{p,p}^{\alpha+k}(\Omega_h^+)} ds$$
$$\leq \int_0^t \int_0^s \|e^{-\Delta(t-\tau)}\delta_0\|_{B_{p,p}^{\alpha+k+1}(\Omega_h^+)} d\tau ds \leq \|\delta_0\|_{B_{p,p}^{\alpha}(\Omega_h^+)} \int_0^t \int_0^s \frac{1}{(t-\tau)^{\frac{k+1}{2}}} d\tau ds.$$

The last integral is bounded, uniformly in $t \in [0,T]$, whenever $k < 3$. Under this condition and under the hypothesis $\alpha < \frac{1}{p} - 1$, we get

$$\|F\|_{L^1([0,t],B_{p,p}^{\alpha+k}(\Omega_h^+))} < C_1.$$

for some $C_1 > 0$, uniformly in $t \in [0,T]$. Applying Lemma 4.6 to the difference norm we have

$$||F(s+\sigma) - F(s)||_{B_{p,p}^{\alpha+k}(\Omega_h^+)} \leq \int_s^{s+\sigma} \frac{1}{\tau^{\frac{1+k}{2}}} d\tau$$
$$\leq \frac{1}{s^{\frac{k+1}{2}\theta + (1-\theta)\frac{k-1}{2}}} \sigma^{\theta}.$$

Now, putting all the estimates together, we finally obtain:

$$||F||_{B^{1-\kappa}_{1,1}([0,t],B^{\alpha+k}_{p,p}(\Omega_h^+))} \leq C_1 + C_2 \int_0^t \int_{|\sigma|<1} \frac{1}{s^{\frac{k+1}{2}\theta+(1-\theta)\frac{k-1}{2}}} \sigma^{\theta+\kappa-2} dh ds$$

Hence the integral on the RHS is finite if

$$\begin{aligned} \theta + \kappa - 2 > -1 \quad &\rightarrow \quad \kappa + \theta > 1 \quad \text{for } h \text{ close to } 0 \\ \frac{k+1}{2}\theta + (1-\theta)\frac{k-1}{2} < 1 \quad &\rightarrow \quad \theta < \frac{3-k}{2} \end{aligned} \tag{4.18}$$

$$\tag{4.19}$$

Indeed the following condition on time regularity κ holds:

$$\kappa > 1 - \theta \tag{4.20}$$

Now, combining (4.20) with (4.18) we get:

$$\kappa \quad > \quad 1 - \theta > 1 + \frac{k-3}{2} = \frac{k-1}{2}$$

Therefore we have found the connection between the time regularity κ and the spatial regularity k. Indeed, from the previous inequalities, we get

$$\kappa > \frac{k-1}{2}.$$

We note that κ is exactly the regularity of ψ. Recalling that $\psi \in C^\kappa$, $\kappa \in \left(\frac{1}{4}, \frac{1}{2}\right)$, in the worst case we have that the regularity of ψ is $\kappa = \frac{1}{4}$. This leads to

$$\frac{1}{4} \geq \frac{k-1}{2} \rightsquigarrow k \leq \frac{3}{2}$$

Since for the spacial variable we are working on $B^{\alpha+k}_{p,p}$, (where $\alpha = \frac{1}{p} - 1$), we could reach the maximum space regularity whenever

$$\alpha + k \leq \frac{1}{p} - 1 + \frac{3}{2} = \frac{1}{p} + \frac{1}{2}$$

By choosing $p = 2$, we gain $\alpha + k = 1$ regularity in space.

Finally, the estimation on u is given by:

$$||u||_{L^\infty_t W^{p,r}_x} \leq C||\psi||_{C^\kappa_t}, \quad \frac{1}{p} + 2\kappa > r,$$

and, in particular, we get

$$||u||_{L^\infty_t H^1_x} \leq C||\psi||_{C^\kappa_t}, \quad \kappa \in \left(\frac{1}{4}, \frac{1}{2}\right).$$

When $r = 1, p = 2$ we obtain the case $\kappa = \frac{1}{4}$. Since κ is the regularity of a diffusion process, it has necessarily to be less than $1/2$. □

Remark 4.11. An alternative way to prove that the maximum regularity that we can gain in space is 1 is to fix κ and derive k in terms of κ:

$$k < 2(\kappa + \frac{1}{2}) = 2\kappa + 1$$

The maximum regularity we can gain in space is given by

$$\begin{aligned} \alpha + 2\kappa + 1 &> 1 \\ \frac{1}{p} - 1 + 2\kappa + 1 &> 1 \\ \kappa &> \frac{p-1}{2p} \end{aligned}$$

Again, by choosing $p = 2$ we get $\kappa > \frac{1}{4}$, which is the lowest regularity admissible for the boundary condition ψ.

Remark 4.12. We note that, even though it has no meaning in our case, by choosing $\kappa = 0$ one has

$$\begin{aligned} 0 = \kappa = \frac{k-1}{2} \quad &\rightsquigarrow \quad k < 1 \\ 0 = \kappa = \frac{p-1}{2p} \quad &\rightsquigarrow \quad p > 1 \end{aligned}$$

Remark 4.13. Since by Remark 4.7 we have for $x \geq h$

$$D_x^- u(t,x) = \int_0^t H^D(t-s, x-h)\dot{\psi}(s)ds + \int_0^t H^D(t-s,x)\dot{\psi}(s)ds$$

differentiating with respect to x we get

$$D_x^+ D_x^- u(t,x) = \int_0^t D_x^+ H^D(t-s, x-h)\dot{\psi}(s)ds + \int_0^t D_x^+ H^D(t-s,x)\dot{\psi}(s)ds$$

By Proposition 4.7 we then obtain for $x \geq h$

$$||D_x^+ D_x^- u||_{L_t^\infty W_x^{p,r}} \leq C' ||\dot{\psi}||_{L_t^\infty}$$

4.4 A priori estimates for a quasi-linear system

Following [82], we provide a linearization to equation (4.6) by introducing a Borel function $f : [0,T] \times \Omega_h^+ \to \mathbb{R}$ satisfying, for some $K > 0$.

$$\begin{aligned} & f \in C_t(L_x^2) \cap L_t^2(W_x^{1,2}) \\ & \|f\|^2_{C_t(L_x^2)} + \|D_x^+ f\|^2_{L^2_{t,x}} \leq K \\ & f \geq 0, \\ & f(\cdot, 0) = \psi, \\ & \|f\|_{L^\infty_{t,x}} \leq \widetilde{\eta}. \end{aligned} \tag{4.21}$$

and we consider the following quasi-linear version of the semi-discrete system (4.6)-(4.7) in $[0,T]\times\Omega_h^+$:

$$\begin{aligned}\partial_t s &= \Delta_x^D s + b_g(t,x)[D_x^+ c D_x^+ s + D_x^- c D_x^- s] + \gamma_g s(Bf-1)\\ \partial_t g &= -\lambda f \varphi(g) g\end{aligned} \tag{4.22}$$

where

$$b_g = \frac{1}{2}\frac{B}{\varphi(g)}, \qquad \gamma_g = \lambda g \tag{4.23}$$

Let us remark that the solution g of the second equation of (4.22) admits the following explicit expression

$$g(t,x) = \frac{Ac_0}{\varphi(c_0)e^{\lambda A\int_0^t f(\tau,x)d\tau} - Bc_0} \tag{4.24}$$

The idea now is to prove a uniform bound for the solution s of the linear PDE in $[0,T]\times\Omega_h^+$:

$$\begin{aligned}\partial_t s &= \Delta_x^D s + b_g(t,x)[D_x^+ c D_x^+ s + D_x^- c D_x^- s] + \gamma_g s(Bf-1)\\ s(0,x) &= s_0\\ s(t,0) &= \psi(t)\end{aligned}$$

Again, we split the solution $s = u + v$, where u is the solution of the initial boundary problem for the homogeneous heat equation

$$\begin{aligned}\partial_t u &= \Delta_x^D u \qquad \text{in } [0,T]\times\Omega_h^+\\ u(0,x) &= 0 \qquad \text{in } \Omega_h^+\\ u(t,0) &= \psi(t) \qquad \text{in } [0,T]\end{aligned}$$

while for v we have

$$\begin{aligned}\partial_t v &= \Delta_x^D v + b_g[D_x^+ g D_x^+ v + D_x^- g D_x^- v] - \gamma_g(1-Bf)v\\ &\quad + b_g[D_x^+ g D_x^+ u + D_x^- g D_x^- u] - \gamma_g(1-Bf)u \qquad \text{in } [0,T]\times\Omega_h^+\\ v(0,x) &= s_0 \qquad \text{in } \Omega_h^+\\ v(t,0) &= 0 \qquad \text{in } [0,T]\end{aligned}$$

where b_g and γ_g are defined in (4.23).

4.4.1 A priori estimates

In view of proving the convergence we provide an a priori uniform estimate for the variable s. To this scope, we need to give some a priori bounds both to u and v. Let us recall that in (4.17) we have already found an a priori estimate for the solution u. In the following proposition, we ensure bounds for $D_x^+ u$:

Proposition 4.8. *Given u solution of the semi-discrete heat equation, then the following estimation holds:*

$$\|D_x^+ u\|_{L_t^\infty L_x^2} \leq C_1' \|\psi\|_{C_t^\kappa}$$

Proof. The estimation is a direct application of Proposition 4.7 by setting $p = 2, r = 1$. □

On the other hand, to give an estimate for v and, thus, for s, we need to control the norm $\|D^+\varphi\|_{L_t^\infty L_x^2}$. Since $D^+\varphi = BD^+ g$, we can find an explicit expression for $D_x^+ g$ by applying the Leibniz rule in Proposition 4.1.

An easy calculation gives the finite difference derivative rule for the quotient:

Lemma 4.7. *Given two general functions f, g, then*

$$D_x^+ \left(\frac{f}{g}\right) = \frac{g(x) D_x^+ f(x) - f(x) D_x^+ g(x)}{g(x+h)g(x)} \tag{4.25}$$

Proof. The claim is a natural consequence of the definition of forward difference operator applied to the quotient:

$$\begin{aligned} D_x^+ \left(\frac{f}{g}\right) &= \frac{1}{h}\left(\frac{f(x+h)}{g(x+h)} - \frac{f(x)}{g(x)}\right) \\ &= \frac{1}{h}\left(\frac{f(x+h)g(x) - g(x+h)f(x)}{g(x+h)g(x)}\right) \\ &= \frac{1}{h}\left(\frac{g(x)[f(x+h) - f(x)] - f(x)[g(x+h) - g(x)]}{g(x+h)g(x)}\right) \\ &= \frac{g(x) D_x^+ f(x) - f(x) D_x^+ g(x)}{g(x+h)g(x)} \end{aligned}$$

□

Proposition 4.9. *Let f satisfy assumptions (4.21), $0 < c_m \leq c_0(x) \leq C_0$, $0 \leq s_0(x) \leq \widetilde{\eta}$ and $A > BC_0$. Moreover, let the boundary condition satisfy the following assumption:*

$$\begin{aligned} \psi \in C_t^\beta, \qquad t \in [0,T],\ \beta \in \left(\frac{1}{4}, \frac{1}{2}\right) \\ \psi(0) = 0 \\ 0 \leq \psi \leq \widetilde{\eta} \end{aligned}$$

Then, there exists constants c, κ such that the solution g in (4.24) admits the following estimates:

$$\|D_x^+ g\|_{L_t^\infty L_x^2}^2 \leq cT \left(\|D_x^+ c_0(x)\|_{L^2(\Omega_h^+)}^2 + \kappa \|D_x^+ f\|_{L_t^\infty L_x^2}^2 \right). \tag{4.26}$$

Moreover, the previous estimate could be extended to $\|D_x^+ \varphi\|_{L_t^\infty L_x^2}$ up to a constant factor $|B|$.

Proof. Let us introduce the following notation:

$$g(t,x) = \frac{Ac_0(x)}{\zeta(t,x)}, \quad \zeta(t,x) := \varphi(c_0(x))\tilde{h}(t,x) - Bc_0(x), \quad \tilde{h}(t,x) := e^{\lambda A \int_0^t f(\tau,x)d\tau}.$$

By applying the quotient rule for finite difference operator in (4.25) to the function g we get:

$$\begin{aligned} D_x^+ g(t,x) &= D_x^+ \left(\frac{Ac_0(x)}{\zeta(t,x)} \right) \\ &= \frac{\zeta(t,x) D_x^+ (Ac_0(x)) - Ac_0(x) D_x^+ \zeta(t,x)}{(\tau_h \zeta(t,x)) \cdot \zeta(t,x)}, \end{aligned} \tag{4.27}$$

where

$$D_x^+ \zeta(t,x) = \varphi(c_0(x) D_x^+ \tilde{h}(t,x) + \tilde{h}(x+h,t) D_x^+ \varphi(c_0(x)) - B D_x^+ c_0(x)$$

and

$$\begin{aligned} D_x^+ \tilde{h}(t,x) &= \frac{1}{h} \left(e^{\lambda A \int_0^t f(x+h,\tau)d\tau} - e^{\lambda A \int_0^t f(\tau,x)d\tau} \right) \\ &= \frac{1}{h} \left(e^{\lambda A \int_0^t hD_x^+ f(x,\tau) + f(x,\tau)d\tau} - e^{\lambda A \int_0^t f(\tau,x)d\tau} \right) \\ &= \frac{1}{h} \int_0^1 \left(e^{\lambda A \int_0^t f(x,\tau) + \theta h D_x^+ f(x,\tau)d\tau} \right) \left(\lambda A \int_0^t hD_x^+ f(x,\tau)d\tau \right) d\theta \\ &= \int_0^1 \left(e^{\lambda A \int_0^t f(x,\tau) + \theta h D_x^+ f(x,\tau)d\tau} \right) \left(\lambda A \int_0^t D_x^+ f(x,\tau)d\tau \right) d\theta \end{aligned}$$

In any case, we can provide estimates of the previous quantities by recalling that both φ and c_0 are bounded from above ($0 < \varphi_m \leq \varphi(x) \leq \varphi_M < 1$, $c_0 \leq c(t,x) \leq C_0$). In particular, the estimates for $D_x^+ \tilde{h}$ are given by

$$\begin{aligned} \|D_x^+ \tilde{h}\|_{L_t^\infty L_x^2}^2 &\leq \exp\left(C_1 T \|f\|_{L_t^\infty L_x^\infty} + C_2 T \left\|D_x^+ f\right\|_{L_t^\infty L_x^\infty} \right) \left\| \lambda A \int_0^t D_x^+ f(\tau,x)d\tau \right\|_{L_t^\infty L_x^2} \\ &\leq \exp\left(C_1 T \|f\|_{L_t^\infty L_x^\infty} + C_2 T \left\|D_x^+ f\right\|_{L_t^\infty L_x^\infty} \right) \left(\lambda A T \left\|D_x^+ f(\tau,x)d\tau\right\|_{L_t^\infty L_x^2} \right). \end{aligned}$$

Furthermore

$$\begin{aligned} \|\zeta(t,x)\|_{L_t^\infty L_x^2}^2 &= \sup_{t\in[0,T]} \|\varphi(c_0) e^{\lambda A \int_0^t f(\tau,x)d\tau} - Bc_0\|^2 \\ &\leq |\varphi(c_0)| \exp\left(\lambda A T \|f\|_{L_{t,x}^\infty} \right) + |B| C_0 \\ &\leq \varphi_M e^{\lambda T K} + |B| C_0. \end{aligned}$$

and

$$\begin{aligned}
\|D_x^+\zeta(t,x)\|^2_{L_t^\infty L_x^2} &= \sup_{t\in[0,T]} \|D_x^+\varphi(c_0(x))\tilde{h} + \varphi(c_0(x))D_x^+\tilde{h} - D_x^+ Bc_0(x)\|^2_{L^2(\Omega_h^+)} \\
&\leq \sup_{t\in[0,T]} \|D_x^+\varphi(c_0)\tilde{h}\|^2_{L^2(\Omega_h^+)} + \|\varphi(c_0)D_x^+\tilde{h}\|^2_{L^2(\Omega_h^+)} + \|D_x^+ Bc_0\|^2_{L^2(\Omega_h^+)} \\
&\leq \sup_{t\in[0,T]} \left\|D_x^+ c_0 e^{\lambda A\int_0^t f}\right\|^2_{L^2(\Omega_h^+)} + M\|D_x^+\tilde{h}\|^2_{L^2(\Omega_h^+)} + B\|D_x^+ c_0\|^2_{L^2(\Omega_h^+)} \\
&\leq \sup_{t\in[0,T]} (Me^{c_1 t} + |B|)\|D_x^+ c_0\|^2_{L^2(\Omega_h^+)} + M\|D_x^+\tilde{h}\|^2_{L^2(\Omega_h^+)} \\
&\leq (Me^{c_1 T} + |B|)\|D_x^+ c_0(x)\|^2_{L^2(\Omega_h^+)} + M\lambda ATe^{c_1 T}\|D_x^+ f\|^2_{L^2(\Omega_h^+)}
\end{aligned}$$

where we have exploited the hypothesis (4.21) on the data f.

Concerning (4.27) we can verify that $\zeta(t,x) > 0$ and therefore, going back to the definition of $D_x^+ g$ in (4.27)

$$\begin{aligned}
\|D_x^+ g(t,x)\|_{L_t^\infty L_x^2} &= \frac{\|\zeta(t,x)D_x^+(Ac_0(x)) - Ac_0(x)D_x^+\zeta(t,x)\|_{L_t^\infty L_x^2}}{\|(\tau_h\zeta(t,x))\cdot\zeta(t,x)\|_{L_t^\infty L_x^2}} \\
&\leq \|\zeta(t,x)D_x^+(Ac_0(x)) - Ac_0(x)D_x^+\zeta(t,x)\|_{L_t^\infty L_x^2}
\end{aligned}$$

In conclusion, by rearranging all the estimates combined with the hypothesis for f in (4.21) we obtain the following estimation on $D_x^+ g$:

$$\|D_x^+ g\|^2_{L_t^\infty L_x^2} \leq cT(\|D_x^+ c_0(x)\|^2_{L^2(\Omega_h^+)} + \kappa\|D_x^+ f\|^2_{L_t^\infty L_x^2}).$$

The estimate for the term $\|D_x^+\varphi\|_{L_t^\infty L_x^2(\Omega_h^+)}$ is related to the previous estimate for g since

$$\begin{aligned}
\|D_x^+\varphi\|^2_{L_t^\infty L_x^2} &= \sup_{t\in[0,T]} \|D_x^+\varphi\|_{L_x^2} \\
&= \sup_{t\in[0,T]} \|D_x^+(A + Bg)\|^2_{L_x^2} \\
&\leq \sup_{t\in[0,T]} |B|\|D_x^+ g\|^2_{L_x^2}
\end{aligned}$$

□

Finally, estimates for the quasi-linear equation for v are provided in the following:

Proposition 4.10 (Estimate for v)**.** *Suppose the previous hypothesis in Proposition 4.9 holds. Then there exist constants $\varepsilon, C'_\varepsilon, \kappa$ such that the solution v to quasi-linear system* (4.4) *satisfies the following bound*

$$\sup_{t\in[0,T]}\left(\int_0^\infty v_t^2 dx + \int_0^\infty\int_0^t [(D_x^- v)^2 + (D_x^+ v)^2)]drds\right) \leq C'_\varepsilon + \frac{\varepsilon T}{\varphi_M}\kappa\|D_x^+ f\|^2_{L_t^\infty L_x^2} \quad (4.28)$$

Proof. Let us calculate the following time-derivative

$$\begin{aligned}\partial_t(\varphi v^2) &= 2\varphi v\partial_t v + v^2\partial_t\varphi(g)\\ &= 2\varphi v[\Delta_x^D v + b_g(D_x^+ gD_x^+ v + D_x^- gD_x^- v) - \lambda g(1-Bf)v+\\ &\quad + b_g(D_x^+ gD_x^+ u + D_x^- gD_x^- u) - \lambda g(1-Bf)u] + v^2\partial_t\varphi(g)\\ &= \varphi(g)v(D_x^+D_x^- + D_x^-D_x^+)v + vB(D_x^+ gD_x^+ v + D_x^- gD_x^- v) - 2\lambda\varphi(g)g(1-Bf)v^2\\ &\quad + vB(D_x^+ gD_x^+ u + D_x^- gD_x^- u) - 2\lambda\varphi(g)g(1-Bf)uv - \lambda B\varphi(g)gfv^2\\ &= v[D_x^+(D_x^- v)\varphi) + D_x^-((D_x^+ v)\varphi)] - 2\lambda\varphi(g)g(1-Bf)v^2\\ &\quad + vB(D_x^+ gD_x^+ u + D_x^- gD_x^- u) - 2\lambda\varphi(g)g(1-Bf)uv - \lambda B\varphi(g)gfv^2)\end{aligned}$$

since $D_x^\pm\varphi(g) = D_g^\pm\varphi(g)D_x^\pm g$ and $D_g^+\varphi(g) = D_g^-\varphi(g) = B$.

We integrate over $[0,T]$ and sum in $(0,+\infty)$ by parts in x using the fact that $v(t,0) = 0$ and $v(t,+\infty) = 0$:

$$\begin{aligned}\int_0^\infty \varphi(g_t)v_t^2dx - \int_0^\infty \varphi(g_0)v_0^2dx - \int_0^\infty\int_0^t v[D_x^+((D_x^- v)\varphi) + D_x^-((D_x^+ v)\varphi)]drds =\\ = -\int_0^\infty\int_0^t \lambda\varphi(g)g(2-Bf)v^2 + \int_0^\infty\int_0^t (D_x^+ uD_x^+\varphi + D_x^- uD_x^-\varphi)v\,drds\\ -\int_0^\infty\int_0^t 2\lambda\varphi(g)g(1-Bf)vu\,drds\\ = R1 + R2 + R3.\end{aligned}$$

We first focus on the third term on the LHS: integrating by parts we obtain

$$\begin{aligned}\int_0^\infty\int_0^t v[D_x^+((D_x^- v)\varphi) + D_x^-((D_x^+ v)\varphi)]drds =\\ -\int_0^\infty\int_0^t [(D_x^- v)(D_x^- v) + (D_x^+ v)(D_x^+ v)]\varphi drds\\ = -\int_0^\infty\int_0^t [(D_x^- v)^2 + (D_x^+ v)^2)]\varphi drds\end{aligned}$$

Concerning R1, since $f \le M < 1$ whenever $B = 1$ we have $2 - f > 0$ and for $B = -1$ we get $2 + f > 0$. So R1 is non-positive.

The second step consists in bounding the term R2. We split R2 in two parts as $R2 = R2_+ + R2_-$, the first $R2_+$ involving the D^+ discrete derivatives and $R2_-$ the D^- derivatives. We provide a detailed proof on the bound for $R2_+$, being the $R2_-$ case completely analogous. For the semi-discrete case we would like to give an estimation for v_t^2 in the interpoleted space $L^{\frac{2}{\theta}}([0,T],H^\theta)$. By applying the interpolation's inequality with $\theta = 1$ we get (see D.1):

$$v \in L^2([0,T],H^1) \cap L^\infty([0,T],L^2)$$

then

$$v \in L^p([0,T], H^s), \quad \frac{1}{p} = \frac{\theta}{2} + \frac{(1-\theta)}{\infty}, \quad s = 1 \cdot \theta + 0 \cdot (1-\theta)$$

and the following estimation holds:

$$||v||^{\frac{2}{\theta}}_{L^2([0,T],H^1)} \leq ||v||^{\theta}_{L^2_t H^1_x} \cdot ||v||^{1-\theta}_{L^\infty_t L^2_x}$$

Applying the generalized Hölder inequality to all the three terms, both in the time and space variable and using $\frac{1}{1} = \frac{1}{2} + \frac{1}{2} + \frac{1}{\infty}$, we get for the $R2_+$ term

$$\begin{aligned}
|R2_+| &= \left| \int_0^\infty \int_0^t (D_x^+ u D_x^+ \varphi) v dr ds \right| \\
&\leq 2 \|D_x^+ u\|_{L^\infty_t L^2_x} \|D_x^+ \varphi\|_{L^\infty_t L^2_x} \|v\|_{L^1_t L^\infty_x} \\
&\leq 2\tilde{c} T^{\frac{1}{2}} \|D_x^+ u\|_{L^\infty_t L^2_x} \|D_x^+ \varphi\|_{L^\infty_t L^2_x} \left(\|v\|_{L^2_t H^1_x} + \|v\|_{L^\infty_t L^2_x} \right) \\
&\leq 2\tilde{c} C_\varepsilon T^{\frac{1}{2}} \widetilde{\eta} \|\psi\|_{C^\beta} + \varepsilon T \left(c \|D_x^+ c_0\|_{L^2_x} + \kappa \|D_x^+ f\|_{L^\infty_t L^2_x} \right), \\
&\leq 2\tilde{c} C_\varepsilon T^{\frac{1}{2}} \|D_x^+ u\|_{L^\infty_t L^2_x} \left(\|v\|_{L^2_t H^1_x} + \|v\|_{L^\infty_t L^2_x} \right) + \varepsilon \|D_x^+ \varphi\|_{L^\infty_t L^2_x} \\
&\leq 2\tilde{c} C_\varepsilon T^{\frac{1}{2}} \widetilde{\eta} \|\psi\|_{C^\beta} + \varepsilon T \left(c \|D_x^+ c_0\|_{L^2_x} + \kappa \|D_x^+ f\|_{L^\infty_t L^2_x} \right),
\end{aligned}$$

where we have used the estimates for $\|D^+ u\|_{L^\infty_t L^2_x}$,$\|D^+ \varphi\|_{L^\infty_t L^2_x}$ and the L^∞-bound on v depending on the parameter $\widetilde{\eta}$ given in [8]. Furthermore for the $||v||_{L^1_t L^\infty_x}$ we have applied a direct consequence of the Hölder's inequality (D.1) [See Appendix D] with $p = 2$:

$$\begin{aligned}
||v||_{L^1_t L^\infty_x} &\leq T^{\frac{1}{2}} \cdot ||v||_{L^2_t L^\infty_x} \\
&\leq T^{\frac{1}{2}} (\|v\|_{L^2_t H^1} + \|v\|_{L^\infty_t L^2_x}),
\end{aligned}$$

and the estimate of u in terms of the boundary function ψ given in Proposition 4.7.

Finally, for handle the $R3$ term we apply Hölder inequality with $p = 1, q = \infty$ and we can carry $||v||_{L^\infty_{t,x}}$ in the interpolated space $L^2([0,T], H^1)$ as follows:

$$\begin{aligned}
|R3| &= \left| \int_0^t \int_0^\infty -2\lambda \varphi(g) g u (1 - Bf) v \, dx dr \right| \\
&\leq C\lambda T ||g||_{L^\infty_x} (A + |B| ||g||_{L^\infty_x}) ||v||_{L^1_t L^\infty_x} ||u||_{L^\infty_t L^1_x} \\
&\leq C\lambda T ||g||_{L^\infty_x} (A + |B| ||g||_{L^\infty_x}) [T^{\frac{1}{2}} (||v||_{L^2_t H^1_x} + ||v||_{L^\infty_t L^2_x})] ||u||_{L^\infty_t L^1_x} \\
&\leq C\lambda T ||g||_{L^\infty_x} (A + |B| ||g||_{L^\infty_x}) [T^{\frac{1}{2}} (||v||_{L^2_t H^1_x} + ||v||_{L^\infty_t L^2_x})] k_1 ||\psi||_{C^\beta_t} \\
&\leq C\lambda T \eta^2 C_0 (A + |B| C_0).
\end{aligned}$$

Since the hypothesis on f given in (4.21) hold, then g admits an upper bound ($0 \leq g \leq C_0$) and thus $\varphi(g) < A + |B| C_0$. Moreover, the L^1 bound on u gives the bound $|\psi| < \eta$. Again, the L^∞_x bound on v are recalled in (3.39) (see [8] for more details).

Finally, following [82], by combining the estimation for v we obtain an important L^2- bound for v and its (symmetric) difference derivative

$$\begin{aligned}\int_0^\infty v_t^2 dx + \int_0^\infty \int_0^T [(D_x^+ v)^2 + (D_x^- v)^2] \leq \\ &\leq \int_0^\infty \frac{\varphi(g_t)}{\varphi_m} v_t^2 dx - \int_0^\infty \int_0^t \frac{\varphi(g)}{\varphi_m} \left[(D_x^- v)^2 + (D_x^+ v)^2\right] dr dx \\ &\leq \frac{R_1 + R_2 + R_3}{\varphi_m} \leq \frac{R_2 + R_3}{\varphi_m} \\ &\leq \frac{\tilde{c} C_\varepsilon T \widetilde{\eta}}{\varphi_m} \|\psi\|_{C^\beta} + \frac{\varepsilon T}{\varphi_m} \left(c \|D_x^+ c_0\|_{L_x^2(\Omega_h)} + \kappa \|D_x^+ f\|_{L_t^\infty L_x^2} \right) \\ &\quad + \frac{C \lambda \widetilde{\eta}^2}{\varphi_m} C_0 (A + |B| C_0) \\ &\leq C'_\varepsilon + \frac{\varepsilon T}{\varphi_m} \kappa \|D_x^+ f\|_{L_t^\infty L_x^2}\end{aligned}$$

□

Finally, we can provide the following uniform estimate for s.

Proposition 4.11 (Estimates for the linearized equation in s)**.** *Let s be the solution of* (4.22)*, then for $T > 0$, the following estimate on s holds with K a constant depending on T and the constants in inequality* (4.28)*:*

$$\sup_{t \in [0,T]} \|s(t,\cdot)\|^2_{L^2(\Omega_h^+)} + \int_0^T \|D_x^+ s(t,\cdot)\|_{L^2(\Omega_h^+)} dt \leq K \tag{4.29}$$

Proof. Combining the estimates obtained for u in (4.7) and v in (4.10) we could finally give a bound on the linearized solution $s = u + v$, only depending on the final time T:

$$\begin{aligned}\int_0^\infty s_t^2 dx + \int_0^\infty \int_0^T [(D_x^+ s)^2 + (D_x^- s)^2] \leq 2 \int_0^\infty u_t^2 dx + 2 \int_0^\infty \int_0^T [(D_x^+ u)^2 + (D_x^- u)^2] + \\ + 2 \int_0^\infty v_t^2 dx + 2 \int_0^\infty \int_0^T [(D_x^+ v)^2 + (D_x^- v)^2] \\ \leq C_1 T \|\psi\|^2_{C_t^\beta} + C_\varepsilon \kappa T \|D_x^+ f\|^2_{L_t^\infty L_x^2}\end{aligned} \tag{4.30}$$

By taking ε sufficiently small we get that $C_\varepsilon \kappa < 1$. Finally we can say that there exists a constant K such that the statement of the proposition is true. □

Remark 4.14. From the Proposition 4.11 one can easily derive that the same estimate is true for the original non-linear system. Indeed, we can consider $f = s$. By inequality (4.30) and by taking ε small enough, we obtain the bound on s.

Remark 4.15. The bound (4.29) on s, which is uniform in $0 < h \leq 1$, and Remark 4.14 guarantee that the solution (s, c) to equation (3.2) exists in $L^\infty([0,T], H^1(\Omega_h^+))$.

We conclude this subsection by stating a uniform bound for the variable c.

Proposition 4.12. *The norm* $\|c\|_{L^\infty([0,T],H^1(\Omega_h^+))}$ *is uniformly bounded with respect to* $0 < h \leq 1$.

Proof. We have the following explicit representation for c:

$$c(t,x) = \frac{c_0(x)}{\varphi(c_o(x))e^{\lambda \int_0^t s(\tau,x)d\tau} - Bc_0(x)}.$$

Starting from the explicit definition for g in (4.24), if we impose $f = s$, then we get $g = c$. Thus, from (4.26) and the uniform bound for s in (4.29), we can obtain the following bound for the discrete derivative of c:

$$\sup_{[0,T]} \|D_x^+ c(t,x)\|_{L^2(\Omega_h^+)} \leq cT \left(\|D_x^+ c_0(x)\|^2_{L^2(\Omega_h^+)} + \kappa \|D_x^+ f\|^2_{L_t^\infty L^2} \right),$$

and thus the statement is proved. □

4.5 Convergence results

In this section the convergence of the weak solution of the semi-discrete system (4.14) to the weak solution of the original system (3.7) - (3.8) is provided. To this end, following [74] and [29], we first define a piecewise constant extension of the grid functions introduced in Definition 4.1 and the related extension operators in order to be able to extend the *a priori* estimation on s to the whole space $\Omega = \mathbb{R}_+$. We recall some relevant properties of the piecewise constant extension operators and other preliminary technical results. The convergence of the semi-discrete system to the one in the continuum is shown by a compactness argument of Besov spaces as the spatial discretization step Δ_x tends to 0.

4.5.1 Interpolation and Compactness

Let the space $\Omega = \mathbb{R}_+$ be decomposed to the corresponding set $\Omega_h = h\mathbb{Z} \cap \mathbb{R}_+$ as described in Definition (4.1). Our proposed semi-discrete scheme (4.14) gives us a solution which, by definition, consists of two functions $s_h : \mathbb{R}_+ \times \Omega_h \to \mathbb{R}$ and $c_h : \mathbb{R}_+ \times \Omega_h \to \mathbb{R}$. Since we aim to obtain a convergence result of the functions s_h, c_h to the solutions of the equations (3.7) and (3.8), we need to extend the definition of s_h, c_h from the lattice space $\mathbb{R}_+ \times \Omega_h^+$ to the continuum product space $\mathbb{R}_+ \times \Omega$. A standard technique is to apply the *piecewise-linear interpolation*. Since we have to consider the composition of the functions s_h and c_h with some non-linear functions it is more useful to use the *piecewise constant extension*. More precisely, let us introduce the following definition.

Definition 4.5 (Piecewise constant extension)**.** Let $w : \Omega_h^+ \to \mathbb{R}$ be a grid function. Then, for every $x \in \Omega$ we define

$$\mathcal{E}_h(w)(x) := w_h(x) = \sum_{z \in \Omega_h^+} w(z) \mathbb{I}_{[z,z+h)}(x)$$

where $\mathbb{I}_K$ is the indicator function of the subset $K \subset \Omega$. We call w_h the piecewise constant extension of the function grid w in each interval of the space discretization, and the operator $\mathcal{E}_h$ the (piecewise constant) extension operator.

Concerning the operator $\mathcal{E}_h$ introduced in the previous definition, we report the following results, proved in [13].

Theorem 4.2 (Extension operator properties)**.** *Let $0 < s \leq 1$.*

The operator $\mathcal{E}_h$ is continuous from $W^{s,p}(\Omega_h^+)$ to $B_{p,\infty}^{s \wedge \frac{1}{p}}(\Omega)$.

- *For any $p \in [1, +\infty)$ we have*

$$\sup_{0<h\leq 1} \|\mathcal{E}_h\|_{\mathcal{L}(W^{s,p}(\Omega_h^+), B_{p,\infty}^{s\wedge\frac{1}{p}}(\mathbb{R}_+))} < +\infty.$$

- *In the case $s = 1$, $\mathcal{E}_h$ is continuous from $W^{1,p}(\Omega_h^+)$ into $B_{p,p}^{\frac{1}{p}}(\Omega)$ with the operator norm uniformly bounded in $0 < h \leq 1$.*

- *Let f_h be a sequence of functions in $W^{s,p}(\Omega_h^+)$ such that*

$$\sup_{0<h\leq 1} \|f_h\|_{W^{s,p}(\Omega_h^+)} < +\infty, \qquad \mathcal{E}_h(f_h) \to f \quad in \quad L^p(\Omega)$$

  then $f \in B_{p,\infty}^s(\Omega)$.

- *When $s = 1$ and $1 < p < +\infty$ then $f \in W^{1,p}(\Omega)$, where $W^{1,p}(\Omega)$ is the Sobolev space of one time weakly differentiable functions with weak derivatives in $L^p(\Omega)$.*

Proof. The proof can be found in Theorem 2.23 and Theorem 2.25 in [13]. □

Definition 4.6. We introduce the notion of *discretization operator* $\mathcal{D}^h$ from the space of $L^p(\Omega)$, where $p \in [1, +\infty]$, into $L^p(\Omega_h^+)$ defined as

$$\mathcal{D}^h(\varphi)(z) = \frac{1}{h} \int_z^{z+h} \varphi(x)dx, \quad \varphi \in L^p(\Omega), \quad z \in \Omega_h^+.$$

Remark 4.16. It is simple to see that for $g \in L^p(\Omega)$ and $f \in L^q(\Omega_h^+)$, with $\frac{1}{p} + \frac{1}{q} = 1$, it holds

$$\int_\Omega g(x)\mathcal{E}_h f(x)dx = \int_{\Omega_h^+} \mathcal{D}^h g(z) f(z)dz. \tag{4.31}$$

Definition 4.7. Let $g \in C^\infty(\Omega)$ be a smooth function. Hereafter we denote by g_h the function defined by applying the discretization operator $\mathcal{D}^h$ to g, namely

$$g_h(z) = \mathcal{D}^h(g)(z), \quad z \in \Omega_h^+.$$

In the following, we prove some technical results which will be useful for establishing our convergence theorem. The first states that, starting from a smooth function, a good approximation of it in the Besov spaces setting is provided by the extension of its space discretized version.

Lemma 4.8. *Let $g \in C_0^\infty(\Omega)$ be a smooth function with compact support. Then, for any $p \in [1, +\infty]$, $s < \frac{1}{p}$, we have*

$$\lim_{h\to 0} \|\mathcal{E}_h(g_h) - g\|_{B^s_{p,p}(\Omega)} = 0.$$

Furthermore, we get

$$\lim_{h\to 0} \|\mathcal{E}_h(D^+ g_h) - \partial_x g\|_{B^s_{p,p}(\Omega)} = \lim_{h\to 0} \|\mathcal{E}_h(D^- g_h) - \partial_x g\|_{B^s_{p,p}(\Omega)} = \lim_{h\to 0} \|\mathcal{E}_h(\Delta^D g_h) - \partial_x^2 g\|_{B^s_{p,p}(\Omega)}.$$

Proof. Since g is a compactly supported smooth function, we obtain $g_h(z) = \mathcal{D}^h(g)(z) = g(z) + o(z)$, $D^+ g_h(z) = \frac{1}{h}\int_0^h D^+ g(z+s)ds = \mathcal{D}^h(\partial_x(g))(z) + o(h) = \partial_x(g)(z) + o(h)$, and similarly for other terms.
From these relations, it is very simple to prove that $\mathcal{E}_h(g_h)$, $\mathcal{E}_h(D^- g_h)$, $\mathcal{E}_h(D^+ g_h)$ and $\mathcal{E}_h(\Delta^D g_h)$ converge weakly, as distributions in $\mathcal{S}'(\mathbb{R})$, to g, $\partial_x(g)$, $\Delta_x g$, respectively.
By Theorem 4.2, we get

$$\sup_{0<h\leq 1} \left\{ \|\mathcal{E}_h(g_h)\|_{B^{1/p}_{p,p}}, \|\mathcal{E}_h(D^+ g_h)\|_{B^{1/p}_{p,p}}, \|\mathcal{E}_h(D^- g_h)\|_{B^{1/p}_{p,p}}, \|\mathcal{E}_h(\Delta^D g_h)\|_{B^{1/p}_{p,p}} \right\} < +\infty,$$

and thus, for any $s < \frac{1}{p}$, using the compactness of the immersion of $B^{1/p}_{p,p}(\Omega)$ into $B^s_{p,p}(\Omega)$, the result follows. □

The previous lemma allows us to establish the following technical result concerning the convergence of the products of converging sequences.

Proposition 4.13. *Let $f_h \in H^1(\Omega_h^+)$ be such that $\mathcal{E}_h(f_h)$ converges to $f \in H^1(\Omega)$ in $L^2(\Omega)$. Then $\mathcal{E}_h(D^+ f_h)$ and $\mathcal{E}_h(D^- f_h)$ converge to $\partial_x f$ weakly in $L^2(\Omega)$, which is the weak derivatives of the function $f \in H^1(\Omega)$.*
Furthermore, for any other $k_h \in H^1(\Omega_h^+)$, such that $\mathcal{E}_h(k_h)$ converges to $k \in H^1(\Omega)$, then, for any $p \in [1, +\infty)$, $\mathcal{E}_h(k_h f_h)$ converges to kf strongly in $L^p(\Omega)$.

Proof. Let $g \in C_0^\infty(\Omega)$ be a smooth function with compact support. Denoting by $g_h = \mathcal{D}^h(g)$ its discretization according with Definition 4.7, by Remark 4.16 and the discrete integration by parts formula, we note that

$$\int_\Omega g(x)\mathcal{E}_h(D^+ f)(x)dx = \int_{\Omega_h^+} g_h(z) D^+ f_h(z)dz = -\int_{\Omega_h^+} D^- g_h(z) f_h(z)dz.$$

Using the fact that $D^- g_h$ converges to $\partial_x g$ in L^2, and f_h converges weakly to f in L^2 the convergence of $\mathcal{E}_h(D^+ f_h)$ to $\partial_x f$ in $\mathcal{S}'(\Omega)$ is provided.

Since $\|f_h\|_{H^1(\Omega_h^+)}$ is uniformly bounded, we obtain that $\|\mathcal{E}_h(D^+ f)\|_{L^2(\Omega)}$ is uniformly bounded too and thus $\mathcal{E}_h(D^+ f_h)$ converges to $\partial_x f$ weakly in $L^2(\Omega)$.

The second part of the proposition follows from the fact that $\mathcal{E}_h(k_h f_h) = \mathcal{E}_h(k_h)\mathcal{E}_h(f_h)$, the previous results on the boundedness of $\mathcal{E}_h$ and on the properties of compact embeddings of Besov spaces. □

4.5.2 A convergence result

In view of the numerical convergence, we introduce the weak formulation for the original non-linear problem:

Definition 4.8. We say that the couple $(\bar{s}, \bar{c})$ is a weak solution for the system (3.1) if

$$\int_0^T \int_\Omega \partial_t(\varphi \bar{s})\Phi_1 dtdx + \int_0^T \int_\Omega \varphi(\bar{c})\nabla \bar{s} \nabla \Phi_1 dtdx = -\int_0^T \int_\Omega \lambda \varphi(\bar{c}) \bar{s}\bar{c}\, \Phi_1 dtdx \tag{4.32}$$

$$\int_0^T \int_\Omega \partial_t \bar{c}\, \Phi_2 dtdx = -\int_0^T \int_\Omega \lambda \varphi(\bar{c}) \bar{s}\bar{c}\, \Phi_2 dtdx \tag{4.33}$$

for every $(\Phi_1, \Phi_2) \in C_0^\infty([0,T] \times \Omega) \times C_0^\infty([0,T] \times \Omega)$.

Author in [12] proves that, under the hypothesis that the operator in (3.7) ∂_{xx} generates a strongly continuous semigroup of bounded linear continuous operator and the term in $b_c \partial_x s + \tilde{\gamma_c} s$ is L^1 bounded, then the weak solution is a mild solution of (4.6). We can directly apply the previous result, but we still need to ensure that the *weak formulation* in Definition 4.8 is equivalent to the weak formulation for (3.7). In doing this, we should consider an opportune test function Φ_1.

Lemma 4.9. *The couple of weak solutions* $(\bar{s}, \bar{c})$ *defined in* (4.32)-(4.33) *is a mild solution for the system* (3.1) *in the sense of Definition 3.1.*

Proof. Let (s, c) be the mild solution to equations (3.7) and (3.8). By the result in [12], the mild solution to equations (3.7) and (3.8) is the same as the *weak solution* to the equations (3.7) and (3.8), i.e. (s, c) is a mild solution to equations (3.7) and (3.8) if and only if for any $g_0 \in C_0^\infty([0,T] \times \Omega)$ (namely g_0 is a smooth function with compact support) we have

$$\begin{aligned} -\int_0^T \int_\Omega \partial_t g_0(t,x) s(t,x) dtdx = &\int_0^T \int_\Omega \partial_x^2 g_0(t,x) s(t,x) dtdx \\ &+ \int_0^T \int_\Omega g_0(t,x)(b_c(t,x)\partial_x s + \gamma_c(t,x) s(Bs - 1)) dtdx \end{aligned} \tag{4.34}$$

where b_c and γ_c are given by equations (3.9) and (3.10) and c is given by the explicit formula (3.11). So, what remains to prove is that the weak formulation (4.32) in Definition 4.8 implies the weak formulation given by equation (4.34).

In order to prove this statement, we consider $g_0 \in C_0^\infty([0,T]\times\Omega)$ and a smooth mollifier $a \in C_0^\infty(\mathbb{R}^2)$ with compact support. Then, we choose $\Phi_1(t,x) = g_0(t,x)\left(a_\varepsilon^{t,x} * \frac{1}{\varphi}\right)$ as a test function. By integrating by parts the first integral in (4.32) we get:

$$\begin{aligned}
\int_0^T\int_\Omega \partial_t(\varphi(c)s)g_0(t,x)\left(a_\varepsilon^{t,x}*\frac{1}{\varphi}\right) &= \\
&= -\int_0^T\int_\Omega \varphi(c)s\partial_t\left(g_0(t,x)\left(a_\varepsilon^{t,x}*\frac{1}{\varphi}\right)\right) \\
&= -\int_0^T\int_\Omega \varphi(c)\left(a_\varepsilon^{t,x}*\frac{1}{\varphi}\right)s\partial_t g_0 - \int_0^T\int_\Omega \varphi(c)sg_0\partial_t\left(a_\varepsilon^{t,x}*\frac{1}{\varphi}\right) \\
&= -\int_0^T\int_\Omega \varphi(c)\left(a_\varepsilon^{t,x}*\frac{1}{\varphi}\right)s\partial_t g_0 - \int_0^T\int_\Omega \varphi(c)sg_0\left(a_\varepsilon^{t,x}*\partial_t\frac{1}{\varphi}\right) \\
&= -\int_0^T\int_\Omega \varphi(c)\left(a_\varepsilon^{t,x}*\frac{1}{\varphi}\right)s\partial_t g_0 - \int_0^T\int_\Omega \varphi(c)sg_0\left(a_\varepsilon^{t,x}*\frac{1}{\varphi^2}\partial_t\varphi(c)\right) \\
&= -\int_0^T\int_\Omega \varphi(c)\left(a_\varepsilon^{t,x}*\frac{1}{\varphi}\right)s\partial_t g_0 - \int_0^T\int_\Omega \varphi(c)sg_0\left(a_\varepsilon^{t,x}*\frac{B\lambda sc}{\varphi}\right)
\end{aligned}$$

Taking the limit for $\varepsilon\to 0$ we have

$$\int_0^T\int_\Omega \partial_t(\varphi(c)s)g_0(t,x)\left(a_\varepsilon^{t,x}*\frac{1}{\varphi}\right) \longrightarrow -\int_0^T\int_\Omega s\partial_t g_0 - \int_0^T\int_\Omega B\lambda s^2 c g_0. \tag{4.35}$$

For the second term in (4.32) we apply the product rule:

$$\begin{aligned}
\int_0^T\int_\Omega \varphi(c)\partial_x s\partial_x\left(g_0\left(a_\varepsilon*\frac{1}{\varphi}\right)\right) &= \\
&= \int_0^T\int_\Omega \varphi(c)\left(a_\varepsilon*\frac{1}{\varphi}\right)\partial_x s\partial_x g_0 + \int_0^T\int_\Omega \varphi(c)\left(a_\varepsilon*\frac{-\partial_x\varphi}{\varphi^2}\right)\partial_x s g_0 \\
&= \int_0^T\int_\Omega \varphi(c)\left(a_\varepsilon*\frac{1}{\varphi}\right)\partial_x s\partial_x g_0 + \int_0^T\int_\Omega \varphi(c)g_0\left(a_\varepsilon*\frac{-B\partial_x c}{\varphi^2}\right)\partial_x s \\
&= \int_0^T\int_\Omega \varphi(c)\left(a_\varepsilon*\frac{1}{\varphi}\right)\partial_x s\partial_x g_0 - \int_0^T\int_\Omega \varphi(c)g_0\left(a_\varepsilon*\frac{b_c(t,x)}{\varphi}\right)\partial_x s.
\end{aligned}$$

Similarly, as $\varepsilon\to 0$, we obtain

$$\int_0^T\int_\Omega \varphi(c)\partial_x s\partial_x\left(g_0\left(a_\varepsilon^{t,x}*\frac{1}{\varphi}\right)\right) \longrightarrow \int_0^T\int_\Omega \partial_x s\partial_x g_0 - \int_0^T\int_\Omega \partial_x s b_c g_0. \tag{4.36}$$

Thus, inserting the limits (4.35) and (4.36) in (4.32) we get

$$-\int_0^T\int_\Omega s\partial_t g_0 - \int_0^T\int_\Omega B\lambda s^2 c g_0 + \int_0^T\int_\Omega \partial_x s\partial_x g_0 - \int_0^T\int_\Omega \partial_x s b_c g_0 = -\int_0^T\int_\Omega \lambda s c g_0$$

It is easy to check that the previous expression is exactly the weak formulation for equation (3.7) against a test function $g_0 \in C_0^\infty$. Indeed, an integration by parts gives:

$$\int_0^T \int_\Omega (\partial_t s) g_0 = \int_0^T \int_\Omega (\partial_{xx} s) g_0 + \int_0^T \int_\Omega \left(\partial_x s + B\lambda s^2 c - \lambda s c)\right) g_0.$$

Let us finally recall that $\tilde{\gamma}_c = -\lambda c$. □

A similar formulation for the semi-discrete system could be obtained in the same way. The following is our main convergence result.

Theorem 4.3 (Convergence theorem)**.** *Let (s_h, c_h) be the unique solution to the semi-discrete system defined in $[0,T] \times \Omega_h^+$:*

$$\begin{cases} \partial_t(\varphi(c_h)s_h) & = \frac{1}{2}\left(D_x^+(\varphi(c_h)D_x^- s_h) + D_x^-(\varphi(c_h)D_x^+ s_h)\right) - \lambda\varphi(c_h)s_h c_h \\ \partial_t c_h & = -\lambda\varphi(c_h)s_h c_h \end{cases} \tag{4.37}$$

Then (s_h, c_h) converges to the solution (s, c) of the system (3.7) - (3.8), in the following sense: denoting by $\tilde{s}_h = \mathcal{E}_h(s_h)$ and $\tilde{c}_h = \mathcal{E}_h(c_h)$, for any $p \in [1,2]$ and for any $k < \frac{1}{p}$, we have that $(\tilde{s}_h, \tilde{c}_h)$ converges in $L^p([0,T], B^k_{p,p}(\Omega)$ to the unique solution (s,c) of the equations (4.32) and (4.33).

Proof. By the a priori estimates proved in Proposition 4.11, we have that

$$\sup_{0<h\leq 1} \|s_h\|_{L^2([0,T],H^1(\Omega_h^+))} < +\infty$$

which implies, up to a suitable subsequence, that $\tilde{s}_h = \mathcal{E}_h(s_h)$, $D\tilde{s}_h^\pm = \mathcal{E}_h(D^\pm s_h)$ converge to some function $\hat{s}$ and to its derivatives $\partial_x \hat{s}$, respectively, weakly in $L^2([0,T] \times \Omega)$.

Consider $k \in C_0^\infty([0,T] \times \Omega)$, and let $k_h = \mathcal{D}^h(k)$ be the discretization of k in the space variable. Integrating by parts we get

$$\begin{aligned} \int_0^T \int_{\Omega_h^+} \partial_t(k_h)(\varphi(c_h)s_h) dz dt = \frac{1}{2}\int_0^T \int_{\Omega_h^+} \Big(D_x^-(k_h)\varphi(c_h)D_x^- s_h + D_x^+(k_h)\varphi(c_h)D_x^+ s_h \Big) dz dt \\ + \lambda \int_0^T \int_{\Omega_h^+} \varphi(c_h) s_h c_h k_h dz dt, \\ \int_0^T \int_{\Omega_h^+} \partial_t(k_h) c_h dz dt = \lambda \int_0^T \int_{\Omega_h^+} k_h \varphi(c_h) s_h c_h dz dt \end{aligned}$$

Using property (4.31) we get that

$$\int_0^T \int_\Omega \partial_t(k)(\varphi(\tilde{c}_h)\tilde{s}_h)dxdt = \frac{1}{2}\int_0^T \int_\Omega \left(\tilde{k}_h^- \varphi(\tilde{c}_h)\tilde{s}_h^- + \tilde{k}_h^+ \varphi(\tilde{c}_h)\tilde{s}_h^+\right) dxdt + \lambda \int_0^T \int_\Omega k\varphi(\tilde{c}_h)\tilde{c}_h\tilde{s}_h dxdt,$$

$$\int_0^T \int_\Omega \partial_t(k)\tilde{c}_h dxdt = \lambda \int_0^T \int_\Omega k\varphi(\tilde{c}_h)\tilde{c}_h\tilde{s}_h dxdt,$$

where $\tilde{c}_h = \mathcal{E}_h(c_h)$ and $\tilde{k}_h^\pm = \mathcal{E}_h(D^\pm k_h)$.

We need that $\tilde{c}_h$ converges at least strongly in $L^2([0,T]\times\Omega)$ to some function $\hat{c}$. We also need that $\tilde{k}^\pm$ converges to k, strongly in $L^\infty([0,T]\times\Omega)$. This holds, by Lemma 4.8. Finally, we need that $\varphi(\tilde{c}_h)\tilde{c}_h$ converges to $\varphi(\hat{c})\hat{c}$ strongly in $L^2([0,T]\times\Omega)$.

From Proposition 4.12, we have that

$$\sup_{0<h\leq 1} \|c_h\|_{L^\infty([0,T],H^1(\Omega_h^+))} < +\infty$$

when $c_0 \in H^1(\Omega)$. We can exploit the second equation of the system (4.37) to deduce that

$$\sup_{0<h\leq 1} \|c_h\|_{H^1([0,T],L^p(\Omega_h^+))} < +\infty$$

Using interpolation inequalities on the previous two inequalities we get that for any $q \in [1,+\infty)$ there exists $\alpha, \delta > 0$ small enough

$$\sup_{0<h\leq 1} \|c_h\|_{B^\alpha_{\infty,\infty}([0,T],B^\delta_{q,q}(\Omega_h^+))} < +\infty.$$

By Theorem 4.2, this implies that

$$\sup_{0<h\leq 1} \|\varphi(\tilde{c}_h)\tilde{c}_h\|_{B^\alpha_{\infty,\infty}([0,T],B^\delta_{q/2,q/2}(\Omega))} < +\infty$$

and, by compact immersion of Besov spaces and Proposition 4.13, we get that $\varphi(\tilde{c}_h)\tilde{c}_h$ converges to $\varphi(\hat{c})\hat{c}$ strongly in $L^2([0,T],L^2(\Omega)) = L^2([0,T]\times\Omega)$. In a similar way it is possible to prove that $\tilde{c}_h$ converges to $\hat{c}$ in $L^2([0,T]\times\Omega)$.
Putting all the previous convergences together we obtain, taking $h \to 0$, that

$$\int_0^T \int_\Omega \partial_t(k)(\varphi(\hat{c})\hat{s})dxdt = \frac{1}{2}\int_0^T \int_\Omega \left(\partial_x(k)\varphi(\hat{c})\partial_x(s) + \partial_x(k)\varphi(\hat{c})\partial_x(\hat{s})\right) dxdt + \lambda \int_0^T \int_\Omega k\varphi(\hat{c})\hat{c}\hat{s}dxdt$$

$$\int_0^T \int_\Omega \partial_t(k)\hat{c}dxdt = +\lambda \int_0^T \int_\Omega k\varphi(\hat{c})\hat{c}\hat{s}dxdt.$$

Thus, by the uniqueness of weak solution to equation (3.7) - (3.8), we get that $(\hat{s}, \hat{c}) = (s, c)$, where (s, c) is the unique solution to the equation (3.7) - (3.8). Since $\tilde{s}_h = \mathcal{E}_h(s_h)$ and $\tilde{c}_h = \mathcal{E}_h(c_h)$ converge to $\hat{s} = s$ and $\hat{c} = c$ respectively, we have that the solution to the semi-discrete equation converges to the solution to the continuum one. □

Since we have stated the convergence of the solution to the semi-discrete system to the solution of the original system in the continuum, in a future work we plan to complete our study by facing the convergence of the solution of the discrete (splitting) scheme to the unique mild solutions provided in [82].

Appendix A

A finite element scheme

For the convenience of the reader, we here present the derivation of the finite elements scheme in detail, which was proposed by Natalini et al. in [9]. We are dealing with a problem with non-homogeneous Dirichlet boundary conditions: it is necessary to construct a false variational formulation by introducing the variable $\sigma(t,x) = s(t,x) - s(t,0)$, $\sigma \in H = \{u \in H^1(]0,1[), u(0) = 0\}$. We rewrite the first equation as:

$$\partial_t(\varphi\sigma) - \partial_x(\varphi(c)\partial_x\sigma) = F(\sigma, c, t)$$

and writing the classical variational formulation: we look for a couple $(\sigma, c) \in C^1([0,+\infty[, H \times L^2(]0,1[)$ such that for all $(p,q) \in H \times L^2(]0,1[)$

$$\begin{cases} \int_{]0,1[} \partial_t\varphi\sigma p dy & + \int_{]0,1[} \partial_x(\varphi\partial_x\sigma)p dy = \int_{]0,1[} pF dy \\ \int_{]0,1[} \partial_t c q dy = & - \int_{]0,1[} \rho_s c q dy \end{cases} \tag{A.1}$$

By integrating by parts the first equation, by changing the derivative with respect to t and the integral and by substituting the expression for ρ_s in the second equation we obtain:

$$\begin{cases} \partial_t \int_{]0,1[} \varphi\sigma p dy & + \int_{]0,1[} \varphi\partial_x\sigma\partial_x p dy - [\varphi\partial_x\sigma p]_0^1 = \int_{]0,1[} pF dy \\ \partial_t \int_{]0,1[} c q dy = & - \int_{]0,1[} \varphi(\sigma + s(0,\cdot))c q dy \end{cases} \tag{A.2}$$

The term $[\varphi\partial_x\sigma p]_0^1$ is equal to 0 because $p \in H$ and we have imposed the boundary condition $\partial_x\sigma(1,t)$ to be equal to 0.

In conclusion, we obtain the following variational form:

$$\begin{cases} \partial_t \int_{]0,1[} \varphi\sigma p dx & + \int_{]0,1[} \varphi\partial_x\sigma\partial_x p dx = \int_{]0,1[} pF dx \\ \partial_t \int_{]0,1[} c q dx = & - \int_{]0,1[} \varphi(\sigma + s(0,\cdot))c q dx \end{cases} \tag{A.3}$$

Let us begin the discretization of the problem. We first discretize in space by defining the regular mesh:

$$[0,1] = \bigcup_{1 \le i \le N} [x_i, x_{i-1}], \quad x_i = (i-1)\Delta x,\ \Delta x = \frac{1}{N}$$

and denoting by P1 the classical basis functions $\{p_i, i = 1, \dots N+1\}$

$$p_i(x) = \begin{cases} \frac{x-x_{i-1}}{\Delta x} & \text{if } x \in [x_{i-1}, x_i], \\ \frac{x_{i+1}-x}{\Delta x} & \text{if } x \in [x_i, x_{i+1}], \\ 0 & \text{else} \end{cases} \tag{A.4}$$

while we consider the characteristic function on the interval $[x_i, x_{i+1}[$ as basis $\{q_i, i = 1 \dots N\}$. Under these hypothesis, the couple of the solutions (s, c) can be approximated as:

$$s_h(t,x) = \sum_{i=1}^{N+1} \xi_i(t) p_i(x), \quad c_h(t,x) = \sum_{k=1}^{N} \eta_k(t) q_k(x)$$

Moreover, we define the porous density of SO_2 by:

$$\rho_{s_h}(t,x) = \varphi(c_h(t,x)) s_h(t,x)$$

In the numerical discretization, the coefficients $\xi_i(t)$ of the solution s_h are located in the nodes. In contrast, the coefficients $\eta_k(t)$ are located in the mean value of each interval of the spatial discretization $[x_k, x_{k+1}]$. To consider the boundary condition, when $x = 0$, we put $\xi_1(t) = \frac{\rho_{s0}}{\varphi(\eta_1(t)}$

The spatial discretization is given by the classical finite elements scheme; as we are dealing with non homogeneous Dirichlet boundary condition, we have written a "false" variational formula with N+1 basis functions $\{p_1, \dots, p_{N+1}\}$ and the boundary conditions are set a posteriori.

Let us rewrite the problem (A.3):

$$\begin{cases} \partial_t \int_{]0,1[} \varphi_h s_h p_i dx & + \int_{]0,1[} \varphi_h \partial_x s_h \partial_x p i dx = - \int_{]0,1[} \varphi_h s_h c_h p_i dx, \\ \partial_t \int_{]0,1[} c_h q_k dx = & - \int_{]0,1[} \varphi_h s_h c_h q_k dx \end{cases} \tag{A.5}$$

where $\varphi_h = \varphi(c_h) = \sum_{k=1}^{N} \varphi(\eta_n) q_k$. Starting from the first equation of the system and by substituting s_h with its expression in terms of the basis p_i we obtain:

$$\partial_t \sum_{j=1}^{N+1} \xi_j \int_{]0,1[} \varphi_h p_j p_i dx + \sum_{j=1}^{N+1} \xi_j \int_{]0,1[} \varphi_h \partial_x p_j \partial_x p_i dx \tag{A.6}$$

$$= - \sum_{j=1}^{N+1} \xi_j \int_{]0,1[} \varphi_h c_h p_j p_i dx, \quad i = 1, \dots, N+1 \tag{A.7}$$

As $\varphi_h = \sum_{k=1}^{N} \varphi(\tilde{\eta_k}) q_k$, we can rewrite the first equation in a vectorial form:

$$\partial_t (M(\eta(t))\xi(t)) + K(\eta(t))\xi(t) = 0. \tag{A.8}$$

Matrices M and K are respectively the Mass Matrix and the Stiffness Matrix associated with the spatial discretization by finite elements. It is easy to find an expression for the

matrices M and K by calculating the integrals that appear in the equation (A.6). Starting from M, we got:

$$M(\eta) = \begin{bmatrix} \int_{]0,1[} \varphi_1 p_1 p_1 dx & \int_{]0,1[} \varphi_1 p_1 p_2 dx & \dots & \int_{]0,1[} \varphi_1 p_1 p_N dx \\ \int_{]0,1[} \varphi_2 p_2 p_1 dx & \int_{]0,1[} \varphi_2 p_2 p_2 dx & \dots & \int_{]0,1[} \varphi_2 p_2 p_N dx \\ \dots & \dots & \dots & \dots \\ \int_{]0,1[} \varphi_{N+1} p_{N+1} p_1 dx & \int_{]0,1[} \varphi_{N+1} p_{N+1} p_2 dx & \dots & \int_{]0,1[} \varphi_{N+1} p_{N+1} p_{N+1} dx \end{bmatrix}$$

By exploiting the definition of the p_i basis, we can note that the only contributes without null entries are the one in correspondence of the indices $j = i, i-1, i+1$. By computing the integrals, we have an explicit form of the matrix M:

$$M(\eta) = \frac{\Delta x}{6} \begin{bmatrix} 2\varphi_1 & \varphi_1 & 0 & \dots & 0 \\ \varphi_1 & 2(\varphi_1 + \varphi_2) & \varphi_2 & \dots & 0 \\ \dots & \dots & \dots & \dots & \dots \\ 0 & \dots & \varphi_N & 2(\varphi_N + \varphi_{N+1}) & \varphi_{N+1} \\ 0 & \dots & 0 & \varphi_{N+1} & 2\varphi_{N+1} \end{bmatrix}$$

In an analogous way, we can compute the other contributes of the equation (A.6): we split the matrix K by the sum of two contributes $K1$ and $K2$ and we get:

$$K(\eta) = \frac{1}{\Delta x} \begin{bmatrix} 2\varphi_1 & -\varphi_1 & 0 & \dots & 0 \\ -\varphi_1 & (\varphi_1 + \varphi_2) & -\varphi_2 & \dots & 0 \\ \dots & \dots & \dots & \dots & \dots \\ 0 & \dots & -\varphi_N & (\varphi_N + \varphi_{N+1}) & -\varphi_{N+1} \\ 0 & \dots & 0 & -\varphi_{N+1} & \varphi_{N+1} \end{bmatrix}$$

$$+ \frac{\Delta x}{6} \begin{bmatrix} 2\varphi_1\tilde{\eta_1} & \varphi_1\tilde{\eta_1} & 0 & \dots & 0 \\ \varphi_1\tilde{\eta_1} & 2(\varphi_1\tilde{\eta_1} + \varphi_2\tilde{\eta_2}) & \varphi_2\tilde{\eta_2} & \dots & 0 \\ \dots & \dots & \dots & \dots & \dots \\ 0 & \dots & \varphi_N\tilde{\eta_N} & 2(\varphi_N\tilde{\eta_N} + \varphi_{N+1}\tilde{\eta_{N+1}}) & \varphi_{N+1}\tilde{\eta_{N+1}} \\ 0 & \dots & 0 & \varphi_{N+1}\eta_{N+1} & 2\varphi_{N+1}\eta_{N+1} \end{bmatrix}$$

The second equation of the system (A.3) can be written as:

$$\Delta x \partial_t \eta_k = -\eta_k (B\eta_k + A) \sum_{j=1}^{N+1} \xi_j(t) \int_{]x_k, x_{k+1}[} p_j(x) dy, \quad k = 1, \dots, N \tag{A.9}$$

or equivalently

$$\partial_t \eta_k = -\frac{(\xi_k + \xi_{k+1})}{2} \eta_k (B\eta_k + A) = -\gamma_k \eta_k (B\eta_k + A), \quad k = 1, \dots, N \tag{A.10}$$

Once the spatial discretization is done, we work with the temporal discretization of the problem. Let us consider the interval $t = [0, T_{max}]$ with time step Δt. For $t \in [t_n, t_{n+1}[$ we put $s_h(t,x) = s_h^n(x)$, $c_h(t,x) = c_h^n(x)$ The initial and boundary conditions are:

$$\begin{cases} \xi_1^0 = \frac{\rho_{s_0}}{\varphi(c_0)}, \quad \xi_j^0 = 0, & \text{for } j = 2, \dots, N+1 \\ \eta_k^0 = c_0 & \text{for } k = 1, \dots, N \end{cases}$$

To deal with the resolution either in spatial either in temporal discretization the solutions ξ and η are represented as:

$$\xi_k^n = \begin{bmatrix} \xi_1^0 & \xi_1^1 & \xi_1^2 & \dots & \xi_1^N \\ \xi_2^0 & \xi_2^1 & \xi_2^2 & \dots & \xi_2^N \\ \dots & \dots & \dots & \dots & \dots \\ \xi_{N+1}^0 & \xi_{N+1}^1 & \xi_{N+1}^2 & \dots & \xi_{N+1}^N \end{bmatrix} = \begin{bmatrix} \frac{\rho_{s0}}{\varphi(c_0)} & \xi_1^1 & \xi_1^2 & \dots & \xi_1^N \\ 0 & \xi_2^1 & \xi_2^2 & \dots & \xi_2^N \\ \dots & \dots & \dots & \dots & \dots \\ 0 & \xi_{N+1}^1 & \xi_{N+1}^2 & \dots & \xi_{N+1}^N \end{bmatrix}$$

$$\eta_k^n = \begin{bmatrix} \eta_1^0 & \eta_1^1 & \eta_1^2 & \dots & \eta_1^N \\ \eta_2^0 & \eta_2^1 & \eta_2^2 & \dots & \eta_2^N \\ \dots & \dots & \dots & \dots & \dots \\ \eta_N^0 & \eta_N^1 & \eta_N^2 & \dots & \eta_N^N \end{bmatrix} = \begin{bmatrix} c_0 & \eta_1^1 & \eta_1^2 & \dots & \eta_1^N \\ c_0 & \eta_2^1 & \eta_2^2 & \dots & \eta_2^N \\ \dots & \dots & \dots & \dots & \dots \\ c_0 & \eta_N^1 & \eta_N^2 & \dots & \eta_N^N \end{bmatrix}$$

We start by discretizing the second equation (A.10) by fixing for all $n = 1, \dots, N$ the spatial component $\xi_k = \xi_k^n$ and solving excatly the ODE (A.10). We first look for the primitive:

$$\begin{aligned} \frac{1}{-\gamma\eta(B\eta + A)} &= \frac{C_1}{-\gamma\eta} + \frac{C_2}{B\eta + A} \\ 1 &= C_1(B\eta + A) - C_2(\gamma\eta) \\ 1 &= \eta(BC_1 - C_2\gamma) + C_1 A \end{aligned}$$

And we get the parameters C_1, C_2:

$$\begin{cases} BC_1 - C_2\gamma &= 0 \\ C_1 A &= 1 \end{cases} \quad \begin{cases} C_1 &= \frac{1}{A} \\ C_2 &= \frac{B}{\gamma A} \end{cases}$$

We now solve the ODE (A.10) by the separation of variables method:

$$\begin{aligned} \int_{x_0}^{x} \frac{1}{-\gamma\eta(B\eta + A)d\eta} &= \int_{t_n}^{t_{n+1}} 1ds \\ \int_{x_0}^{x} \frac{1}{-\gamma A\eta} d\eta + \int_{x_0}^{x} \frac{B}{\gamma A(B\eta + A} d\eta &= \Delta t \\ \left[-\frac{1}{\gamma A} \ln \eta + \frac{1}{\gamma A} \ln (B\eta + A) \right]_{x_0}^{x} &= \Delta t \\ \left[\frac{1}{\gamma A} \ln \frac{B\eta + A}{\eta} \right]_{x_0}^{x} &= \Delta t \\ \ln \frac{Bx + A}{x} \frac{x_0}{Bx_0 + A} &= \gamma A \Delta t \\ (B + \frac{A}{x}) \frac{x_0}{Bx_0 + A} &= e^{\gamma A \Delta t} \end{aligned}$$

And we get the following solution with a general initial condition x_0:

$$x = \frac{Ax_0 e^{A\gamma\Delta t}}{(Bx_0 + A)e^{\gamma A\Delta t} - Bx_0} \tag{A.11}$$

By multiplying by $e^{-\gamma A\Delta t}$ we obtain

$$x = \frac{Ax_0}{Bx_0 + A - Bx_0 e^{-\gamma A\Delta t}}$$

Since the parameters B, A are nonnegative, if ξ_j^n, η_k^n are also non negative, we can approximate at each time step n the intermediate value $\eta_k^{n+1/2}$ by considering η_k^n as initial value:

$$\eta_k^{n+1/2} = A\eta_k^n \frac{e^{-\gamma_k A\Delta t}}{B\eta_k^n + A - B\eta_k^n e^{-\gamma_k A\Delta t}} \tag{A.12}$$

Remark A.1. We can also find the stationary solutions by imposing $\partial_t x = 0$:

$$\partial_t x = -\gamma x(Bx + A) = 0$$

$$\begin{cases} x &= 0 \\ x &= -\frac{A}{B} \end{cases}$$

We now solve the problem (A.6) by the θ-method, ($\theta \in [0, 1]$): $\forall n, \forall k$

$$\frac{M(\eta^{n+1/2})\xi^{n+1/2} - M(\eta^n)\xi^n}{\Delta t} + (1-\theta)K(\eta^n)\xi^n + \theta K(\eta^{n+1/2})\xi^{n+1/2} = 0 \tag{A.13}$$

For every n we got a tridiagonal system $UX = G$, where the matrix $U \in \mathcal{M}^{(N+1)\times(N+1)}$ and the vector $G \in \mathcal{M}^{(N+1)\times 1}$ are defined as:

$$U = M^{n+1/2} + \Delta t\theta K^{n+1/2}$$
$$G = (M^n - (1-\theta)\Delta t K^n)\xi^n$$

The vector X contains the spatial solution at time t^{n+1}:

$$X = \xi^{n+1} = \begin{bmatrix} \xi_1^{n+1} \\ \xi_2^{n+1} \\ \xi_3^{n+1} \\ \cdots \\ \xi_{N+1}^{n+1} \end{bmatrix}$$

The matrix U and the vector G are modified at each step of the temporal discretization to take into consideration the boundary conditions: the term g_1 is replaced by $g_{1,mod} = \frac{\rho_{s0}}{\varphi_1^{n+1/2}}$, $g_{2,mod} = g_2 - u_{2,1}\frac{\rho_{s0}}{\varphi_1^{n+1/2}}$, while $u_{1,j,mod} = \delta_{1,j}$ e $u_{i,1,mod} = \delta_{i,1}$

Once ξ^{n+1} is computed, we impose

$$\eta_k^{n+1} = \eta_k^{n+1/2} \tag{A.14}$$

to get the coefficients η_k of the solution of the second equation of the starting problem.

A.1 Stability results for the finite elements scheme

Let us recall that given the linear porosity $\varphi(c) = A + Bc$, let us say $\varphi_{\tilde{g}}$ the porosity as $c = 0$, that is at the end of the reaction, and φ_0 the initial state when $c = c_0$, then

$$B = \frac{1}{c_0}(\varphi_0 - \varphi_{\tilde{g}}), \quad A = \varphi_{\tilde{g}}.$$

In [9] an extended study of the numerical scheme, in particular a stability analysis, has been carried out in the case of a positive B, that is equivalent to say that $\varphi_0 > \varphi_{\tilde{g}}$. For completeness, here we give conditions on parameters to establish stability and positivity of the solution, in the case $B < 0$, following the analogous proposition discussed by Natalini et al. in [9] in the case of positive B. The case $B < 0$, is more appropriate in the case of marble sulphation since marble has a porosity much lower than the gypsum.

Proposition A.1. *Let $A \in \mathbb{R}_+$ and $B < 0$. Suppose that $\theta \in \left]\frac{1}{3}, 1\right]$ and $\Delta x^2 < \frac{3(3\theta-1)}{c_0}$. If the time step Δt satisfies the following condition*

$$\frac{\Delta x^2}{\theta(6 - c_0\Delta x^2)} < \Delta t \leq \frac{\Delta x^2}{(1-\theta)(3 + c_0\Delta x^2)} \tag{A.15}$$

then for all $x \in [0,1]$, $c_h(x,\cdot)$ is a non-increasing function of t, $\forall t \geq 0$ and

$$\rho_{s,h}(t,x) \geq 0, \quad c_h(t,x) \in]0, c_0]$$

Moreover, the condition (A.15) is not empty.

Proof. The goal is to prove that for all $x \in [0,1]$, $c_h(x,\cdot)$ is a non-increasing function of t, $\forall t \geq 0$, i.e.:

$$0 < \eta_k^{n+1/2} \leq \eta_k^n, \quad \forall n = 1, \ldots, N, \tag{A.16}$$

and $\rho_{s,h}(t,x) \geq 0$, i.e.

$$\xi_j^n \geq 0, \quad \forall j, n = 1, \ldots, N+1, \tag{A.17}$$

The result is true for $t \in [0, t_1[$. In fact, after imposing the initial conditions we have for all k that $\eta_k^0 = c_0$, $\gamma_k^0 = \frac{\xi_{k+1} - \xi_k}{2} = 0$. By exploiting the conditions (A.10),(A.12) we get

$$\eta_k^{1/2} = \frac{Ac_0 e^{-\gamma A \Delta t}}{(Bc_0 + A) - Bc_0 e^{-\gamma A \Delta t}} > 0 \tag{A.18}$$

The last inequality holds if the denominator is positive, i.e.

$$(Bc_0 + A) - Bc_0 e^{-\gamma A \Delta t} > 0$$

and this is always verified if $Bc_0 + A = \varphi_0 > 0$. This condition implies $A > -Bc_0$.
To prove that $\eta_k^{n+1/2} \leq \eta_k^n$ we use the same argument of Natalini's work:

$$\begin{aligned}
\eta_k^{n+1/2} &\leq \eta_k^n \\
\frac{Ae^{-\gamma A\Delta t}}{B\eta_k^n + A - B\eta_k^n e^{-\gamma A\Delta t}} &\leq 1 \\
Ae^{-\gamma A\Delta t} &\leq B\eta_k^n + A - B\eta_k^n e^{-\gamma A\Delta t} \\
e^{-\gamma A\Delta t}(B\eta_k^n + A) &\leq B\eta_k^n + A \\
e^{-\gamma A\Delta t} &\leq 1
\end{aligned}$$

which holds. By induction, we can now prove that

$$0 < \eta_k^{n+1/2} \leq \eta_k^n \leq c_0 \tag{A.19}$$

By the assumption $B < 0$, we note that as η_k^n decreases, $\varphi(\eta_k^n)$ increases. Thus, being φ a linear combination of the calcite density c, i.e. $\varphi(c) = Bc + A$, we obtain

$$0 < \varphi_0 \leq \varphi(\eta_k^n) \leq \varphi(\eta_k^{n+1/2}) \leq A = \varphi_{\tilde{g}} \tag{A.20}$$

The initial condition on ρ is equivalent to $\xi_j^0 = 0,$ for $j = 2, \ldots, N+1$ and this proves that $\rho_{s,h}(x, 0) \geq 0$.
Now we would like to prove that $\xi_j^n \geq 0$, $\forall j, n$. After the modification due to the boundary conditions, we got a $(N+1) \times (N+1)$ with a symmetric irreducibly diagonally dominant matrix: $U = M^{n+1/2} + \Delta t\theta K^{n+1/2}$. Then the matrix U^{-1} is positive if $u_{ii} > 0$, $\forall i$ and $u_{ij} < 0, \forall j = i \pm 1$. We consider now the right-hand side for $i \geq 2$ that could be written as:

$$g_i = \sum_{j=i-1}^{i+1} (m_{ij}^n - (1-\theta)\Delta t k_{ij}^n)\xi_j^n, \quad \xi_1^n = \frac{\rho_{s_0}}{\varphi_1^n} \tag{A.21}$$

by imposing the boundary conditions we have:

$$g_{2,mod} = g_2 - \frac{u_{21}\rho_{s_0}}{\varphi_1^{n+1/2}} \tag{A.22}$$

Where

$$\begin{aligned}
u_{21} &= m_{21}^{n+1/2} + \Delta t\theta k_{21}^{n+1/2} \\
&= \frac{\Delta x}{6}\varphi_1^{n+1/2} + \Delta t(-\frac{1}{\Delta x}\varphi_1^{n+1/2} + \frac{\Delta x}{6}\varphi_1^{n+1/2}\eta_1^{n+1/2})
\end{aligned}$$

And so equation (A.22) becomes:

$$\begin{aligned}
g_{2,mod} = &\sum_{j=1}^{3}(m_{2j}^n - (1-\theta)\Delta t k_{2j}^n)\xi_j^n \\
&- \frac{\rho_{s_0}}{\varphi_1^{n+1/2}}\left[\frac{\Delta x}{6}\varphi_1^{n+1/2} + \Delta t\theta\varphi_1^{n+1/2}(-\frac{1}{\Delta x} + \frac{\Delta x}{6}\eta_1^{n+1/2})\right]
\end{aligned}$$

We now explicit the term in the summation for $j = 1$:

$$m_{21}^n - (1-\theta)\Delta t k_{21}^n = \frac{\Delta x}{6}\varphi_1^n - (1-\theta)\Delta t(-\frac{\varphi_1^n}{\Delta x} + \frac{\Delta x}{6}\varphi_1^n\eta_1^n)$$
$$= \frac{\Delta x}{6}\varphi_1^n - \Delta t(-\frac{\varphi_1^n}{\Delta x} + \frac{\Delta x}{6}\varphi_1^n\eta_1^n) + \theta\Delta t(-\frac{\varphi_1^n}{\Delta x} + \frac{\Delta x}{6}\varphi_1^n\eta_1^n)$$

Going back in the equation for $g_{2,mod}$:

$$\begin{aligned} g_{2,mod} &= \sum_{j=2}^{3}(m_{2j}^n - (1-\theta)\Delta t k_{2j}^n)\xi_j^n \\ &+ \rho_{s_0}\left[\frac{\Delta x}{6} + \frac{\Delta t}{\Delta x} - \frac{\Delta x}{6}\eta_1^n + \theta\Delta t(-\frac{1}{\Delta x} + \frac{\Delta x}{6}\eta_1^n)\right] \\ &- \rho_{s_0}\left[\frac{\Delta x}{6} + \theta\Delta t(-\frac{1}{\Delta x} + \frac{\Delta x}{6}\eta_1^{n+1/2})\right] \\ &= \sum_{j=2}^{3}(m_{2j}^n - (1-\theta)\Delta t k_{2j}^n)\xi_j^n \\ &+ \rho_{s_0}\cdot\frac{\Delta t}{\Delta x}\left[1 - \frac{\Delta x^2}{6}\eta_1^n + \theta\frac{\Delta x^2}{6}(\eta_1^n - \eta_1^{n+1/2})\right] \end{aligned}$$

To ensure the positivity of the right hand side G of the system $UX = G$, we have the summation to be positive: this because the last line of the expression for $g_{2,mod}$ is non-negative if we choose a space step Δx small enough and because we have already proved that η_1^n is non-increasing.
We now combine the conditions we have imposed on U and G to guarantee the positivity of the solution. Thus we need to satisfy the following conditions:

1. $m_{ij}^{n+1/2} + \theta\Delta t k_{ij}^{n+1/2} < 0$, $\forall j = i \pm 1$, $i \geq 1$
2. $m_{ii}^{n+1/2} + \theta\Delta t k_{ii}^{n+1/2} > 0$, $\forall i \geq 2$
3. $m_{ij}^n - (1-\theta)\Delta t k_{ij}^n \geq 0$, $\forall j = i \pm 1$, i

Let us study first the case when $j \neq i$: we choose $j = i-1$ (the case $j = i+1$ is analogous for symmetry).

$$k_{ij} = -\frac{\varphi_{i-1}}{\Delta x} + \frac{\Delta x}{6}\varphi_{i-1}\eta_{i-1} \leq 0$$

This is true because φ_{i-1} and η_{i-1} are non-negative and Δx is small, so the term $\frac{1}{\Delta x}$ explodes. For the mass matrix M we have:

$$m_{ij} = \frac{\Delta x}{6}\varphi_{i-1} > 0$$

Let us focus now on the case $j = i$, $(i \geq 2)$:

$$k_{ii} = \frac{1}{\Delta x}(\varphi_{i-1} + \varphi_i) + \frac{\Delta x}{3}(\varphi_{i-1}\eta_{i-1} + \varphi_i\eta_i)) > 0$$
$$m_{ii} = \frac{\Delta x}{3}(\varphi_{i-1} + \varphi_i) > 0$$

The case when $i = 1$ is analogous:

$$k_{11} = \frac{1}{\Delta x}\varphi_1 + \frac{\Delta x}{3}(\varphi_1\eta_1) > 0$$
$$m_{11} = \frac{\Delta x}{3}\varphi_1 > 0$$

We can see that condition 2. is always true and also condition 3. when $j \neq i$. In conclusion, condition 1. and condition 3. (when $j = i$) are the conditions we need to prove to guarantee the positivity.

$$1. \iff \Delta t > -\frac{m_{ij}^{n+1/2}}{\theta k_{ij}^{n+1/2}}$$
$$3.\,(j = i) \iff \Delta t \leq \frac{m_{ii}^n}{(1-\theta)k_{ii}^n}$$

Thus

$$-\frac{m_{ij}^{n+1/2}}{\theta k_{ij}^{n+1/2}} < \Delta t \leq \frac{m_{ii}^n}{(1-\theta)k_{ii}^n} \tag{A.23}$$

If $2 \leq i \leq N$:

$$\begin{aligned}\frac{m_{ii}}{(1-\theta)k_{ii}} &= \frac{\frac{\Delta x}{3}(\varphi_{i-1} + \varphi_i)}{(1-\theta)[(\varphi_{i-1} + \varphi_i)(\frac{1}{\Delta x} + \frac{\Delta x}{3}(\eta_{i-1} + \eta_i))]} \\ &= \frac{\Delta x^2}{(1-\theta)(3 + \Delta x^2(\eta_{i-1} - \eta_i))} \\ &\leq \frac{\Delta x^2}{(1-\theta)(3 + c_0\Delta x^2)}\end{aligned}$$

where we have used the fact that η is non-increasing in the last line. For $i = N + 1$ the same low estimate holds.
If $j = i - 1$:

$$\begin{aligned}-\frac{m_{ij}}{\theta k_{ij}} &= \frac{-\frac{\Delta x}{6}\varphi_{i-1}}{\theta[-\frac{\varphi_{i-1}}{\Delta x} + \frac{\Delta x}{6}\varphi_{i-1}\eta_{i-1}]} \\ &= \frac{\Delta x^2}{\theta(6 - \Delta x^2\eta_{i-1})} \\ &\leq \frac{\Delta x^2}{\theta(6 - \Delta x^2 c_0)}\end{aligned}$$

The fact that the condition (A.15) is not empty, i.e.:

$$\frac{\Delta x^2}{\theta(6 - c_0\Delta x^2)} < \frac{\Delta x^2}{(1-\theta)(3 + c_0\Delta x^2)}$$

is ensured by the condition

$$\Delta x^2 < \frac{3(3\theta - 1)}{c_0}, \quad \theta > 1/3$$

As it is enough to consider the case where $\eta^{n+1} = \eta^{n+1/2}$, the proof is complete. □

Remark A.2. The proof can be extended in the case where the boundary condition is a positive, measurable bounded function.

Appendix B

Finite differences scheme

Following Natalini [9], we discretize system (1.10) by the finite differences scheme. Let us remark that for one-dimensional space problem, finite differences and finite elements are equivalent.

Again, we mesh $[0,1]$ with a spatial step $\Delta x = \frac{1}{N}$ and with a time step $\Delta t = \frac{1}{M}$. We look for a couple $u_n^m = (\rho_{s_m}^n, c_m^n)$, $textfor n = 1, \cdots, M$, $m = 1, \cdots, N-$ numerical solution for the system:

$$\begin{cases} \partial_t \rho_s - \partial_x \left(\varphi(c) \partial_x \frac{\rho_s}{\varphi(c)} \right) & = \mathrm{S(u)} \\ \partial_t c & = \mathrm{S(u)} \end{cases} \tag{B.1}$$

where $S(u) = -\rho_s c$ is the reaction term.
Note that c_m^n plays the same role as η_n^k in the finite elements approach.

Firstly, we would like to approximate the diffusion term for the first equation by means of Taylor's expansion of first order:

$$\Delta_m(a, r) = \frac{(a_m + a_{m+1})(r_{m+1} - r_m) - (a_{m-1} + a_m)(r_m - r_{m-1})}{2\Delta x^2} \tag{B.2}$$

The scheme is comparable to the finite element one: we firstly solve the second equation of (B.2) by fixing $\rho_{s,m}^n$ and solve:

$$c_m^{n+1} = c_m^n \, e^{-\Delta t \rho_{s,m}^n} \tag{B.3}$$

and then by time-discretizing the first equation of the system by the θ-Euler:

$$\frac{\rho_{s,m}^{n+1} - \rho_{s,m}^n}{\Delta t} - \Delta_m \left(\varphi^n, \frac{\rho_s^n}{\varphi^n} \right) = S((1-\theta)\rho_{s,m} + \theta \rho_{s,m}^{n+1}, c_m^{n+1}) \tag{B.4}$$

where $\theta \in [0,1]$.

B.1 Stability results for finite differences

We prove the stability analysis for the finite differences scheme following Natalini et al. The proposed finite difference scheme preserve the positivity under a suitable time step restriction:

Proposition B.1. *For all $n \geq 0$, $m = 1, \ldots, N$*

$$\rho_{s,m}^n \geq 0, \quad c_m^n \in [0, c_0]$$

under the time step restriction

$$\Delta t \leq \frac{A\Delta x^2}{\varphi(c_0) + A(1 + \Delta x^2 c_0(1-\theta))} \tag{B.5}$$

Proof. We need to check only the first order in time. From (B.3) it follows that $c_m^{n+1} \in [0, c_0]$. This is true for $n = 0$:

$$c_m^1 = c_0 e^{-t_1 \rho_{s_0}}$$

where $\rho_{s_0}, c_0 > 0$. It follows $c_m^1 > 0$, $c_m^1 \leq c_0$. Let us now suppose it is true for $k \leq n$, then $c_m^{n+1} \in [0, c_0]$. Then $c_m^{n+1} \in [0, c_0]$ and, when $B < 0$

$$\varphi(c_0) \leq \varphi_m^n \leq A, \quad \forall n$$

Thus going back to the scheme (B.4) we have

$$\begin{aligned}\rho_{s,m}^{n+1}(1 + \Delta t\theta c_m^{n+1}) = \rho_{s,m}^n \left[1 - \mu\left(1 + \frac{\varphi_{m+1}^n + \varphi_{m-1}^n}{2\varphi_m^n}\right) - \Delta t(1-\theta)c_m^{n+1}\right] \\ + \mu\rho_{s,m-1}^n \frac{\varphi_{m+1}^n + \varphi_{m-1}^n}{2\varphi_m^n} + \mu\rho_{s,m+1}^n \frac{\varphi_{m+1}^n + \varphi_{m-1}^n}{2\varphi_m^n}\end{aligned}$$

The positivity in ensured as soon as condition (B.5) is satisfied. □

Remark B.1. The proof for the case where $B > 0$ treated by Natalini in [9] is the same.

Appendix C

Besov Spaces

Following [62], let us start by recalling the definition of Fourier transform. We denote by $\mathcal{S}(\mathbb{R}^d)$ the *Schwartz space* and its dual by $\mathcal{S}'$, which is the space of the tempered distributions on $\mathbb{R}^d$. This because one can naturally extend the Fourier transform to a very large class of distributions on $\mathbb{R}^d$. Let us briefly introduce the following settings.

Definition C.1. Let $\alpha \in \mathbb{N}^d$ be a *multi-index*, $x \in \mathbb{R}^d$, f a smooth function of $\mathbb{R}^d$, then the length of α is given by

$$|\alpha| = \alpha_1 + \alpha_2 + \cdots + \alpha_d$$

and the derivatives of f are given by

$$\partial^\alpha f = \partial_1^{\alpha_1} \dots \partial_d^{\alpha_d} f.$$

Then, the *Schwartz space* $\mathcal{S}(\mathbb{R}^d)$ is defined as the set of smooth functions f on $\mathbb{R}^d$ such that for any $k \in \mathbb{N}$ we have

$$\|f\|_{k,\mathcal{S}} := \sup_{|\alpha| \leq k, x \in \mathbb{R}^d} (1 + |x|)^k |\partial^\alpha f(x)| < \infty$$

Now, the Fourier transform can be defined as a continuous map $\mathcal{F} : \mathcal{S}(\mathbb{R}^d) \to \mathcal{S}(\mathbb{R}^d)$:

$$\mathcal{F}(f)(\xi) = \hat{f}(\xi) = \int_{\mathbb{R}^d} e^{-i(k,\xi)} f(x) dx, \quad \xi \in \mathbb{R}^d, f \in \mathcal{S}(\mathbb{R}^d)$$

and by $\mathcal{F}^{-1}$ we denote is inverse:

$$\mathcal{F}^{-1}(\hat{f})(x) = \frac{1}{(2\pi)^d} \int_{\mathbb{R}^d} e^{i(\xi,x)} \hat{f}(\xi) d\xi, \quad x \in \mathbb{R}^d, \hat{f} \in \mathcal{S}(\mathbb{R}^d)$$

The definition could be extended to the space of tempered distribution $\mathcal{S}'$ by a duality argument.

We start by introducing the Besov space and some preliminary definitions. Let

$$B(r) = \left\{ y \in \mathbb{R}^d : |x - y| \leq r \right\}$$

denotes the ball of radius r.

Definition C.2 (Dyadic partition of unity)**.** A pair (ξ, φ) is a dyadic partition of unity if $\xi, \varphi : \mathbb{R}^d \to [0, 1]$ are two smooth compactly supported functions satisfying the following conditions:

- $supp(\chi) \subset B_{\frac{4}{3}}(0), \quad supp(\varphi) \subset B_{\frac{8}{3}}(0) \cap B_{\frac{3}{4}}(0)$
- $\chi(y) + \sum_{j \geq 0} \varphi(2^{-j}) = 1, \quad \forall y \in R^n$
- $supp(\chi) \cap supp(\varphi(2^{-j}\cdot)) = \emptyset, \quad j \geq 1$
- $supp(\varphi(2^{-j}\cdot) \cap supp(\varphi(2^{-i}\cdot) = \emptyset, \quad |i - j| > 1$

Definition C.3. Given a function $\sigma \in C^\infty(\mathbb{R}^d)$ growing at most polynomially at infinity, we define the operator $\sigma(D) : S(\mathbb{R}^d) \to S(\mathbb{R}^d)$ given by

$$\sigma(D) = \mathcal{F}^{-i}(\sigma(\xi)\mathcal{F}(f)(\xi)), \quad f \in S(\mathbb{R}^n)$$

Definition C.4. Let us fixed a *dyadic partition of unity* (see [62][11] for more details) (ξ, φ). The Littlewood-Paley blocks are the following operators, Δ_j, $j \geq -1$ defined as:

$$\begin{aligned} \Delta_{-1} &= \chi(D) \\ \Delta_j &= \varphi(2^{-j}D), \quad j \geq 0. \end{aligned}$$

Also, let $K_{-1} = \mathcal{F}^{-1}(\chi)$ and $K_j = \mathcal{F}^{-1}(\varphi(2^{-j}\cdot))$, if $j \geq 0$.

Now, if $f \in \mathcal{S}'(\mathbb{R}^d)$ then $\forall j \geq -1$

$$\Delta_j f = K_j * f.$$

Remark C.1. One can prove that when $f \in \mathcal{S}'(\mathbb{R}^d)$ then

$$\lim_{n \to +\infty} \sum_{j=-1}^{n} \Delta_j f = f$$

Furthermore we note that $\Delta_j f$ is a function since it has a compactly supported Fourier transform, in spite of the fact that f is a tempered distribution.

Finally, following [62][11], the definition of Besov space is provided:

Definition C.5. Consider $s \in \mathbb{R}$, and $p, q \in [1, +\infty]$. We say that a function $f \in \mathcal{S}'(\mathbb{R}^d)$ belongs to the Besov space $B^s_{p,q}(\mathbb{R}^d)$ if the following norm is finite

$$\|f\|_{B^s_{p,q}(\mathbb{R}^d)} := \left(\sum_{j \geq -1} 2^{qsj} \|\Delta_j f\|^q_{L^p} \right)^{1/q}$$

The following property holds:

Proposition C.1. *Embedding Let* $1 \leq p_1 \leq p_2 \leq +\infty$ *and* $1 \leq q_1 \leq q_2 \leq +\infty$*, then*

$$B^s_{p_1,q_1} \hookrightarrow B^{s-n\left(\frac{1}{p_1}-\frac{1}{p_2}\right)}_{p_2,q_2}$$

and the embedding is continuous.

Following [81][13], one can extend the definition of a discrete Besov space on the lattice. Let $\varepsilon > 0$ and define the set $\varepsilon\mathbb{Z}^d$ i.e. $<\in \varepsilon\mathbb{Z}^d$ if $z = (\varepsilon n_1, \ldots, \varepsilon n_d)$, with $n_1, n_2, \ldots, n_d \in \mathbb{Z}$. We restrict to our case of interest $d = 1$. With the discrete topology and with the Lebesgue measure we have, for any integrable function $f : \varepsilon\mathbb{Z} \to \mathbb{R}$ as

$$\int_{\varepsilon\mathbb{Z}} f(z)dz = \varepsilon \sum_{z\in\varepsilon\mathbb{Z}} f(z)$$

One can also define the Lebesgue space $L^p_\ell(\varepsilon\mathbb{Z})$, with $p \in [1, +\infty], \ell \in \mathbb{R}$, with the norm

$$\|f\|_{L^\infty_\ell(\varepsilon\mathbb{Z})} = \sup_{z\in\varepsilon\mathbb{Z}} |f(z)\rho_\ell(z)|$$

where $\rho_\ell(x)$ are the weights (see [81] for more details). Now, the *Schwartz space* on $\varepsilon\mathbb{Z}$ equipped with the semi-norm $\{\|\cdot\|_{L^\infty_\ell}\}_{\ell<0}$ as

$$\mathcal{S}(\varepsilon\mathbb{Z}) = \bigcap_{\ell<0} L^\infty_\ell(\varepsilon\mathbb{Z})$$

and its topological dual space $\mathcal{S}'(\varepsilon\mathbb{Z})$.

Lately, the Fourier transform is well-defined $\mathcal{F}_\varepsilon : \mathcal{S}(\varepsilon\mathbb{Z}) \to C^\infty\left(\mathbb{T}_{\frac{1}{\varepsilon}}\right)$, where $\mathbb{T}_{\frac{1}{\varepsilon}}$ is the torus of length $\frac{2\pi}{\varepsilon}$, is given by:

$$\mathcal{F}_\varepsilon(f)(h) := \hat{f}(h) = \int_{\varepsilon\mathbb{Z}} e^{-i\,x\cdot h} f(z)dz, \quad h \in \mathbb{T}_{\frac{1}{\varepsilon}}$$

and its inverse

$$\mathcal{F}^{-1}_\varepsilon(\hat{f})(z) := \frac{1}{2\pi} \int_{\mathbb{T}_{\frac{1}{\varepsilon}}} e^{i\,x\cdot z} \hat{f}(h)dh, \quad h \in \mathbb{T}_{\frac{1}{\varepsilon}}$$

Appendix D

Sobolev Spaces

Following [22], let us briefly recall the definition of the Sobolev space H^1 in view of the estimations.

Definition D.1. Let $I = (a, b)$ an open interval and let $1 \leq p \leq \infty$. Then, the Sobolev space $W^{1,p}(I)$ is defined to be:

$$W^{1,p}(I) = \left\{ w \in L^2(\mathbb{R}^+) : \exists g \in L^p(I) \text{ such that } \int_I u\chi' = -\int_I g\chi \quad \forall \chi \in C_c^\infty(I) \right\}$$

If $u \in W^{1,p}(I)$, then we denote $u' = g$. Moreover, let us recall that $H^1(I) = W^{1,2}(I)$.

The Sobolev space is equipped with the norm

$$\|u\|_{W^{1,p}} = \|u\|_{L^p} + \|u'\|_{L^p}$$

and for H^1 we have the associated norm

$$\|u\|_{H^1} = \left(\|u\|_{L^2}^2 + \|u'\|_{L^2}^2\right)^{1/2}$$

Definition D.2. Given $1 \leq p < \infty$, the space $H_0^1(I) = W_0^{1,p}$ is defined by the closure in $C_c^1(I)$ of $W^{1,p}(I)$.

Lemma D.1 (Hölder's Inequality for L^p spaces)**.** *Let $f \in L^p$ and $g \in L^q$ with $1 \leq p \leq \infty$ then $fg \in L^1$ and*

$$\int |fg| \leq ||f||_{L^p} ||g||_{L^q}$$

Remark D.1. A direct consequence is the following estimation when $g \equiv 1$.

Let $h \in L^p$, then

$$\int_0^T |h(t)|dt \leq ||h||_{L^p} \cdot T^{\frac{1}{q}} \tag{D.1}$$

D.1 Interpolation

Theorem D.1 (Sobolev embedding)**.** *Let $\Omega \subset \mathbb{R}^n$ be the whole space, half space or a bounded Lipschitz domain. Let $p, p_1, p_2 \leq \infty$ positive extended real quantities, s, s_1, s_2 non-negative real numbers.*

Let $\theta \in (0,1)$ and assume $s_1 \leq s_2$ such that

$$s = \theta s_1 + (1 - \theta s_2)$$

$$\frac{1}{p} = \frac{\theta}{p_1} + \frac{1-\theta}{p_2}$$

Then

$$||u||_{W^{s,p}(\Omega)} \leq c \cdot ||u||^{\theta}_{W^{s_1,p_1}(\Omega)} \cdot ||u||^{1-\theta}_{W^{s_2,p_2}(\Omega)}$$

for any $u \in W^{s_1,p_1}(\Omega) \cap W^{s_2,p_2}(\Omega)$ if and only if at least one of the following conditions is false:

$$\begin{cases} s_2 \in \mathbb{N}, & s_2 \geq 1 \\ p_2 = 1 \\ 0 < s_2 - s_1 \leq 1 - \frac{1}{p_1} \end{cases}$$

The previous result can be generalized in Besov spaces. See [15], Theorem 6.4.5.

Bibliography

[1] G. Alì, V. Furuholt, R. Natalini, and I. Torcicollo. "A mathematical model of sulphite chemical aggression of limestones with high permeability. Part I". In: *Modeling and qualitative analysis, Transport in Porous Media* 69 (2007), pp. 109–122.

[2] G. Alì, V. Furuholt, R. Natalini, and I. Torcicollo. "A mathematical model of sulphite chemical aggression of limestones with high permeability. Part II". In: *Numerical approximation, Transport in Porous Media* 69 (2007), pp. 175–188.

[3] G. Alì, R. Natalini, and I. Torcicollo. "Global existence for a 1D parabolic–elliptic model for chemical aggression in permeable materials". In: *Nonlinear Analysis: Real World Applications* 21 (2015), pp. 1–12.

[4] L. Angelini, F. Ardizzone, E. Roubin, and A. Suma. "Effects of boundary conditions in non-homogeneous birth-and-death processes". In: *Journal of Statistical Physics* (2020).

[5] F. Arceci, F. De Vecchi, D. Morale, and S. Ugolini. "Semi-discretization of a reaction-diffusion system with dynamical stochastic boundary conditions: convergence results." In: *arXiv preprint arXiv:* (2024).

[6] F. Arceci, L. M. Giordano, M. Maurelli, D. Morale, and S. Ugolini. "Randomness in a nonlinear model of sulphation phenomena". In: *Mathematical Modeling in Cultural Heritage, MACH2021*. Ed. by G. Bret, C. Cavaterra, M. Solci, and M. Spagnuolo. Springer Nature, 2023.

[7] F. Arceci, M. Maurelli, D. Morale, and S. Ugolini. "A reaction diffusion model with a stochastic boundary condition". In: *MACH2023. Mathematical Modeling in Cultural Heritage*. To appear. Springer Nature, 2024.

[8] F. Arceci, D. Morale, and S. Ugolini. *A numerical study of a PDE-ODE system with a stochastic dynamical boundary condition: a nonlinear model for sulphation phenomena*. 2024. arXiv: `2412.16307`.

[9] D. Aregbda-Driollet, F. Diele, and R. Natalini. "A mathematical model for the sulphur dioxide aggression to calcium carbonate stones: numerical approximation and asymptotic analysis". In: *SIAM J. APPL. MATH.* 64.5 (2004), pp. 1936–1667.

[10] ARPA Lombardia. *ARPA Lombardia Home Page*. `https://www.arpalombardia.it/Pages/ARPA_Home_Page.aspx`.

[11] H. Bahouri, J.-Y Chemin, and R. Danchin. *Fourier Analysis and Nonlinear Partial Differential Equations*. Vol. 343. Grundlehren der mathematischen Wissenschaften. Springer Science & Business Media, 2011, p. 524. ISBN: 9783642168307.

[12] J. Ball. "Strongly continuous semigroups, weak solutions, and the variation of constants formula". In: *Proceedings of the American Mathematical Society* 63 (Apr. 1977), pp. 370–373. DOI: 10.1090/S0002-9939-1977-0442748-6.

[13] N. Barashkov and F. C. De Vecchi. "Elliptic stochastic quantization of Sinh-Gordon QFT". In: *arXiv preprint arXiv:2108.12664* (2021). arXiv: 2108.12664 [math-ph].

[14] V. Barbu, S. Bonaccorsi, and L. Tubaro. "Stochastic parabolic equations with nonlinear dynamical boundary conditions". In: *Journal of Mathematical Analysis and Applications* 427.1 (2015), pp. 484–498.

[15] J. Bergh and J. Löfström. *Interpolation Spaces*. Vol. 223. Grundlehren der Mathematischen Wissenschaften. Berlin-New York: Springer-Verlag, 1976.

[16] S. Bonaccorsi and G. Ziglio. "A Semigroup Approach to Stochastic Dynamical Boundary Value Problems". In: *Systems, Control, Modeling and Optimization*. Ed. by F. Ceragioli, A. Dontchev, H. Furuta, K. Marti, and L. Pandolfi. Boston, MA: Springer US, 2006, pp. 55–65.

[17] A. Bonazza, P. Messina, C. Sabbioni, C. Grossi, and P. Brimblecombe. "Mapping the impact of climate change on surface recession of carbonate buildings in Europe". In: *The Science of the total environment* 407 (2009), pp. 2039–50.

[18] E. Bonetti, C. Cavaterra, F. Freddi, M. Grasselli, and R. Natalini. "A nonlinear model for marble sulphation including surface rugosity: theoretical and numerical results". In: *Communications on Pure & Applied Analysis* 18.2 (2019), pp. 977–998.

[19] E. Bonetti, C. Cavaterra, F. Freddi, M. Grasselli, and R. Natalini. "A nonlinear model for marble sulphation including surface rugosity and mechanical damage". In: *Nonlinear Analysis: Real World Applications* 73 (2023), p. 103886.

[20] E.A. Borisova and P.M. Adler. "Deposition in porous media and clogging on the field scale". In: *Physical Review E: Statistical, Nonlinear, and Soft Matter Physics* 71 (2005). DOI: 10.1103/PhysRevE.71.016311.

[21] E. Bouillaguet, M. Cadoni, and P. Galgani. "Spontaneous emission of a Brownian particle, friction and zero-point energy". In: *Annals of Physics* 433 (2021), p. 168594.

[22] H. Brezis. *Functional Analysis, Sobolev Spaces and Partial Differential Equations*. Universitext. Springer New York, NY, 2010. ISBN: 978-0-387-70913-0. DOI: 10.1007/978-0-387-70914-7.

[23] Z. Brzeźniak, B. Goldys, S. Peszat, and F. Russo. "Second order PDEs with Dirichlet white noise boundary conditions". In: *J. Evol. Equ.* 15 (2015).

[24] Dangerfield C.E., Kay D., MacNamara S., and Burrage K. "Boundary preserving semi-implicit schemes for reflected SDEs with application to population dynamics". In: *IMA Journal of Numerical Analysis* 42 (2022), pp. 1808–1834.

[25] J. Campbell. "The SMM model as a boundary value problem using the discrete diffusion equation". In: *Theoretical population biology* 72 (Jan. 2008), pp. 539–46. DOI: 10.1016/j.tpb.2007.08.001.

[26] V. Capasso and D. Bakstein. *An Introduction to Continuous-Time Stochastic Processes: Theory, Models, and Applications to Finance, Biology, and Medicine*. Springer, 2021.

[27] J. Carrera, M. W. Saaltink, J. Soler-Sagarra, J. Wang, and C. Valhondo. "Reactive Transport: A Review of Basic Concepts with Emphasis on Biochemical Processes". In: *Energies* 15 (2022), p. 925. DOI: 10.3390/en15030925.

[28] J. Chadam, Hoff, E. Merino, P. Ortoleva, and A. Sen. "Reactive infiltration instabilities". In: *IMA Journal of Applied Mathematics* 36.3 (1986), pp. 207–221.

[29] V. Chalupecky and A. Muntean. "Semi-discrete finite difference multiscale scheme for a concrete corrosion model: a priori estimates and convergence". In: *Japan Journal of Industral and Applied Mathematics* 29.2 (2012), pp. 289–316. DOI: 10.1007/s13160-012-0060-6.

[30] L. Chen and S. Gan. "Strong convergence and stationary distribution of an explicit scheme for the Wright-Fisher model". In: *Journal of Computational and Applied Mathematics* 424 (Dec. 2023), p. 115017. DOI: 10.1016/j.cam.2022.115017.

[31] L. Chen, S. Gan, and X. Wang. "First order strong convergence of an explicit scheme for the stochastic SIS epidemic model". In: *Journal of Computational and Applied Mathematics* 392 (Feb. 2021), p. 113482. DOI: 10.1016/j.cam.2021.113482.

[32] I. Chueshov and B. Schmalfuss. "Parabolic stochastic partial differential equations with dynamical boundary conditions". In: *Differential Integral Equations* 17 (2004).

[33] F. Clarelli, A. Fasano, and R. Natalini. "Mathematics and monument conservation: free boundary models of marble sulphation". In: *SIAM J. Appl. Math.* 69.1 (2008), pp. 149–168.

[34] C. Coletti. "Climate Change Threats to Stone Cultural Heritage: State of the Art of Quantitative Damage Functions and New Challenges for a Sustainable Future". In: *Heritage* 7.6 (2024), pp. 3276–3290. ISSN: 2571-9408. URL: https://www.mdpi.com/2571-9408/7/6/154.

[35] V. Comite, A. Bergomi, M. Formenti, C.A. Lombardi, M. Borelli, D. Morale, S. Ugolini, P. Fermo, C. Cavaterra, C. Castellano, and C. Cristina Della Pina. "Experimental study on the catalytic action of heavy metals in the sulphation process and formation of black crusts by accelerated ageing tests". In: *Construction and Building Materials* 449 (2024), p. 138378. URL: https://www.sciencedirect.com/science/article/pii/S0950061824035207.

[36] V. Comite, A. Miani, M. Ricca, M. La Russa, M. Pulimeno, and P. Fermo. "The impact of atmospheric pollution on outdoor cultural heritage: an analytic methodology for the characterization of the carbonaceous fraction in black crusts present on stone surfaces". In: *Environmental Research* 201 (2021), p. 111565. ISSN: 0013-9351. DOI: https://doi.org/10.1016/j.envres.2021.111565. URL: https://www.sciencedirect.com/science/article/pii/S0013935121008598.

[37] V. Comite, J. S. Pozo-Antonio, C. Cardell, T. Rivas, L. Randazzo, M. F. La Russa, and P. Fermo. "Environmental". In: *International Journal of Conservation Science* 11 (2020).

[38] V. Comite, M. Ricca, S. Antonio Ruffolo, S. F. Graziano, N. Rovella, C. Rispoli, C. Gallo, L. Randazzo, D. Barca, P. Cappelletti, and M. F. La Russa. "Multidisciplinary Approach for Evaluating the Geochemical Degradation of Building Stone Related to Pollution Sources in the Historical Center of Naples (Italy)". In: *Applied Sciences* 10 (2020), pp. 42–41.

[39] A. Costa. "Permeability-porosity relationship: A reexamination of the Kozeny-Carman equation based on a fractal pore-space geometry assumption". In: *Geophysical Research Letters* 33 (2006).

[40] A. d'Onofrio. *Bounded Noises in Physics, Biology, and Engineering*. Birkhäuser, 2013.

[41] G. d'Onofrio, P. Patie, and L. Sacerdote. "Jacobi processes with jumps as neuronal models: A first passage time analysis". In: *SIAM Journal on Applied Mathematics* (2023).

[42] G. Da Prato and J. Zabczyk. "Evolution equations with whitenoise boundary conditions". In: *Stochastics: An International Journal of Probability and Stochastic Processes* (1993).

[43] C.E. Dangerfield, D. Kay, S. MacNamara, and K. Burrage. "A boundary preserving numerical algorithm for the Wright-Fisher model with mutation". In: *BIT Numer. Math.* 52 (2012), pp. 283–304.

[44] C.E. Dangerfield, D. Kay, S. MacNamara, and K. Burrage. "A boundary preserving numerical algorithm for the Wright-Fisher model with mutation". In: *BIT Numerical Mathematics* 52.2 (2012), pp. 283–304.

[45] A. Debussche, M. Fuhrman, and G. Tessitore. "Optimal control of a stochastic heat equation with boundary-noise and boundary-control". In: *ESAIM: Control, Optimisation and Calculus of Variations* (2007).

[46] F. Delbaen and H. Shirakawa. "An interest rate model with upper and lower bounds". In: *Asia-Pacific Financial Markets* 9.3 (2002), pp. 191–209.

[47] S. Dereich, A. Neuenkirch, and L. Szpruch. "An Euler-type method for the strong approximation of the Cox-Ingersoll-Ross process". In: *Royal Society of London Proceedings Series A* 468 (Dec. 2011), pp. 1105–1115. DOI: 10.1098/rspa.2011.0505.

[48] D. Domingo, A. d'Onofrio, and F. Flandoli. "Boundedness vs unboundedness of a noise linked to Tsallis q-statistics. The role of the overdamped approximation". In: *Journal of Mathematical Physics* 58.3 (2017).

[49] M. Frémond. *Phase change in mechanics*. Vol. 13. Springer Science & Business Media, 2012.

[50] F. Garbassi, E. Mello, and M. Laurenzi Tabasso. "In situ XPS observation of the first stages of marble sulphation by atmospheric SO2". In: *Durability Build. Mater.* 3 (1985), pp. 51–58.

[51] K.L. Gauri, R. Popli, and A.C. Sarma. "Effect of relative humidity and grain size on the reaction rates of marble at high concentrations of SO2". In: *Durability Build. Mater.* 1 (1982), pp. 209–216.

[52] B. Ghayebi, S. M. Hosseini, and D. Blömker. "Numerical Solution of the Burgers Equation With Neumann Boundary Noise". In: *Journal of Computational and Applied Mathematics* 311 (July 2016). DOI: 10.1016/j.cam.2016.07.005.

[53] C. Giavarini, M.L. Santarelli, R. Natalini, and F. Freddi. "A non-linear model of sulphation of porous stones: Numerical simulations and preliminary laboratory assessments". In: *Journal of Cultural Heritage* 9 (2008), pp. 14–22.

[54] L. M. Giordano and D. Morale. "A Fractional Brownian–Hawkes Model for the Italian Electricity Spot Market: Estimation and Forecasting". In: *Journal of Energy Markets* 14.3 (2021).

[55] C. Gouriéroux and C. Pascale Valéry. "Estimation of a Jacobi process". In: 2002. URL: https://api.semanticscholar.org/CorpusID:18103395.

[56] R. C. Griffiths, P. A. Jenkins, and D. Spanó. "Wright–Fisher diffusion bridges". In: *Theoretical Population Biology* 122 (2018), pp. 67–77.

[57] R. C. Griffiths and D. Spanó. "Diffusion processes and coalescent trees". In: *Probability and Mathematical Genetics*. Vol. 378. London Mathematical Society Lecture Note Series. Cambridge: Cambridge University Press, 2010, pp. 358–379.

[58] F. R. Guarguaglini and R. Natalini. "Global existence of solutions to a nonlinear model of sulphation phenomena in calcium carbonate stones". In: *Nonlinear Analysis: RealWorld Applications* 6 (2005), pp. 477–494.

[59] F. R. Guarguaglini and R. Natalini. "Fast Reaction Limit and Large Time Behavior of Solutions to a Nonlinear Model of Sulphation Phenomena". In: *Communications in Partial Differential Equations* 32.2 (2007), pp. 163–189.

[60] F. R. Guarguaglini and R. Natalini. "Global existence and uniqueness of solutions for multidimensional weakly parabolic systems arising in chemistry and biology". In: *Communications on Pure & Applied Analysis* 1.6 (2007), pp. 287–309.

[61] F.R. Guarguaglini and R. Natalini. "Nonlinear transmission problems for quasilinear diffusion systems". In: *Netw. Heterog. Media* 2 (2007), pp. 359–381.

[62] M. Gubinelli and M. Hofmanová. "A PDE construction of the Euclidean φ^4_3 quantum field theory". In: *arXiv preprint arXiv:1810.01700* (2018). arXiv: 1810.01700 [math-ph].

[63] N. Halidias and I. S. Stamatiou. In: *Computational Methods in Applied Mathematics* 16.1 (2016), pp. 105–132. DOI: doi:10.1515/cmam-2015-0028. URL: https://doi.org/10.1515/cmam-2015-0028.

[64] N. Halidias and I. S. Stamatiou. "Boundary preserving explicit scheme for the Aït-Sahalia mode". In: *Discrete and Continuous Dynamical Systems - B* 28.1 (2023), pp. 648–664. ISSN: 1531-3492. DOI: 10.3934/dcdsb.2022092. URL: https://www.aimsciences.org/article/id/627e24542d80b75a35c2ba8c.

[65] H. Holden, B. Øksendal, J. Ubøe, and T. Zhang. *Stochastic partial differential equations*. Springer, 2010.

[66] T. Huillet. "On the Karlin-Kimura approaches to the Wright-Fisher diffusion with fluctuating selection". In: *Journal of Statistical Mechanics: Theory and Experiment* (2011).

[67] M. Hutzenthaler, A. Jentzen, and P. Kloeden. "Strong convergence of an explicit numerical method for SDEs with nonglobally Lipschitz continuous coefficients". In: *The Annals of Applied Probability* 22 (Oct. 2010). DOI: 10.1214/11-AAP803.

[68] C. Jordan. *Calculus of Finite Differences*. New York, NY : Chelsea Publ. Comp., 1960.

[69] I. Karatzas and S. E. Shreve. *Brownian Motion and Stochastic Calculus*. Second Edition. Vol. 113. Graduate Texts in Mathematics. Springer, 1991. ISBN: 978-0-387-97655-6.

[70] S. Karlin and H.M. Taylor. *A Second Course in Stochastic Processes*. Academic Press, 1981.

[71] D. P. Kingma and J. Ba. "Adam: A method for stochastic optimization". In: *arXiv preprint arXiv:1412.6980* (2014).

[72] Peter E Kloeden and Eckhard Platen. *Numerical Solution of Stochastic Differential Equations*. Vol. 23. Applications of Mathematics. Berlin, Heidelberg: Springer-Verlag, 1992. ISBN: 978-3-662-12616-5. DOI: 10.1007/978-3-662-12616-5.

[73] N. P. Kulshreshtha, A. R. Punuru, and K. L. Gauri. "Kinetics of reaction of SO2 with marble". In: *J. Mater. Civil Engrg.* 1 (1989), pp. 60–72.

[74] O. A. Ladyženskaja, V. A. Solonnikov, and N. N. Ural'ceva. *Linear and Quasi-linear Equations of Parabolic Type*. American Mathematical Society, 1968.

[75] R. LeVeque. *Finite Difference Methods for Ordinary and Partial Differential Equations: Steady-State and Time-Dependent Problems (Classics in Applied Mathematics Classics in Applied Mathemat)*. USA: Society for Industrial and Applied Mathematics, 2007. ISBN: 0898716292.

[76] Z. Libasin, A. Z. Ul-Saufie, H. Ahmat, and W. N. Shaziayani. "Single and Multiple Imputation Method to Replace Missing Values in Air Pollution Datasets: A Review". In: *IOP Conference Series: Earth and Environmental Science* 616 (2020).

[77] J.-L. Lions. *Quelques méthodes de résolution des problèmes aux limites non linéaires*. Paris: Dunod, 1969.

[78] W.T. Lipfert. "Atmospheric damage to calcareous stone: comparison and reconciliation of recent experimental findings". In: *Atmos. Environ.* 23 (1989), pp. 415–429.

[79] Z. Liu, Y. Lin, Y. Cao, H. Hu, Y. Wei, Z. Zhang, S. Lin, and B. Guo. "Swin Transformer: Hierarchical Vision Transformer using Shifted Windows". In: *arXiv preprint arXiv:2104.03468* (2021).

[80] R. Lord, R. Koekkoek, and D.V. Dijk. "A comparison of biased simulation schemes for stochastic volatility models". In: *Quantitative Finance* 10.2 (2010), pp. 177–194.

[81] J. Martin and N. Perkowski. "Paracontrolled distributions on Bravais lattices and weak universality of the 2d parabolic Anderson model". In: *Ann. Inst. H. Poincaré Probabilités et Statistiques* 55.4 (2019), pp. 2058–2110.

[82] M. Maurelli, D. Morale, and S. Ugolini. *Well-posedness of a reaction-diffusion model with stochastic dynamical boundary conditions*. 2023. arXiv: 2308.06847 [math.PR].

[83] A.I. Middya and S. Roy. "Pollutant specific optimal deep learning and statistical model building for air quality forecasting". In: *Environmental Pollution* 301 (2022), p. 118972.

[84] G. N. Milstein, Eckhard Platen, and H. Schurz. *Balanced Implicit Methods for Stiff Stochastic Systems*. Published Paper Series 1998-1. Finance Discipline Group, UTS Business School, University of Technology, Sydney, Jan. 1998. URL: https://ideas.repec.org/p/uts/ppaper/1998-1.html.

[85] J. K. Møller and H. Madsen. *From State Dependent Diffusion to Constant Diffusion in Stochastic Differential Equations by the Lamperti Transform*. Tech. rep. IMM-Technical Report-2010-16. Technical University of Denmark, DTU Informatics, Building 321, 2010.

[86] D. Morale, G. Rui, and S. Ugolini. "A stochastic interacting particle model for the marble sulphation process". In: *MACH2023. Mathematical Modeling in Cultural Heritage*. Springer (to appear), 2024.

[87] D. Morale, L. Tarquini, and S. Ugolini. *A probabilistic interpretation of a non-conservative and path-dependent nonlinear reaction-diffusion system for the marble sulphation in Cultural Heritage*. 2024. arXiv: 2407.19301.

[88] P. Moropoulou, T. Theoulakis, and T. Chrysopakis. "Correlation between stone weathering and environmental factors in marine atmosphere". In: *Atmospheric Environment* 29 (1995), pp. 895–903.

[89] T. Nakagawa, D. Taguchi, and T. Yuasa. "Semi-implicit Euler–Maruyama scheme for polynomial diffusions on the unit ball". In: *Journal of Mathematical Analysis and Applications* 519 (Nov. 2022), p. 126829. DOI: 10.1016/j.jmaa.2022.126829.

[90] R. Natalini, C. Nitsh, G Pontrelli, and S. Sbaraglia. "A numerical study of a nonlocal model of damage propagation under chemical aggression". In: *J. of Applied Mathematics* 14 (2003), pp. 447–464.

[91] A. Neuenkirch and L. Szpruch. "First order strong approximations of scalar SDEs defined in a domain". In: *Numer. Math.* 128.1 (2014), pp. 103–136.

[92] J. Nowotarski, J. Tomczyk, and R. Weron. "Estimation and forecasting of the long-term seasonal component of electricity spot prices". In: *Energy Economics* 39 (2013), pp. 13–27.

[93] B. Øksendal. *Stochastic Differential Equations: An Introduction with Applications*. 6th. Berlin, Germany: Springer, 2003. ISBN: 978-3-540-04758-2. URL: https://books.google.it/books?id=gizqCAAAQBAJ.

[94] S. Pal. "Wright-Fisher diffusion with negative mutation rates". In: *Annals of Probability* 41.2 (2013), pp. 503–526.

[95] D. Pasquale, A. Airoldi, and Beatriz N. Rodriguez. "Salt transport and distribution in marble at variable temperatures: experimental characterization and numerical simulations". In: *Construction and Building Materials* 218 (2019), pp. 212–222.

[96] K. Pini. "Time series analysis. A statistical study for air pollutant daily concentration in Milano". MA thesis. (Advisor D. Morale), Università degli studi di Milano, 2023.

[97] D. Revuz and M. Yor. *Continuous Martingales and Brownian Motion*. Springer-Verlag, 1991.

[98] L. C. G. Rogers and D. Williams. *Diffusions, Markov Processes, and Martingales: Volume 2, Itö Calculus*. Cambridge University Press, 2000.

[99] M. Saba, E.E. Quiñones-Bolañosa, and A. L. Barbosa López. "A review of the mathematical models used for simulation of calcareous stone decay". In: *Environmental Science and Pollution Research* 25 (2018), pp. 28677–28686.

[100] S. Särkkä and A. Solin. *Applied Stochastic Differential Equations*. Institute of Mathematical Statistics Textbooks. Cambridge University Press, 2019. DOI: 10.1017/9781108186735.

[101] S. Sciarra. "Pearson diffusions: from well-posedness to statistical estimation via an optimal martingale approach." MA thesis. (Advisors D. Morale, S. Ugolini), Università degli studi di Milano, 2024.

[102] A. M. Sefidian and N. Daneshpour. "Estimating missing data using novel correlation maximization based methods". In: *Applied Soft Computing Journal* 91 (2020).

[103] A.V. Skorohod. *Studies in the theory of random processes*. Addison-Wisley, 1965.

[104] M. Sorensen and J. L. Forman. "The Pearson diffusions: A class of statistically tractable diffusion processes". In: *Scandinavian Journal of Statistics* 35.3 (2008), pp. 438–465.

[105] I. Spinelli, S, S. cardapane, and A. Uncini. "Missing data imputation with adversarially-trained graph convolutional networks". In: *Neural Networks* 129 (2020), pp. 249–260.

[106] J. C. Strikwerda. *Finite Difference Schemes and Partial Differential Equations, Second Edition*. Society for Industrial and Applied Mathematics, 2004.

[107] S. Tambe, K. L. Gauri, S. Li, and W. G. Cobourn. "Kinetic study of SO2 reaction with dolomite". In: *Environ. Sci. Technol.* 25 (1991), pp. 2071–2075.

[108] L. Teng, M. Ehrhardt, and M. Günther. "Modelling stochastic correlation". In: *Journal of Mathematics in Industry* 6 (2016), p. 2.

[109] J. W. Thomas. *Numerical Partial Differential Equations: Finite Difference Methods*. USA: Springer-Verlag New York, Inc., 1995, pp. 205–258.

[110] C. Tomasi. "Mathematical models of sulphation of limestone and marble under atmospheric and aqueous pollutants: a review". In: *Environ. Sci. Pollut. Res.* 28 (2021), pp. 65339–65364.

[111] M. Turra. "Infinitesimal analysis of singular stochastic partial differential equations". PhD thesis. University of Bonn, 2022.

[112] T. Wei. "Crosswind stability of high-speed trains". PhD thesis. Delft University of Technology, 2019. URL: https://repository.tudelft.nl/islandora/object/uuid:948769c8-49e5-4175-9990-76b3235f7a25.

[113] S. Xu and J. Duan. "A Taylor expansion approach for solving partial differential equations with random Neumann boundary conditions". In: *Applied Mathematics and Computation* 217 (Aug. 2011), pp. 9532–9542. DOI: 10.1016/j.amc.2011.03.137.

[114] T. Yamada and S. Watanabe. "On the uniqueness of solutions of stochastic differential equations". In: *J. Math. Kyoto Univ.* 1.11 (1971), pp. 155–167.

[115] J. Yang, W. Chen, D Yang, and H.-M Tian. "Investigating the Permeability of Marble under Moderate Pressure and Temperature". In: *Geofluids* 2017 (Sept. 2017), pp. 1–8.

[116] A. Zanin. "Poisson and Hawkes processes: modeling and estimation of jumps in time series. Applications to real data." MA thesis. (Advisor D. Morale), Università degli studi di Milano, 2024.

[117] Z. Zhang and G. Karniadakis. *Numerical Methods for Stochastic Partial Differential Equations with White Noise*. Jan. 2017. ISBN: 978-3-319-57510-0. DOI: 10.1007/978-3-319-57511-7.

[118] X. Zong, F. Wu, and C. Huang. “Convergence and stability of the semi-tamed Euler scheme for stochastic differential equations with non-Lipschitz continuous coefficients”. In: *Applied Mathematics and Computation* 228 (Feb. 2014), pp. 240–250. DOI: 10.1016/j.amc.2013.11.100.